TRANSITION METAL COMPLEXES OF SCHIFF BASES WITH AZIDE AND THIOCYANATE AS COLIGANDS: SPECTRAL AND STRUCTURAL INVESTIGATIONS

Thesis

Submitted to Cochin University of Science and Technology

in partial fulfilment of the requirements

for the award of the degree of

DOCTOR OF PHILOSOPHY

in

CHEMISTRY

by

SREESHA SASI

Department of Applied Chemistry

Cochin University of Science and Technology

Kochi - 22

October 2008

Department of Applied Chemistry
Cochin University of Science and Technology
Kochi-682 022

Phone Off: 0484-2575804
Telex: 885 – 5019 CUIN
Fax: 0484 – 2577595
Email: mrp@cusat.ac.in

Dr. M.R. Prathapachandra Kurup
Professor of Inorganic Chemistry

14th October 2008

Certificate

Certified that the thesis entitled "**TRANSITION METAL COMPLEXES OF SCHIFF BASES WITH AZIDE AND THIOCYANATE AS COLIGANDS: SPECTRAL AND STRUCTURAL INVESTIGATIONS**", submitted by Ms. Sreesha Sasi, in partial fulfilment of the requirements for the degree of Doctor of Philosophy in Chemistry to Cochin University of Science and Technology, is an authentic and bonafide record of the original research work carried out by her under my supervision at the Department of Applied Chemistry. Further, the results embodied in this thesis, in full or in part, have not been submitted previously for the award of any other degree.
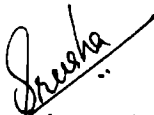
M.R. Prathapachandra Kurup
(Supervising Guide)

DECLARATION

I hereby declare that the work presented in this thesis entitled **"TRANSITION METAL COMPLEXES OF SCHIFF BASES WITH AZIDE AND THIOCYANATE AS COLIGANDS: SPECTRAL AND STRUCTURAL INVESTIGATIONS"**, is based on the original work carried out by me under the guidance of Dr. M.R. Prathapachandra Kurup, Professor, Department of Applied Chemistry, Cochin University of Science and Technology and has not been included in any other thesis submitted previously for the award of any degree.

Kochi – 22

14-10-2008

Sreesha Sasi

Acknowledgement

At the outset, I bow before the Almighty for His countless blessings and first of all, submit my thesis at his feet.

A journey is easier when we travel together. During my research work I have been accompanied and supported by many people. It is a pleasant aspect that I now have the opportunity to acknowledge with sincere respect, my deep sense of gratitude for all those who have been instrumental in bringing this thesis to completion.

I express my profound gratitude towards my supervising guide Dr. M.R. Prathapachandra Kurup, Professor, Department of Applied Chemistry, Cochin University of Science & Technology for his dynamic guidance, meticulous efforts, constructive discussions, persistent encouragement and whole hearted co-operation to bring this project to completion. It has been an honour and pleasure to work with him and I shall always cherish this association.

I wish to express my heartiest thanks to Dr. K. Girish Kumar, Head, Department of Applied Chemistry, CUSAT for his valuable advices and support. I am greatly indebted to Dr. K.K. Mohammed Yusuff, Professor, Department of Applied Chemistry, CUSAT for all the help extended. I owe my sincerest thanks to Dr. S. Sugunan, Former Head for providing necessary help. I express my gratitude to all other teaching and non-teaching staff of the Department of Applied Chemistry, CUSAT for their support.

I deeply acknowledge the Council of Scientific and Industrial Research, New Delhi for the financial assistance. I am grateful to Dr. H.-K. Fun, X-ray Crystallography Unit, School of Physics, Universiti Sains Malaysia, Peneng, Malaysia and Dr. E. Suresh, CSMCRI, Bhavnagar, Gujarat for single crystal X-ray diffraction studies. I extend my thanks to the head of the institutions of SAIF Kochi, IISc Bangalore, IIT Roorkee and IIT Mumbai for the services rendered in analyses.

I acknowledge my seniors Dr. Suni V., Dr. P.F. Rapheal, Mini Kuriakose and Dr. Seena E.B. for their help and valuable suggestions. A special word of thanks to Dr. Seena E.B. who has been particularly helpful with her suggestions. Seena chechi, I have always enjoyed your company and our travel in the University bus. I would specially like to thank my colleagues Bessy, Manoj, Leji, Binu, Suja, Laly miss, Jayakumar sir, Sheeja, Nancy, Reena, Renjusha and Neema for providing a friendly working

The interaction of transition metal ions with biologically active ligands provides one of the most fascinating areas of coordination chemistry. Metal chelation has spurred interest in the present day in medicine and chemical investigations.

Recently, inorganic chemistry witnessed a great outflow of coordination compounds, with unique structural characteristics and diverse applications. The diversity in structures exhibited by the coordination complexes of multidentate ligands have led to their usage as sensors, models for enzyme mimetic centers, medicines etc. The present work deals with the complexation of Schiff bases with various transition metal ions in presence of pseudohalides like azide and thiocyanate. Schiff bases exhibit a wide variety of properties like antimicrobial, antifungal and anticancer activities and are useful as catalysts in many reactions. The pseudohalogens azide and thiocyanate have been demonstrated to be versatile bridging ligands. They are excellent candidates for the design of molecule based magnetic materials. In addition, the azide and thiocyanate anions are observed to inhibit several enzymes like ATPases, cytochrome C oxidase, human carboxy peptidase etc. This makes the study of the metal complexes of these anions very useful for the understanding of biological processes. The use of these anions in conjugation with the Schiff bases for the synthesis of metal complexes can bring about interesting results.

Coordination complexes of transition metal ions like copper, manganese, nickel, cobalt and cadmium have been synthesized. Various spectral techniques have been employed for characterization of the metal complexes. The structures of some of the complexes have been established by single crystal X-ray diffraction studies.

This Ph.D thesis contains the description of the work done by the researcher from March 2004 to October 2008. The work done is presented in seven chapters and a brief summary and conclusions is also included in the last part of the thesis.

Contents

Chapter 7

Syntheses, structural and spectral investigations of cadmium(II) complexes of Schiff bases with azide and thiocyanate

Chapter 8

Summary and Conclusions

Transition metal complexes of Schiff bases and pseudohalogens, their bonding aspects and applications

1.1 Introduction

Metallo-organic chemistry, incorporating the frontiers of both inorganic and organic chemical aspects, is a topic of utility concern. The first exploration of coordinated metal complexes dates back to the nineteenth century, during the days of Alfred Werner [1]. Thereafter, the inorganic chemistry witnessed a great outflow of coordination compounds, with unique structural characteristics and diverse applications. In the modern ages, the stereochemistry of most of the coordination compounds can be explored by accommodating the concepts of electronic energy levels and bonding, but however there are several instances where unusual structures and theoretical challenges are observed.

The stereochemistry of coordination compounds is one of the major interests of the coordination chemist. Coordination complexes can assume a wide variety of structures depending on the metal ion, its coordination number and the denticity of the ligands used. The ligands also range from monodentate to polydentate based on the potential donor sites available in their structural skeleton. The presence of more

electronegative nitrogen, oxygen or sulfur atoms on the ligand structure is established to enhance the coordinating possibilities of ligands. Hence there has been a continuous quest over the many years for nitrogen or sulfur donor ligands, which possess a variety of coordination possibilities.

Hugo Schiff described the condensation between a carbonyl compound and an amine leading to a Schiff base in 1864 [2]. A Schiff base contains the azomethine group, $-CH=N-$ and is obtained as per the following scheme:
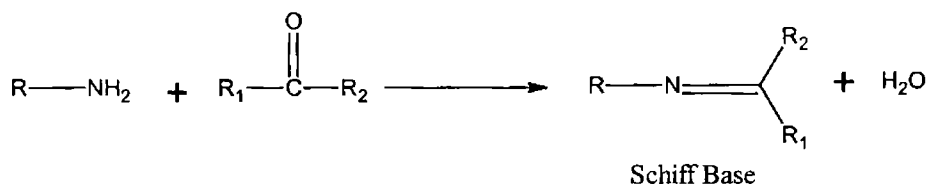
Schiff Base

where R, R_1 and R_2 may be alkyl or aryl groups. If the reactant is an aldehyde, the group R_2 will be hydrogen. Schiff bases of aliphatic aldehydes are relatively unstable and readily polymerizable [3,4], while those of aromatic aldehydes having effective conjugation are more stable [5,6]. Schiff bases prepared from aromatic amines are known as anils.

1.2 Importance of Schiff bases

Schiff base ligands are able to coordinate metals through imine nitrogen and another group, usually linked to the aldehyde/ketone. Modern chemists still prepare Schiff bases, and nowadays active and well-designed Schiff base ligands are considered 'privileged ligands' [7]

because they are easily prepared by the condensation between aldehydes and amines. Synthetic catalysts which are enantioselective over a wide range of different reactions were defined as 'privileged' by Jacobsen. Schiff base ligands are able to coordinate many different metals, and to stabilize them in various oxidation states, enabling the use of Schiff base metal complexes for a large variety of useful catalytic transformations. Stereogenic centers or other elements of chirality (planes, axes) can be introduced in the synthetic design.

Schiff bases are interesting due to their preparational accessibilities, structural varieties and varied denticities [8-18]. Metal-organic frameworks are widely regarded as promising materials for application in catalysis, separation, magnetism and molecular recognition [19-30]. One of the possible approaches to the synthesis of such compounds can be carried out from coordination chemistry.

Metal complexes of Schiff bases are useful in the catalysis of many reactions like carbonylation, hydroformylation, reduction, oxidation, epoxidation and hydrolysis etc [31]. This is due to the fact that Schiff bases offer opportunities for inducing substrate chirality, tuning the metal centered electronic factor, enhancing the solubility and stability of either homogeneous or heterogeneous catalysts. The flexibility of disposition of different donor sites is the secret behind their successful performance in mimicking peculiar geometries around the metal centers, leading to very interesting spectroscopic properties with varied magnetic activities [32]. Optically active Schiff base

complexes are especially important due to their importance as catalysts in several industrial redox processes [33-37].

Schiff bases are important in enzyme catalysis for three reasons (at least). They maintain the oxidation state of the carbonyl group. They form a covalent bond to the substrate, so that the substrate cannot diffuse away in the middle of the reaction. And they act as electron sinks and sources for further chemistry.

Antimicrobial and antifungal activities of various Schiff bases have also been reported [38,39]. Sahu *et al.* [40] reported fungi toxicity of some Schiff bases. Gawad *et al.* [41] synthesized some Schiff bases and observed high antimicrobial activities. Many Schiff bases are known to be medicinally important and are used to design medicinal compounds [42-44].

Metal complexes with nitrogenous Schiff bases are becoming increasingly relevant for their biochemical, analytical and antimicrobial activities [45-47]. It has been shown that Schiff base complexes derived from 4-hydroxysalicylaldehyde and amines have strong anticancer activity, e.g. against *Ehrlich Ascites Carcinoma* (EAC) [48]. It is well known that some drugs have greater activities when administered as metal complexes than as free organic ligands only [49]. A large number of reports are available on the biochemistry and the microbial activities of transition metal complexes containing O, N and S, N donor atoms. The transition metal complexes having oxygen and nitrogen donor Schiff bases possess unusual configuration, structural

4

lability and are sensitive to molecular environment [49]. The environment around the metal center as coordination geometry, number of coordinated ligands and their donor groups are the key factors for metallo-proteins to carry out specific physiological functions [50].

1.3 The pseudohalogens – azide and thiocyanate

The synthesis of pseudohalide complexes of metals is a subject of much interest, and intensive investigations have taken place as a result of their diverse structures and potential applications in magnetic materials. Pseudohalide anions are excellent ligands for obtaining discrete, one-dimensional, two-dimensional or three-dimensional systems. Indeed, both anions have been frequently used as crystallizing agents in protein crystal growth [51] and, much more importantly, are known to be competitive inhibitors in many enzymes. Both entities, thiocyanate and azide, are small, triatomic, linear monoanions wherein the negative charge can be localized on one of the terminal atoms or delocalized over the whole anion.

1.3.1 The azide anion

The azido-bridged complexes have attracted intense interest, due to the coordination versatility of the azido bridge and the magnetic diversity of the complexes [52-55]. Among all the pseudohalogens, the flexidentate azide ion is the most efficient ligand with regard to the superexchange pathways between the paramagnetic centers. The use of azide as a ligand affords a great variety of structural types spanning from discrete molecules to three-dimensional compounds [56-58]. The

diversity and efficiency of azide lies in its functionality as a terminal monodentate or bridging bi-, tri- and tetradentate ligand [59,60]. The various coordination modes exhibited by the azide ion is depicted in Fig. 1.1.

μ-1,1
(*end-on*)

μ_3-1,1,1

μ_4-1,1,1,1

μ-1,3
(*end-to-end*)

μ_3-1,1,3

μ_4-1,1,3,3
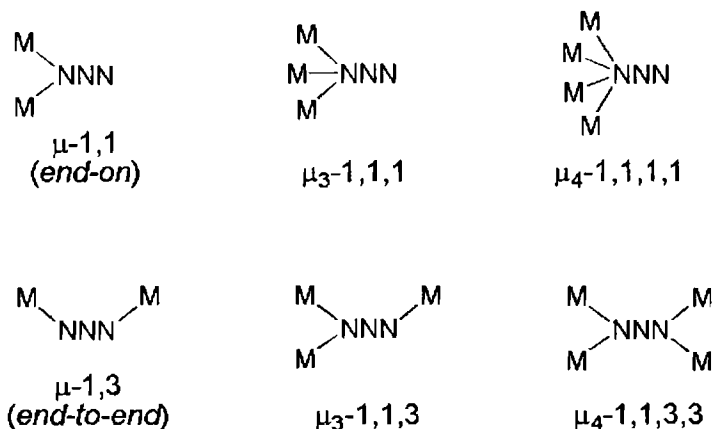
Fig.1.1. Possible coordination modes of azide ion.

The two major bidentate bridging modes observed are the μ-1,1 (end-on) and μ-1,3 (end-to-end) azido modes; the latter offering the possibility of various geometric isomers. Several other less common modes have also been reported. The nature of the link in azido-bridged paramagnets is reflected in both size and sense of magnetic interaction thereby mediated.

The remarkable ability of the azido ligand to transmit large ferro or antiferromagnetic interactions when adopting the end-on or end-to-end bridging modes makes it versatile. When the azido group acts as a bridging ligand with an end-on coordination mode the resulting complexes usually show ferromagnetic behavior [61-63], whereas

6

end-to-end coordination results in antiferromagnetic behavior [63,64].
Finally, in complexes with asymmetric end-to-end azide bridges the
interaction is either negligible [65] or weakly antiferromagnetic [66].
A small change in the coligands can lead to astonishing variation in the
structure and properties of the resulting complexes [67].

Inorganic azides have long enjoyed industrial usefulness as
detonators, generators of pure nitrogen gas in safety cushions (air bags)
and photographic materials [68]. The ability of the azide ions to act as
detonators or as effective generators of nitrogen gas has been found to
be a property of the polarization of the ordinarily symmetric azide
anion brought about by complexation with a metal ion.

Besides, azide is also used as a ligand to study the interaction
between small molecules and metal centres of metalloenzymes [69-71].
Since the azide group is bioactive [72] and the azide ion inhibits
photosynthetic phosphorylation [73], phosphate transfer [74] and
endogenous respiration [75], the complexes which contain azide as the
ligand show some interesting behaviour.

The azide ion, being very reactive, acts as an inhibitor in various
biological systems by blocking the substrate binding sites [68]. In
manganese biosystems, the azide ion is known to inihibit the
superoxide dismutation in mononuclear superoxide dismutases *via*
binding to the metal at the active site in both the Mn(II) and Mn(III)
oxidation states [76]. The function of dinuclear active sites in Mn
catalases, which catalyze the conversion of toxic peroxide to oxygen

and water in certain bacteria, is also dramatically inhibited by azide [77-83].

The study of the transition metal complexes with Schiff bases and azide anion becomes interesting in view of all the above observations.

1.3.2 The thiocyanate anion

The ambidentate character of thiocyanate and its bidentate function give rise to a wide variety of coordination geometries [84,85]. The pseudohalide NCS^- is known to coordinate to metals in both terminal and bridging modes [13].

As a bridging ligand, the thiocyanate can link a pair of metal centers in either an end-on (1,1'-SCN, 1,1'-NCS) or end-to-end (1,3'-SCN) configuration. The thiocyanate anion may link a third or even fourth metal atom giving rise to a 1,1,3'-SCN or 1,1,1,3'-SCN mode (Fig. 1.2).

The coordination through the soft base S of the thiocyanate ion appears to be common with second and third transition series metal ions of soft acid character. Owing to the two different donor groups (N and S) within it, the thiocyanate has less versatility and is less efficient as a transmitter of magnetic interactions than the azide. Thiocyanate complexes of various dimensionalities have been obtained [86,87]. The chemistry and bonding properties of transition metal-thiocyanate complexes have been the subject of several reviews [88].

M—N—C—S—M   N—C—S$<^M_M$ S—C—N$<^M_M$

1,3-μ-NCS   1,1-μ-SCN   1,1-μ-NCS

M—N—C—S$<^M_M$ M—N—C—S$\diagup^M_{\diagdown M}^M$

1,1,3-μ-SCN   1,1,1,3-μ-SCN
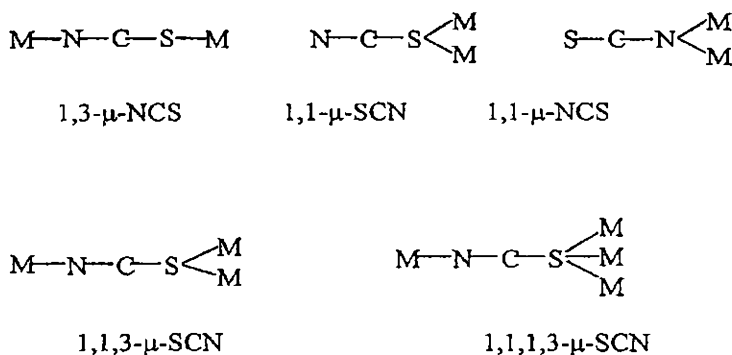
Fig.1.2. Possible coordination modes of thiocyanate anion.

Thiocyanate metal-coordination complexes have received special attention because they exhibit interesting electrochemical, magnetic, and photomagnetic properties [89,90]. In this regard, a great variety of thiocyanate-bridged extended networks have been prepared [90-95], in which thiocyanate ligands act as linkers between metals centers.

Thiocyanate plays a diverse role in the structural chemistry and the kinetics of the reactions [96]. It is interesting that thiocyanates have been found in human biofluids, saliva and cerebrospinal fluid and recently it was established that psychological stress induces them in oral cavities [97,98].

1.4 Objectives of the present work

The chemical properties of Schiff bases and their complexes are widely explored in recent years owing to their coordinative capability, their pharmacological activity, their catalytic activity and their use in bioinorganic chemistry. Also, the pseudohalides like azide and thiocyanate complexes have been widely investigated because of their capability to form a wide variety of structures. The pseudohalides are

also observed to act as inhibitors for many enzymes and proteins. This prompted us to investigate the transition metal complexes of Schiff bases, utilizing these pseudohalides as the coligands. It is observed that even a small change in the secondary ligand used can cause astonishing variation in the properties of metal-pseudohalide complexes. With this in mind, we synthesized seven Schiff bases and used the Schiff bases to synthesize copper(II), manganese(II), nickel(II), cobalt(II/III) and cadmium(II) complexes having azide/thiocyanate. The metal complexes were characterized by various spectroscopic techniques and by crystallographic studies. Magnetic studies were also conducted.

1.5　Physical measurements

Elemental analyses were carried out on a Vario EL III elemental analyzer at Sophisticated Analytical Instruments Facility, CUSAT, Kochi. The magnetic susceptibility measurements were done in the polycrystalline state at room temperature on a PAR model 155 Vibrating Sample Magnetometer at 5 k Oersted field strength at Indian Institute of Technology, Roorkee. IR spectra were recorded on a Thermo Nicolet AVATAR 370 DTGS FT-IR spectrophotometer instrument using KBr pellets, in 4000-400 cm^{-1} region at SAIF, CUSAT, Kochi. Electronic spectra were recorded on a Spectro UV-VIS Double Beam UVD-3500 spectrophotometer in the 200-900 nm range. NMR spectra were recorded using Bruker AMX 400 FT-NMR Spectrometer using TMS as the internal standard at Sophisticated Instruments Facility, Indian Institute of Science, Bangalore. EPR spectral measurements were carried out on a Varian E-112

X-band spectrometer using TCNE as standard at the SAIF, Indian Institute of Technology, Mumbai.

References

[1]   J.E. Huheey, E.A. Keiter, R.L. Keiter, Inorganic Chemistry, Principles of Structure and Reactivity, 4th ed., Harper Collins College Publishers, New York (1993).

[2]   H. Schiff, Ann. Suppl. 3 (1864) 343.

[3]   K.N. Campbell, H. Sommers, B.K. Campbell, J. Am. Chem. Soc. 66 (1944) 82.

[4]   J. Hine, C.Y. Yeh, J. Am. Chem. Soc. 89 (1967) 2669.

[5]   H. Tazoki, K. Miyano, J. Chem. Soc. (1959) 9769.

[6]   C.M. Brewster, J. Am. Chem. Soc. 46 (1924) 2463.

[7]   T.P. Yoon, E.N. Jacobsen, Science 299 (2003) 1691.

[8]   A.D. Garnovskii, A.L. Nivorozhkin, V.I. Minkin, Coord. Chem. Rev. 126 (1993) 1.

[9]   V. Alexander, Chem. Rev. 95 (1995) 273.

[10]   T.K. Karmakar, S.K. Chandra, J. Ribas, G. Mostafa, T.-H. Lu, B.K. Ghosh, Chem. Commun. (2002) 2364.

[11]   P. Bamfield, R. Price, R.G.J. Miller, J. Chem. Soc. A (1962) 1447.

[12]   R. Paschke, S. Liebsch, C. Tschierske, M.A. Oakley, E. Sinn, Inorg. Chem. 42 (2003) 8230.

[13]   H. Zhang, X. Wang, K. Zhang, B.K. Teo, Coord. Chem. Rev. 183 (1999) 157.

[14]   A. Mondal, G. Mostafa, A. Ghosh, I.R. Laskar, N.R. Chaudhuri, J. Chem. Soc., Dalton Trans. (1999) 9.

[15]   N. Mondal, M.K. Saha, S. Mitra, V. Gramlich, J. Chem. Soc., Dalton Trans. (2000) 3218.

[16] J.M. Clemente-Juan, B. Chansou, B. Donnadieu, J.-P. Tuchagues, Inorg. Chem. 39 (2000) 5515.

[17] M.K. Saha, D.K. Dey, B. Samanta, A.J. Edwards, W. Clegg, S. Mitra, J. Chem. Soc., Dalton Trans. (2003) 488.

[18] E.-Q. Gao, S.-Q Bai, Y.-F. Yue, Z.-M. Wang, C.-H. Yan, Inorg. Chem. 42 (2003) 3642.

[19] C. Janiak, Angew. Chem. Int. Ed. 36 (1997) 1431.

[20] S.L. James, Chem. Soc. Rev. 32 (1997) 276.

[21] J. Costamagna, J. Vargas, R. Latorre, A. Alvarado, G. Mena, Coord. Chem. Rev. 119 (1992) 67.

[22] S.C. Bhatia, J.M. Bindlish, A.R. Saini, P.C. Jain, J. Chem. Soc., Dalton Trans. (1981) 1773.

[23] M.H. Chisholm, J.C. Gallucci, H. Zhen, J.C. Huffman, Inorg. Chem. 40 (2001) 5051.

[24] D.M. Epstein, S. Choudhary, M.R. Churchill, K.M. Keil, A.V. Eliseev, J.R. Morrow, Inorg. Chem. 40 (2001) 1591.

[25] S. Yamada, Coord. Chem. Rev. 190–192 (1999) 537.

[26] R.T. Ruck, E.N. Jacobsen, J. Am. Chem. Soc. 124 (2002) 2882.

[27] H.-J. Kim, W. Kim, A.J. Lough, B.M. Kim, J. Chin, J. Am. Chem. Soc. 127 (2005) 16776.

[28] R. Paschke, S. Liebsch, C. Tschierske, M.A. Oakley, E. Sinn, Inorg. Chem. 42 (2003) 8230.

[29] H.-L. Zhu, S.-Y. Li, Z.-D. Wang, F. Yang, J. Chem. Cryst. 34 (2004) 203.

[30] X.-B. Wan, C.-M. Jin, Z.-W. Shi, G.-Y. Lu, J. Chem. Cryst. 34 (2004) 57.

[31] M.M.T. Khan, S. Shukla, J. Shark, J. Mol. Catal. 57 (1990) 301.

[32] D.E. Fenton, Chem. Soc. Rev. 28 (1999) 159.

[33] M. Suzuki, T. Ishikawa, A. Harada, S. Ohba, M. Sakamoto, Y. Nishida, Polyhedron 16 (1997) 2553.

[34] J. Du Bois, J. Hong, E.M. Carreira, M.W. Day, J. Am. Chem. Soc. 118 (1996) 915.

[35] N.S. Finney, P.J. Pospisil, E.N. Jacobsen, Angew. Chem. Int. Ed. Engl. 36 (1997) 1720.

[36] C. Linde, M. Arnold, Angew. Chem. Int. Ed. Engl. 36 (1997) 1723.

[37] L. Canali, D.C. Sherrington, Chem. Soc. Rev. 28 (1999) 85.

[38] S. Shah, R. Vyas, R.H. Mehta, J. Indian Chem. Soc. 69 (1992) 590.

[39] N. Raman, A. Kulandaisamy, A. Shunmugasundaram, K. Jeyasubramaniam, Trans. Met. Chem. 26 (2001) 131.

[40] K. Sahu, R.K. Behera, R.C. Pathaik, A. Nayak, G.B. Behera, Indian J. Chem. 18B (1979) 557.

[41] M. Abdul-Gawad, Y.M. Issa, S.M. Abd-Alhamid, Egypt J. Pharm. Sci. 34 (1993) 219.

[42] S.K. Chakraborti, B. Kumar De, J. Indian Chem. Soc. LP (1973) 137.

[43] S. Rao, A.S. Mittra, J. Indian Chem. Soc. LV (1978) 420.

[44] S.A. Khan, A.A. Siddiqui, S. Bhatt, Asian J. Chem. 14 (2002) 1117.

[45] E. Kimura, R. Machida, M. Kochima, J. Am. Chem. Soc. 106 (1984) 5497.

[46] J.W. Pyrz, A.I. Roe, L.J. Stern, J.R. Que, J. Am. Chem. Soc. 107 (1985) 614.

[47] M. Tumer, B. Erdogan, H. Koksal, S. Serin, M.Y. Nutku, Synth. React. Inorg. Met. Org. Chem. 28 (1998) 529.

[48] W. Zishen, L. Zhiping, Y. Zhenhuan, Trans. Met. Chem. 18 (1993) 291.

[49] J. Chakraborty, R.N. Patel, J. Ind. Chem. Soc. 73 (1996) 191.

[50] R. Klement, F. Stock, H. Elias, H. Paulus, P. Pelikan, M. Valko, M. Muzur, Polyhedron 18 (1999) 3617.

[51] A. Ducruix, R. Giegé, Crystallization of proteins and nucleic acids, IRL /Oxford Press (1992).

[52] A. Escuer, R. Vicente, M.A.S. Goher, F.A. Mautner, M.A.M. Abu-Youssef, Chem. Commun. (2002) 64.

[53] C.S. Hong, J. Koo, S.K. Son, Y.S. Lee, Y.S. Kim, Y. Do, Chem. Eur. J. 7 (2001) 4243.

[54] M.A.S. Goher, J. Cano, Y. Journaux, M.A.M. Abu-Youssef, F.A. Mautner, A. Escuer, R. Vicente, Chem. Eur. J. 6 (2000) 778.

[55] A.H. Fu, X.Y. Huang, J. Li, T. Yuen, C.L. Lin, Chem. Eur. J. 8 (2002) 2239.

[56] M.H.W. Lam, Y.Y. Tang, K.M. Fung, X.Z. You, W.T. Wong, Chem. Commun. (1997) 957.

[57] A. Escuer, R. Vicente, M.S. El Fallah, M.A.S. Goher, F.A. Mautner, Inorg. Chem. 37 (1998) 4466.

[58] A. Escuer, R. Vicente, M.A.S. Goher, F.A. Mautner, Inorg. Chem. 35 (1996) 6386.

[59] M.A.S. Goher, F.A. Mautner, J. Chem. Soc., Dalton Trans. (1999) 1535.

[60] A. Escuer, M. Font-Bardia, E. Peñalba, X. Solans, R. Vicente, Polyhedron 18 (1998) 211.

[61] S. Sikorav, I. Bkouche-Waksman, O. Kahn, Inorg. Chem. 23 (1984) 490.

[62] R. Cortés. J.L. Pizarro, L. Lezama, M.I. Arriortua, T. Rojo, Inorg. Chem. 33 (1994) 2697.

[63] E. Ruiz, J. Cano, S. Alvarez, P. Alemany, J. Am. Chem. Soc. 120 (1998) 11122.

[64] Y. Agnus, R. Louis, R. Weiss, J. Am. Chem. Soc. 101 (1979) 3381.

[65] J. Comardmon, P. Plumeré, J.M. Lehn, Y. Agnus, R. Louis, R. Weiss, O. Kahn, I. Morgenstern-Badarau, J. Am. Chem. Soc. 104 (1982) 6330.

[66]   T.R. Felthouse, D.N. Hendrickson, Inorg. Chem. 17 (1978) 444.

[67]   J. Ribas, A. Escuer, M. Monfort, R. Vicente, R. Cortés, L. Lezama, T. Rojo. Coord. Chem. Rev. 193–195 (1999) 1027.

[68]   H.D. Fair, R.F. Walker (eds), Energetic Materials, Plenum Press, New York 1-2 (1977).

[69]   M.M. Whittaker, J.W. Whittaker, Biophys. J. 64 (1993) 762.

[70]   M.M. Whittaker, V.L.Devito, S.A. Asher, J.W. Whittaker, J. Biol. Chem. 264 (1989) 7104.

[71]   F. Tuczek, E.I. Solomon, Inorg. Chem. 32 (1993) 2850.

[72]   R.W.F. Hardy, R.C. Burns, Ann. Rev. Biochem. 2 (1968) 332.

[73]   J.S.C. Wessels, Biochim. Biophys. Acta 29 (1958) 113.

[74]   W.O. James, Ann. Rev. Plant Physiol. 4 (1953) 59.

[75]   G.C. Wabster, A.W. Frenkel, Plant Physiol. 28 (1953) 63.

[76]   J.W. Whittaker, M.M. Whittaker, J. Am. Chem. Soc. 113 (1991) 5528.

[77]   Y. Kono, I. Fridovich, J. Bacteriol. 155 (1983) 742.

[78]   Y. Kono, I. Fridovich, J. Biol. Chem. 258 (1983) 6015.

[79]   W.F. Beyer Jr., I. Fridovich, Biochemistry 24 (1985) 6460.

[80]   R.M. Fronko, J.E. Penner-Hahn, C.J. Bender, J. Am. Chem. Soc. 110 (1988) 7554.

[81]   G.S. Waldo, R.M. Fronko, J.E. Penner-Hahn, Biochemistry 30 (1991) 10486.

[82]   G.S. Waldo, S. Yu, J.E. Penner-Hahn, J. Am. Chem. Soc. 114 (1992) 5869.

[83]   S.V. Khangulov, V.V. Barynin, S.V. Antonyuk-Barynina, Biochim. Biophys. Acta 102 (1990) 25.

[84]   S. Sailaja, K.R. Reddy, M.V. Rajasekharan, C. Hureau, E. Riviere, J. Cano, J.-J. Girerd, Inorg. Chem. 42 (2003) 180.

[85]   S.K. Dey, N. Mondal, M.S. El Fallah, R. Vicente, A. Escuer, X. Solans, M. Font-Bardia, T. Matsushita, V. Gramlich, S. Mitra, Inorg. Chem. 43 (2004) 2427.

[86]   W. Zhang, X. Wu, B. Wu, S. Yu, G. Santoni, D. Rehder, Inorg. Chem. 42 (2003). 1130.

[87]   B. Zurowska, J. Mrozinski, M. Julve, F. Lloret, A. Maslejova, W. Sawka-Dobrowolska, Inorg. Chem. 41 (2002) 1771.

[88]   J.L. Burmeister, Coord. Chem. Rev. 3 (1968) 225.

[89]   A. Rodriguez, H. Sakiyama, N. Masciocchi, Inorg. Chem. 44 (2005) 8399.

[90]   P. Kulkarni, S. Padhye, E. Sinn, Inorg. Chim. Acta 332 (2002) 167.

[91]   D.J. Chesnut, D. Plewak, J. Zubieta, J. Chem. Soc., Dalton Trans. (2001) 2567.

[92]   D.J. Chesnut, A. Kussnetzow, R. Birge, J. Zubieta, J. Chem. Soc., Dalton Trans. (2001) 2581.

[93]   D.J. Chesnut, A. Kussnetzow, R. Birge, J. Zubieta, Inorg. Chem. 38 (1999) 5484.

[94]   D.J. Chesnut, A. Kussnetzow, J. Zubieta, J. Chem. Soc., Dalton Trans. (1998) 4081.

[95]   D.J. Chesnut, J. Zubieta, Chem. Commun. (1998) 1707.

[96]   M. Amirnasr, K.J. Schenk, S. Meghdadi, Inorg. Chim. Acta 338 (2002) 19.

[97]   P.B. Paul, M.L. Smith, J. Anal. Toxicol. (2006) 511.

[98]   M. Rosin, T. Kocher, A. Kramer, J. Clin. Periodontol. 28 (2001) 270.

❋❋❋ℰℭ❋❋❋

Syntheses of bidentate Schiff base ligands - Characterisation of the ligand derived from 2-hydroxy-4-methoxybenzaldehyde and aniline

2.1 Introduction

The condensation of primary amines with carbonyl compounds yields Schiff bases that are regarded as one of the most potential group of chelators for the facile preparations of metallo-organic hybrid materials [1]. The exceptional qualities of Schiff bases such as facile syntheses, easily tunable steric, electronic properties and good solubility in common solvents have led to their extensive study [2]. In the past two decades, the synthesis, structure and properties of Schiff base complexes have stimulated much interest for their noteworthy contributions in the development of single molecule magnets, material science [3,4], catalysis of many reactions like carbonylation, hydroformylation, reduction, oxidation, epoxidation, hydrolysis etc [5-10]. This is due to the fact that Schiff bases offer opportunities for inducing substrate chirality, tuning the metal centered electronic factor, enhancing the solubility and stability of either homogeneous or heterogeneous catalysts. The flexibility of disposition of different donor sites is the secret behind their successful performance in mimicking peculiar geometries around the metal centers, leading to very interesting spectroscopic properties with varied magnetic activities [11]. Schiff bases also display biological

activity and play an important role in biological systems [12-16]. Moreover, Schiff bases are found to have wide applications as antibacterial, antiviral and antifungal agents [17].

Transition metal complexes containing pseudohalogens like azide or thiocyanate ions have been extensively investigated due to their excellent magnetic properties [18]. The use of Schiff bases as auxiliary ligands in such metal-pseudohalogen complexes lead to interesting results [19-27]. This is because even a very small change in the coligands can lead to astonishing variation in the structure and magnetism of the resulting complexes. The stereochemical properties of the coligands certainly influence the structural diversity of the metal complexes [26]. The metal-pseudohalogeno complexes containing Schiff base coligands are not as extensively investigated as the complexes without Schiff bases.

In view of the above observations, the following seven Schiff base ligands were prepared by varying the aldehyde and the amine.

    a.   Pyridine-2-carbaldehyde-aniline (paa)

    b.   Pyridine-2-carbaldehyde-1-phenylethylamine (papea)

    c.   Pyridine-2-carbaldehyde-2-aminopyrimidine (paap)

    d.   2-Benzoylpyridine-aniline (bzpa)

    e.   Di-2-pyridyl ketone-aniline (dpka)

    f.   Quinoline-2-carbaldehyde-aniline(qaa)

    g.   2-Hydroxy-4-methoxybenzaldehyde-aniline (Hhmba)

18

The structures of the seven ligand systems are shown below (Fig. 2.1).

paa

papea

paap

bzpa

dpka

qaa

Hhmba
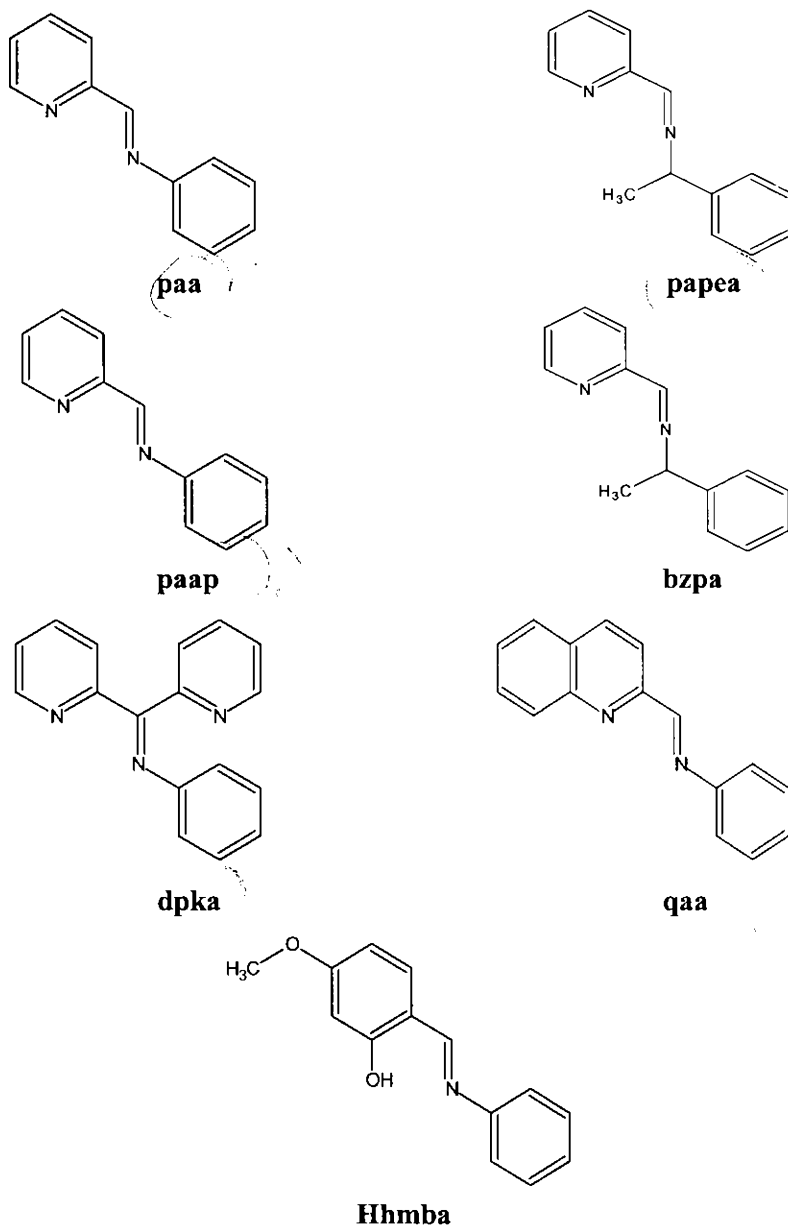
Fig. 2.1. Structures of the ligands.

The ligands paa, papea, bzpa and qaa are neutral bidentate *N, N* donor ligands. The ligands paap and dpka are also neutral ligands, but they have additional N donors, which may or may not be coordinated. If all the N atoms of these ligands coordinate to the same metal centre, paap and dpka becomes quadridentate and terdentate respectively. The involvement of the additional N atoms in coordination to the same metal is less probable because of their spatial disposition and the distance from the metal centre. The possibility of the formation of a bridged complex, utilizing these additional coordination sites, cannot however be neglected. The ligand Hhmba is monoprotic bidentate *N, O* ligand, which usually coordinates to the metal through deprotonation.

2.2 Experimental
2.2.1 Materials

Pyridine-2-carbaldehyde (Sigma Aldrich), 2-benzoylpyridine (Sigma Aldrich), di-2-pyridyl ketone (Sigma Aldrich), quinoline-2-carbaldehyde (Sigma Aldrich), 2-hydroxy-4-methoxybenzaldehyde (Sigma Aldrich), aniline (S. D. Fine), *R*-1-phenylethyl amine (Alfa Aeser), 2-aminopyrimidine (Sigma Aldrich) and methanol (Merck) were used as received.

2.2.2 Syntheses of ligands

Equimolar ratios of corresponding carbonyl compound and the amine were refluxed in a suitable solvent to obtain the ligand. Minor changes required in the case of each ligand, such as time required for the reaction, the use of catalysts etc were incorporated accordingly. The general scheme of the reaction (Scheme 2.1) is given below.

20
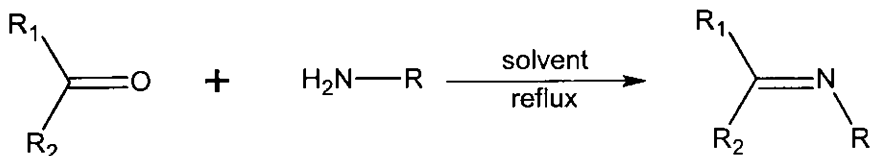
Scheme 2.1

paa: A mixture of pyridine-2-carbaldehyde (0.107 g, 1 mmol) in methanol and aniline (0.093 g, 1 mmol) in methanol was refluxed for 2 hours. The resulting yellow solution of the ligand after reflux was used directly for the synthesis of the complexes without further purification.
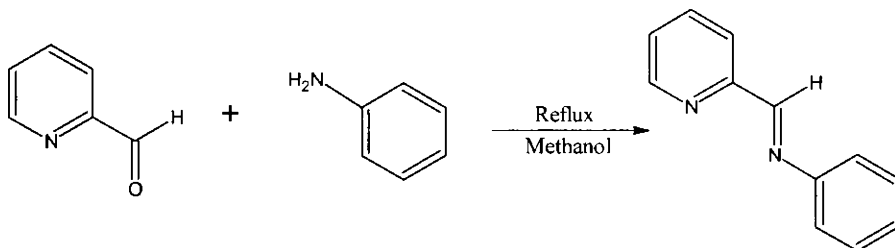
Scheme 2.2

papea: Pyridine-2-carbaldehyde (0.107 g, 1mmol) and R-1-phenylethyl amine (0.121 g, 1 mmol) was refluxed in methanol for 2 hours. The yellow solution of the ligand obtained was directly used for the synthesis of the complexes without further purification.

Scheme 2.3

21
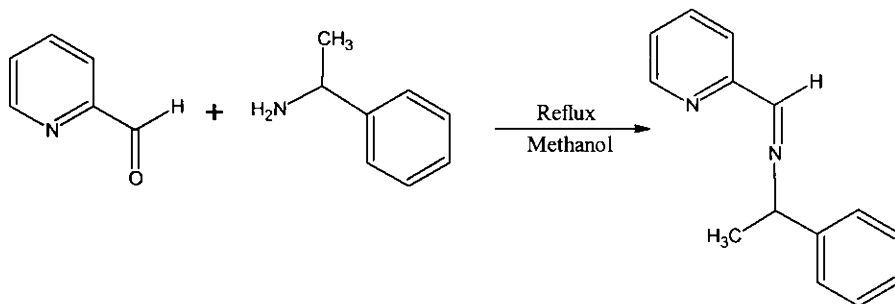
paap:A mixture of pyridine-2-carbaldehyde (0.107 g, 1 mmol) and 2-aminopyrimidine (0.094 g, 1 mmol) in methanol was refluxed for 2 hours. The deep yellow solution of the ligand obtained was directly used for the synthesis of the complexes without further purification.
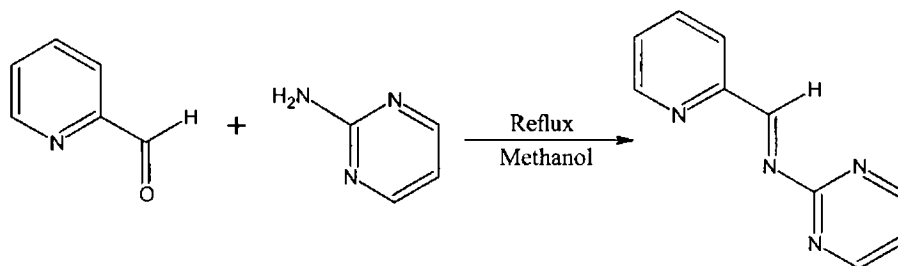
Scheme 2.4

bzpa: 2-Benzoylpyridine (0.183 g, 1 mmol) was dissolved in methanol and to this aniline (0.093 g, 1 mmol) was added. The mixture was refluxed for 6 hours. The yellow solution of the ligand obtained was used directly for the synthesis of the complexes without further purification.
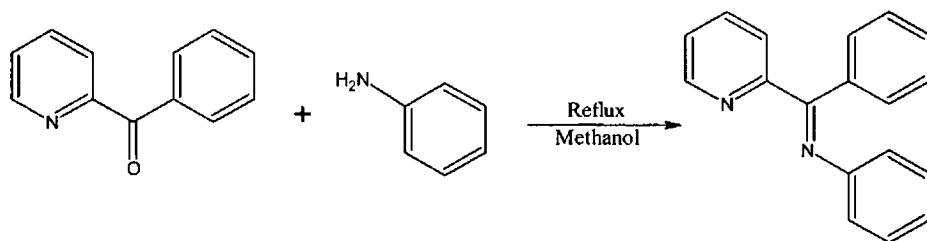
Scheme 2.5

dpka: Di-2-pyridyl ketone (0.187 g, 1 mmol) was dissolved in methanol. Aniline (0.093 g, 1 mmol) was added to this. About 4-5 drops of glacial acetic acid was also added and refluxed for 6 hours. The brownish-yellow solution of the ligand obtained after reflux was used directly without any further purification.
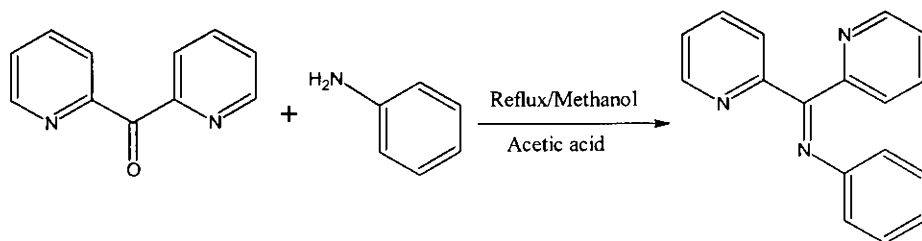
Scheme 2.6

qaa: Quinoline-2-carbaldehyde (0.157 g, 1 mmol) was dissolved in methanol. Aniline (0.093 g, 1 mmol) was added to this. A few drops of glacial acetic acid was also added and refluxed for 4 hours. The deep yellow solution of the ligand obtained after reflux was used directly without any further purification.
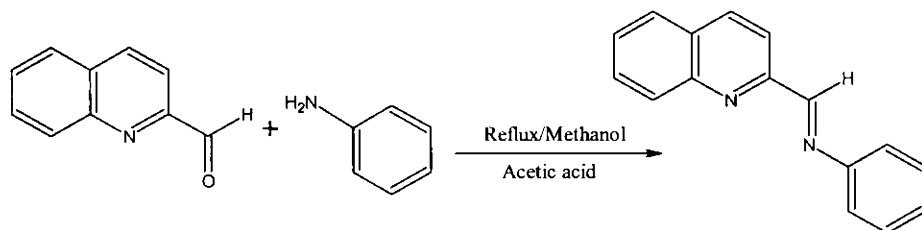
Scheme 2.7

Hhmba: 2-Hydroxy-4-methoxybenzaldehyde (0.152 g, 1 mmol) was dissolved in methanol. To this aniline (0.093 g, 1 mmol) was added. The mixture was refluxed for 2 hours. The yellow product obtained on the evaporation of the solvent was filtered, washed with methanol and dried over P_4O_{10} _in vacuo._ The product was recrystallized from methanol. Elemental Anal. Found (Calcd.) (%): C, 73.52 (73.99); H, 6.49 (5.77); N, 6.10 (6.16).
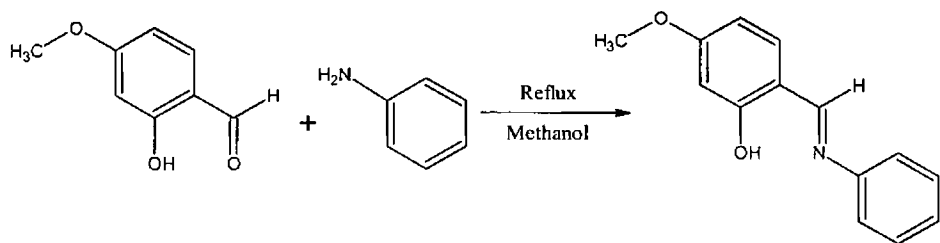
Scheme 2.8

2.3 Results and discussion

The ligands were prepared in methanol by the direct refluxing of the respective aldehydes or ketones with the corresponding amines. Except Hhmba, all other ligands were obtained as yellow oils and could not be isolated in the solid form even after repeated trials. These compounds were thus used directly for the synthesis of the complexes without further purification. Even though Hhmba could be isolated in the solid form, the yield was very low. So the method similar to that employed for the for the syntheses of complexes of other ligands was used in the case of the complexes of Hhmba also.

2.3.1 Characterisation of the ligand Hhmba

2.3.1a *Electronic spectrum*

The electronic spectrum of the ligand Hhmba in acetonitrile solution (10^{-6} M) (Fig. 2.2) shows a band at 334 nm, which corresponds to the $n \rightarrow \pi^*$ transition of the azomethine chromophore. The band observed at 291 nm is assigned to the $\pi \rightarrow \pi^*$ transitions in the azomethine group and the phenyl ring of the ligand. The band due to $n \rightarrow \pi^*$ transition is of greater intensity when compared to that of the $\pi \rightarrow \pi^*$ transition [28].
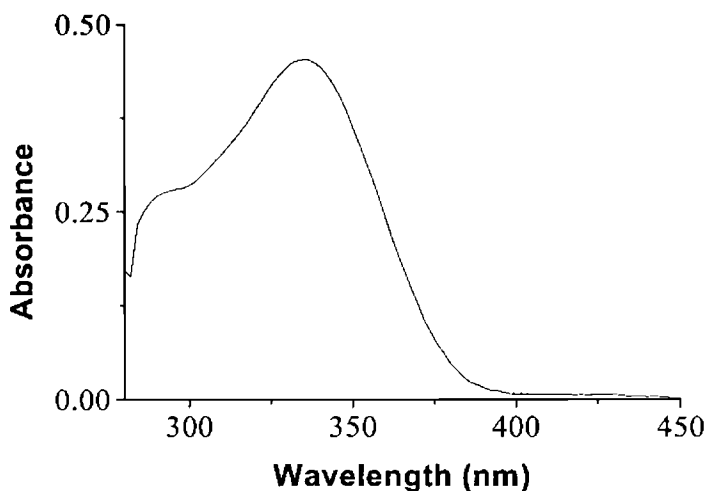
Fig. 2.2. Electronic spectrum of ligand Hhmba in acetonitrile.

2.3.1b *Infrared spectrum*

IR spectroscopy is a useful tool to confirm the coordination of various atoms and groups to the metal atom from the positions and natures of the bands associated with them.

The IR spectra of all compounds were recorded in the 4000-400 cm^{-1} range using KBr pellet. IR spectral analysis (Fig. 2.3) confirms the presence of characteristic groups present in the compound. A broad band at 3440 cm^{-1} is assigned to the ν(O–H) stretching of the phenolic –OH group [28]. The broadness of the band is probably due to intramolecular hydrogen bonding existing in the compound. The strong band at 1614 cm^{-1} can be attributed to the ν(C=N) stretching mode of the azomethine function of the ligand. The ν(C=C) stretching vibrations of the phenyl ring appear as a strong band at 1565 cm^{-1} and the ν(C–O) band is observed as a strong band at 1287 cm^{-1}. Aromatic

25

C–H stretching bands occur at 2940 cm^{-1}. The ν(C–C) stretching vibrations within the phenyl ring occurs at 1486 cm^{-1}.
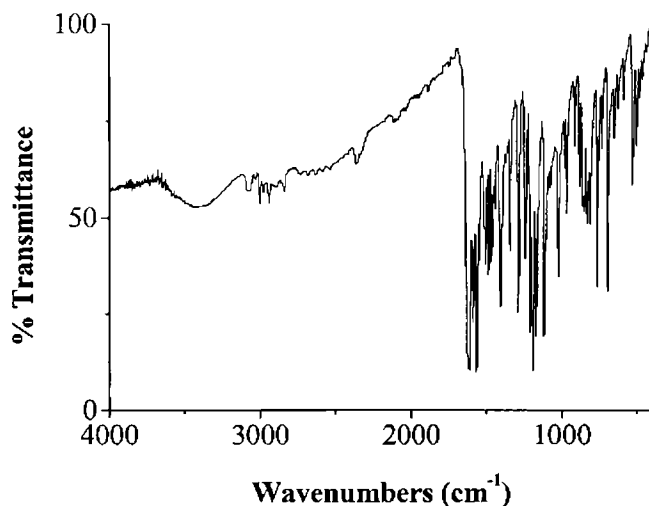
Fig. 2.3. IR spectrum of ligand Hhmba.

2.3.1c *^1H NMR spectral studies*

The ^{1}H NMR spectrum of the ligand Hhmba is represented in Fig. 2.4. The ^{1}H resonance of the −OH group of the ligand is the most downfield one in the NMR spectrum and is observed as a singlet at 11.49 ppm. Such a downfield shift is attributed to the intramolecular hydrogen bonding [29]. The singlet appearing at 9.72 ppm is due to the single proton of the azomethine moiety, H−C=N [30,31]. The protons of the aromatic rings are obtained in the region 6-8 ppm, slight variations are observed as a result of the difference in the environments. The C5−H and C6−H resonate near 6.50 ppm as doublets by coupling with each other. C3−H occurs as a singlet at 6.80 ppm. The higher δ value for this proton is explained by its position between the −OH group and the methoxy

group in the benzene ring. The methoxy protons appear as a singlet at 3.85 ppm. The singlet appearing at 8.58 ppm is assigned to the resonance of the C12–H proton. Such a low- field value is due to its position para to the N atom of the azomethine group. All other aromatic protons resonate at 7.20-7.50 ppm and is observed as a complex multiplet due to spin-spin coupling.
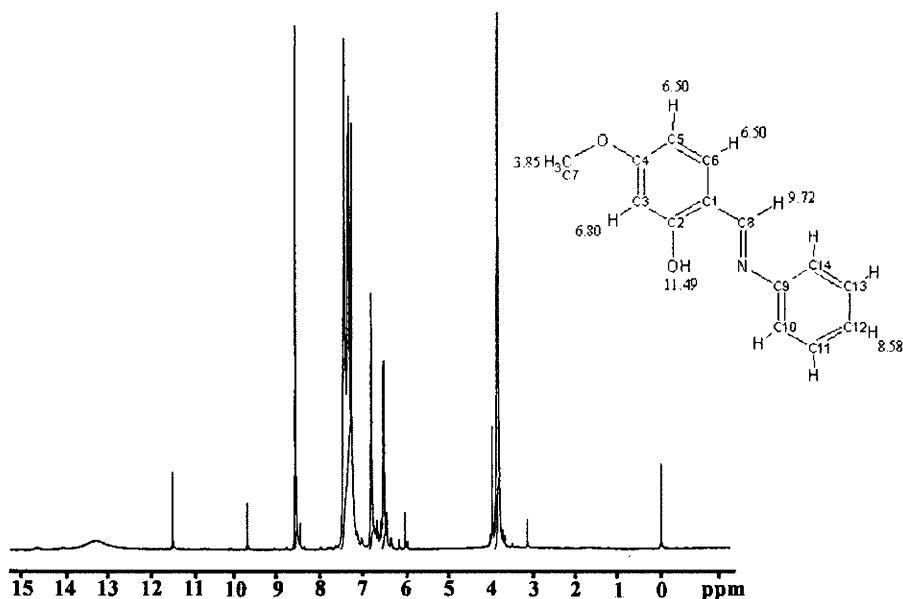
Fig. 2.4. ^{1}H NMR spectrum of ligand Hhmba.

References

[1]   U. Casellato, P.A. Vigato, Coord. Chem. Rev. 23 (1977) 31.

[2]   Q. Shi, L. Xu, J. Ji, Y. Li, R. Wang, Z. Zhou, R. Cao, M. Hong, A.S.C. Chan, Inorg. Chem. Commun. 7 (2004) 1254.

[3]   I. Ramade, O. Kahn, Y. Jeannin, F. Robert, Inorg. Chem. 36 (1977) 930.

[4]   H. Miyasaka, H. Ieda, N. Matsumoto, R. Crescenzi, C. Floriani, Inorg. Chem. 37 (1998) 255.

[5]   M.M.T. Khan, S. Shukla, J. Shark, J. Mol. Catal. 57 (1990) 301.

[6]   E. Fujita, B.S. Brunschwig, T. Ogata, S. Yanagida, Coord. Chem. Rev. 132 (1994) 195.

[7]   E. Kimura, S. Wada, M. Shiyonoya, Y. Okazaki, Inorg. Chem. 33 (1994) 770.

[8]   B. De Clercq, F. Verpoort, Macromolecules 35 (2002) 8943.

[9]   T. Opstal, F. Verpoort, Angew. Chem. Int. Ed. 42 (2003) 2876.

[10]   B. De Clercq, F. Lefebvre, F. Verpoort, Appl. Catal. A 247 (2003) 345.

[11]   D.E. Fenton, Chem. Soc. Rev. 28 (1999) 159.

[12]   V. Razakantoanina, P.P. Nguyen Kim, G. Jaureguiberry, Parasitol Res. 86 (2000) 665.

[13]   R.E. Royer, L.M. Deck, T.J.V. Jagt, F.J. Martinez, R.G. Mills, S. Young, A.D.L.V. Jagt, J. Med. Chem. 38 (1995) 2427.

[14]   M.R. Flack, R.G. Pyle, N. Mullen, M.B. Lorenzo, Y.W. Wu, R.A. Knazek, B.C. Nusule, M.M. Reidenberg, J. Clin. Endocrinol. Metab. 76 (1993) 1019.

[15]   R. Baumgrass, M. Weiwad, F. Edmann, J. Biol. Chem. 276 (2001) 47914.

[16]   P.J.E. Quintana, A. Peyster de, S. Klatzke, H. Park, J. Toxicol Lett. 117 (2000) 85.

[17]   S. Chandra, X. Sangeetika, Spectrochim. Acta A60 (2004) 147.

[18]   K. Vrieze, G. van Koten, Comprehensive Coordination Chemistry, G. Wilkinson, R.D. Gillard, J.A. McCleverty (Eds.), Pergamon Press : Oxford, England 2 (1987) 225.

[19]   P.S. Mukherjee, T.K. Maji, A. Escuer, R. Vicente, J. Ribas, G. Rosair, F.A. Mautner, N.R. Chaudhuri, Eur. J. Inorg. Chem. (2002) 943.

[20]   S. Deoghoria, S. Sain, B. Moulton, M.J. Zaworotko, S.K. Bera, S.K. Chandra, Polyhedron 21 (2002) 2457.

[21]   E.-Q. Gao, S.-Q. Bai, Y.-F. Yue, Z.-M. Wang, C.-H. Yan, Inorg. Chem. 42 (2003) 3642.

[22]   M.S. Ray, A. Ghosh, S. Chaudhuri, M.G.B. Drew, J. Ribas, Eur. J. Inorg. Chem. (2004) 3110.

[23]   C.-L. Yuan, Synth. React. Inorg. Met.-Org. Nano-Met. Chem. 37 (2007) 567.

[24]   E.-Q. Gao, Y.-F. Yue, S.-Q. Bai, Z. He, C.-H. Yan, Cryst. Growth Design 5 (2005) 1119.

[25]   H.-R. Wen, C.-F. Wang, Y. Song, J.-L. Zuo, X.-Z. You, Inorg. Chem. 44 (2005) 9039.

[26]   C. Adhikary, D. Mal, K.-I. Okamoto, S. Chaudhuri, S. Koner, Polyhedron 25 (2006) 2191.

[27]   S. Chattopadhyay, M.S. Ray, M.G.B. Drew, A. Figuerola, C. Diaz, A. Ghosh, Polyhedron 25 (2006) 2241.

[28]   R.M. Silverstein, G.C. Bassler, T.C. Morrill, Spectrometric Identification of Organic Compounds, 4th Ed., Wiley, New York (1981).

[29]   L. Lindoy, W.E. Moody, D. Taylor, Inorg. Chem. 16 (1977) 1962.

[30]   V.G. Gnanasoundari, K. Natarajan, Trans. Met. Chem. 29 (2004) 511.

[31]   M. Tümer, H. Köksal, M.K. Sener, S. Serin, Trans. Met. Chem. 24 (1999) 414.

❀❀❀ℰℭ❀❀❀

Syntheses, structural and spectral investigations of copper(II) complexes of Schiff bases with azide and thiocyanate

3.1 Introduction

Copper is a bioelement and an active site in several metalloenzymes and proteins [1-4]. Copper ions are found in the active sites of a large number of metalloproteins such as hemocyanin, tyrosinase, cytochrome c oxidase, laccase and ascorbate oxidase. These proteins are involved in various biological processes such as biological electron-transfer reaction, oxygen atom insertion into substrates, dioxygen reduction to hydrogen peroxide or water and hydrolytic reactions. Often better structural and functional models to metalloproteins have been prepared by altering the substituents of the ligands in order to match with the required spectral properties of the metalloproteins. The most important contribution to copper chemistry must be the role that biological copper [5-8] has played in stimulating research in the inorganic chemistry of copper, not only in the chemistry of copper proteins, for which Cu(I), Cu(II) and Cu(III) species are relevant, but also in systems where more than one type of Cu is considered to be present. The blue copper proteins have received considerable interest because of their unusual spectral and structural properties. The geometry around copper in blue copper proteins is

intermediate between tetrahedral and square planar. Several model systems, including those with bidentate Schiff base ligands, have been reported correlating the molecular structure with the electronic ground state of those complexes [9-11] in redox reactions involving copper containing enzymes. This is an essential factor for many of the properties of these enzymes.

Among all the transition metal complexes, copper(II) Schiff base complexes with pseudohalogens are well known for their preparational accessibilities, exhibiting the flexibility of the coordination geometry around the metal center. Many metalloproteins are inhibited by the azide ion [14-18], and hence the metal-azido complexes of such proteins were studied extensively [19,20] in order to understand the electronic nature, geometrical properties as well as the role of the metal in the biological processes involving these metalloproteins. Azide-copper(II) complexes are also of great interest for bioinorganic chemists to explore the structure and role of active sites in copper proteins such as metazido hemocyanins and tyrosinases [21,22]. The chemistry of copper(II)-azido complexes has also received great deal of attention to enhance the fundamental knowledge about the magnetic interactions between the paramagnetic centers and for developing new functional molecule-based materials [23,24]. Examples of Cu(II)-azide systems with bidentate coligands are numerous and their structures are much diverse and sensitive to the coligands used. Hence a variety of mononuclear, binuclear and polymeric complexes have been obtained, not only due to the coordination diversity of the azide ion, but also due

to the coordination flexibility of the Cu(II) ion. Two one dimensional azido-bridged Cu(II) coordination polymers with bidentate Schiff bases obtained by the condensation of pyridine-2-carbaldehyde and aniline and p-chloroaniline respectively have been synthesized and studied. Both contains Cu(II) in a distorted square pyramidal geometry interlinked by single end-on azido bridges which mediate weak antiferromagnetic interactions [25]. Ferromagnetic interactions mediated through single end-to-end azide bridges in helical chains of chiral Cu(II) complexes, where a Schiff base obtained from pyridine-2-carbaldehyde and _R_ and _S_ forms of 1-phenylethyl amine is used as the auxiliary ligand have been reported [26].

Even though thiocyanate is not as good a mediator of magnetic exchange between metal centers as the azide ion, still many copper complexes have been reported with thiocyanate and Schiff bases having ferromagnetic as well as antiferromagnetic interactions. Also the thiocyanate-bridged metal-coordination complexes have received special attention because they exhibit interesting electrochemical, zeolitic, magnetic, and photomagnetic properties [27,28]. The tetranuclear copper(II) chain complexes designed using the dipyridylmethanediol ligand has been found to promote ferromagnetic coupling between the copper(II) centers, thus opening a new avenue for the synthesis of molecular magnets [29]. Serna _et al._ reported dimeric and polymeric Cu(II) complexes synthesized from the methylated di-2-pyridyl ketone and thiocyanate with the same empirical formula [30]. These compounds contain double (_N_, _S_)-thiocyanate bridges and single

end-to-end thiocyanate bridges respectively and are weakly antiferromagnetic as expected.

3.2 Stereochemistry

The Cu(II) ion with $3d^9$ outer electron configuration lacks cubic symmetry and hence yields distorted forms of the basic stereochemistries such as tetrahedral, square planar, square pyramidal and octahedral [31]. Coordination numbers of four, five and six predominate, but variations of each structure occur through bond length or bond angle distortions. The four coordinate complexes may be tetrahedral, square planar or a distorted mixture thereof, and the five coordinate complexes, square pyramidal, trigonal bipyramidal or a mixed version thereof. Jahn Teller effect plays a major role in deciding the distortion effect on stereochemistries of Cu(II) complexes. The typical distortion involved in octahedral geometry is elongated structures with the odd electron residing in the $d_{x^2-y^2}$ orbital resulting in four short Cu–L bonds and two *trans* long bonds, which are usually more energetically favourable than the compressed structures, consistent with their more frequent occurrence. In the six coordinate species, the structures vary from compressed tetragonal through regular octahedral to elongated tetragonal but also include examples where the bond angles are clearly not 90°.

3.3 Experimental

3.3.1 Materials

Pyridine-2-carbaldehyde (Sigma Aldrich), 2-benzoylpyridine (Sigma Aldrich), di-2-pyridyl ketone (Sigma Aldrich), quinoline-2-

carbaldehyde (Sigma Aldrich), 2-hydroxy-4-methoxybenzaldehyde (Sigma Aldrich), aniline (S. D. Fine), _R_-1-phenylethyl amine (Alfa Aeser), 2-aminopyrimidine (Sigma Aldrich), $Cu(ClO_4)_2 \cdot 6H_2O$ (Sigma Aldrich), $Cu(OAc)_2 \cdot H_2O$ (Qualigens), NaN_3 (Reidel-De Haen), KCNS (BDH) and methanol (Merck) were used as received.

3.3.2 Preparation of copper(II) complexes

$[Cu_2(paa)_2(N_3)_4] \cdot \frac{1}{2} H_2O$ (1): A mixture of pyridine-2-carbaldehyde (0.107 g, 1 mmol) in methanol and aniline (0.093 g, 1 mmol) in methanol were refluxed for 2 hours. To this $Cu(ClO_4)_2 \cdot 6H_2O$ (0.370 g, 1 mmol) dissolved in methanol and a methanolic solution of NaN_3 (0.130 g, 2 mmol) containing minimum amount of water was added with stirring. The resulting brown colored solution was stirred for half an hour. The brown precipitate obtained on stirring was filtered, washed with methanol followed by ether and dried over P_4O_{10} _in vacuo_. Elemental Anal. Found (Calcd.) (%): C, 43.30 (43.11); H, 3.17 (3.17); N, 33.12 (33.52). $\mu = 1.06$ B.M.

$[Cu_2(paa)_2(NCS)_4] \cdot H_2O$ (2): A mixture of pyridine-2-carbaldehyde (0.107 g, 1 mmol) in methanol and aniline (0.093 g, 1 mmol) in methanol was refluxed for 2 hours. $Cu(OAc)_2 \cdot H_2O$ (0.199 g, 1 mmol) dissolved in methanol was added to this followed by a methanolic solution of KCNS (0.194 g, 2 mmol) and refluxed for 4 hours. Brown solid, which separated out, was filtered, washed with methanol and ether and dried over P_4O_{10} _in vacuo_. Elemental Anal. Found (Calcd.) (%): C, 45.76 (45.33); H, 2.91 (2.99); N, 15.53 (15.10). $\mu = 1.27$ B.M.

35

[Cu$_2$(papea)$_2$(N$_3$)$_4$]·H$_2$O (3): Pyridine-2-carbaldehyde (0.107 g, 1 mmol) and *R*-1-phenylethyl amine (0.121 g, 1 mmol) was refluxed in methanol for 2 hours. A methanolic solution of Cu(OAc)$_2$·H$_2$O (0.199 g, 1 mmol) was added to this. To the green solution obtained, an aqueous solution of NaN$_3$ (0.130 g, 2 mmol) was added drop wise. The resulting mixture was stirred for 30 minutes and the green product separated out was filtered, washed with methanol followed by ether and dried over P$_4$O$_{10}$ *in vacuo*. Elemental Anal. Found (Calcd.) (%): C, 46.08 (45.83); H, 3.76 (4.12); N, 30.50 (30.54). $\mu = 1.10$ B.M.

([Cu(pyox)$_2$]·2H$_2$O)$_n$ (4): Pyridine-2-carbaldehyde (0.107 g, 1 mmol) and *R*-1-phenylethyl amine (0.121 g, 1 mmol) was refluxed in methanol for 2 hours. Cu(OAc)$_2$·H$_2$O (0.199 g, 1 mmol) dissolved in methanol was added followed by an aqueous solution of KCNS (0.194 g, 2 mmol) and refluxed for 3 hrs. Blue prismatic single crystals were obtained within a period of one week. The crystals were separated, washed with methanol followed by ether and dried over P$_4$O$_{10}$ *in vacuo*. Elemental Anal. Found (Calcd.) (%): C, 42.60 (42.42); H, 3.39 (3.56); N, 16.11 (16.49). $\mu = 1.55$ B.M.

[Cu$_2$(apm)$_2$(N$_3$)$_2$]·$\frac{1}{2}$CH$_3$OH·3H$_2$O (5): A mixture of pyridine-2-carbaldehyde (0.107 g, 1 mmol) in methanol and 2-aminopyrimidine (0.094 g, 1 mmol) in methanol was refluxed for 2 hours. To this, Cu(OAc)$_2$·H$_2$O (0.199 g, 1 mmol) dissolved in water was added followed by the slow addition of aqueous NaN$_3$ (0.130 g, 2 mmol) solution. The green solution obtained was stirred for 3 hours. The green product separated out was collected, washed with methanol

followed by ether and dried over P_4O_{10} _in vacuo_. Elemental Anal. Found (Calcd.) (%): C, 21.66 (21.75); H, 2.94 (3.44); N, 35.58 (35.81). $\mu = 0$ B.M.

[Cu₂(pa)₂(NCS)₄]·5CH₃OH (6): A mixture of pyridine-2-carbaldehyde (0.107 g, 1 mmol) in methanol and 2-aminopyrimidine (0.094 g, 1 mmol) in methanol was refluxed for 2 hours. $Cu(OAc)_2 \cdot H_2O$ (0.199 g, 1 mmol) dissolved in water added to this followed by the addition of an aqueous solution of KCNS (0.194 g, 2 mmol). The resulting green solution was refluxed for 2 hours. The green product separated out was filtered, washed with methanol followed by ether and dried over P_4O_{10} _in vacuo_. Elemental Anal. Found (Calcd.) (%): C, 34.26 (33.71); H, 2.95 (2.33); N, 14.38 (13.88). $\mu = 1.24$ B.M.

[Cu₂(bzpa)₂(N₃)₄]·H₂O (7): 2-Benzoylpyridine (0.183 g, 1 mmol) was dissolved in methanol and to this aniline (0.093 g, 1 mmol) was added. The mixture was refluxed for 6 hours. To the yellow solution thus obtained, a methanolic solution of $Cu(ClO_4)_2 \cdot 6H_2O$ (0.370 g, 1 mmol) was added slowly followed by an aqueous solution of NaN_3 (0.130 g, 2 mmol). The green solution obtained was stirred for 30 minutes. The dark green product which separated out within one week was filtered, washed with methanol and ether and dried over P_4O_{10} _in vacuo_. Elemental Anal. Found (Calcd.) (%): C, 51.54 (52.11); H, 3.60 (3.64); N, 26.36 (27.01). $\mu = 1.15$ B.M.

[Cu₂(dpk·OH·OCH₃)₂(N₃)₄]·CH₃OH·4H₂O (8): Di-2-pyridyl ketone (0.187 g, 1 mmol) was dissolved in methanol and aniline (0.093 g, 1 mmol)

was added to this. About 4-5 drops of glacial acetic acid was also added and refluxed for 6 hours. To this, $Cu(OAc)_2 \cdot H_2O$ (0.199 g, 1 mmol) dissolved in hot methanol was added followed by an aqueous solution of NaN_3 (0.130 g, 2 mmol) slowly with stirring. Stirring was continued for 6 hours. The green product formed was filtered, washed with methanol and ether and dried over P_4O_{10} *in vacuo*. Elemental Anal. Found (Calcd.) (%): C, 36.06 (36.10); H, 4.08 (4.36); N, 27.07 (26.94). $\mu = 0$ B.M.

[Cu(dpk·OCH₃)(NCS)₂]·2H₂O (9): Di-2-pyridyl ketone (0.187 g, 1 mmol) was dissolved in methanol and aniline (0.093 g, 1 mmol) was added to this. About 4-5 drops of glacial acetic acid was also added and refluxed for 6 hours. To this, an aqueous solution of $Cu(OAc)_2 \cdot H_2O$ (0.199 g, 1 mmol) and an aqueous solution of KCNS (0.194 g, 2 mmol) was added. The formation of a green product was spontaneous and the mixture was stirred for 3 hours in order for the completion of the reaction. The product was filtered, washed with methanol, water and ether and dried over P_4O_{10} *in vacuo*. Elemental Anal. Found (Calcd.) (%): C, 39.13 (38.93); H, 4.08 (3.73); N, 12.60 (12.97). $\mu = 1.69$ B.M.

[Cu₂(qaa)₂(N₃)₄]·H₂O (10): Quinoline-2-carbaldehyde (0.157 g, 1 mmol) was dissolved in methanol and aniline (0.093 g, 1 mmol) was added to this. A few drops of glacial acetic acid was also added and refluxed for 4 hours. To the deep yellow solution of the ligand thus obtained, $Cu(OAc)_2 \cdot H_2O$ (0.199 g, 1 mmol) dissolved in hot methanol and an aqueous solution of NaN_3 (0.130 g, 2 mmol) was added. The formation of a brown product was spontaneous and the mixture was stirred for

4 hours in order for the completion of the reaction. The product was filtered, washed with methanol, water and ether and dried over P_4O_{10} *in vacuo*. Elemental Anal. Found (Calcd.) (%): C, 48.95 (49.42); H, 3.22 (3.37); N, 28.42 (28.81). $\mu = 0$ B.M.

[Cu(qaa)(NCS)$_2$]·$\frac{1}{2}$CH$_3$OH·H$_2$O (11): Quinoline-2-carbaldehyde (0.157 g, 1 mmol) was dissolved in methanol and aniline (0.093 g, 1 mmol) was added to this. A few drops of glacial acetic acid was also added and refluxed for 4 hours. To the deep yellow solution of the ligand thus obtained, a solution of Cu(OAc)$_2$·H$_2$O (0.199 g, 1 mmol) in hot methanol was added followed by the addition of a solution of KCNS (0.194 g, 2 mmol) in methanol. Refluxed for 2 hours. The brown product separated out was filtered, washed with methanol and ether and dried over P_4O_{10} *in vacuo*. Elemental Anal. Found (Calcd.) (%): C, 50.40 (49.82); H, 2.95 (3.62); N, 11.91 (12.56). $\mu = 1.65$ B.M.

[Cu$_2$(hmba)$_2$(N$_3$)$_2$]·CH$_3$OH·2H$_2$O (12): 2-Hydroxy-4-methoxybenzaldehyde (0.152 g, 1 mmol) was dissolved in methanol. To this aniline (0.093 g, 1 mmol) was added. The mixture was refluxed for 2 hours. An aqueous solution of Cu(OAc)$_2$·H$_2$O (0.199 g, 1 mmol) and an aqueous solution of NaN$_3$ (0.130 g, 2 mmol) was added to the above solution of the ligand. The mixture was stirred for 3 hours and the green product formed was filtered, washed with methanol and ether and dried over P_4O_{10} *in vacuo*. Elemental Anal. Found (Calcd.) (%): C, 47.23 (47.60); H, 4.08 (4.41); N, 15.86 (15.31). $\mu = 1.16$ B.M.

[Cu₂(hmba)₂(NCS)₂] (13): 2-Hydroxy-4-methoxybenzaldehyde (0.152 g, 1 mmol) was dissolved in methanol. To this aniline (0.093 g, 1 mmol) was added. The mixture was refluxed for 2 hours. An aqueous solution of Cu(OAc)₂·H₂O (0.199 g, 1 mmol) and an aqueous solution of KCNS (0.194 g, 2 mmol) was added and the resulting solution was refluxed for 2 hours. The brown product separated out was filtered, washed with methanol followed by ether and dried over P₄O₁₀ *in vacuo.* Elemental Anal. Found (Calcd.) (%): C, 51.10 (51.79); H, 3.66 (3.48); N, 7.97 (8.05). μ = 1.27 B.M.

Caution! Although not encountered in our experiments, azide complexes are potentially explosive. Only a small amount of the material should be prepared, and it should be handled with care.

3.4 Results and discussion

The reaction between the aldehyde/ketone and amine in 1:1 molar ratio yielded the Schiff base ligands, which were used without further purification for the synthesis of the complexes by reaction in presence of pseudohalides NaN₃/ KCNS. The complexes **1** and **2** obtained from the Schiff base synthesized by the reaction between pyridine-2-carbaldehyde and aniline, complex **7** obtained from the Schiff base prepared by the reaction between 2-benzoylpyridine and complexes **10** and **11** obtained from the Schiff base synthesized by the reaction between quinoline-2-carbaldehyde and aniline were found to have the Schiff bases paa, bzpa and qaa respectively as neutral bidentate *N, N* donor ligands.

40

However, the complexes **5** and **6**, obtained from the Schiff base synthesized from the condensation between pyridine-2-carbaldehyde and 2-aminopyrimidine, did not have the Schiff base, instead these complexes had the parent amine coordinated in **5** and the parent aldehyde coordinated in **6**.

The complex synthesized from the ligand obtained by the condensation between pyridine-2-carbaldehyde and *R*-1-phenylethyl amine within in presence of NaN_3 gave the azido complex **3**. However, the reaction in presence of KCNS yielded a polymeric copper complex **4** in which the Schiff base ligand has undergone oxidation and cleavage to form a deprotonated pyridine-2-carboxamide (pyox). The oxidation of azomethine group to deprotonated amide group through metal binding has been well documented. The oxygen atom of the amide group originates from the water molecule [32,33]. There has been previous reports of the synthesis of copper(II) complexes with pyridine-2-carboxamide starting from pyridine-2-carbonitrile and copper(II) salts [34-36]. The above reaction occurs due to the copper(II) assisted hydrolysis of pyridine-2-carbonitrile to pyridine-2-carboxamide. Copper(II) has been found to promote the hydrolysis of 2,4,6-tris (2-pyridyl)-1,3,5-triazine (tptz) to yield Cu(II) complexes of pyridine-2-carboxamide [37]. In the present case, the transformation of azomethine function of the Schiff base to deprotonated amide group is activated through Cu(II) coordination to the Schiff base and then the deprotonated amide hydrolyses to pyridine-2-carboxamide and the

Cu(II) complex with a one dimensional polymeric structure was formed.

In the case of the copper complexes **8** and **9**, the ligand used was the Schiff base obtained by the reaction between di-2-pyridyl ketone and aniline. But it appears that in the copper complexes, the Schiff base has undergone hydrolysis in presence of Cu(II) to the alcohol adduct of di-2-pyridyl ketone. The ability of di-2-pyridyl ketone to undergo metal-mediated nucleophilic addition of small molecules like water or alcohol to the carbonyl group results in the formation of hydrate or hemiacetal [30,38-40]. The driving force for such a reaction may be the release of strain and steric interactions on changing the hybridization of the central carbon atom from sp^2 to sp^3 [41,42]. Additional driving force may be supplied by the hydrated ligand functioning as a vicinal tridentate [42]. Thus in complexes **8** and **9**, the alcohol adduct of di-2-pyridyl ketone coordinates to Cu(II).

The ligand prepared by the reaction between 2-hydroxy-4-methoxybenzaldehyde was found to be a bidentate *N, O* donor, which coordinates through the deprotonated O atom and the azomethine N in its Cu(II) complexes **12** and **13**.

The complexes prepared were either green or dark brown in color, except **4**, which is blue. All the complexes except **4** were found to be soluble in CH_3CN, DMF and DMSO, but only partially soluble in other organic solvents such as $CHCl_3$, ethanol, methanol etc. The compound **4** was found to be partially soluble only in DMF and DMSO

probably due to its polymeric structure. The room temperature magnetic susceptibility measurements revealed all the complexes to have lower values of effective magnetic moments, which can be attributed to the presence of strong antiferromagnetic interactions between the Cu(II) centers in the complexes. The strong antiferromagnetic interactions present in complexes **5, 8** and **10** made them diamagnetic.

3.4.1 Crystallographic data collection and structure analysis

Single crystal X-ray diffraction measurements of compound **4** were carried out on a Nonius MACH3 diffractometer at the Indian Institute of Technology, Bombay. The unit cell parameters were determined and the data collections were performed using a graphite-monochromated Mo Kα (λ = 0.71073 Å) radiation at 293(2) K. The collected data were reduced using MAXUS program [43]. The trial structure was solved by direct methods [44] using SHELXS-97 and refinement was carried out by full-matrix least squares on F^2 using SHELXL-97 [45]. The graphics tools used was DIAMOND [46]. All non-hydrogen atoms and the hydrogen atoms in complex **4** were refined anisotropically.

3.4.2 Crystal structure

[Cu(pyox)$_2$·2H$_2$O]$_n$ (5): The structure of **[Cu(pyox)$_2$·2H$_2$O]$_n$** (Fig. 3.1) consists of an infinite one dimensional polymeric chain of Cu(II) with pyridine-2-carboxamide (pyox) ligands. The structural refinement parameters are given in Table 3.1 and the selected bond distances and bond angles are given in Table 3.2.

Table 3.1. Crystal data and structure refinement of $[Cu(pyox)_2 \cdot 2H_2O]_n$

Parameters	$[Cu(pyox)_2 \cdot 2H_2O]_n$
Empirical formula	$C_{12}H_{12}CuN_4O_4$
Formula weight	339.80
Color	Blue
Wavelength (Mo Kα) (Å)	0.71073
Crystal system	Triclinic
Space group	$P\bar{1}$
Unit cell dimensions	
a (Å)	5.1278(4)
b (Å)	7.6293(12)
c (Å)	9.2290(8)
α (˚)	74.877(9)
β (˚)	84.416(6)
γ (˚)	71.479(9)
Volume V ($Å^3$), Z	330.46(6), 1
Calculated density (ρ) (Mg m^{-3})	1.707
Absorption coefficient μ(mm^{-1})	1.675
F(000)	173
Crystal size (mm^3)	0.40x0.35x0.30
θ range for data collection	2.29 – 24.95
Limiting indices	$-6 \leq h \leq 5$, $-9 \leq k \leq 0$, $-10 \leq l \leq 10$
Reflections collected / unique	1228/1140 [R(int) = 0.0183]
Completeness to 2θ = 24.95	99.0%
Absorption correction	Psi-scan
Maximum and minimum transmission	0.6335, 0.5539
Refinement method	Full-matrix least-squares on F^2
Data / restraints / parameters	1140/0/121
Goodness-of-fit on F^2	1.157
Final R indices [I>2σ(I)]	$R_1 = 0.0382$, $wR_2 = 0.1009$
R indices (all data)	$R_1 = 0.0424$, $wR_2 = 0.1038$
Largest diff. peak and hole(e $Å^{-3}$)	0.853 and -0.658

The Cu(II) ion is located on the inversion centre of a distorted 4+1+1 elongated tetragonal octahedral geometry. The equatorial positions of the Cu(II) octahedron are defined by two nitrogen atoms from pyridyl rings and two amide nitrogens from pyridine-2-carboxamide moiety. There are four short in-plane bonds. The Cu–$N_{pyridyl}$ lengths [1.967(3) Å] in the complex are in agreement with those previously reported for similar Cu(II) systems, but is longer than Cu(II) bond with amide N [1.947(2) Å] [35,36,47,48]. This indicates the stronger bonding of the amide N to Cu(II) than pyridyl N. The apical positions are occupied by two oxygen atoms from two neighbouring pyridine-2-carboxamides. The Cu(II)–O bonds [2.748(2) Å] are highly elongated due to Jahn-Teller effect.
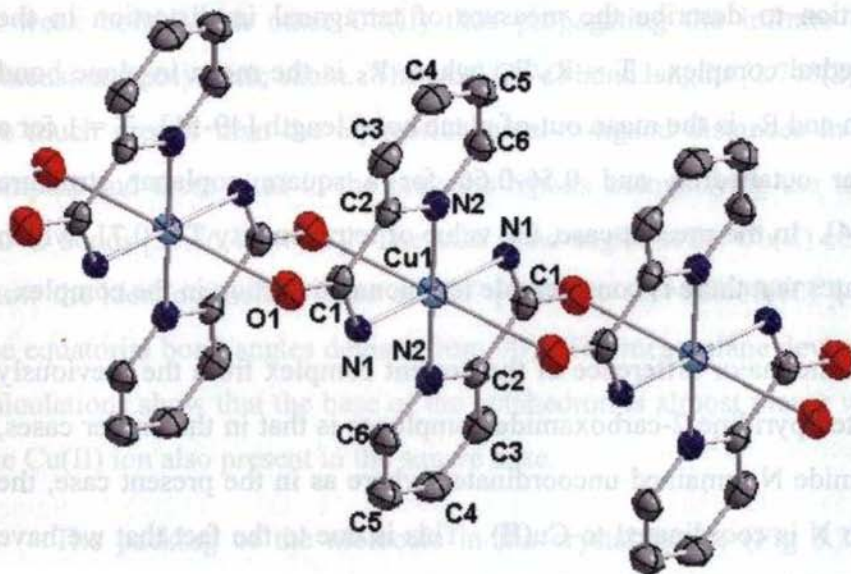
Fig.3.1. Molecular structure of [Cu(pyox)$_2$·2H$_2$O]$_n$ (5). Hydrogen atoms and water molecules are omitted for clarity.

Table 3.2. Selected bond lengths (Å) and bond angles (°) of $[Cu(pyox)_2 \cdot 2H_2O]_n$

Bond lengths		Bond angles	
Cu1−N1	1.947(2)	N(1)−Cu(1)−N(2)	83.54(10)
Cu(1)−N(1)[a]	1.947(2)	N(1)−Cu(1)−N(2)[a]	96.46(10)
Cu(1)−N(2)[a]	1.967(3)	N(1)[a]−Cu(1)−N(2)	96.46(10)
Cu(1)−N(2)	1.967(3)	N(1)[a]−Cu(1)−N(2)[a]	83.54(10)
N(1)−C(1)	1.279(4)	N(1)−Cu(1)−N(1)[a]	180.0
N(2)−C(2)	1.338(4)	N(2)[a]−Cu(1)−N(2)	180.0
N(2)−C(6)	1.339(4)		
O(1)−C(1)	1.226(4)		

a = -x,-y,-z

It is useful to define a term T called the tetragonality or tetragonal distortion to describe the measure of tetragonal in distortion in the octahedral complex. $T = R_S/R_L$, where R_S is the mean in-plane bond length and R_L is the mean out-of plane bond length [49-51]. $T = 1$ for a regular octahedron and 0.56-0.66 for a square coplanar structure [52-54]. In the present case, the value of tetragonality $T = 0.71$, which indicates that there is considerable tetragonal distortion in the complex.

The major difference of the present complex from the previously reported pyridine-2-carboxamide complexes is that in the earlier cases, the amide N remained uncoordinated where as in the present case, the amido N is coordinated to Cu(II). This is due to the fact that we have not used the pyridine-2-carboxamide directly for the preparation of the complex; instead the pyridine-2-carboxamide moiety came as a result of the metal-supported oxidation followed by hydrolysis of the Schiff

base papea as discussed earlier. This is also the reason for the absence of H atoms on the amide N of the pyridine-2-carboxamide.

It is interesting to note that both the C–O and C–N bonds of the amide function of the pyridine-2-carboxamide in the complex shows significant double bond character [C1–O1 = 1.226(4) Å and C1–N1 = 1.279(4) Å]. The C–N bond lengths of the amide group in all the earlier cases were greater than 1.3 Å and this difference reveals the extent of the double bond character of the C–N bond of the amide group. Coordination through amide N of pyridine-2-carboxamide or its derivatives is reported only in those cases where the amide N is not terminal, rather it is a secondary or tertiary N or as azomethine N [55-57]. The oxygen atom of the pyridine-2-carboxamide is involved in weak bonds with other Cu(II) thus propagating the infinite one dimensional polymeric chain. The axial Cu–O bond lengths [2.748(2) Å] are much greater than the equatorial metal-to-ligand distances in the complex and those cited in the previous reports exemplifying the weak Cu–O bonds [35,36,47,48,58]. The axial bond angles at the Cu(II) centre show the ideal octahedral value of 180° [O1–Cu1–O1=180.00(10)°], but the equatorial bond angles deviate from 90°. The mean plane deviation calculations show that the base of the octahedron is almost planar with the Cu(II) ion also present in the square base.

The packing of the molecule in the crystal lattice (Fig 3.2) is under the combined effect of hydrogen bonding, $\pi \cdots \pi$ and C–H$\cdots \pi$ interactions [Table 3.3].
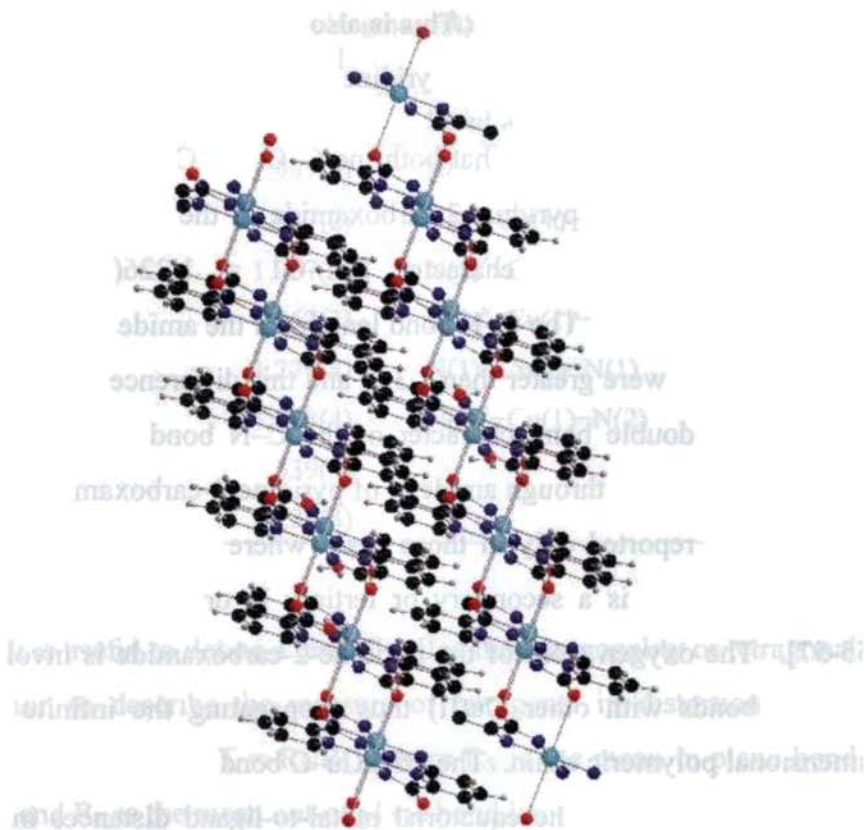
Fig. 3.2. Molecular packing diagram of **[Cu(pyox)₂·2H₂O]ₙ (5)**.

The oxygen atom O1 forms a hydrogen bond with the water molecule [OW–H111···O1; OW–H111 = 0.68(7) Å, H111···O1 = 2.33(7) Å, OW···O1 = 2.931(5) Å, OW–H111···O1 = 148(8)°]. A C–H···π interaction is also noted [C3–H3···O1; O3–H3 = 0.77(5) Å, H3···O1 = 0.77(5) Å, O3···O1 = 2.907(4) Å, OW–H111···O1 = 111(5)°]. Some π···π interactions observed in the crystal structure also reinforce the packing of the molecule.

Table 3.3. Interaction parameters of $[Cu(pyox)_2 \cdot 2H_2O]_n$

D–H⋯A	D–H (Å)	H⋯A (Å)	D⋯A (Å)	D–H⋯A (°)
OW–H111⋯O1	0.68(7)	2.33(7)	2.931(5)	148(8)
C3–H3⋯O1	0.77(5)	0.77(5)	2.907(4)	111(5)

π⋯π interactions

Cg(I)–Res(I)⋯Cg(J)	Cg⋯Cg (Å)	α°	β°	γ°
Cg(1)[1]⋯Cg(1)[a]	3.4089(17)	0.03	30.36	30.36
Cg(1)[1]⋯Cg(2)[b]	3.4089(17)	0.03	30.36	30.36
Cg(2)[1]⋯Cg(1)[c]	3.4089(17)	0.03	30.36	30.36
Cg(2)[1]⋯Cg(2)[d]	3.4089(17)	0.03	30.36	30.36

Equivalent position codes : a = 1-x, -y, -z; b = 1+x, -1+y, z; c = -1+x, y, z; d = -1-x,-y, -z
Cg(1) = Cu1, N1, C1, C2, N2; Cg(2) = Cu1, N1_c, C1_c, C2_c, N2_c.

Even though we tried to isolate the single crystals of other copper complexes repeatedly, we were unsuccessful.

3.4.3 Spectral characteristics of Cu(II) complexes

3.4.3a *Electronic spectra*

The d^9 Cu^{2+} ion with a ^2D ground state free ion term has an electron vacancy or hole in its d level and can be regarded as the inverse of a simple d^1 arrangement. The d^9 Cu^{2+} ion is stereochemically flexible, so a wide range of stereochemistries are possible. The presence of nine electrons, together with the Jahn-Teller effect in appropriate cases give rise to a range of distorted stereochemistries of uncertain description. The four coordinate complexes may be tetrahedral, square or a distorted mixture thereof, and the five coordinate complexes, square pyramidal, trigonal bipyramidal or a mixed version thereof. In the six coordinate

species, the structures vary from compressed tetragonal through regular octahedral to elongated tetragonal.

The ground state will be split by an octahedral field into a lower ^2E_g and upper $^2T_{2g}$ level [59]. But usually due to the lower symmetry of environments around the Cu(II) ion the energy levels again split resulting in more transitions. A very broad band with a peak maximum near 600 nm is observed for most geometries [60]. Thus the electronic spectrum of Cu(II) is often of little value in structural assignment making it difficult to use electronic spectroscopy alone as a definitive tool for identifying the geometry.

Tetragonal distortion is usually assumed to be the most common example of Cu^{2+} coordination. The energy levels of an axially elongated octahedron are shown in Fig. 3.3.
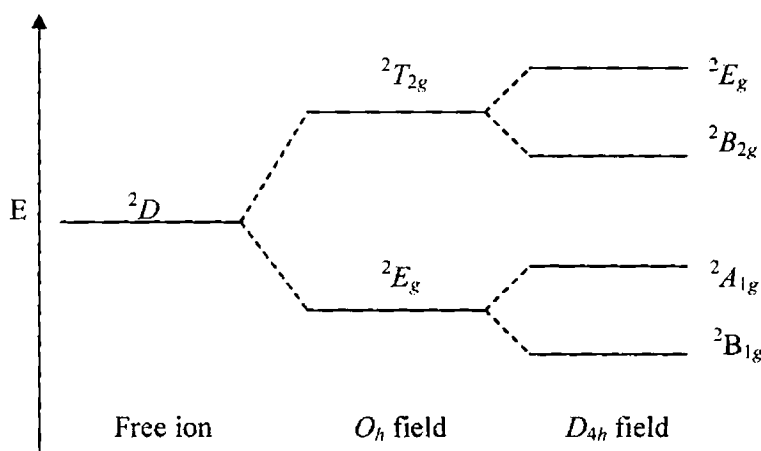
Fig. 3.3. Energy levels for axially elongated octahedral Cu(II) complexes.

The ground state of Cu(II) ion in an elongated tetragonally distorted octahedral crystal field of D_{4h} symmetry may be described as a single electron in $d_{x^2-y^2}$ (b_{1g}) orbital, or a $^2B_{1g}$ spectroscopic state. In a tetragonal field, transitions expected are $^2A_{1g} \leftarrow {}^2B_{1g}$, $^2B_{2g} \leftarrow {}^2B_{1g}$ and $^2E_g \leftarrow {}^2B_{1g}$ and they occur in the range 850-550, 645-555 and 580-500 nm respectively. Due to Jahn-Teller distortion, the axial ligands of the octahedron are farther away from the metal ion than the equatorial ligands. The absorption spectra of Cu^{2+} complexes broadened by geometrical distortion from octahedral symmetry may be further broadened by spin-orbit coupling.

In the case of square planar complexes also three allowed *d-d* transitions are expected in the visible region as in the case of octahedral complexes, but often these theoretical expectations are unseen in practice and these bands usually appear overlapped due to the very small energy difference between the *d* levels. For five coordinated complexes two extreme structures, the square pyramid and trigonal bipyramid are possible, along with many distorted intermediates. Although the electronic spectra of Cu(II) complexes do not in general provide a good indication of geometry, a criterion for distinguishing between square pyramidal and trigonal bipyramidal geometries has been proposed [61-63]. A regular trigonal bipyramidal complex is characterized by peaks extending from 850-800 nm, with the greater absorption intensity for the lower energy. The square pyramid has a similar band envelope with peaks extending from 670-530 nm, but with greater intensity in the higher energy [64].

The electronic spectra of all the copper(II) complexes were recorded in acetonitrile solutions.

Compound **1** exhibited (Fig. 3.4) a broad peak *ca.* 610 nm characteristic of Cu^{2+} complex with a square pyramidal geometry [64]. So the transition is characteristic of a Cu(II) ion with the single electron residing in the $d_{x^2-y^2}$ orbital. The broadness of the band did not permit its resolution into various components.
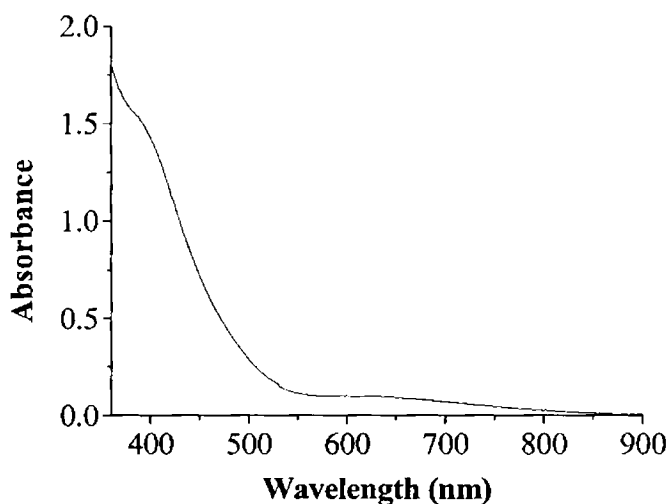
Fig. 3.4. Electronic spectrum of compound **1**.

Two intense charge transfer bands are observed at 480 and 380 nm. The existence of a charge transfer band in the vicinity of 500 nm should be taken as μ-1,1 N_3^-→Cu(II) LMCT [65-67]. So the one at 480 nm is assigned as μ-1,1 N_3^-→Cu(II) LMCT and such a band is a strong evidence for the presence of μ-1,1 azide bridges in the complex.

The above mentioned band is obviously not a _d-d_ band as evidenced by its high molar extinction coefficient. The CT band at 380 nm is due to terminal $N_3^- \rightarrow$ Cu(II) LMCT. The $\pi \rightarrow \pi^*$ transitions of the ligand are seen as a highly intense peak at 295 nm. The $n \rightarrow \pi^*$ transitions of the ligand are obscured by the broad and intense CT bands.

For the **2** (Fig. 3.5), the _d-d_ band is observed at 600 nm. Due to the broadness of the band only one transition could be distinguished. Two charge transfer bands were visible at 424 and 366 nm. The lower energy CT band may be assigned to $NCS^- \rightarrow$ Cu(II) LMCT and the higher energy band is due to N$\rightarrow$Cu(II) LMCT. The $n \rightarrow \pi^*$ and $\pi \rightarrow \pi^*$ transitions due to the ligand are observed at 311 and 290 nm respectively.

Fig. 3.5. Electronic spectrum of compound **2**.

Compound **3** exhibits (Fig. 3.6) a single broad band at 615 nm. The position of this band is consistent with a square-pyramidal geometry around the copper(II) centres [52,64,68]. The existence of a charge transfer band in the vicinity of 500 nm should be taken as μ-1,1 $N_3^- \rightarrow$Cu(II) LMCT [65-67]. Thus the absorption band *ca.* 470 nm in **3** may be considered to be due to μ-1,1 $N_3^- \rightarrow$Cu(II) LMCT and such a band is a strong evidence for the presence of μ-1,1 azide bridges in the complex. An intense charge transfer band at 395 nm is due to the terminal $N_3^- \rightarrow$Cu(II) LMCT. The $\pi \rightarrow \pi^*$ ligand transitions were observed at 295 nm and the $n \rightarrow \pi^*$ transitions were not observed as it was masked by the broad and intense charge transfer transitions.
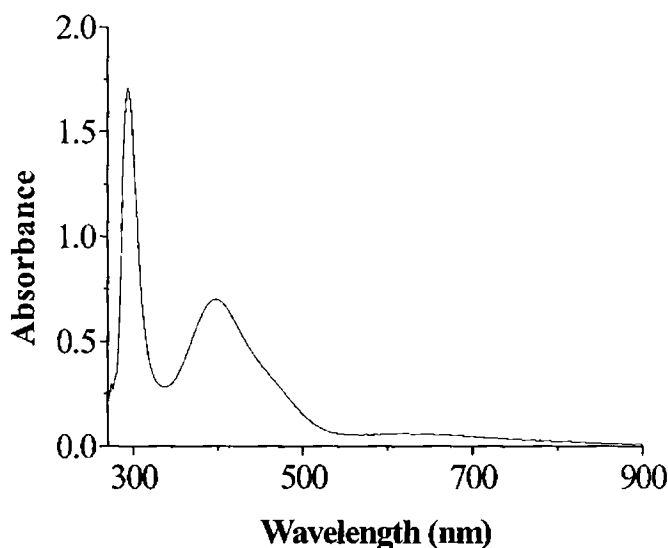
Fig. 3.6. Electronic spectrum of compound **3**.

The d-d transition for the complex **4** (Fig. 3.7) was observed as a broad band ca. 630 nm typical of Cu(II) ions in a distorted octahedral environment. They can be attributed to the components of the $^2T_{2g} \leftarrow {}^2E_g$ [69]. Due to the broadness of the band only one transition could be distinguished. The ligand to metal charge transfer band was observed as a strong band ca. 423 nm. Generally, we cannot see a charge transfer transition from axial ligands in tetragonal complexes with long axial Cu–L bonds. The strong charge transfer absorption in a tetragonal Cu(II) complex is an indicator of equatorial binding for the ligands concerned. So the CT band in the present case is due to N$\rightarrow$Cu LMCT and not O$\rightarrow$Cu LMCT [64]. The $n \rightarrow \pi^*$ and $\pi \rightarrow \pi^*$ transitions of the ligand are found at 358 (sh) and 290 nm respectively.
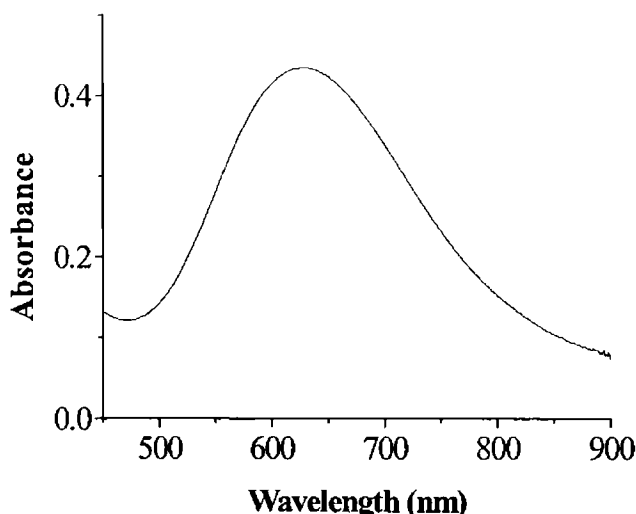
Fig. 3.7. Electronic spectrum of compound 4.

In complex **5** (Fig. 3.8), *d-d* transition was observed as very low intensity broad band at 625 nm. Ligand to metal charge transfer band appeared at 460 nm assigned as the N_3^- →Cu(II) LMCT. The $n \to \pi*$ transitions of the ligand were obtained in conjugation with another LMCT due to N→Cu(II) at around 385 nm with very high intensity almost equivalent to the intensity of the $\pi \to \pi*$ transition of the ligand, which was viewed at 290 nm. The higher intensity of the $n \to \pi*$ transitions is due to the intensity borrowing from the nearby charge transfer band [64].
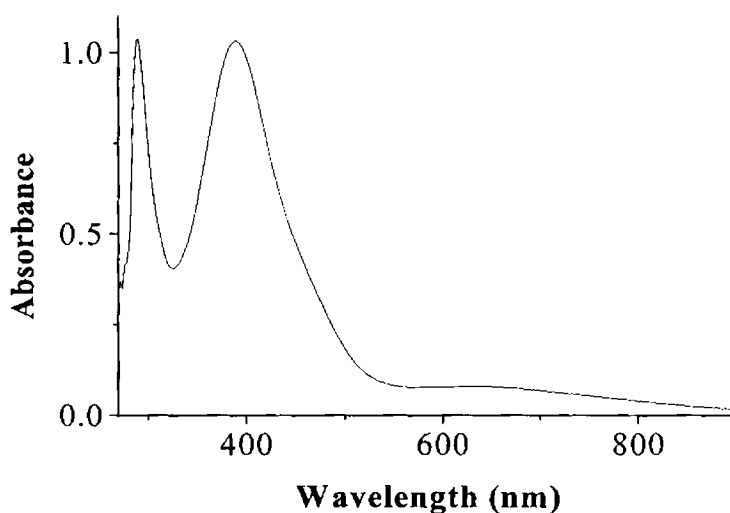
Fig. 3.8. Electronic spectrum of compound **5**.

Complex **6** (Fig. 3.9) exhibits a broad *d-d* band at 645 nm. The charge transfer band appears at 438 nm. The ligand centered transitions are seen at 350 and 290 nm.
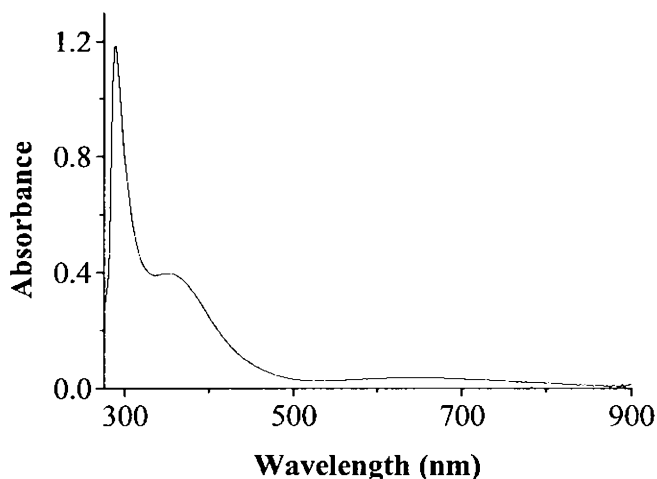
Fig. 3.9. Electronic spectrum of compound **6**.

Complex **7** (Fig. 3.10) has a broad band at 600 nm, which can be assigned as the *d-d* transition of the Cu^{2+} ion. The charge transfer transition overlaps with the $n \rightarrow \pi^*$ transitions of the ligand and is observed at 390 nm. The peak at 292 nm corresponds to the $\pi \rightarrow \pi^*$ transition of the ligand.
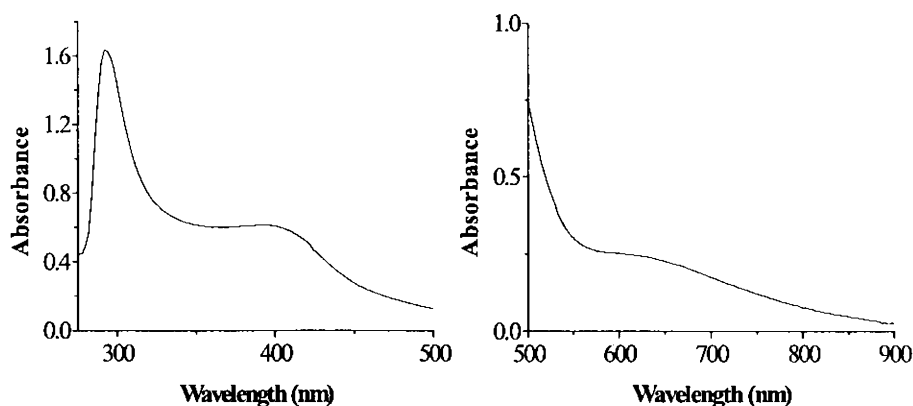
Fig. 3.10. Electronic spectrum of compound **7**.

57

In complex **8** (Fig. 3.11), the *d-d* transition was observed as a very broad band at 685 nm. The intraligand transitions were obtained at 384 ($n \to \pi$ *) and 292 nm ($\pi \to \pi$ *).
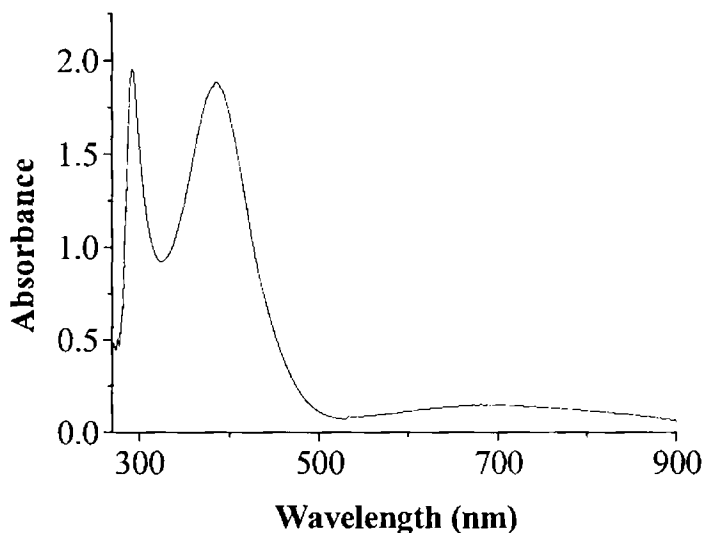
Fig. 3.11. Electronic spectrum of compound **8**.

The *d-d* transition in complex **9** (Fig. 3.12) was obtained as a broad band in the range 530-880 nm with the band centre at around 700 nm. The NCS¯ →Cu(II) LMCT is seen at 420 nm and a higher energy charge transfer band occurs due to N→Cu(II) transition at 365 nm. The $n \to \pi$ * and $\pi \to \pi$ * transitions of the ligand are viewed at 311 and 288 nm respectively.
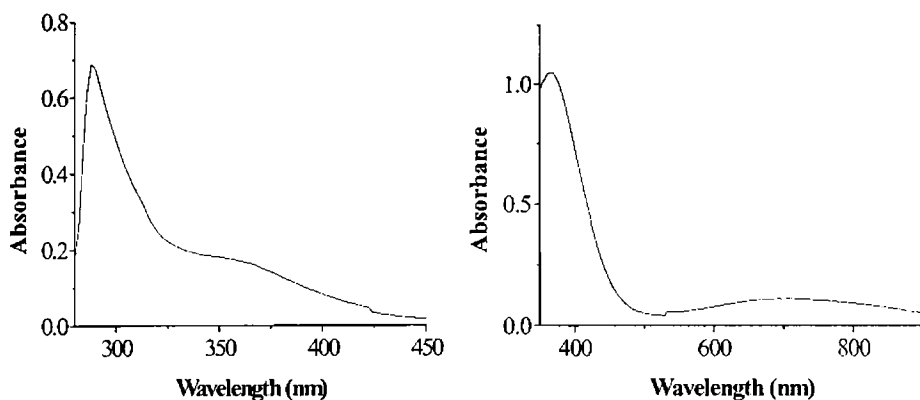
Fig. 3.12. Electronic spectrum of compound 9.

The d-d transition in complex **10** (Fig. 3.13) was obtained as a broad band at 630 nm. The charge transfer transition observed at 425 nm is due to $N_3^-{\rightarrow}Cu(II)$ LMCT. The $n \rightarrow \pi^*$ and $\pi \rightarrow \pi^*$ transitions of the ligand are viewed at 323 (sh) and 295 nm respectively.
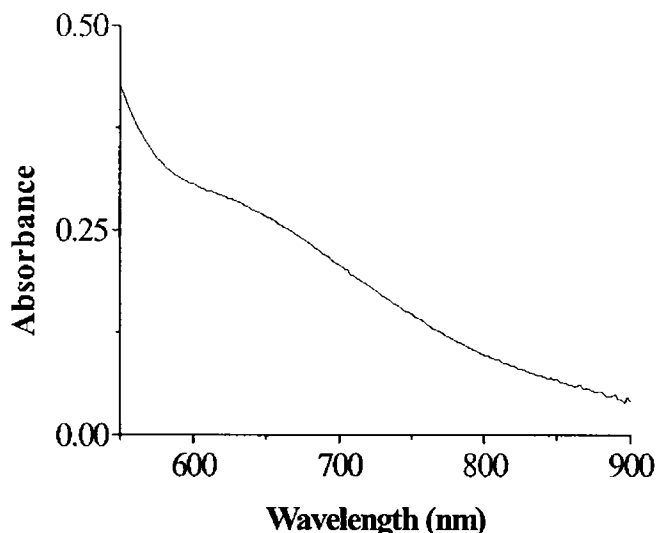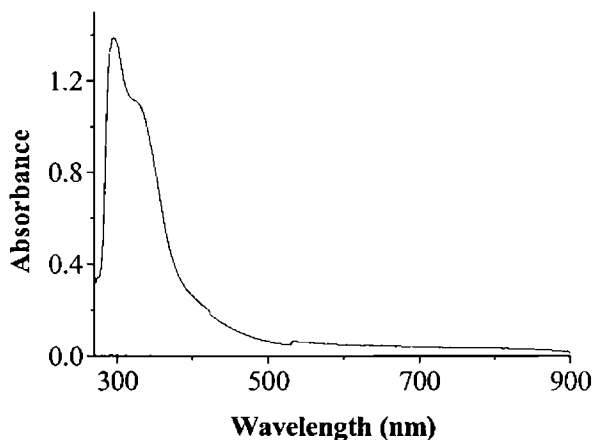

Fig. 3.13. Electronic spectrum of compound **10**.

The thiocyanato complex **11** (Fig. 3.14) displays a *d-d* transition at 561 nm with a lower energy shoulder at 655 nm, corresponding to a

five coordinate square pyramidal geometry for Cu(II). The charge transfer band in the complex is viewed at 423 nm and the ligand centered transitions are seen at 325 and 293 nm.
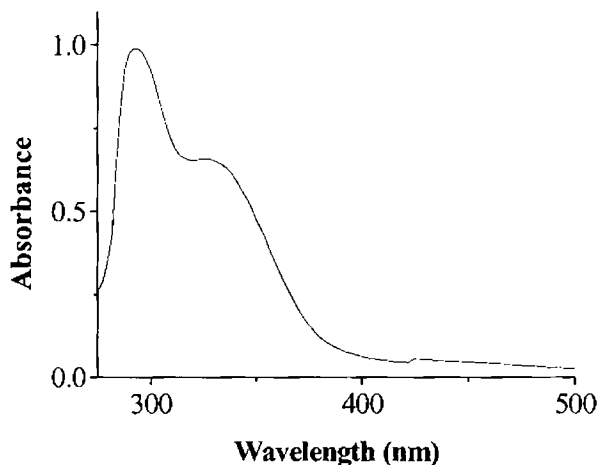
Fig. 3.14. Electronic spectrum of compound **11**.

For the Cu(II) complex **12** (Fig. 3.15), the ligand field transition is obtained as a broad band *ca.* 650 nm. Due to the broadness of the band, this band could not be resolved. The charge transfer band that also contributes to the observed green color, for the compound is observed in the visible region at 445 nm. The $n \rightarrow \pi^*$ and $\pi \rightarrow \pi^*$ transitions of the ligand are viewed at 370 and 295 nm respectively in complex **12**. These transitions were observed at 334 and 291 nm respectively in the ligand. The $\pi \rightarrow \pi^*$ transitions of the ligand thus show a shift to longer wavelengths in the complex upon complexation. The red shift in the case of $n \rightarrow \pi^*$ transition indicates coordination of the azomethine nitrogen atom of the Schiff base [64].
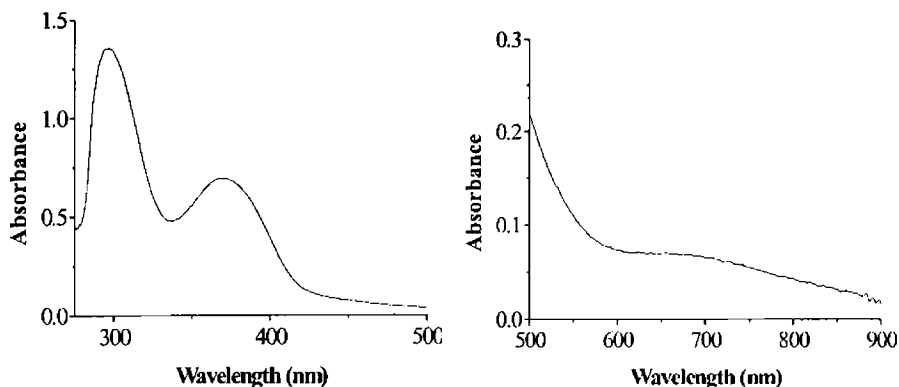
Fig. 3.15. Electronic spectrum of compound **12**.

The d-d electronic transition for the single electron in Cu^{2+} in complex **13** was observed as a broad band at 700 nm (Fig. 3.16). The charge transfer band was obtained in conjugation with the $n \to \pi^*$ transition. The $n \to \pi^*$ and $\pi \to \pi^*$ transitions due to the ligand are viewed at 365 and 297 nm respectively. These transitions were observed at 334 and 291 nm in the free ligand. The red shift observed for these transitions in the complex is indicative of coordination.
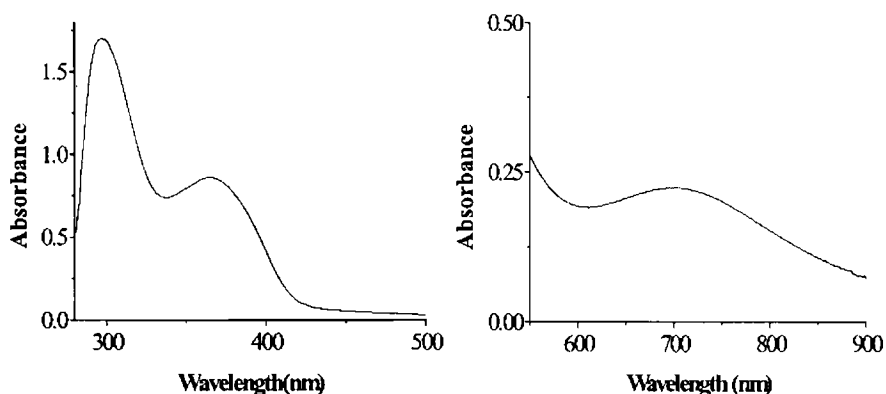
Fig. 3.16. Electronic spectrum of compound **13**.

3.4.3b *Electron paramagnetic spectra*

Electron paramagnetic resonance (EPR) spectroscopy is a powerful tool in the study of the structures and environments of species that contain unpaired electrons, such as transition-metal ions, organic free radicals and electronically excited states. An easy application of EPR spectroscopy uses the Cu(II) ion ($3d^9$ electronic configuration), a particularly favourable example of a metal ion that exhibits a wide range of stereochemistries (tetra-, penta- and hexa-coordinated) along with a variety of intermediate situations. The geometry of the complex affects the electronic properties of the Cu(II) ion, establishes the order of the energy levels of the d orbitals, and consequently the ground state for a particular arrangement. Thus EPR spectroscopy plays a significant role in identifying the existence or otherwise of the compressed tetragonal or rhombic octahedral stereochemistry for the Cu(II) ion its six coordinate complexes [52,53,70]. The Cu(II) ion with the d^9 configuration, has an effective spin of s = ½ and associated spin angular momentum of m_s = ±½ leads to a doubly degenerate spin energy state in the absence of magnetic field. On applying a magnetic field, this degeneracy is removed and transitions occur between the two levels, whose energy difference is given by

$$\Delta E = h\nu = g\beta H$$

where h is Planck's constant, ν is the frequency, g is the Landé splitting factor, β is the electron Bohr magneton and H is the magnetic field.

The factors that determine the type of EPR spectrum are:

  a.   the nature of the electronic ground state

  b.   the symmetry of the effective ligand-field about the copper(II) ion

  c.   the mutual orientations of the local molecular axes of the separate copper(II) chromophores.

The factors a and b deal with the mode of splitting of the five-fold degenerate 3d-*orbitals* by crystal fields of octahedral and tetrahedral symmetries which are inverse of each other. The orbital sequences of the various stereochemistries determine their ground states. For coordination geometries corresponding to an elongated octahedron, a square pyramid and square planar, the ground state is $d_{x^2-y^2}$. When the coordination around copper ion is a compressed octahedron or a trigonal bipyramid, the ground state is d_{z^2}. EPR spectroscopy can distinguish the ground states a $d_{x^2-y^2}$ and d_{z^2} on the basis of the principal values of the g tensor in the anisotropic spectra. The third factor c, determines the amount of exchange coupling present, which is the major factor in reducing the amount of stereochemical information available from the EPR spectra [71].

The value of g is the primary empirical parameter that characterizes the response of a paramagnetic molecule and is loosely analogous to the chemical shift in NMR spectroscopy [72]. The g factors for the metal complexes are quite different from the g factor of a

free electron (g_e ≈ 2.0023) and they can be smaller or larger than g_e. The shifts in the g value are caused by the influence of spin-orbit coupling.

The EPR spectra of the compounds **1-13** were recorded in the X-band frequency. The various magnetic interaction parameters are summarized in Table 3.4.

The X-band EPR spectrum of complex **1** in the polycrystalline state at room temperature exhibited a broad isotropic spectrum with a g_{iso} of 2.099. The broadness of the spectrum may be attributed to the strong dipolar and exchange interactions present between the Cu^{2+} ions in the polycrystalline sample. Such broad spectrum is not informative in interpreting the geometry of the complex. The Cu^{2+} signal was very weak and could be obtained only at very high receiver gains. The broadness of the spectrum and the weak signal maybe due to the large antiferromagnetic interaction between the metal ions decreasing the paramagnetism due to Cu(II) centers [73,74]. The EPR spectrum of compound **1** in solution at 77 K (Fig. 3.17) is a typical axial spectrum with $g_{\parallel}$ = 2.194 and $g_{\perp}$ = 2.046. g_{av} calculated as g_{av} =$^1/_3(g_{\parallel}$ +2 $g_{\perp})$ has the value 2.096. The parallel region of the spectrum is well resolved and consists of a set of four hyperfine line due to the interaction of the electron with the Cu(II) nucleus (No: of hyperfine lines = 2nI+1 and for ^{65}Cu, I = $^3/_2$). The hyperfine lines will be separated by the nuclear hyperfine splitting constant A. The nuclear hyperfine splitting constant in the parallel region, i.e., $A_{\parallel}$ is found to be

187.8×10^{-4} cm^{-1}. The perpendicular region of the spectrum is devoid of hyperfine splitting. The trend in the g values, $g_{\parallel} > g_{\perp} > 2.0023$ indicates square pyramidal geometry for Cu(II) with the $d_{x^2-y^2}$ ground state [75-77]. The $g_{\parallel} > g_{\perp} > 2.0023$ rules out the possibility of a trigonal bipyramidal structure for which $g_{\perp} > g_{\parallel} = 2.0023$ is expected. The $g_{\parallel}$ value provides information regarding the nature of metal-ligand bond [78]. The value $g_{\parallel}$ is normally 2.3 or larger for ionic and less than 2.3 for covalent metal-ligand bonds. The $g_{\parallel}$ value obtained indicates a significant degree of covalency in the metal-ligand bonds.
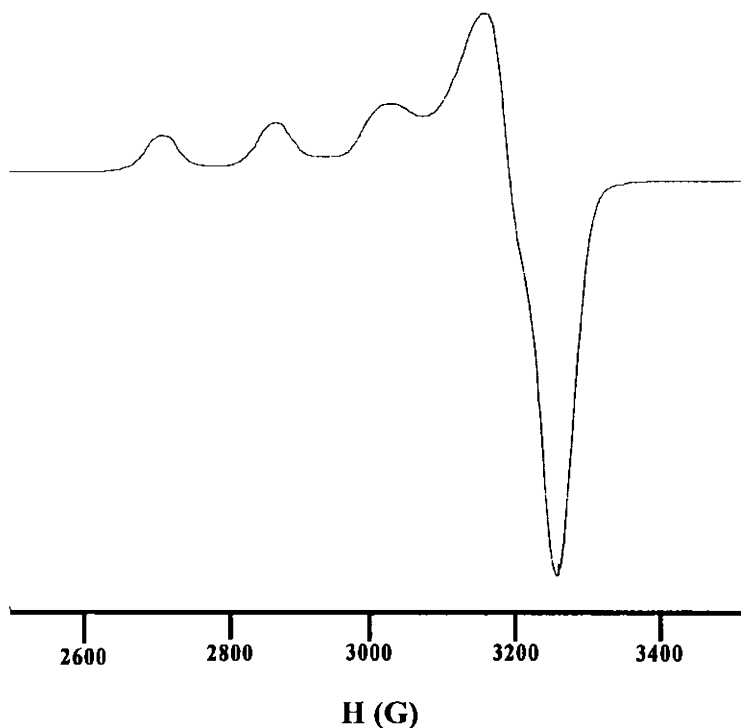
Fig. 3.17. EPR spectrum of compound **1** in DMF at 77 K.

The compound **2** in the polycrystalline state at room temperature (Fig. 3.18) exhibited a broad isotropic spectrum with a g_{iso} of 2.102. The broadness of the spectrum may be attributed to the strong dipolar and exchange interactions present between the Cu^{2+} ions in the polycrystalline sample. Such broad spectrum is not informative in interpreting the geometry of the complex.

2400 2600 2800 3000 3200 3400 3600 3800

H (G)
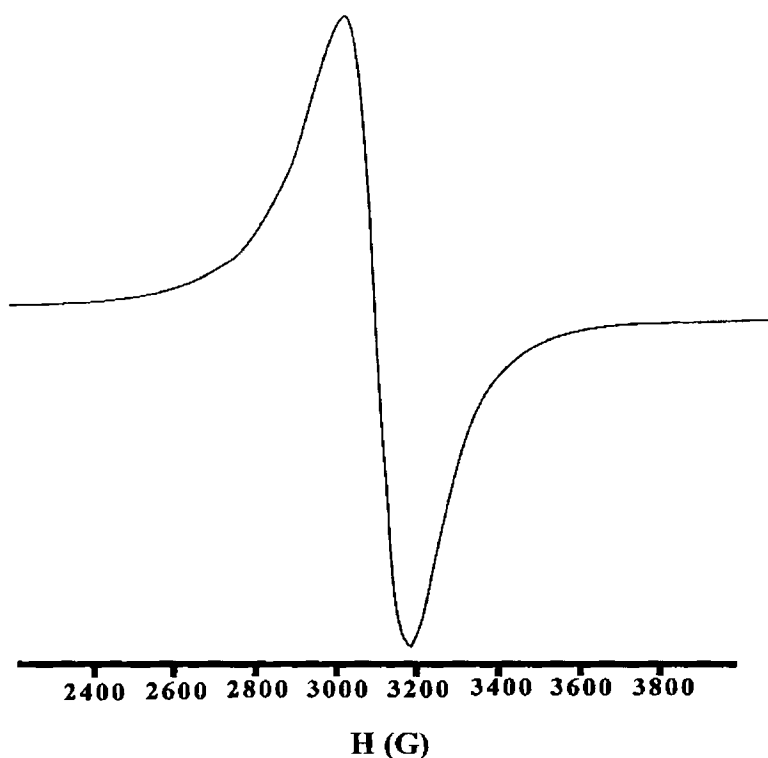
Fig. 3.18. EPR spectrum of compound **2** in polycrystalline state at 298 K.

The spectrum in solution at 77 K (Fig. 3.19) is a typical axial spectrum with $g_{\parallel} = 2.238$ and $g_{\perp} = 2.059$, $g_{av} = 2.118$. $g_{\parallel} > g_{\perp} > 2.0023$ indicates an axial symmetry for Cu(II) with the $d_{x^2-y^2}$

ground state. The $g_\parallel$ value (>2.3) indicates the covalent character of the Cu(II)–N bonds. The parallel region of the spectrum is well-defined and shows a multiplet structure consisting of seven lines corresponding to the hyperfine interaction with two copper atoms. The $A_\parallel$ value is found to be 102.7×10^{-4} cm^{-1} and the perpendicular region is devoid of hyperfine lines.
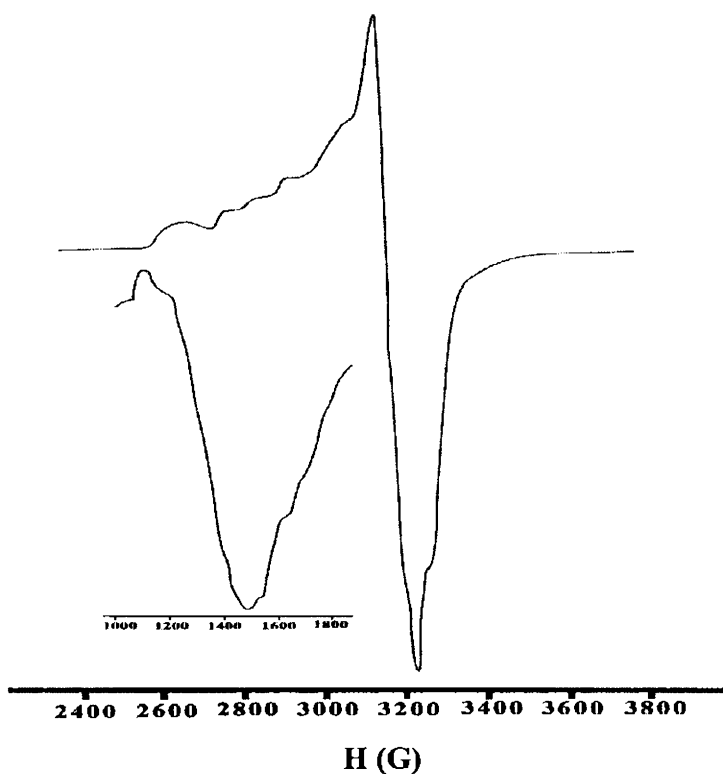
Fig. 3.19. EPR spectrum of compound **2** in DMF at 77 K.

In polynuclear copper(II) complexes, due to Cu-Cu dipolar interaction, the zero field splitting parameter, D gives rise to transitions corresponding to $\Delta M_s = \pm 2$ [79]. In the X-band spectra, $\Delta M_s = \pm 1$

transitions are associated with fields of 3000 Gauss, while the $\Delta M_s = \pm 2$ transition generate an absorption at the half field value of 1500 Gauss and the presence of this half field band is a useful criterion for dipolar interaction from the presence of some dinuclear (or polynuclear) complex formation. In the solution spectrum of **2** at 77 K, there is a signal at 1380 G with a *g* value 4.760 due to the half-field $\Delta M_s = \pm 2$ forbidden transition, indicating that the complex is dimeric and thus the presence of magnetic exchange interaction between the copper ions in solution. Thus a partial dissociation of the complex on coordination with solvent in solution, but with the dimeric structure retained is suggested.

Compound **3** in polycrystalline state at 298 K (Fig. 3.20) displayed an axial spectrum with $g_{\parallel} = 2.136$, $g_{\perp} = 2.065$. $g_{\parallel} > g_{\perp} > 2.0023$ indicates square pyramidal geometry for Cu(II) with the $d_{x^2-y^2}$ ground state. The $g_{\parallel}$ value (<2.3) indicates the covalent character of the Cu(II)−N bonds. The geometric parameter *G*, which is a measure of the exchange interaction between copper centers in the polycrystalline compound, is calculated using the equation $G = (g_{\parallel}-2)/(g_{\perp}-2)$ [49]. If $G > 4$, then the local tetragonal axes are aligned parallel or only slightly misaligned and the g values are near to the molecular *g* values. So exchange interaction is negligible and the unit cell of the complex contains magnetically equivalent sites. *G* value less than 4 indicates significant exchange interaction among the Cu(II) ions in the unit cell. So the *g* values of the polycrystalline sample will be different from the molecular *g*

values [49,71,80]. G is found to be less than 4.0 in the present complex, suggesting considerable exchange coupling interactions in the complex in the polycrystalline state. The $g_{\parallel}$ value is relatively small and this can be attributed to a small influence of the spin-orbit coupling in the parallel direction and hence a large $d_{x^2-y^2} \rightarrow d_{xy}$ energy gap [81].
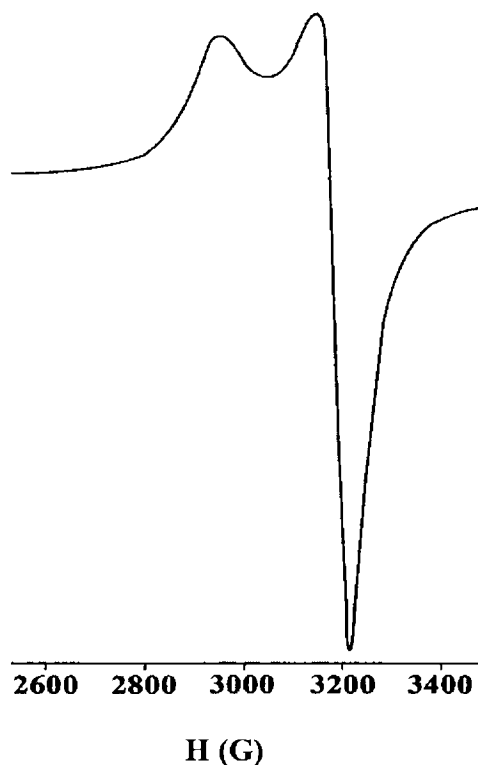
Fig. 3.20. EPR spectrum of compound **3** in polycrystalline state at 298 K.

The frozen solution EPR spectrum (Fig. 3.21) of the compound in DMF at 77 K revealed axial characters. At 77 K, the signal appears more resolved with $g_{\parallel} = 2.189$ and a very intense $g_{\perp} = 2.052$. $g_{\parallel} < 2.3$ indicates a fair degree of covalent character in the Cu–L bonding and

69

$g_\parallel > g_\perp > 2.0023$ is consistent with a square pyramidal geometry and the $d_{x^2-y^2}$ ground state and negates the trigonal bipyramidal structure. For Cu(II) complexes, the g values may display evidence for copper nuclear hyperfine splitting, $2nI+1$, for ^{65}Cu, $I = \frac{3}{2}$ and the g value in the parallel region is split into four lines, separated by the nuclear hyperfine splitting constant A. $A_\parallel$ is found to be 191.4 x 10^{-4} cm^{-1} and the perpendicular region is devoid of hyperfine lines.

H (G)
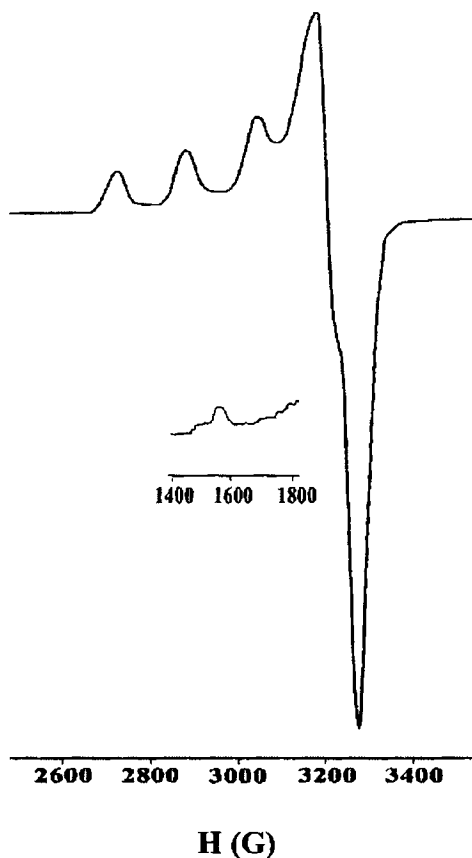
Fig. 3.21. EPR spectrum of compound 3 in DMF at 77 K.

The solution EPR spectrum of compound **3** at 77 K, exhibited a half field signal at approximately 1575 G (g = 4.1708), which indicate that indeed a weak interaction between two Cu(II) ions within this compound is present. Thus a dimeric structure could be proposed for the square pyramidal complex **3**. The g values in the polycrystalline state and solution do not show much difference suggesting that the complex retains its structure in solution.

Compound **4** displayed a complicated EPR spectrum in the polycrystalline state at 298 K (Fig. 3.22) and in solution at 77 K (Fig. 3.23). This is probably due to complex exchange coupling interactions between the Cu(II) centers both in the solid state and in solution. The solid state spectrum is almost axial with a $g_{\parallel}$ = 2.155, $g_{\perp}$ = 2.066 and g_{av} = 2.096. The hyperfine splitting observed in the parallel region is not clearly defined, so the determination of $A_{\parallel}$ was not possible. This also restricted the calculation of the bonding parameters. G value for the complex is less than 4 and this suggests the existence of strong exchange interactions in the Cu(II) complex in the solid state. Hexacoordinated Cu(II) complexes exhibit a tetragonal distortion due to Jahn Teller effect which reduces its symmetry from O_h to D_{4h} [82,83]. This results in anisotropy of the g-tensor. As the coordinated groups are not equivalent, only static distortion can occur [71,84,85]. As $g_{\parallel} > g_{\perp}$, a tetragonal distortion is suggested, corresponding to an elongation along the Z axis. The unpaired electron still remains in the $d_{x^2-y^2}$ orbital in the distorted octahedral structure

71

because the Jahn Teller induced distortion generally favours $d_{x^2-y^2}$ while d_{z^2} configuration are rare. The g values in the complex are less than 2.3 and it means that considerable covalent character is imparted to the metal-ligand bonds. The results are in accordance with the crystal structure of **4**.

2700 2800 2900 3000 3100 3200 3300 3400

H (G)
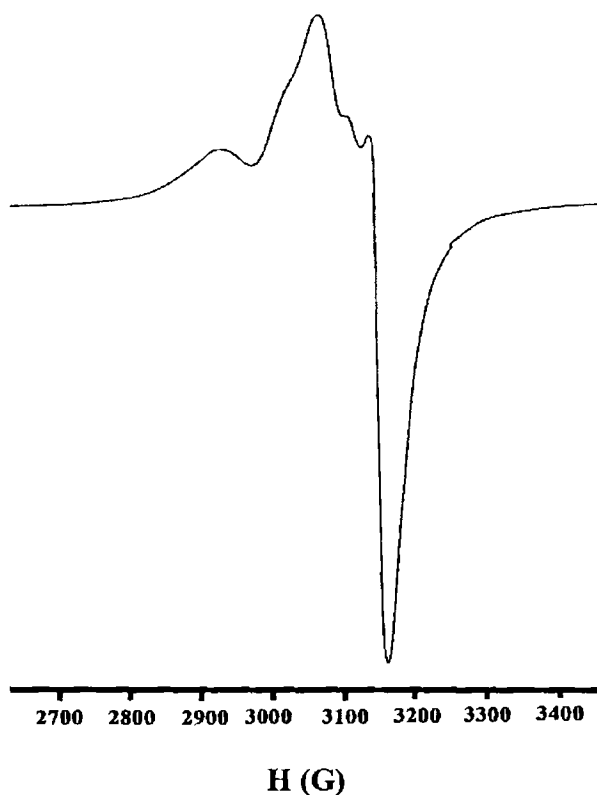
Fig. 3.22. EPR spectrum of compound **4** in polycrystalline state at 298 K.

The EPR spectrum of **4** in DMF at 77 K is very similar to the spectra reported for other Cu(II) systems where considerable exchange interactions are present [40,86-88].

2500 2600 2700 2800 2900 3000 3100 3200 3300

H (G)
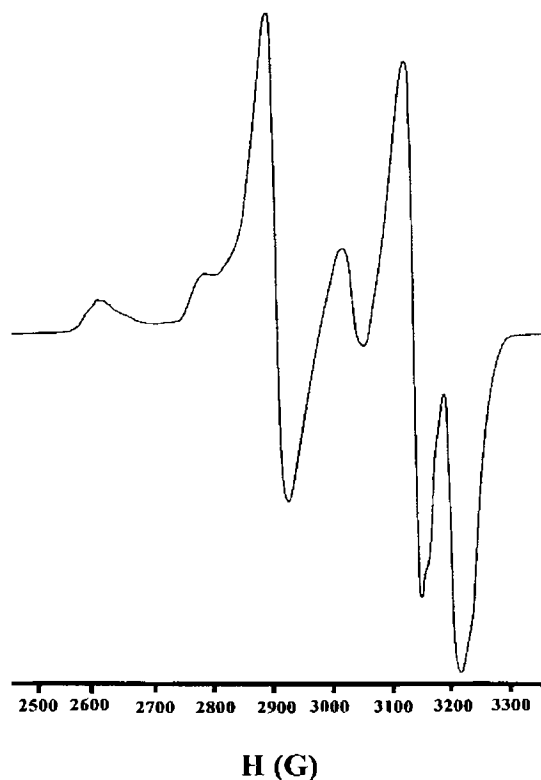
Fig. 3.23. EPR spectrum of compound **4** at 77 K in DMF.

The X-band EPR spectrum of complex **5** in the solid state at room temperature was very broad that the broadness of the spectrum restricted the accurate measurement of the *g* value. The broadness of the spectrum, almost equivalent to EPR silence maybe due to the large antiferromagnetic interaction between the metal ions [73,74]. The solution spectrum at 77 K (Fig. 3.24) displayed a typical axial spectrum with $g_{\parallel}$ = 2.245, $g_{\perp}$ = 2.065 and g_{av}= 2.125. The parallel region is well resolved into six hyperfine splittings and the seventh one is hidden under the perpendicular features suggesting a dimeric state with two

73

copper centres. $A_{\parallel}$ = 106.5 x 10^{-4} cm^{-1}. The perpendicular part is not resolved. $g_{\parallel} > g_{\perp} > 2.0023$ suggests a $d_{x^2-y^2}$ ground state and a square planar geometry around Cu(II). $g_{\parallel} < 2.3$ and the molecular bonding parameters imply a significant degree of covalent character in the Cu–L bonding. The parameter $f(g_{\parallel}/A_{\parallel})$ is used as an index to express the range of tetrahedral distortion from planarity. If the parameter lies between 105 and 150 cm, the complex is square planar and a value between 150 and 200 cm indicates a distorted tetrahedral geometry [89]. For the present case f = 193.7 cm, which indicates large tetrahedral distortion in the square planar complex.
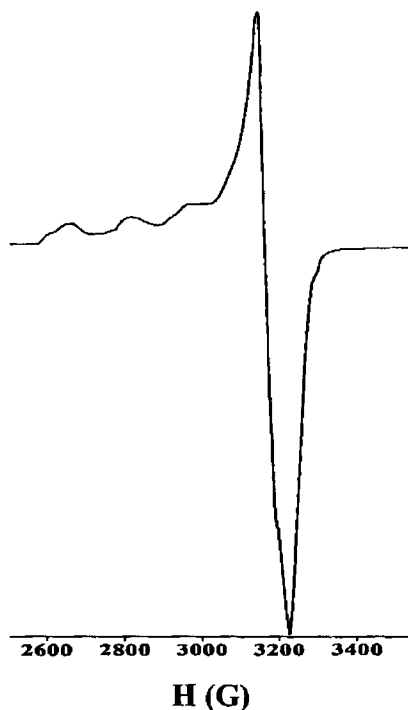
Fig. 3.24. EPR spectrum of compound **5** in DMF at 77 K.

Compound **6** (Fig. 3.25) in the solid state at room temperature exhibits an axial spectrum with $g_{\parallel} = 2.219$, $g_{\perp} = 2.078$ and $g_{av} = 2.125$. There are no hyperfine or superhyperfine lines. $g_{\parallel} > g_{\perp} > 2.0023$ implies the geometry of the complex to be square pyramidal or square planar, with a $d_{x^2-y^2}$ ground state and rules out the possibility of a trigonal bipyramidal structure. The G value for the complex in the polycrystalline state is found to be 2.782, which is less than 4 and indicates exchange interactions between the Cu(II) ions in the solid state. But the absence of a signal at half-field corresponding to $\Delta M_s = \pm 2$ forbidden transition indicates that the exchange interaction is weak.

| 2600 | 2800 | 3000 | 3200 | 3400 | 3600 |

H (G)
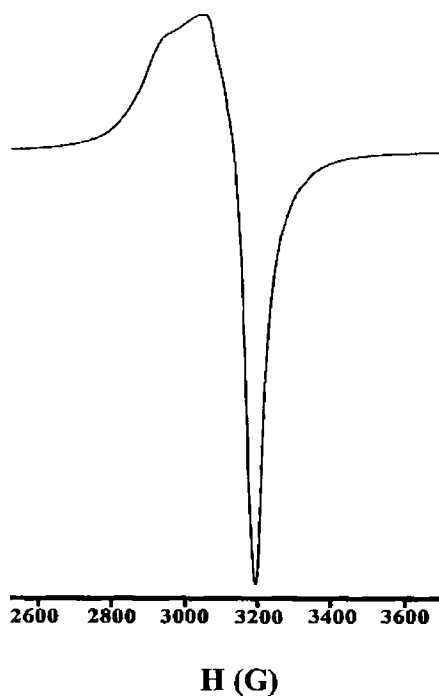
Fig. 3.25. EPR spectrum of compound **6** in polycrystalline state at 298 K.

75

The three signals observed for the compound **6** in solution at 77 K (Fig. 3.26) are in complete agreement with the rhombic distortion of the coordination sphere around the Cu(II) ion. The g values calculated are found to be $g_1 = 1.999$; $g_2 = 2.065$; $g_3 = 2.269$. The hyperfine splittings are observed only in the higher g value region ($A_3 = 180.0 \times 10^{-4}$ cm^{-1}). $g_{\parallel} = g_3 = 2.269$ and $g_{\perp} = (g_1 + g_2)/2 = 2.032$.
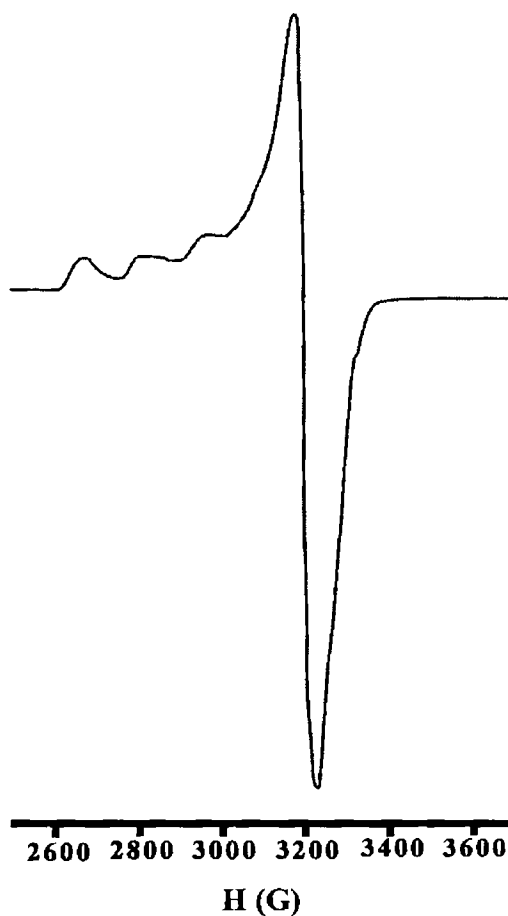
Fig. 3.26. EPR spectrum of compound 6 in DMF at 77 K.

In the rhombic spectra with $g_1 < g_2 < g_3$, the rhombic spectral value, $R = (g_2 - g_1) / (g_3 - g_2)$ may be significant. If $R > 1$, a predominant d_{z^2} ground state is present and if $R < 1$, a predominant $d_{x^2-y^2}$ ground state is present. When $R = 1$, then the ground state involves an approximately equal mixture of $d_{x^2-y^2}$ and d_{z^2}, and the structure is intermediate between square planar and trigonal bipyramidal geometries [53,76,90,91]. In the present case, $R < 1$ ($R = 0.3245$) and is consistent with a square pyramidal geometry. This ground state is supported by the fact that the low field side of the spectrum is less intense than the high field side [92].

The X-band EPR spectrum of copper complex 7 (Fig. 3.27) exhibited a featureless axial spectrum in the polycrystalline state at 298 K. The values $g_{\parallel} = 2.197$, $g_{\perp} = 2.085$ and $g_{av} = 2.123$ can be obtained from the $\Delta M_s = \pm 1$ transition signal at 298 K. The pattern $g_{\parallel} > g_{\perp} > 2.0023$ is indicative of a copper(II) $3d_{x^2-y^2}$ ground state, which points out the square pyramidal or square planar geometry of the complex. The $g_{\parallel} > g_{\perp} > 2.0023$ rules out the possibility of a trigonal bipyramidal structure. $g_{\parallel} < 2.3$ was observed and this indicates a fair degree of covalent character in the Cu–L bonding. For the spectrum of 7 in the polycrystalline state, the exchange interaction parameter G is 2.28, which points out to the existence of considerable Cu----Cu interactions and thus the possibility of a dimeric structure for the complex. The signal detected at about 1600 G ($g = 4.093$) is attributable to the "half-field" $\Delta M_s = \pm 2$ forbidden transition and it

confirms the presence of dimeric system and the existence of magnetic exchange interaction between the copper ions.
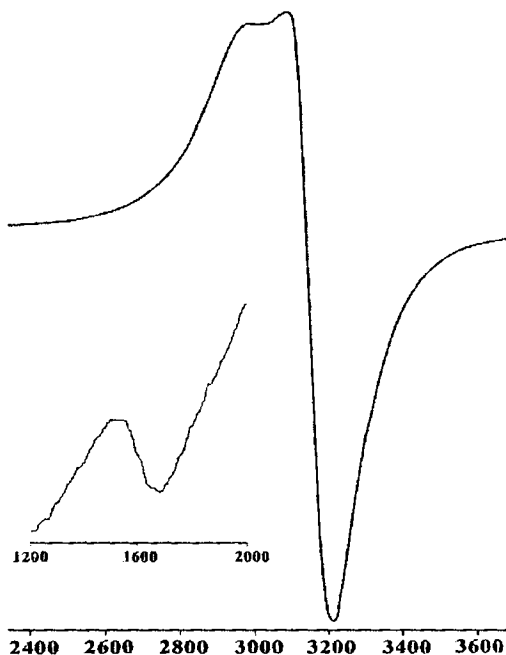
Fig. 3.27. EPR spectrum of compound **7** in polycrystalline state at 298 K.

The solution spectrum of **7** at 77 K (Fig. 3.28) is very similar to the above, but the parallel region is resolved into a set of four hyperfine lines. The values $g_{\parallel} = 2.197$, $g_{\perp} = 2.072$, $g_{av} = 2.113$, $A_{\parallel} = 184.6 \times 10^{-4}$ cm^{-1} can be obtained at 298 K. The trend $g_{\parallel} > g_{\perp} > 2.0023$ is indicative of a copper(II) $3 d_{x^2-y^2}$ ground state, which points out the square pyramidal geometry of the complex. $g_{\parallel} < 2.3$ indicates a fair degree of covalent character in the Cu–L bonding. There is a half-field signal at 1590 G with a g value 4.131, which indicates that the dimeric structure of the

78

complex is retained in the solution also. Moreover, the Cu–L bonds are fairly strong that the dimer is not getting dissociated by the coordination of the solvent molecules. One of the most interesting features of this EPR spectrum is that it exhibits strong half field transition signals at both room temperature and 77 K, which is rarely observed in copper(II) complexes, and the strong half field signal may be a sign of strong magnetic coupling between the bridging copper(II) ions. The second interesting feature of this EPR spectrum is that its strong and sharp signal is in contradistinction to the rule that the line width is proportional to the magnetic interaction and the strong magnetic interaction may lead to ESR silence [93,94].

H (G)
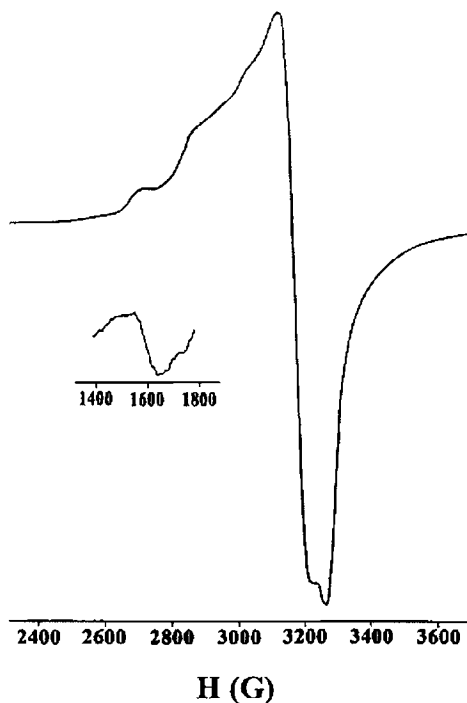
Fig. 3.28. EPR spectrum of compound 7 in DMF at 77 K.

The X-band EPR spectrum of complex **8** in the solid state at room temperature was EPR silent. This fact maybe due to the large antiferromagnetic interaction between the metal ions which could be responsible for a broadening in the signal [73,93-95]. The solution spectrum at 77 K (Fig. 3.29) displays a typical axial spectrum with $g_{\|}$ = 2.242, $g_{\perp}$ = 2.052 and g_{av} = 2.115, $A_{\|}$ = 160.4 x 10^{-4} cm^{-1}. $g_{\|} > g_{\perp} > 2.0023$ suggests a $d_{x^2-y^2}$ ground state and a square pyramidal geometry around Cu(II). $g_{\|} < 2.3$ and the molecular bonding parameters imply a significant degree of covalent character in the Cu–L bonding. There is a half-field signal of reasonable intensity at 1680 G with a *g* value 3.910, which confirms the dimeric structure for **8**.
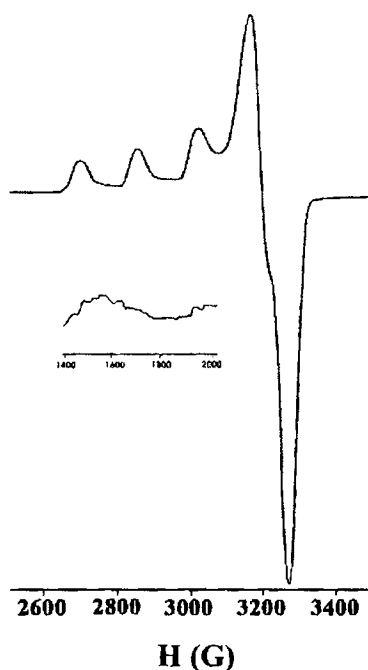
Fig. 3.29. EPR spectrum of compound **8** in DMF at 77 K.

Complex **9** has a broad quasi-isotropic EPR spectrum (Fig. 3.30) in the polycrystalline state at room temperature with $g_{iso} = 2.072$, suggesting Cu-Cu interactions as found in other Cu(II) systems [66,96-99]. Small g value suggests dipolar broadening and enhanced spin lattice relaxation.

2600 2800 3000 3200 3400 3600

H (G)
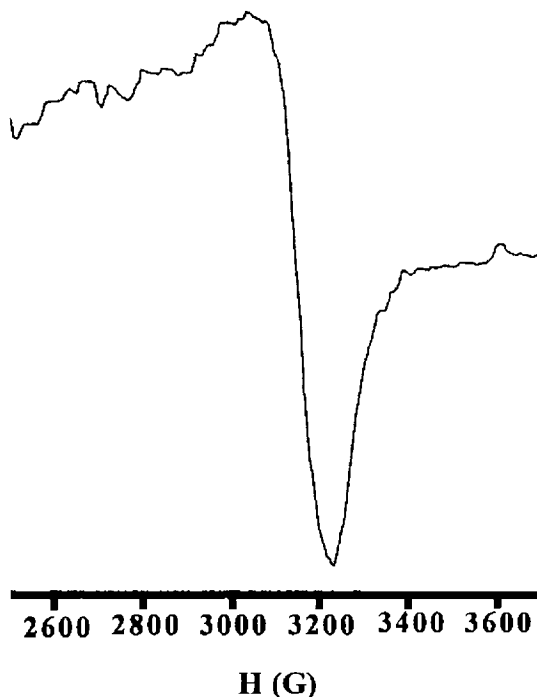
Fig. 3.30. EPR spectrum of compound **9** in polycrystalline state at 298 K.

The spectrum of **9** in solution at 77 K (Fig. 3.31) is a typical axial type, with hyperfine lines in the parallel and perpendicular regions. $g_{\parallel} = 2.262$, $g_{\perp} = 2.052$, $g_{av} = 2.122$, $A_{\parallel} = 172.5 \times 10^4 \, \text{cm}^{-1}$, $A_{\perp} = 76.6 \times 10^4 \, \text{cm}^{-1}$. It should be mentioned here that the splittings observed in the perpendicular region were not well resolved, so the copper hyperfine splitting constant $A_{\perp}$ was calculated by taking one third of the line widths

at half maximum [100,101]. The pattern observed for the g values, $g_{\parallel} > g_{\perp} > 2.0023$ indicates a square planar geometry for Cu(II) with the unpaired electron present in the $d_{x^2-y^2}$ orbital in the ground state.

H (G)
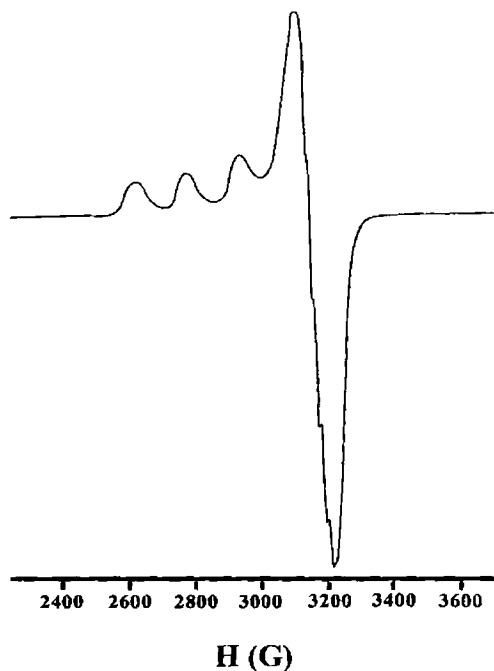
Fig. 3.31. EPR spectrum of compound **9** in DMF at 77 K.

The contribution of the s electrons to the hyperfine interaction can be estimated by the value of Fermi contact hyperfine interaction term (K_0) using the equation [102]:

$$K_0 = A_{iso} / P\beta^2 + (g_{av} - 2.0023) / \beta^2$$

where P is taken as 0.036 cm^{-1}, A_{iso} as $1/3(A_{\parallel} + 2A_{\perp})$ and g_{av} as $1/3(g_{\parallel} + 2g_{\perp})$. K_0 is a dimensionless quantity and is generally found to have a value of 0.3. The value calculated for complex **9** is 0.450,

82

which is in agreement with those estimated by Assour [103] and Abragam and Pryce [104]. The parameter f $(g_{\parallel}/A_{\parallel})$ is found to be 131.1 cm in the present case, which confirms our assumption of a square planar geometry for complex **9**. The $g_{\parallel}$ value implies a fair amount of covalent character in the metal-ligand bond.

The EPR spectrum of compound **10** in the polycrystalline sample at 298 K (Fig. 3.32) was much less informative in interpreting the geometry as the broad spectrum revealed isotropic features, g_{iso} 2.109. The Cu^{2+} signal was very weak and the spectrum was obtained only at very high receiver gains. The above two observations may be due to strong dipolar and exchange interactions between the Cu (II) ions in the unit cell.

2600 2800 3000 3200 3400 3600

H (G)
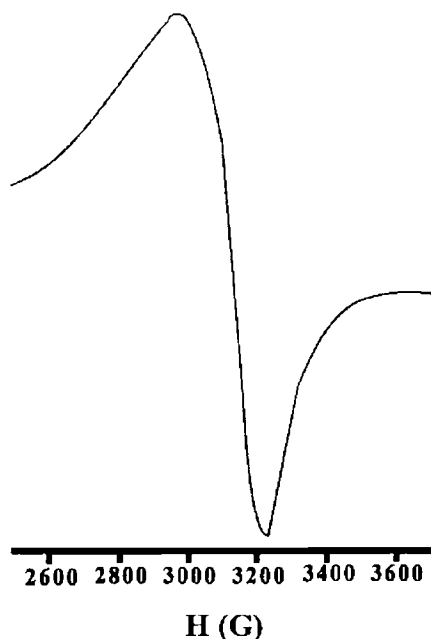
Fig. 3.32. EPR spectrum of compound **10** in polycrystalline state at 298 K.

Complex **10** exhibited an axial spectrum in DMF solution at 77 K (Fig. 3.33). The values of the g factor ($g_{\parallel}$ = 2.257, $g_{\perp}$ = 2.065 and g_{av} = 2.129) are in accordance with an axial symmetry and $d_{x^2-y^2}$ as ground state. This indicates a square pyramidal geometry for Cu(II) in complex **10**.
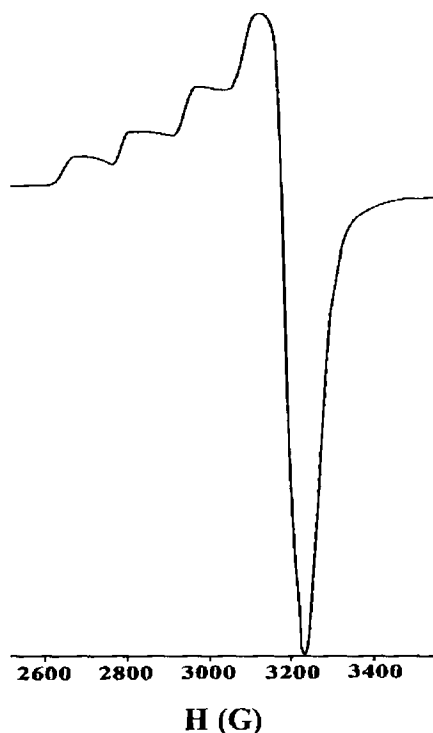
Fig. 3.33. EPR spectrum of compound **10** in DMF at 77 K.

The hyperfine splittings in the $g_{\parallel}$ region are clearly visible with an $A_{\parallel}$ = 147.5 x 10^{-4} cm^{-1}. There is a weak signal at 1680 G with a g value 3.910 corresponding to the half-field ΔM_s = ± 2 forbidden transition, indicating the presence of dimeric system and the presence of magnetic

exchange interaction between the copper ions. The complex has probably undergone a partial dissociation in solution due to the coordination of DMF molecules.

The spectrum of compound **11** in the solid state at 298 K (Fig. 3.34) displayed a very weak Cu^{2+} signal which is quasi-isotropic and centered at g_{iso} = 2.115. This observation may be due to the presence of very strong antiferromagnetic spin-coupling between the Cu^{2+} ions in the solid state. Broad isotropic signals are not informative about the geometry of the complex.
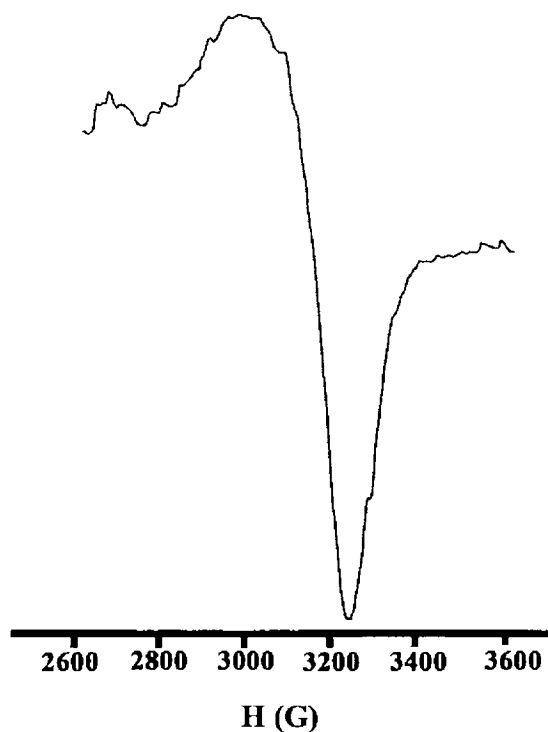
Fig. 3.34. EPR spectrum of compound **11** in polycrystalline state at 298 K.

The spectrum in DMF solution at 77 K (Fig. 3.35) exhibits an axial pattern and the parallel part of the spectrum is well resolved into a set of four hyperfine lines owing to the coupling with the Cu(II) nucleus. $g_{\parallel}$ = 2.249, $g_{\perp}$ = 2.072 and g_{av} = 2.131. $g_{\parallel} > g_{\perp} > 2.0023$ indicates a $d_{x^2-y^2}$ ground state and a square planar geometry for Cu(II). $A_{\parallel}$ = 143.2 x 10^{-4} cm^{-1} for the complex. The value of $g_{\parallel}$ and the bonding parameters confirms significant covalent character for the Cu–N bonds. For the present case f = 157.0 cm, which indicates slight tetrahedral distortion in the square planar complex. The results are in accord with a monomeric square planar Cu(II) complex.
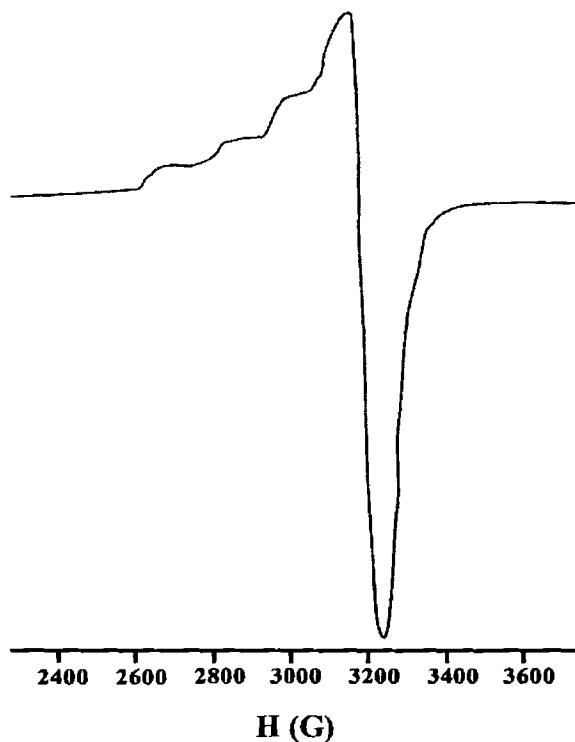
Fig. 3.35. EPR spectrum of compound **11** in DMF at 77 K.

The EPR spectrum of compound **12** in the polycrystalline sample at 298 K was not informative in interpreting the geometry as the spectrum was very broad, which restricted the calculation of the g values. The Cu^{2+} signal was very weak and the spectrum was obtained only at very high receiver gains. The above two observations may be due to strong dipolar and exchange interactions between the Cu(II) ions in the unit cell. The spectrum of **12** in DMF at 77 K (Fig. 3.36) was axial in character, $g_{\parallel} = 2.263$, $g_{\perp} = 2.059$ and $g_{av} = 2.127$.
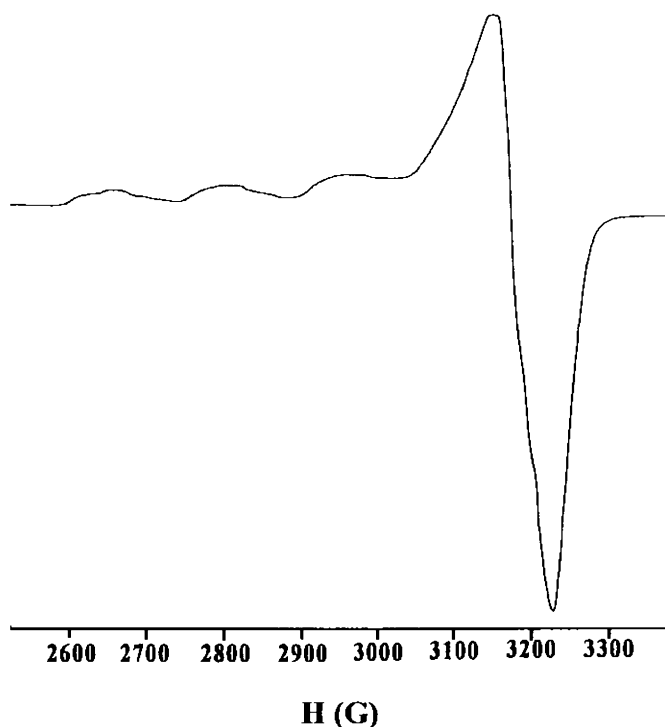
Fig. 3.36. EPR spectrum of compound **12** in DMF at 77 K.

The parallel region is well resolved into a set of seven hyperfine lines as a result of the interaction of the electron spin with the spin of two nuclei of ^{65}Cu ($A_{\parallel}$ = 96.8 x 10^{-4} cm^{-1}). The perpendicular region also shows evidences of hyperfine interaction, but is not well resolved as in the parallel region. So the calculation of $A_{\perp}$ was done by taking one sixth of the line widths at half maximum. $A_{\perp}$ = 19.2 x 10^{-4} cm^{-1}. $g_{\parallel} > g_{\perp} > 2.0023$ points out the square planar structure of the Cu(II) complex with a $d_{x^2 - y^2}$ ground state. The $g_{\parallel}$ value and the bonding parameters show a fair amount of covalency in the metal-ligand bonds. The value of K_0 calculated for complex **12** is 0.1912, which is in agreement with the previous reports.

The EPR spectrum of complex **13** in the solid state at room temperature displayed a very weak signal, which was obtained only at higher receiver gains. This may attributed to very strong antiferromagnetic spin-coupling occurring between the Cu(II) ions in the dimeric complex. G value could not be estimated from the powder spectrum since there was only one broad signal and hence only one g value was obtained. The spectrum was much less informative in interpreting the geometry as the broad spectra revealed quasi-isotropic isotropic features with g_{iso} = 2.223. However, the spectrum measured in solution at 77 K (Fig. 3.37) is axial in character ($g_{\parallel}$ = 2.238, $g_{\perp}$ = 2.052, g_{av} = 2.114) with hyperfine splitting only in the parallel region ($A_{\parallel}$ = 212.5 x 10^{-4} cm^{-1}). The pattern observed for the g values, i.e. $g_{\parallel} > g_{\perp} > 2.0023$ points out the square planar structure of the Cu(II) complex with a $d_{x^2 - y^2}$ ground state. The $g_{\parallel}$ value and the

bonding parameters show a fair amount of covalency in the metal-ligand bonds. In the present case f = 105 cm, an observation which reinforces the assumption of a four coordinate square planar complex. The shape of the spectrum in DMF at 77 K (a dip associated with each hyperfine line) reveals the presence of two types of Cu(II) in solution. This observation is probably due to the dissociation of the dimeric complex by coordination of the solvent molecule replacing the weakest ligated N atom in some of the Cu(II) sites.
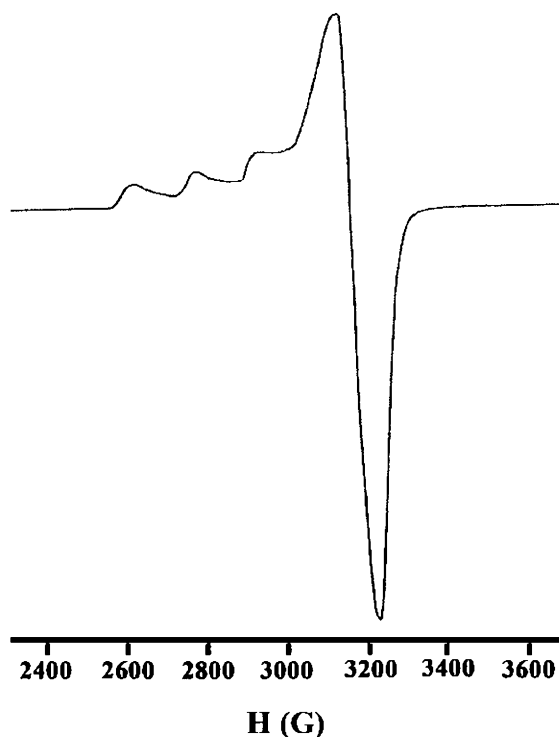
Fig. 3.37. EPR spectrum of compound **13** in DMF at 77 K.

The values of experimental magnetic parameters and the energies of the electronic d-d transitions have been used for evaluating the bonding parameters (molecular orbital coefficients) α^2, β^2 and γ^2. α^2 measures the

89

covalency of the in-plane σ bonds, i.e. the fraction of the unpaired electron density on the copper ion. α^2 was estimated using the expression [78,105].

$$\alpha^2 = -\frac{A_{\parallel}}{0.036} + (g_{\parallel} - 2.0023) + \frac{3(g_{\perp} - 2.0023)}{7} + 0.04$$

where $A_{\parallel}$ is the parallel coupling constant. If the value of $\alpha^2 = 0.5$, it indicates complete covalent bonding, while the value of $\alpha^2 = 1.0$ suggests complete ionic bonding. The calculated values of the bonding parameters for the complexes are within ranges and imply a significant covalent character in the metal-ligand bonds.

The orbital reduction factors $K_{\parallel}$ and $K_{\perp}$ and molecular orbital coefficients β^2 and γ^2 are calculated using expressions [106]:

$$K_{\parallel}^2 = (g_{\parallel} - 2.0023)\frac{\Delta E(d_{xy} \to d_{x^2-y^2})}{8\lambda_0}$$

$$K_{\perp}^2 = (g_{\perp} - 2.0023)\frac{\Delta E(d_{xz}, d_{yz} \to d_{x^2-y^2})}{2\lambda_0}$$

$$K_{\parallel} = \alpha^2\beta^2$$

$$K_{\perp} = \alpha^2\gamma^2$$

where λ_0 is the spin-orbit coupling constant and is of value -828 cm^{-1} for Cu(II) d^9 system, α is the σ bonding, β the in-plane π-bonding and γ, the out-of-plane π-bonding. Hathaway proposed that, for pure σ bonding, $K_{\parallel} \sim K_{\perp} \sim 0.77$; for in-plane π-bonding, $K_{\parallel} < K_{\perp}$ and for out-of-plane π-bonding, $K_{\perp} < K_{\parallel}$ [35]. The values of $K_{\parallel}$ and $K_{\perp}$ calculated for the complexes are listed in Table 3.4.

Table 3.4. Magnetic parameters from the EPR spectra of the copper complexes.

Complex	g	g_{av}	G	A $(10^{-4}\ cm^{-1})$	K	α^2	β^2	γ^2
(1) Solid (298 K)	g_{iso} 2.099	-	-	-	-	-	-	-
(1) DMF (77 K)	$g_{\parallel}$ 2.194 $g_{\perp}$ 2.046	2.096	-	$A_{\parallel}$ 187.8	$K_{\parallel}$ 0.689 $K_{\perp}$ 0.662	0.773	0.892	0.857
(2) Solid (298 K)	g_{iso} 2.102	-	-	-	-	-	-	-
(2) DMF (77 K)	$g_{\parallel}$ 2.238 $g_{\perp}$ 2.059	2.118	-	$A_{\parallel}$ 102.7	$K_{\parallel}$ 0.770 $K_{\perp}$ 0.757	0.585	1.315	1.293
(3) Solid (298 K)	$g_{\parallel}$ 2.136 $g_{\perp}$ 2.065	2.089	2.074	-	-	-	-	-
(3) DMF (77 K)	$g_{\parallel}$ 2.189 $g_{\perp}$ 2.052	2.098	-	$A_{\parallel}$ 191.4	$K_{\parallel}$ 0.678 $K_{\perp}$ 0.704	0.780	0.868	0.901
(4) Solid (298 K)	$g_{\parallel}$ 2.1553 $g_{\perp}$ 2.066	2.096	2.338	-	-	-	-	-
(5) DMF (77 K)	$g_{\parallel}$ 2.245 $g_{\perp}$ 2.065	2.125	-	$A_{\parallel}$ 106.5	$K_{\parallel}$ 0.766 $K_{\perp}$ 0.782	0.606	1.263	1.289
(6) Solid (298 K)	$g_{\parallel}$ 2.219 $g_{\perp}$ 2.078	2.125	2.782	-	-	-	-	-
(6) DMF (77 K)	g_1 1.999 g_2 2.065 g_3 2.269	-	-	A_3 180.0	$K_{\parallel}$ 0.790 $K_{\perp}$ 0.533	0.814	0.970	0.655
(7) Solid (298 K)	$g_{\parallel}$ 2.197 $g_{\perp}$ 2.085	2.123	2.283	-	-	-	-	-
(7) DMF (77 K)	$g_{\parallel}$ 2.197 $g_{\perp}$ 2.072	2.113	-	$A_{\parallel}$ 184.6	$K_{\parallel}$ 0.699 $K_{\perp}$ 0.839	0.777	0.900	1.079

Complex	g	g_{av}	G	A (10^{-4} cm^{-1})	K	α^2	β^2	γ^2
(8) DMF (77 K)	$g_{\parallel}$ 2.242 $g_{\perp}$ 2.052	2.115	-	$A_{\parallel}$ 160.4	$K_{\parallel}$ 0.726 $K_{\perp}$ 0.667	0.776	0.936	0.859
(9) Solid (298 K)	g_{iso} 2.072	-	-	-	-	-	-	-
(9) DMF (77 K)	$g_{\parallel}$ 2.262 $g_{\perp}$ 2.052	2.122	-	$A_{\parallel}$ 172.5 $A_{\perp}$ 76.6	$K_{\parallel}$ 0.751 $K_{\perp}$ 0.663	0.802	0.936	0.826
(10) Solid (298 K)	g_{iso} 2.109	-	-	-	-	-	-	-
(10) DMF (77 K)	$g_{\parallel}$ 2.2574 $g_{\perp}$ 2.0657	2.129	-	$A_{\parallel}$ 147.5	$K_{\parallel}$ 0.781 $K_{\perp}$ 0.779	0.732	1.067	1.064
(11) Solid (298 K)	g_{iso} 2.115	-	-	-	-	-	-	-
(11) DMF (77 K)	$g_{\parallel}$ 2.249 $g_{\perp}$ 2.072	2.131	-	$A_{\parallel}$ 143.2	$K_{\parallel}$ 0.815 $K_{\perp}$ 0.868	0.715	1.140	1.213
(12) DMF (77 K)	$g_{\parallel}$ 2.263 $g_{\perp}$ 2.059	2.127	-	$A_{\parallel}$ 96.8 $A_{\perp}$ 19.2	$K_{\parallel}$ 0.778 $K_{\perp}$ 0.729	0.594	1.309	1.227
(13) Solid (298 K)	g_{iso} 2.223	-	-	-	-	-	-	-
(13) DMF (77 K)	$g_{\parallel}$ 2.238 $g_{\perp}$ 2.052	2.114	-	$A_{\parallel}$ 212.5	$K_{\parallel}$ 0.714 $K_{\perp}$ 0.660	0.888	0.803	0.747

3.4.3c *IR spectral studies*

IR spectroscopy is a useful tool to confirm the coordination of various atoms and groups to the metal atom from the positions and natures of the bands associated with them. However, it cannot be used alone to determine the stereochemistry and has to be coupled with other spectral techniques like EPR, electronic spectroscopy etc.

The IR spectrum of compound **1** (Fig. 3.38) reveals a broad band around 3440 cm^{-1} which corresponds to the lattice water present in the compound. The medium sharp peak at 1598 cm^{-1} is assigned as the v(C=N) stretching mode of the azomethine function of the Schiff base, the position of which is in agreement with the previous reports and is thus indicative of the coordination of azomethine N [25,107]. The band (medium) at 1445 cm^{-1} is attributed to pyridyl ring stretching and the band at 1019 cm^{-1} is due to pyridyl ring breathing. The in-plane ring deformation of the pyridyl ring and the pyridyl ring out-of-plane bending are observed at 652 and 493 cm^{-1} as weak bands. The above observations indicate the pyridyl N coordination.

The most relevant and the interesting bands in the IR spectrum of **1** are those associated with the azido groups. A triplet pattern is seen in the spectrum, with a sharp strong peak at 2080 cm^{-1}, a very strong sharp peak at 2060 cm^{-1} and a strong sharp feature at 2028 cm^{-1}. A single strong peak at 2033 cm^{-1} is observed for sodium azide. A shift from that wavenumber (both to higher and lower wavenumbers) of the v_{as}(N$_3$) stretching of the azide indicates that it must be coordinated. The triplet structure is due to the existence of three different kinds of azido groups. The peaks at higher wavenumbers may be assigned to be due to different kinds of bridging

azides. These different groups may either be both $\mu_{1,1}$ and $\mu_{1,3}$ azide bridges present in the complex or even the asymmetric nature of the complex can reasonably account for the observation of two peaks for any one kind of azide bridge. It seems that the second reason is the most probable on the basis of previous reports [108]. In the absence of X-ray crystal structure results, it is not possible to draw any definite conclusions. The lower peak at 2028 cm^{-1} is due to terminally bound azide. The $v_s(N_3)$ stretching mode of the azide group is observed at 1359 and 1337 cm^{-1} as bands of medium intensity. This also indicates the presence of two kinds of azide groups. The $v_s(N_3)$ vibration mode in inactive in end-to-end bridges which possess high symmetry [109]. The term high symmetry refers to the case where there is very small or negligible difference in the N–N bond lengths of the azide group. The presence of the $v_s(N_3)$ stretching band in the present case rules out the possibility of a highly symmetrical end-to-end azide bridge. The deformation mode of the azido ligand is observed as a weak band at 692 cm^{-1}.
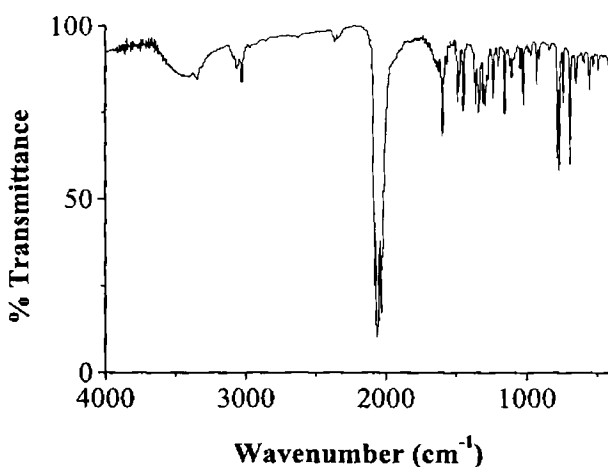
Fig. 3.38. IR spectrum of compound **1**.

A broad band at 3460 cm^{-1} is due to the presence of lattice water in complex **2** (Fig 3.39). The v(C=N) stretch of the azomethine group occurs as a medium band at 1594 cm^{-1} and indicates the azomethine N coordination to the copper. The coordination of the pyridyl nitrogen is confirmed by the presence of pyridyl ring stretch at 1487 cm^{-1}, pyridyl ring breathing at 1027 cm^{-1}, pyridyl in-plane ring deformation at 683 cm^{-1} and pyridyl out-of-plane ring deformation at 415 cm^{-1}.
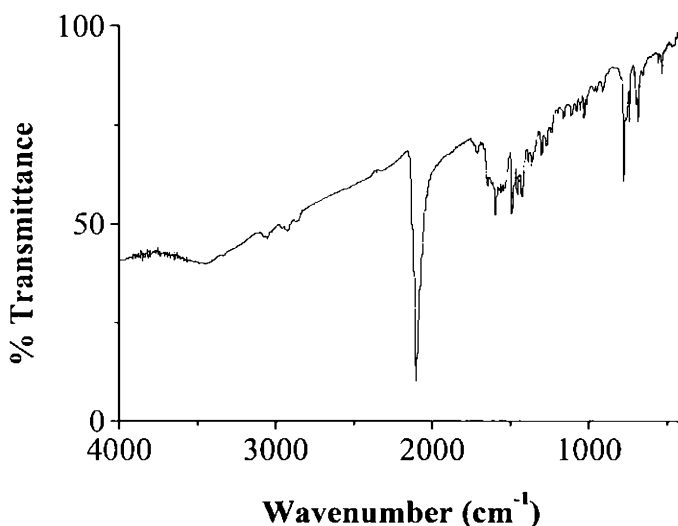
Fig. 3.39. IR spectrum of compound **2**.

The most interesting part of the spectrum is the 2000-2100 cm^{-1} region where the strong absorption bands due to the thiocyanate group is visible. The spectrum of KCNS has a single strong absorption at 2053 cm^{-1} due to the v_{as}(CN) stretching. A shift from this wavenumber evidently indicates the coordination of the NCS group. Several empirical criteria have been developed to determine the bonding mode of thiocyanate ligands in metal complexes.

95

a. The CN stretching frequencies are generally lower in N-bonded complexes (near and below 2050 cm^{-1}) than in S-bonded complexes (near 2100 cm^{-1}) [110]. The bridging (M–NCS–M′) complexes exhibit v(CN) vibrations above 2100 cm^{-1}. But deviations from this rule is frequently observed since v(CN) are affected by many other factors as well [111].

b. v(CS) at 860-780 cm^{-1} are observed for N-bonded and at 720-690 cm^{-1} for S- bonded complexes. But the band due to v(CS) is rather weak and is often obscured by the presence of other bands in the same region [112-114].

c. The N-bonded complex exhibits a single sharp δ(NCS) near 480 cm^{-1}, whereas the S-bonded complex shows bands of low intensity near 420 cm^{-1}. But these bands are also weak and tend to be obscured by other bands [113,114].

The IR spectrum of **2** has a single strong and sharp peak at 2105 cm^{-1} assignable to the v(CN) stretching mode of a thiocyanate group. The number and position of the peak suggests the presence of bridging thiocyanate group. The v(CS) is found at 774 cm^{-1} and the δ(NCS) bending mode is obtained at 533 cm^{-1}.

Complex **3** (Fig. 3.40) shows a medium band at 1600 cm^{-1} assignable to the v(C=N) stretching mode of the azomethine group, indicating the azomethine N coordination. The pyridyl N of the Schiff base is also coordinated as evident from the shifts in the absorption frequencies due to the pyridyl ring. The pyridyl ring stretching is

observed at 1446 cm^{-1}, the breathing mode of the pyridyl ring is at 1025 cm^{-1} and the pyridyl in-plane and out-of-plane ring deformation is at 652 and 416 cm^{-1} respectively. The characteristic $v_{as}(N_3)$ stretch due to the azide ligand is observed as a doublet at 2056 and 2039 cm^{-1}. The band observed at 1581 cm^{-1}, was assigned to be due to the bridging azido group and the one at 2039 cm^{-1} is assigned to the terminal azido group. The $v_s(N_3)$ band at 1339 cm^{-1} suggests the azido bridge to be asymmetric. The bending mode of the azide is observed at 703 cm^{-1}. A broad band at 3440 cm^{-1} is due to the presence of lattice water in the complex.
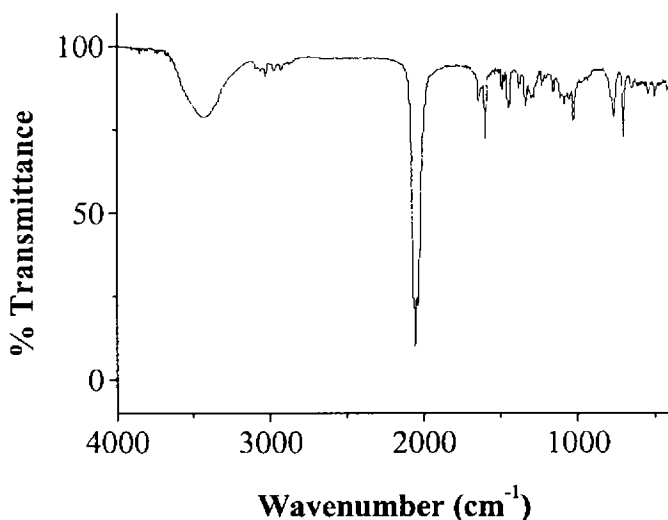
Fig. 3.40. IR spectrum of compound **3**.

Compound **4** (Fig. 3.41) has very strong peaks at 1630 and 1603 cm^{-1}, duly assigned as the $v(C=O)$ and the $v(CN)$ of the amide. The stretching frequencies of the C=O group and the C–N bond suffer shifts to the lower values upon complexation. The absence of the band

corresponding to the $v(NH_2)$ confirms our hypothesis of the formation of the complex **4**. The pyridine N is also coordinated to the metal as evidenced by the peaks at 1448, 1049, 695 and 419 cm^{-1} for the various stretching and deformation modes of the pyridine ring. There are no strong absorptions in the 2100-2000 cm^{-1} region and is in accord with the crystal structure for the complex, in which there are no thiocyanate groups. The crystal structure shows the presence of lattice water, which shows a broad absorption at 3450 cm^{-1}.
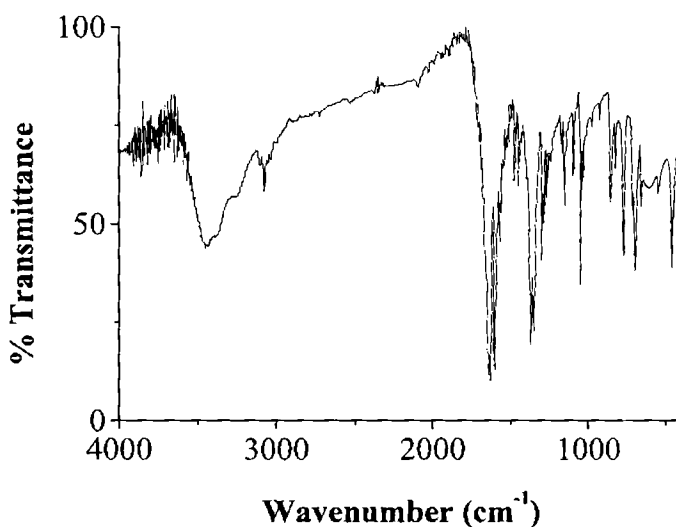
Fig. 3.41. IR spectrum of compound **4**.

The spectrum of **5** (Fig. 3.42) shows a broad band due to $v(NH)$ of the ligand 2-aminopyrimidine at 3350 cm^{-1}. The C=N stretching modes of the pyrimidine ring is at 1607 cm^{-1}. Coordination of azido ligand is confirmed by the presence of four strong bands at 2125, 2095, 2075 and 2054 cm^{-1} for the $v_{as}(N_3)$ stretching vibration. Such an observation is consistent with the presence of both end-to-end and end-

98

on azido bridges in the compound [115]. The azide symmetric stretch, $v_s(N_3)$, appears at about 1300 cm^{-1} in the compounds with the end-on bridging mode. This band is not active for the symmetrical end-to-end coordination mode. For the present compound, it appears at 1346 cm^{-1} due to the presence of end-on bridges in the structure. The band corresponding to the deformation mode (δ) of the azido group can be observed at 652 cm^{-1}.
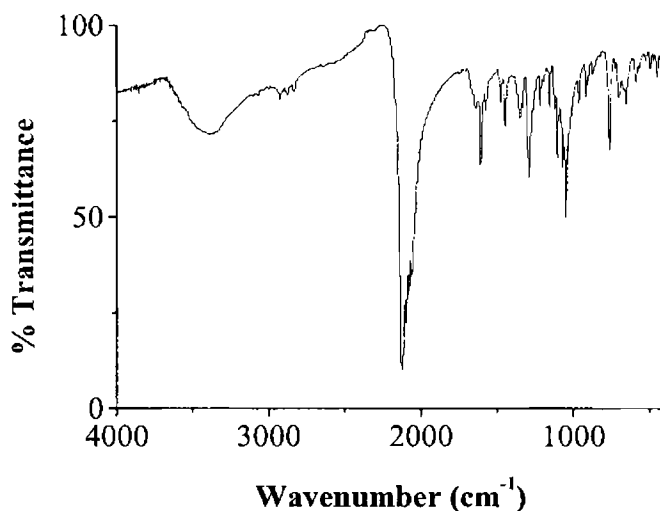
Fig. 3.42. IR spectrum of compound **5**.

Elemental analysis reveals the complex **6** to be formed from the parent aldehyde, pyridine-2-carbaldehyde and not from the Schiff base. IR data supports this statement. The spectrum (Fig 3.43) has a strong band at 1634 cm^{-1} assigned to the v(C=O) of the aldehyde and the shift observed in the frequency compared to that of the free aldehyde confirms its coordination to the metal. The v(C=N) of the pyridine ring is observed at 1603 cm^{-1} and the other characteristic vibrations of the

99

pyridine ring are observed in the usual ranges. The characteristic vibrations due to the thiocyanate group are observed as a complicated pattern consisting of a set of five peaks from 2176-2083 cm^{-1}. It is indicative of the presence of both bridging and terminal NCS ligands in the complex. The lack of single crystal analysis restricts the absolute assignment of these peaks.
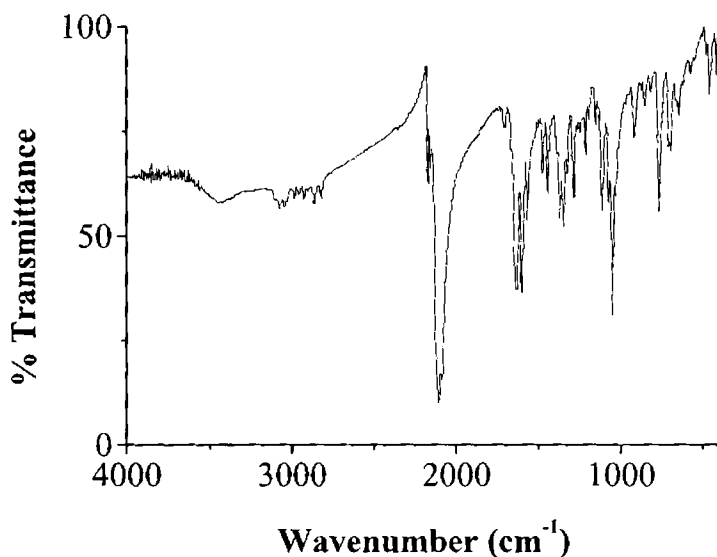
Fig. 3.43. IR spectrum of compound **6**.

Complex **7** (Fig 3.44) exhibits the $v(C=N)$ of the azomethine function of the Schiff base at 1588 cm^{-1} as a medium band. The pyridyl ring vibrations are observed in the usual ranges. The band observed as a doublet at 2055 and 2038 cm^{-1} corresponding to the $v_{as}(N_3)$ stretching suggests the presence of two types of azide groups- bridging and terminal. The $v_s(N_3)$ stretching band at 1333 cm^{-1} confirms the bridging mode of the azide to be end-on since this mode is active for

end-on bridges and inactive for symmetric end-to-end bridges. The bending mode of the azide ligand is observed at 695 cm^{-1}.
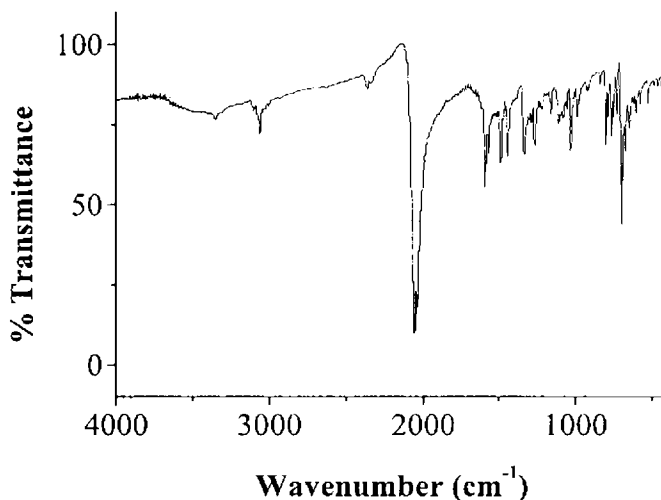
Fig. 3.44. IR spectrum of compound 7.

According to the elemental analysis, the ligand formed between dpk and aniline has undergone hydrolysis to form the unimethylated diol of dpk, which then forms the metal complex **8**. IR data (Fig 3.45) support this observation. The broad and medium intensity band at 3360 cm^{-1} is assigned to the v(OH) vibrations. The broadness and relatively low frequencies of these bands are both indicative of hydrogen bonding [116]. In relation to the absorptions caused by the organic ligand dpk reported previously, it is worth mentioning that the band at 1680 cm^{-1}, assigned to the C=O bond in dpk, is shifted to lower frequencies at 1603 cm^{-1} after solvolysis due to the presence of the C–O bond in the complex [30,117]. The bands assigned to the pyridyl ring stretching modes are also remarkably shifted, relative to the free dpk ligand, due to the loss of coplanarity between the pyridyl rings after

rehybridisation from sp^2 to sp^3. The pyridyl ring stretching modes in the free dpk at 1578 cm^{-1} is shifted to 1439 cm^{-1}, the ring breathing vibrations in dpk at 998 cm^{-1} suffer a negative shift and moves to 1048 cm^{-1}, the pyridyl C–H out-of-plane bending in dpk as a doublet at 753 cm^{-1} and 742 cm^{-1} shifts in the complex to 762 cm^{-1} and the in-plane vibrations of the pyridyl rings shifts to higher frequencies form 662 cm^{-1} to 687 cm^{-1} in the complex. The characteristic $v_{as}(N_3)$ stretching vibrations due to the azide ligand is observed as very strong doublets at 2073 and 2038 cm^{-1}. The presence of two peaks indicates the occurrence of two types of azides in the complex, bridging as well as terminal azide group. The peak at 2073 cm^{-1} is assignable to the bridging azide and the peak at 2038 cm^{-1} is due to terminally bound azide in the complex. The medium band at 1338 cm^{-1} may be assigned to the $v_s(N_3)$ stretch and is suggestive of the bridging azide to be of the end-on type, since the symmetrical $v_s(N_3)$ stretch of end-to-end azide bridge is not IR active.
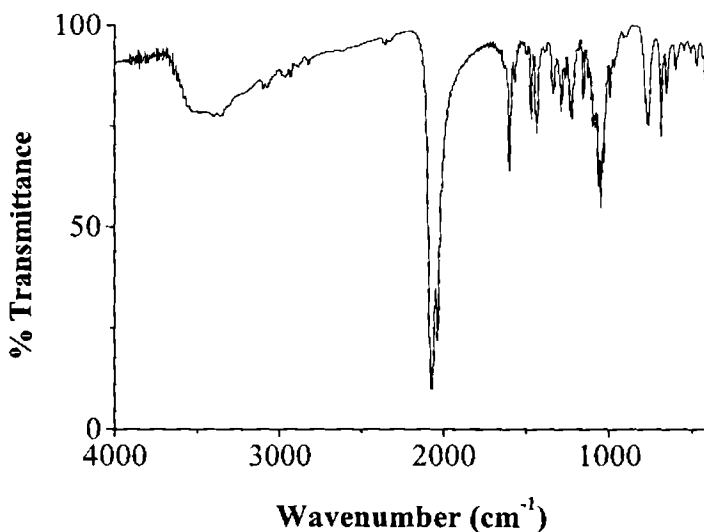
Fig. 3.45. IR spectrum of compound **8**.

In complex **9** (Fig 3.46) also the dpk molecule is coordinating as its unimethylated diol. The IR pattern is very similar to the complex **8** and the main difference lies in the 2100-2000 cm^{-1} region of the spectrum. Complex **9** exhibits a broad band of medium intensity at 3445 cm^{-1} due to the ν(OH) vibrations. The band at 1680 cm^{-1}, assigned to the C=O bond in dpk, is shifted to lower frequencies at 1605 cm^{-1} in the complex due to the conversion to C–O bond on solvolysis. The vibrations of the pyridyl ring in the free ligand also suffers appreciable shift in frequencies upon complexation. In addition a single strong and sharp peak is observed at 2090 cm^{-1}, attributable to the ν(CN) stretching of the N-bonded terminal thiocyanate ligand in the complex. The ν(CS) is at 762 cm^{-1} and the bending vibration of the NCS group is at 473 cm^{-1}, which again confirms the presence of N-bonded terminal NCS group.
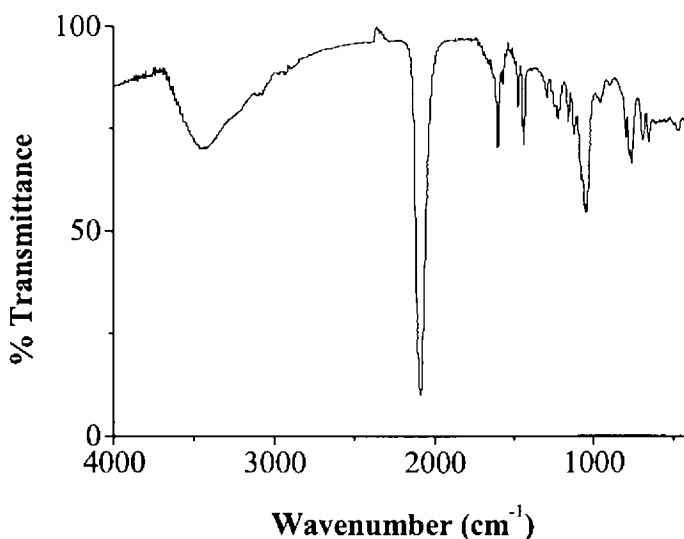
Fig. 3.46. IR spectrum of compound 9.

Complex **10** (Fig. 3.47) has a medium band at 1592 cm^{-1} due to azomethine function, which supports the coordination of imine N to copper. The pyridyl ring vibrations are shifted appreciably in the complex on comparison with the free pyridyl ring and is thus indicative of coordination through pyridyl N. The $v_{as}(N_3)$ stretching vibrations due to the azido ligand exhibits a doublet structure with a very strong band at 2064 cm^{-1}and a strong band at 2032 cm^{-1}. This is consistent with the presence of bridging and terminal azides in the complex. The $v_s(N_3)$ peak at 1340 cm^{-1} rules out the presence of symmetrical end-to-end azide bridges as their $v_s(N_3)$ stretching vibration is IR inactive. So the bridging azide is confirmed as an end-on azide bridge. The bending mode of the azido ligand is observed at 691 cm^{-1}.
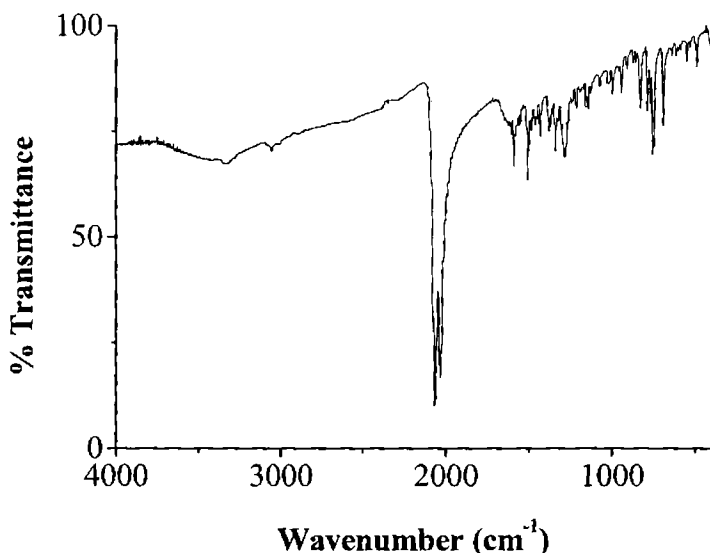
Fig. 3.47. IR spectrum of compound **10**.

In the thiocyanate complex **11** (Fig 3.48), the medium intensity peak at 1591 cm^{-1} is assigned to the absorption of the azomethine function and indicates its coordination. The pyridyl vibrations are observed in the usual ranges and suggest the coordination of pyridyl N. A very strong peak at 2109 cm^{-1} is due to the v(CN) stretching of the thiocyanate group. The position of the peak and its structure (singlet) points out to the presence of N-bonded terminal thiocyanate group in the complex. The v(CS) of the NCS ligand at 748 cm^{-1} and the bending vibration of the NCS group is at 492 cm^{-1} also indicates coordination through N atom of the terminal NCS ligand.
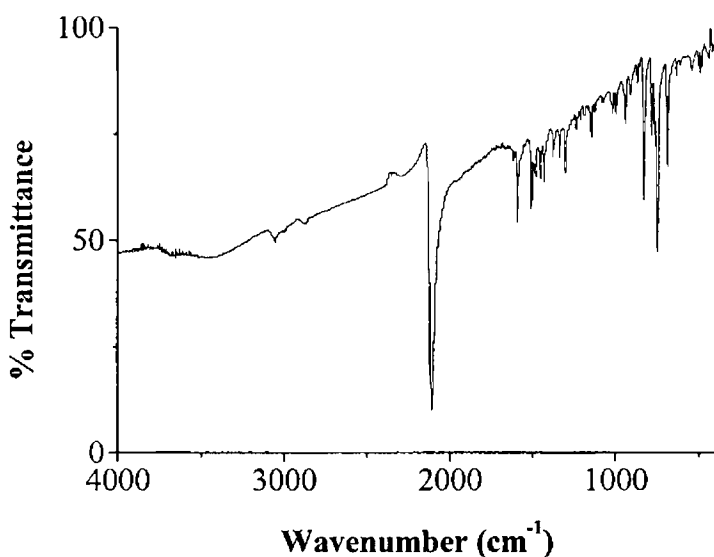
Fig. 3.48. IR spectrum of compound **11**.

The IR spectrum of compound **12** (Fig. 3.49) can be compared with the spectrum of the ligand Hhmba and the differences in the frequencies of various functions and groups can be regarded as the evidence for coordination. The spectrum of ligand has a broad band

105

at 3440 cm^{-1} due to the stretching mode of the O−H group in the ligand. This band is absent in the complex, which means that the deprotonation of the ligand has taken place the oxygen atom is bonded to the metal. The v(C=N) stretching vibration of the azomethine function is observed as a band of medium intensity at 1624 cm^{-1} in the ligand. This band shifts by about 30 cm^{-1} and is seen as a medium intensity band at 1585 cm^{-1} in the spectrum of the complex. This is a very good evidence for the coordination of the azomethine N. Thus, the deprotonated ligand coordinates to the copper ion through the O atom and the azomethine N.
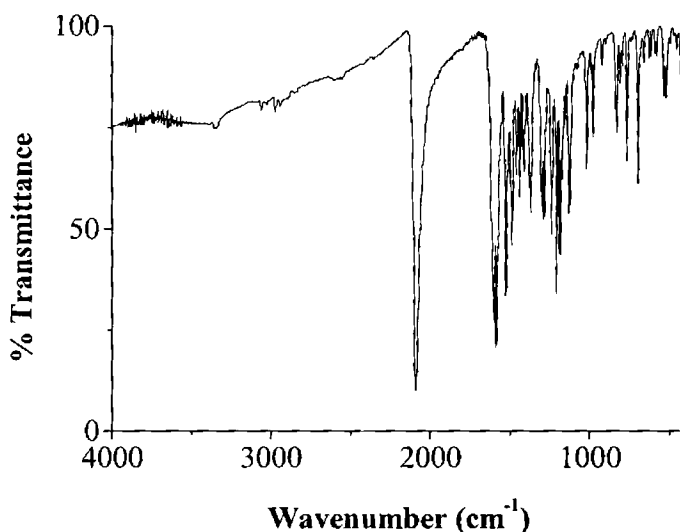
Fig. 3.49. IR spectrum of compound **12**.

The bands assignable to the v_{as}(N$_3$) stretching of the azido ligand is visible as a very strong band at 2090 cm^{-1}. The singlet structure of this band indicates the presence of one type of azide in the complex and the high frequency of absorption suggests that the azide ligand is in the form of bridges. The presence of a medium intensity band at 1369 cm^{-1},

assignable to the symmetric stretching of the azide indicates that the azide bridges are probably of the end-on type since this mode is IR inactive for the end-to-end bridges. The bending vibration of the azide is seen at 695 cm^{-1} as a weak band.

The IR spectrum of complex **13** (Fig 3.50) lacks the band due to the stretching vibrations of the O–H group indicative of the deprotonation of the ligand and coordination through the O atom. The v(C=N) stretching vibration of the azomethine function is observed as a band of medium intensity at 1624 cm^{-1} in the ligand. This shifts to lower frequency and is observed at 1606 cm^{-1} in the complex. In addition a single strong and sharp peak is observed at 2119 cm^{-1}, attributable to the v(CN) stretching of the thiocyanate ligand in the bridged coordination mode in the complex. The v(CS) band is at 837 cm^{-1} and the bending vibration of the NCS group is at 453 cm^{-1}.
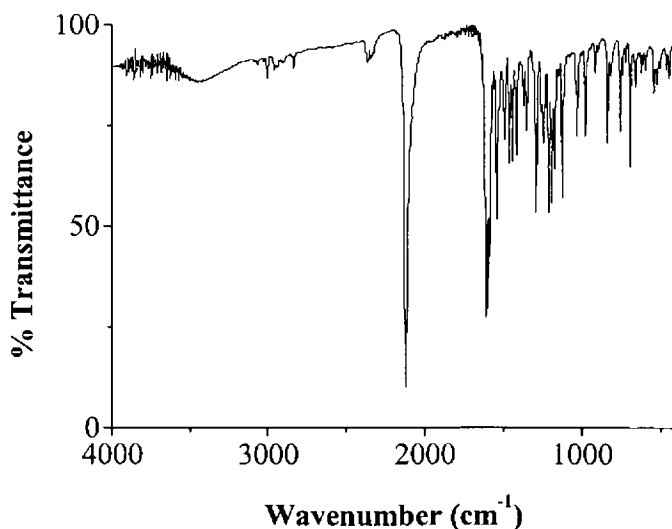
Fig. 3.50. IR spectrum of compound **13**.

References

[1]   R.R. Gay, R.S. Himmelwright, N.C. Eickman, V.A. Norris, H.C. Freeman, E.I. Solomon, J. Am. Chem. Soc. 103 (1981) 4382.

[2]   E.I. Solomon, K.W. Penfield, D.E. Wilcox, Struct. Bonding 53 (1983) 1.

[3]   B. Abolmaali, H.V. Taylor, U. Weser, Struct. Bonding 91 (1998) 91.

[4]   A. Messerschmidt, Struct. Bonding 90 (1998) 37.

[5]   R. Osterberg, Coord. Chem. Rev. 12 (1974) 309.

[6]   J.A. Fee, Struct. Bonding 23 (1975) 1.

[7]   H. Beinert, Coord. Chem. Rev. 23 (1977) 119.

[8]   E.L. Ulrich, J.L. Markey, Coord. Chem. Rev. 27 (1978) 109.

[9]   I. Bertini, G. Canti, R. Grassi, Inorg. Chem. 19 (1980) 2198.

[10]   H. Yokoi, A. Addison, Inorg. Chem. 16 (1977) 1341.

[11]   H. Yokoi, Bull. Chem. Soc. Jpn. 47 (1974) 3037.

[12]   I. Solomon, L.B. La Croix, D.W. Randall, Pure Appl. Chem. 70 (1998) 799.

[13]   K. Pierleot, J.O.A. De Kerpel, U. Ryde, M.H.M. Olsson, B.O. Roos, J. Am. Chem. Soc. 120 (1998) 13156.

[14]   E.I. Solomon, U.M. Sundaram, T.E. Machonkin, Chem. Rev. 96 (1996) 2563.

[15]   K.A. Magnus, H. Ton-That, J.E. Carpenter, Chem. Rev. 94 (1994) 727.

[16]   E.I. Solomon, M.J. Baldwin, M.D. Lowery, Chem. Rev. 92 (1992) 521.

[17]   M. Trémoliéres, J.G. Bieth, Phytochemistry 23 (1984) 501.

[18] A. Rompel, H. Fisher, K. Büldt-Karentzopoulos, D. Miewes, F. Zippel, H.F. Nolting, C. Hermes, B. Krebs, H. Witzel, J. Inorg. Biochem. 59 (1995) 715.

[19] J.L. Cole, P.A. Clark, E.I. Solomon, J. Am. Chem. Soc. 112 (1990) 9534.

[20] J.L. Cole, L. Avigliano, L. Morpurgo, E.I. Solomon, J. Am. Chem. Soc. 113 (1991) 9080.

[21] V. Mckee, M. Zvagulis, J.V. Dagdigian, M.G. Patch, C.A. Reed, J. Am. Chem. Soc. 106 (1984) 4765.

[22] V. Mckee, J.V. Dagdigian, R. Bau, C.A. Reed, J. Am. Chem. Soc. 103 (1981) 7000.

[23] O. Kahn, Molecular Magnetism, VCH, New York (1993).

[24] J. Miller, M. Drilon (Eds.), Magnetism: Molecules to Materials, Wiley-VCH, Weinheim (2002).

[25] E.-Q, Gao, Y.-F. Yue, S.-Q. Bai, Z. He, C.-H. Yan, Cryst. Growth Design 5 (2005) 1119.

[26] H.-R. Wen, C.-F. Wang, Y. Song, J.-L. Zuo, X.-Z. You, Inorg. Chem. 44 (2005) 9039.

[27] A. Rodriguez, H. Sakiyama, N. Masciocchi, Inorg. Chem. 44 (2005) 8399.

[28] P. Kulkarni, S. Padhye, E. Sinn, Inorg. Chim. Acta 332 (2002) 167.

[29] S.R. Breeze, S. Wang, J.E. Greedan, N.P. Raju, Inorg. Chem. 35 (1996) 6944.

[30] Z.E. Serna, R. Cortés, M.K. Urtiaga, M.G. Barandika, L. Lezama, M.I. Arriortua, T. Rojo, Eur. J. Inorg. Chem. (2001) 865.

[31] B.J. Hathaway, G. Wilkinson, R.D. Gillard, J.A. McCleverty, Comprehensive Coordination Chemistry 5 (1987) 558.

[32] M. Menon, A. Pramanik, N. Bag, A. Chakravorty, Inorg. Chem. 33 (1994) 403.

[33] B.K. Dirghangi, M. Menon, A. Pramanik, A. Chakravorty, Inorg. Chem. 36 (1997) 1095.

[34] K.Watanabe, S. Komiya, S.Suzuki, Bull. Chem. Soc. Jpn. 46 (1973) 2792.

[35] L. Seiroń, M. Bukowska-Strzyżewska, Acta Cryst. C53 (1997) 296.

[36] L. Seiroń, M. Bukowska-Strzyżewska, Acta Cryst. C55 (1999) 491.

[37] I. Castro, J. Faus, M. Julve, J.M. Amigó, J. Sletten, T. Debaerdemaeker, J. Chem. Soc., Dalton Trans. 3 (1990) 891.

[38] V. Rattanaphani, W.R. McWhinnie, Inorg. Chim. Acta 9 (1974) 239.

[39] G.S. Papaefstathiou, A. Escuer, C.P. Raptopoulou, A. Terzis, S.P. Perlepes, R. Vicente, Eur. J. Inorg. Chem. (2001) 1567.

[40] J.M. Seco, M. Quirós, M.J.G. Garmendia, Polyhedron 19 (2000) 1005.

[41] M.C. Feller, R.Robson, Aust. J. Chem. 21 (1968) 2919.

[42] M. C. Feller, R. Robson, Aust. J. Chem. 23 (1970) 1997.

[43] S. Mackay, C.J. Gilmore, C. Edwards, N. Stewart, K. Shankland, maXus Computer Program for the Solution and Refinement of Crystal Structures, Bruker Nonius, The Netherlands, Mac-Science, Japan and The University of Glasgow (1999).

[44] G. M. Sheldrick, Acta Cryst. A46 (1990) 467.

[45] G. M. Sheldrick, Program for the solution of Crystal Structures, University of Göttingen, Göttingen, Germany (1997).

[46] K. Bradenburg, H. Putz, DIAMOND Version 3.0, Crystal Impact, GbR, Postfach 1251, D-53002 Bonn, Germany (2004).

[47] L. Seiroń, Acta Cryst. E60 (2004) m297.

[48] I. Uçar, A. Bulut, O.Z. Yeşilel, H. Ölmez, O. Büyükgügör, Acta Cryst. E60 (2004) m1945.

110

[49]   I.M. Procter, B.J. Hathaway, P. Nicholls, J. Chem. Soc. A (1968) 1678.

[50]   B.J. Hathaway, M.J. Bew, D.E. Billing, R.J. Dudley, P. Nicholls, J. Chem. Soc. A (1969) 2312.

[51]   B.J. Hathaway, D.E. Billing, R.J. Dudley, J. Chem. Soc. A (1970) 1420.

[52]   B.J. Hathaway, A.A.G. Tomlinson, Coord. Chem. Rev. 5 (1970) 1.

[53]   B.J. Hathaway, D.E. Billing, Coord. Chem. Rev. 5 (1970) 143.

[54]   B.J. Hathaway, Struct. Bonding 14 (1973) 49.

[55]   M. Menon, A. Pramanik, N. Bag, A. Chakravorty, Inorg. Chem. 34 (1995) 3310.

[56]   S. Banerjee, B.K. Dirghangi, M. Menon, A. Pramanik, A. Chakravorty, J. Chem. Soc., Dalton Trans. (1997) 2149.

[57]   Z.-H. Ni, H.-Z. Kou, L.-F. Zhang, C. Ge, R.-J. Wang, A.-L. Cui, J. Chem. Cryst. 36 (2006) 465.

[58]   G. De Munno, M. Julve, F. Lliret, J. Faus, M. Verdaguer, A. Caneschi, Inorg. Chem. 34 (1995) 157.

[59]   J.E. Huheey, E.A. Keiter, R.L. Keiter, Inorganic Chemistry, Principles of Structure and Reactivity, 4th ed., Harper Collins College Publishers, New York (1993).

[60]   D.N. Sathyanarayana, Electronic Absorption Spectroscopy and Related Techniques, Universities Press Publishers, India (2001).

[61]   B.J. Hathaway, R.J. Dudley, P. Nicholls, J. Chem. Soc. A (1969) 1845.

[62]   B.J. Hathaway, I.M. Procter, R.S. Slade, A.A. Tomlinson, J. Chem. Soc. A (1969) 2219.

[63]   R.J. Dudley, B.J. Hathaway, J. Chem. Soc. A, (1970) 1725.

[64]   A.B.P. Lever, Inorganic Electronic Spectroscopy, 2nd ed., Elsevier Science, Netherlands (1984).

[65] M.A.S. Goher, T.C.W. Mak, Inorg. Chim. Acta 85 (1984) 117.

[66] M.A.S. Goher, T.C.W. Mak, Inorg. Chim. Acta 89 (1984) 119.

[67] M.A.S. Goher, M.A.M. Abu-Youssef, F.A. Mautner, Polyhedron 17 (1998) 3305.

[68] B.J. Hathaway, J. Chem. Soc., Dalton Trans. (1972) 1196.

[69] P.R. Athappan, C. Rajagopal, Polyhedron 15 (1996) 527.

[70] I. Bertini, D. Gattesern, A. Scozzafava, Coord. Chem. Rev. 29 (1979) 67.

[71] J.C. Eisenstein, J. Chem. Phys. 28 (1958) 323.

[72] N.J. Bunce, J. Chem. Educ. 64 (1987) 907.

[73] F. Agaki, Y. Nakao, K. Matsumoto, S. Takamizawa, W. Mori, S. Suzuki, Chem. Lett. (1997) 181.

[74] Y. Song, C. Massera, O. Roubeau, P. Gamez, A.M.M. Lanfredi, J. Reedijk Inorg. Chem. 43 (2004) 6842.

[75] M.J. Bew, B.J. Hathaway, R.R. Faraday, J. Chem. Soc., Dalton Trans. (1972) 1229.

[76] E. Garribba, G. Micera, J. Chem. Educ. 83 (2006) 1229.

[77] D.E. Nickless, M.J. Power, F.L. Vrbach, Inorg. Chem. 22 (1983) 3210.

[78] D. Kivelson, R. Neiman, J. Chem. Phys. 35 (1961) 149.

[79] T.D. Smith, J. Pilbrow, Coord. Chem. Rev. 13 (1974) 173.

[80] J.F. Villa, W.E. Hatfield, Inorg. Chem. 11 (1972) 1331.

[81] J. García-Tojal, L. Lezama, J.L. Pizarro, M. Insausti, M.I. Arriortua, T. Rojo, Polyhedron 18 (1999) 3703.

[82] A. Hudson, J. Mol. Phys. 10 (1966) 575.

[83] I.B. Bersuker, Coord. Chem. Rev. 14 (1975) 357.

[84] M. Maajan, K.N. Saxena, C.P. Saxena, J. Inorg. Nucl. Chem. 43 (1981) 2148.

[85] K.K. Sharma, S. Chandra, Trans. Met. Chem. 9 (1984) 401.

[86] Z.-W. Mao, Q.-W. Hang, W.-X. Tang, S.-X. Liu, Z.-M. Wang, J.-J. Huang, Polyhedron 15 (1996) 321.

[87] S. Sikorav, I.B. Waksman, O. Kahn, Inorg. Chem. 23 (1984) 490.

[88] G.D. Munno, M. Julve, F. Lloret, J. Faus, M. Verdaguer, A. Caneschi, Inorg. Chem. 34 (1995) 157.

[89] U. Sakaguchi, A.W. Addison, J. Chem. Soc., Dalton Trans. (1970) 600.

[90] S. Chandra, L.K. Gupta, Spectrochim. Acta A61 (2005) 269.

[91] R.N. Patel, N. Singh, V.L.N. Gundla, Polyhedron 25 (2006)3312.

[92] B.A. Sastry, S. Md. Asadullah, G. Ponticelli, G. Devoto, J. Mol. Struct. 71 (1981) 343.

[93] B. Scott, U. Geiser, R.D. Willett, B. Patyal, C.P. Landee, R.E. Greeney, T. Manfredini, G.C. Pellacani, A.B. Corradi, L.P. Battaglia, Inorg. Chem. 27 (1988) 2454.

[94] J.A.R. Navarro, M.A. Romero, J.M. Salas, M. Quiros, E.R.T. Tiekink, Inorg. Chem. 36 (1997) 4988.

[95] Y. Song, C. Massera, M. Quesada, A.M.M. Lanfredi, I. Mutikainen, U. Turpeinen, J. Reedijk, Inorg. Chim. Acta 358 (2005) 1171.

[96] M.A.S. Goher, N.A. Al-Salem F.A. Mautner, Polyhedron 15 (1996) 4513.

[97] M.A.S. Goher, F.A. Mautner, N.A. Al-Salem, Polyhedron 16 (1997) 2239.

[98] M.A.S. Goher, F.A. Mautner, Z. Naturforsch. 46B (1991) 687.

[99] F.A. Mautner, M.A.S. Goher, Polyhedron 12 (1993) 2823.

[100] P.S. Zacharias, J.M. Elizabathe, A. Ramachandraiah, Indian J. Chem. 23A (1984) 26.

[101] B. Swamy, J.R. Swamy, Trans. Met. Chem. 16 (1991) 35.

[102] L.S. Lund, J.B. Raynor, J. Chem. Soc., Dalton Trans. (1975) 2477.

[103] M. Assour, J. Chem. Phys. 43 (1965) 2477.

[104] A. Abragam, M.H.L. Pryce, Proc. R. Soc. London Sect. A 206 (1961) 164.

[105] A.H. Maki, B.R. McGarvey, J. Chem. Phys. 29 (1958) 35.

[106] M. Joseph, M. Kuriakose, M.R.P. Kurup, E. Suresh, A. Kishore, S.G. Bhat, Polyhedron 25 (2006) 61.

[107] E.-Q, Gao, S.-Q. Bai, Y.-F. Yue, Z.-M. Wang, C.-H. Yan, Inorg. Chem. 39 (2003) 3642.

[108] S.S. Tandon, L.K. Thompson, M.E. Manuel, J.N. Bridson, Inorg. Chem. 22 (1994) 5555.

[109] J. Nelson, S.M. Nelson, J. Chem. Soc. A (1969) 1597.

[110] P.C.H. Mitchell, R.J.P. Williams, J. Chem. Soc. (1960) 1912.

[111] R.A. Bailey, S.L. Kozak, T.W. Michelsen, W.N. Mills, Coord. Chem. Rev. 6 (1971) 407.

[112] A. Turco, C. Pecile, Nature (London), 191 (1961) 66.

[113] J. Lewis, R.S. Nyholm, P.W. Smith, J. Chem. Soc. (1961) 4590.

[114] A. Sabatini, I. Bertini, Inorg. Chem. 4 (1965) 959.

[115] R. Cortés, M. Drillon, X. Solans, L. Lezama, T. Rojo, Inorg. Chem. 36 (1997) 677.

[116] G.S. Papaefstathiou, A. Escuer, F.A. Mautner, C. Raptopoulou, A. Terzis, S.P. Perlepes, R. Vicente, Eur. J. Inorg. Chem. (2005) 879.

[117] R.R. Osborne, W.R. Mc Whinnie, J. Chem. Soc. A (1967) 2075.

✸✸✸✸℘ℭ✸✸✸✸

Syntheses, structural and spectral investigations of manganese(II) complexes of Schiff bases with azide and thiocyanate

4.1 Introduction

Manganese is relatively abundant element, constituting about 0.085% of the earth's crust. Manganese complexes play important roles ranging from bioinorganic chemistry to solid-state physics. Particularly, over the past decade there has been a considerable interest in synthesizing biomimetic complexes that can act as manganoenzymes such as superoxide dismutase (SOD) [1]. Interest in manganese complexes of varying nuclearities continues to be stimulated by the presence of manganese at the active sites of biological systems such as photosystem II in green plants, ribonucleotide reductase, superoxide dismutase, and the Mn catalases [2-9], the variability in magnetic behavior of polynuclear manganese clusters, which for some systems has been exploited in the development of information storage devices [10-12] and the use of such complexes as catalysts for bleaching and organic synthesis [13-15].

Manganese plays a major key role in many biological redox processes, including water oxidation complex in photosystem II, decomposition of O_2^- radicals catalysed by superoxide dismutases (SODs) and disproportionation of hydrogen peroxide (catalase activity)

in microorganisms, a reaction which is important for cell detoxification. In all these diverse biologically important roles of manganese, it is present either as mononuclear (SOD, manganese dioxygenase) or polynuclear species (WOC, tetranuclear), catalase and ribonucleotide reductase (binuclear). In manganese biosystems, the azide ion is known to inihibit the superoxide dismutation in mononuclear superoxide dismutases *via* binding to the metal at the active site in both the Mn(II) and Mn(III) oxidation states [16]. The function of dinuclear active sites in Mn catalases, which catalyze the conversion of toxic peroxide to oxygen and water in certain bacteria, is also dramatically inhibited by azide [17-22].

Gao *et al.* reports the structure and magnetism of Mn(II) one dimensional coordination polymers built from azide bridges and Schiff base obtained by the condensation of pyridine-2-carbaldehyde with aniline and its derivatives [23]. The complexes synthesized contain alternating end-on and end-to-end azide bridges, which mediate alternating ferromagnetic and antiferromagnetic exchange interactions respectively. Wen and coworkers prepared one dimensional chiral coordination polymers of manganese(II) using azide and a Schiff base (obtained from pyridine-2-carbaldehyde and 1-phenylethyl amine) as the auxiliary ligand [24]. In these complexes, there is weak antiferromagnetic coupling between Mn(II) ions. The use of di-2-pyridyl ketone in conjugation with dicyanamide and azide gave cubane and defective double-cubane clusters of Mn(II) respectively, both of which are found to be antiferromagnetic in nature [25,26].

4.2   Stereochemistry

Manganese shows a wide range of oxidation states ranging from (-III) to (+VII). The divalent state is the most common and most stable oxidation state. The usually exhibited geometry is octahedral. Manganese(II) complexes, in general, belong to a high-spin d^5 system with a ^6S ground state, which do not have strong stereochemical preferences and can exist both in tetrahedral and octahedral coordination environment depending on the structural demand of the coordinated ligands. Five coordinate manganese(II) complexes have also been reported.

4.3   Experimental

4.3.1 Materials

Pyridine-2-carbaldehyde (Sigma Aldrich), di-2-pyridyl ketone (Sigma Aldrich), aniline (S. D. Fine), R-1-phenylethyl amine (Alfa Aeser), $Mn(ClO_4)_2 \cdot 6H_2O$ (Sigma Aldrich), $Mn(OAc)_2 \cdot 4H_2O$ (Merck), $MnCl_2 \cdot 4H_2O$ (Sigma Aldrich), NaN_3 (Reidel-De Haen), KCNS (BDH) and methanol (Merck) were used as received.

4.3.2 Syntheses of manganese(II) complexes

$Mn_2(paa)_2(N_3)_4$ (14): A mixture of pyridine-2-carbaldehyde (0.107 g, 1 mmol) in methanol and aniline (0.093 g, 1 mmol) in methanol were refluxed for 2 hours. To this $Mn(ClO_4)_2 \cdot 6H_2O$ (0.362 g, 1 mmol) dissolved in methanol was added and stirred followed by the slow addition of an aqueous solution of NaN_3 (0.130 g, 2 mmol). The resulting solution was further stirred for 15 minutes to obtain an orange

precipitate. It was then filtered, washed with water, methanol and finally with ether and dried over P_4O_{10} *in vacuo*. Elemental Anal. Found (Calcd.) (%): C, 44.54 (44.87); H, 3.14 (3.14); N, 34.70 (34.89). μ = 5.06 B.M.

[Mn(paa)₂(NCS)₂]·³/₂H₂O (15): A mixture of pyridine-2-carbaldehyde (0.107 g, 1 mmol) in methanol and aniline (0.093 g, 1 mmol) in methanol were refluxed for 2 hours. $Mn(OAc)_2 \cdot 4H_2O$ (0.245 g, 1 mmol) dissolved in methanol and solid KCNS (0.194 g, 2 mmol) was added to this and refluxed for 4 hours. A pale brown solid separated out after two days from the reaction mixture, which was filtered, washed with water, methanol and ether and dried over P_4O_{10} *in vacuo*. Elemental Anal. Found (Calcd.) (%): C, 54.93 (55.51); H, 3.69 (4.12); N, 15.42 (14.94); S, 12.25 (11.40). μ = 6.05 B.M.

Mn(papea)₂(NCS)₂ (16): Pyridine-2-carbaldehyde (0.107 g, 1 mmol) and *R*-1-phenylethyl amine (0.121 g, 1 mmol) were refluxed in methanol for 2 hours. A methanolic solution of $MnCl_2 \cdot 4H_2O$ (0.198 g, 1 mmol) and solid KCNS (0.194 g, 2 mmol) was added to this and refluxed 4 hours. The yellow single crystals suitable for X-ray diffraction were isolated within two days in appreciable yield, which were mechanically separated and dried. Elemental Anal. Found (Calcd.) (%): C, 60.64 (60.90); H, 4.66 (4.77); N, 14.16 (14.20). μ = 5.92 B.M.

[Mn(dpka)₂(NCS)₂]·¹/₂H₂O (17a) and **Mn(dpka)₂(NCS)₂ (17b):** Di-2-pyridyl ketone (0.187 g, 1 mmol) was dissolved in methanol and

aniline (0.093 g, 1 mmol) was added to this. About 4-5 drops of glacial acetic acid was also added and refluxed for 6 hours. To the above solution, $Mn(OAc)_2 \cdot 4H_2O$ (0.245 g, 1 mmol) dissolved in methanol was added. An aqueous solution of KCNS (0.194 g, 2 mmol) was also added. The resulting solution was refluxed for 2 hours. An orange colored crystalline product (17a) was obtained within a week, filtered, washed with ether and dried over P_4O_{10} *in vacuo*. The filtrate on evaporation yielded orange X-ray quality single crystals of 17b. Elemental Anal. of 17a. Found (Calcd.) (%): C, 61.77 (61.88); H, 3.82 (3.89); N, 16.10 (16.04). Elemental Anal. of 17b. Found (Calcd.) (%): C, 62.95 (62.69); H, 3.56 (3.80); N, 15.98 (16.25). $\mu = 5.73$ B.M.

Caution! Although not encountered in our experiments, azide complexes are potentially explosive. Only a small amount of the material should be prepared, and it should be handled with care.

4.4 Results and discussion

The condensation of aldehyde/ketone and amine in 1:1 molar ratio yielded the Schiff base ligands, which were used without further purification for the synthesis of the complexes by reaction in presence of pseudohalides NaN_3/KCNS. All the complexes had the Schiff bases as neutral bidentate *N, N* donor ligands. Even though the Schiff base obtained by the condensation between di-2-pyridyl ketone and aniline has an additional N atom, that N is not coordinated to the metal as evidenced by the crystal studies of **17b**. The compound **17a** separated out from the reaction medium and the filtrate gave out X-ray quality crystals of **17b**. The elemental

analyses indicate that the difference between **17a** and **17b** is the presence of water of crystallization in **17a**, where as in **17b**, it is absent. Because of the absence of sufficient quantity **17b**, the spectral studies were performed using **17a** only.

The room temperature magnetic susceptibility measurements of the compounds **15-17** showed values for magnetic moments in the range 5.73 – 6.05 B.M., which are indicative of a high spin d^5 system [27]. The magnetic moment of compound **14** had a lower value, probably because of interaction between the metal centers. All the complexes were found to be soluble in DMF, DMSO and acetonitrile, but only partially soluble in other organic solvents such as $CHCl_3$, ethanol, methanol etc.

4.4.1 Crystallographic data collection and structure analyses

Single crystal X-ray diffraction measurements of complexes **16** and **17b** were carried out on a Bruker Smart Apex 2 CCD area detector diffractometer at the X-ray Crystallography Unit, School of Physics, Universiti Sains Malaysia, Penang, Malaysia. The unit cell parameters were determined and the data collections were performed using a graphite-monochromated MoKα (λ = 0.71073 Å) radiation at a detector distance of 5 cm at 100(1) K with the Oxford Cyrosystem Cobra low-temperature attachment. The collected data were reduced using SAINT program [28] and the empirical absorption corrections were performed using SADABS program [28]. The structures were solved by direct methods and refinement was carried out by full-matrix least squares on

F^2 using the SHELXTL software package [29]. All non-hydrogen atoms were refined anisotropically. Hydrogen atoms were geometrically fixed at calculated positions and allowed to ride on their parent atoms. Molecular graphics employed were ORTEP-III [30] and DIAMOND [31].

4.4.2 Crystal structures

Mn(papea)₂(NCS)₂ (16) : The molecular structure of the complex along with the atom-numbering scheme is given in Fig. 4.1. The complex crystallizes in a monoclinic crystal system with two molecules in the unit cell. A summary of the key crystallographic information is given in Table 4.1. Selected bond lengths and bond angles are listed in Table 4.2. The complex crystallizes in the chiral space group $P2_1$ (No: 4) and the molecule is chiral due to the asymmetric nature of the Schiff base ligand. The ligand retains its configuration in the complex as well. Based on R and S configuration due to Cahn-Ingold-Prelog, the carbon atoms C7 and C21 have the R configuration, as is the case with the starting amine (_R_-1-phenylethyl amine). Mn(II) is in a distorted octahedral environment, which is occupied by four nitrogen atoms (N1, N2, N3 and N4) from two chelating bidentate Schiff base ligands papea and two nitrogens (N5 and N6) from two thiocyanate ions. The coordination polyhedron consists of MnN₆ chromophore with pairs of _trans_ pyridyl N (N1 and N3), _cis_ azomethine N (N2 and N4) and _cis_ thiocyanate N (N5 and N6) atoms. The thiocyanate ions are coordinated in terminal manner _via_ the nitrogen atom.

Table 4.1. Crystal data and structure refinement

Parameters	Mn(papea)$_2$(NCS)$_2$
Empirical formula	$C_{30}H_{28}MnN_6S_2$
Formula weight	591.64
Crystal colour	Yellow
Crystal morphology	Block
Temperature	100.0(1) K
Wavelength (Mo Kα) (Å)	0.71073
Crystal system	Monoclinic
Space group	$P2_1$ (No: 4)
Unit cell dimensions	
a (Å)	9.0040(2)
b (Å)	15.1618(3)
c (Å)	11.2770(2)
α (˚)	90.00
β (˚)	109.3800(10)
γ (˚)	90.00
Volume V (Å^3), Z	1452.27(5), 2
Calculated density (ρ) (Mg m^{-3})	1.353
Absorption coefficient μ (mm^{-1})	0.629
F(000)	614
Crystal size (mm^3)	0.69x0.40x0.28
θ range for data collection	1.91 – 35.00
Index ranges	-14≤h≤13, -24≤k≤24, -18≤l≤18
Reflections collected / unique	48582/12743 [R(int) = 0.0213]
Completeness to 2θ = 35.00	100 %
Absorption correction	SADABS
Maximum and minimum transmission	0.8432 and 0.6724
Refinement method	Full-matrix least-squares on F^2
Data / restraints / parameters	12743/1/352
Goodness-of-fit on F^2	1.022
Final R indices [I>2σ(I)]	R_1 = 0.0287, wR_2 = 0.0764
R indices (all data)	R_1 = 0.0301, wR_2 = 0.0774
Largest diff. peak and hole(e Å^{-3})	1.141, -0.992

The bond lengths and bond angles reveal significant distortion from the ideal octahedral geometry. The rather small bite angle [N3–Mn1–N4=72.13(3)°] defines the largest distortion of the geometry. The thiocyanates which are almost linear [N5–C29–S1=178.00(11)° and N6–C30–S2=178.77(11)°] are coordinated to Mn(II) in a bent fashion [Mn1–N5–C29=157.95(10)° and Mn1–N6–C30= 139.21(8)°]. The Mn(II)–N bond length is shortest for thiocyanate nitrogens, indicating their stronger coordination than the pyridyl and azomethine nitrogens of the Schiff base. On comparison with earlier reports, all the Mn–N bond lengths are in the normal range as expected for complexes of Mn(II) with thiocyanate ligand [32-35].
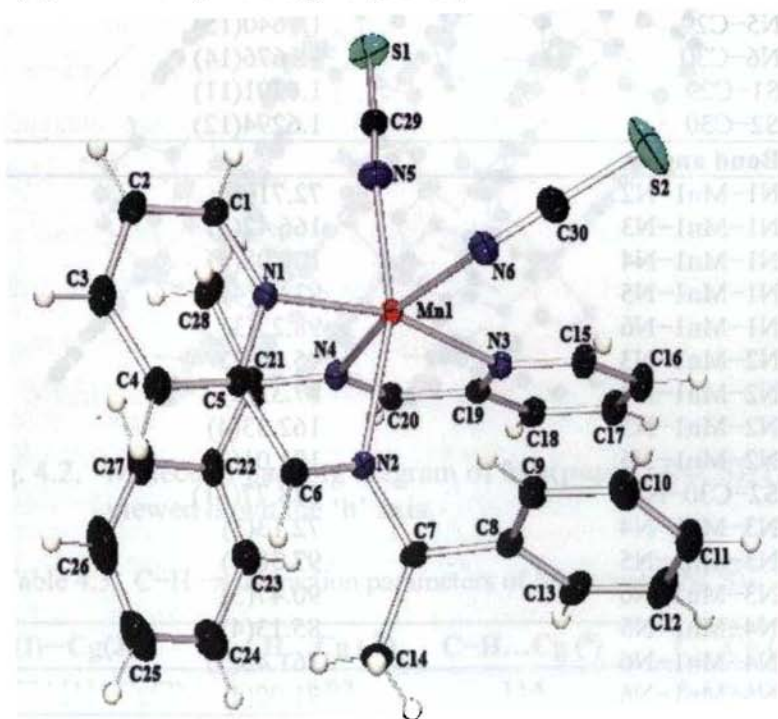
Fig. 4.1. Molecular structure of **Mn(papea)₂(NCS)₂ (16)**

The mean plane deviation calculations show that the metal chelate rings are almost planar. Ring puckering analysis [36] reveals that the metal chelate ring Cg(2) comprising of Mn1, N3, C19, C20 and N4 can be best described as being twisted on Mn1–N3 bond [Q(2) = 0.1000(8) Å and Φ=189.4162(5876)°].

Table 4.2. Selected bond lengths (Å) and bond angles (°) of Mn(papea)$_2$(NCS)$_2$

Bond lengths	
Mn1–N1	2.2871(8)
Mn1–N2	2.2819(9)
Mn1–N3	2.2927(8)
Mn1–N4	2.3775(8)
Mn1–N5	2.1389(11)
Mn1–N6	2.1639(9)
N5–C29	1.1640(15)
N6–C30	1.1676(14)
S1–C29	1.6291(11)
S2–C30	1.6294(12)
Bond angles	
N1–Mn1–N2	72.71(3)
N1–Mn1–N3	166.42(3)
N1–Mn1–N4	100.08(3)
N1–Mn1–N5	92.91(4)
N1–Mn1–N6	98.22(3)
N2–Mn1–N3	95.46(3)
N2–Mn1–N4	87.32(3)
N2–Mn1–N5	162.33(4)
N2–Mn1–N6	101.01(3)
S2–C30–N6	178.77(11)
N3–Mn1–N4	72.13(3)
N3–Mn1–N5	97.38(4)
N3–Mn1–N6	90.47(3)
N4–Mn1–N5	85.13(4)
N4–Mn1–N6	161.46(3)
N5–Mn1–N6	91.00(4)
Mn1–N5–C29	157.95(11)
Mn1–N6–C30	139.20(9)
S1–C29–N5	178.01(11)

The packing in the crystal lattice (Fig. 4.2) is in an ABAB.... manner, which when repeated, one dimensionally forms a layer and the successive layers arranged in a similar manner. No classical hydrogen bonds are observed in the crystal structure. A list of C–H⋯π interactions is listed in Table 4.3. The packing of the molecules in the crystal lattice is stabilized by C–H⋯π interactions and the weak π⋯π interactions (Table 4.4).
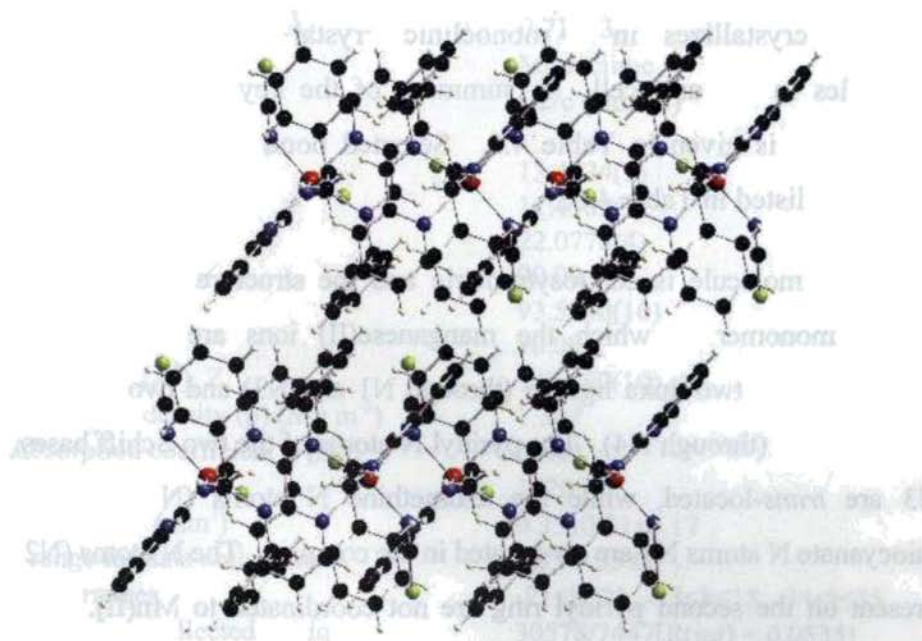
Fig. 4.2. Molecular packing diagram of **Mn(papea)$_2$(NCS)$_2$ (16)** viewed down the 'b' axis.

Table 4.3. C–H⋯π interaction parameters of Mn(papea)$_2$(NCS)$_2$

C–H(I)⋯Cg(J)	H...Cg (Å)	C–H...Cg (°)	C...Cg (Å)
C7–H7A[1]⋯Cg(2)	2.92	114	3.4382(12)

Cg(2) = Mn1, N3, C19, C20, N4

125

Table 4.4. $\pi \cdots \pi$ interactions of Mn(papea)$_2$(NCS)$_2$

Cg(I)–Res(I)···Cg(J)	Cg···Cg (Å)	α°	β°	γ°
Cg(1)[1]···Cg(6)	3.9557(7)	8.53	23.26	29.56
Cg(6)[1]···Cg(1)	3.9557(7)	8.53	29.56	23.26

Cg(1) = Mn1, N1, C5, C6, N2; Cg(6) = C22, C23, C24, C25, C26, C27

Mn(dpka)$_2$(NCS)$_2$ (17b) : The molecular structure of the complex along with the atom numbering scheme is given in Fig. 4.3. The complex crystallizes in a monoclinic crystal system with four molecules in the unit cell. A summary of the key crystallographic information is given in Table 4.5. Selected bond lengths and bond angles are listed in Table 4.6.

The molecule is centrosymmetric and the structure consists of a neutral monomer in which the manganese(II) ions are octahedrally coordinated by two dpka ligands (through N1 and N3) and two terminal NCS⁻ ligands (through N4). The pyridyl N atoms of the two Schiff bases, N3 are *trans*-located, while the azomethine N atoms (N1) and the thiocyanate N atoms N4 are *cis*-located in the complex. The N atoms (N2) present on the second pyridyl ring are not coordinated to Mn(II). The Mn–N distance is shortest for the thiocyanate nitrogens and longest for the azomethine nitrogens. The MnN$_6$ octahedra exhibit a noticeable distortion from the regular geometry. The rather small bite angle of 71.12(4)° corresponding to the N3–Mn–N1 bond angle signifies the extent of distortion. The thiocyanate groups are coordinated in terminal manner to the Mn(II) atom through the nitrogen atom. The NCS groups are quasi-

126

linear with an N4–C18–S1 bond angle of 178.50(14)° and are bonded to the Mn(II) ion through an angle of 164.68(12)°.

Table 4.5. Crystal data and structure refinement

Parameters	Mn(dpka)$_2$(NCS)$_2$
Empirical formula	C$_{36}$H$_{26}$MnN$_8$S$_2$
Formula weight	689.71
Crystal colour	Orange
Crystal morphology	Slab
Temperature	100.0(1) K
Wavelength (Mo Kα) (Å)	0.71073
Crystal system	Monoclinic
Space group	C2/c (No: 15)
Unit cell dimensions	
a (Å)	13.4724(2)
b (Å)	11.4583(2)
c (Å)	22.0778(4)
α (°)	90.00
β (°)	93.5380(10)
γ (°)	90.00
Volume V (Å^3), Z	3401.67(10), 4
Calculated density (ρ) (Mg m^{-3})	1.347
Absorption coefficient μ (mm^{-1})	0.549
F(000)	1420
Crystal size (mm^3)	0.35x0.31x0.17
θ range for data collection	1.85 – 35.00
Index ranges	-21≤h≤21, -18≤k≤18, -34≤l≤35
Reflections collected / unique	30578/7447[R(int) = 0.0535]
Completeness to 2θ = 35.00	99.4 %
Absorption correction	SADABS
Maximum and minimum transmission	0.9129 and 0.8306
Refinement method	Full-matrix least-squares on F^2
Data / restraints / parameters	7447/0/213
Goodness-of-fit on F^2	1.051
Final R indices [I>2σ(I)]	R$_1$ = 0.0464, wR$_2$ = 0.1123
R indices (all data)	R$_1$ = 0.0725, wR$_2$ = 0.1307
Largest diff. peak and hole(e Å^{-3})	0.595, -0.388

Table 4.6. Selected bond lengths (Å) and bond angles (°) of Mn(dpka)₂(NCS)₂

Bond lengths	
Mn1−N1	2.3084(11)
Mn1−N1#1	2.3084(11
Mn1−N3	2.2785(11)
Mn1−N3#1	2.2785(11)
Mn1−N4	2.1194(13)
Mn1−N4#1	2.1194(13)
N4−C18	1.1687(19)
S1−C18	1.6230(15)
Bond angles	
N4#1−Mn1−N4	100.32(7)
N4#1−Mn1−N3	101.08(5)
N4−Mn1−N3	97.85(5)
N4#1−Mn1−N3#1	97.85(5)
N4−Mn1−N3#1	101.08(5)
N3−Mn1−N3#1	150.27(6)
N4#1−Mn1−N1	86.44(5)
N4#1−Mn1−N1	168.13(5)
N3−Mn1−N1	71.12(4)
N3#1−Mn1−N1	87.51(4)
N4#1−Mn1−N1#1	168.13(5)
N4−Mn1− N1#1	86.44(5)
N3−Mn1− N1#1	87.51(4)
N3#1−Mn1−N1#1	71.12(4)
N1#1−Mn1−N1#1	88.65(6)
C18−N4−Mn1	164.68(12)
N4−C18−S1	178.50(14)

Symmetry transformations used to generate equivalent atoms: #1 -x, y,-z+1/2
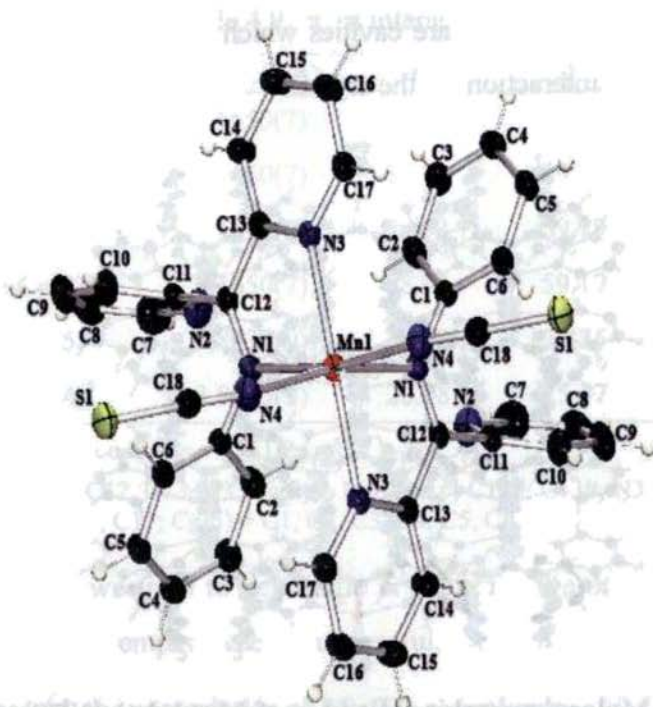
Fig. 4.3. Molecular structure of **Mn(dpka)₂(NCS)₂ (17b)**

The Mn–N bond distances are in agreement with the previous reports [25,26,32-35,37-38]. Mean plane deviation calculations show that the metal-chelate rings, pyridyl rings and the phenyl rings in the complex are almost **planar**.

The packing of the molecules in the crystal lattice (Fig. 4.4) is in a head to tail manner. Classical hydrogen bonds are absent; the weak hydrogen bond interactions present are given in Table 4.7. The C–H···π interactions (Table 4.8) present in the crystal reinforces the packing of the molecules. The crystal structure is further stabilized by significant π···π interactions (Table 4.9). The assembly of molecules in the crystal lattice is

in such a manner that there are cavities which are formed as a result of $\pi\cdots\pi$ and C–H$\cdots\pi$ interactions in the crystal.
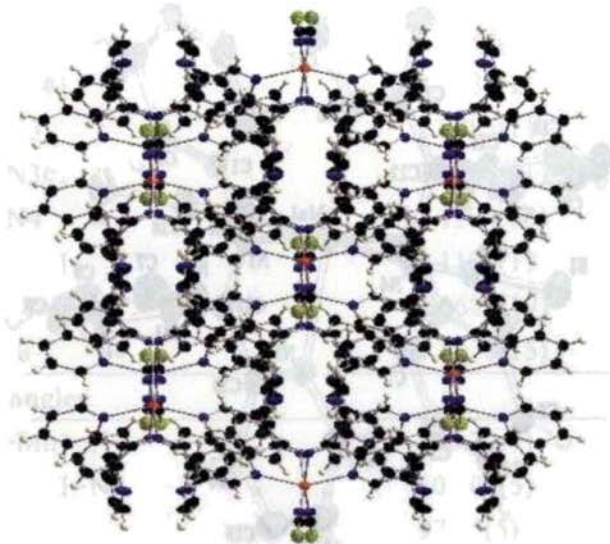
Fig. 4.4. Molecular packing diagram of **Mn(dpka)₂(NCS)₂ (17b)** viewed down the 'c' axis.

Table 4.7. Hydrogen bonding interactions in **Mn(dpka)₂(NCS)₂**

D–H⋯A	D–H (Å)	H⋯A (Å)	D⋯A (Å)	D–H⋯A (°)
C(16)–H(16A)⋯ N(2)[a]	0.9298	2.5888	3.349(2)	139.34

D=donor, A=acceptor; Equivalent position code: a = 1/2-x,-1/2+y, 1/2-z

Table 4.8. C–H⋯π interaction parameters

C–H(I)⋯Cg(J)	H⋯Cg (Å)	C–H⋯Cg (°)	C⋯Cg (Å)
C2–H2A[1]⋯Cg(1)[b]	3.1811	99.37	3.4562(16)
C2–H2A[1]⋯Cg(2)[c]	3.1811	99.37	3.4562(16)
C3–H3A[1]⋯Cg(4)[d]	2.9932	139.68	3.7511(18)
C8–H8A[1]⋯Cg(5)[e]	3.1013	165.06	4.008(2)

Equivalent position code: a = x, 1+y, z; b = -x, y, 1/2-z; c = x, y, z; d =-1/2+x, 1/2+y, z; e = -x, 1-y, 1-z

Cg(1) = Mn1, N1, C12, C13, N3; Cg(2) = Mn1, N1#, C12#, C13#, N3#; Cg(4) = N3, C13, C14, C15, C16, C17; Cg(5) = C1, C2, C3, C4, C5, C6

Table 4.9. $\pi \cdots \pi$ interactions

Cg(I)–Res(I)···Cg(J)	Cg···Cg (Å)	α^o	β^o	γ^o
Cg(1)[1]···Cg(1)[a]	3.1650(7)	88.93	59.19	59.19
Cg(1)[1]···Cg(2)[b]	3.1650(7)	88.93	59.19	59.19
Cg(2)[1]···Cg(1)[b]	3.1650(7)	88.93	59.19	59.19
Cg(2)[1]···Cg(2)[a]	3.1650(7)	88.93	59.19	59.19
Cg(4)[1]···Cg(5)[a]	3.8637(9)	20.08	27.35	25.47
Cg(5)[1]···Cg(4)[a]	3.8635(9)	20.08	25.47	27.35

Equivalent position code: a = –x, y,1/2–z, b = x, y, z

Cg(1) = Mn1, N1, C12, C13, N3; Cg(2) = Mn1, N1#, C12#, C13#, N3#; Cg(4) = N3, C13, C14, C15, C16, C17; Cg(5) = C1, C2, C3, C4, C5, C6

Although we tried to get single crystals for the other manganese complexes, our attempts were unsuccessful.

4.4.3 Spectral characteristics of Mn(II) complexes

4.4.3a *Electronic spectra*

The ground state of tetrahedral and high-spin octahedrally coordinated Mn(II) complex is $^6A_{1g}$. The absence of any other spin sextet terms requires that all transitions in high spin d^5 complexes are spin forbidden. However, some forbidden transitions occur such as $^4A_{1g}(G)$, $^4E_g(G) \leftarrow {}^6A_{1g}$, $^4E_g(D) \leftarrow {}^6A_{1g}$, $^4T_{1g}(G)$, $^4T_{2g}(G) \leftarrow {}^6A_{1g}$ [39]. Also for octahedral complexes, transitions are Laporte forbidden. Thus doubly forbidden transitions are extremely weak. The absorption bands found for the complexes under study are listed in Table 4.10.

Table 4.10. Electronic spectral data for Mn(II) complexes

Compounds	n→π* (nm)	π→π* (nm)	CT (nm)
$Mn_2(paa)_2(N_3)_4$ **(14)**	310	291	400
$[Mn(paa)_2(NCS)_2]\cdot^3/_2H_2O$ **(15)**	310	292	390
$Mn(papea)_2(NCS)_2$ **(16)**	315	294	400
$Mn(dpka)_2(NCS)_2\cdot^1/_2H_2O$ **(17a)**	325	289	410

In the complexes **14-17**, the $\pi \rightarrow \pi*$ transitions are observed as intense peaks at *ca.* 290 nm and the $n \rightarrow \pi*$ transitions of the ligand are seen as intense peaks in the range 310-335 nm. The charge transfer bands are observed at 400 nm. The *d-d* bands in the case of these complexes could not be identified due to their low intensity.

4.4.3b *EPR spectra*

Manganese complexes show a wide variety of bonding geometries and EPR spectroscopy has been used successfully to probe the structures of these compounds [40-44]. The spin Hamiltonian for Mn(II) may be described as

$$\hat{H} = g\beta HS + D[S_z^2 - S(S+1)/3] + E(S_x^2 - S_y^2)$$

where H is the magnetic field vector, D is the axial zero field splitting term, E is the rhombic zero field splitting parameter, g is the spectroscopic splitting factor, β the Bohr Magneton and S is the electron spin vector [45]. If D and E are very small compared to $g\beta HS$, five EPR transitions corresponding to $\Delta m_s = \pm 1$, viz., $|+5/2\rangle\leftrightarrow|+3/2\rangle$, $|+3/2\rangle\leftrightarrow|+1/2\rangle$, $|+1/2\rangle\leftrightarrow|-1/2\rangle$, $|-1/2\rangle\leftrightarrow|-3/2\rangle$ and $|-3/2\rangle\leftrightarrow|-5/2\rangle$ are expected with a g value of 2.0. However, for the case where D or E is

very large, the lowest doublet has effective g values of $g_\parallel = 2$, $g_\perp = 6$ for $D \neq 0$ and $E=0$ but for $D=0$ and $E \neq 0$, the middle Kramers doublet has an isotropic g value of 4.29 [46,47].

The EPR spectrum of compound **14** in the polycrystalline state at room temperature (Fig. 4.5) shows an isotropic signal with a g_{iso} value of 2.009. The spectrum does not present hyperfine transitions.

2600 2800 3000 3200 3400 3600 3800

H (G)
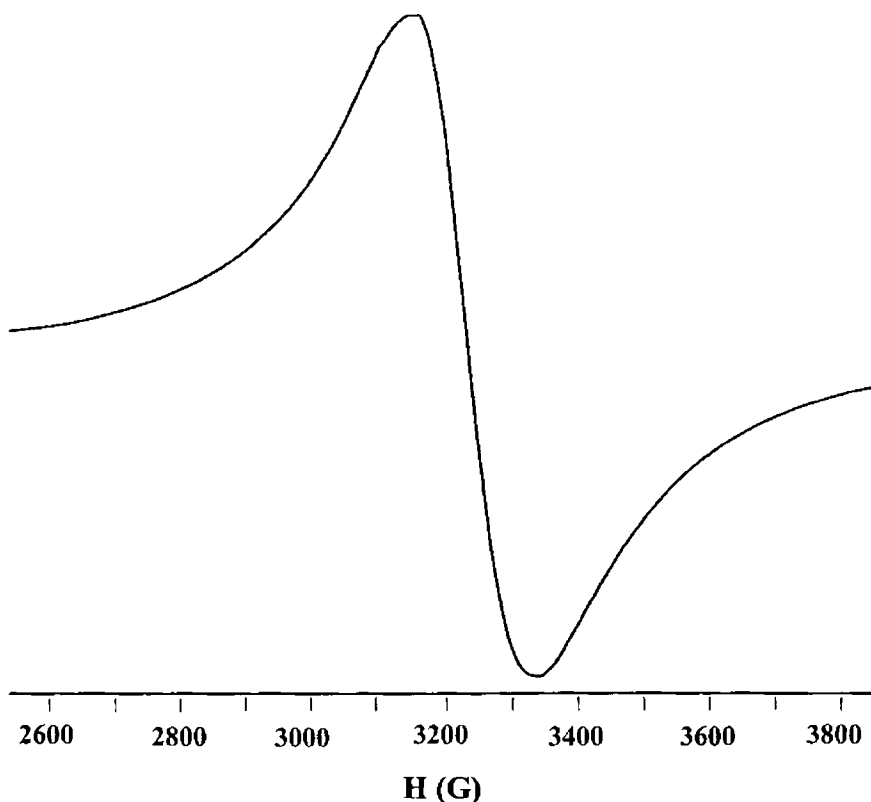
Fig. 4.5. EPR spectrum of compound **1** in polycrystalline state at 298 K.

However, the solution spectrum in DMF at 77 K (Fig. 4.6), displayed two g values, $g_1 = 1.999$ and $g_2 = 4.353$. Both the high field

and low filed signals exhibited hyperfine splitting and a sextet pattern was observed in both the cases. The observance of hyperfine sextet is due to the interaction of the unpaired electron with the Mn(II) nucleus of spin I = 5/2, resulting in $2nI+1$ lines. Thus the six lines observed corresponds to m = +5/2, +3/2, +1/2, -1/2, -3/2, -5/2 with $\Delta m_I = 0$.
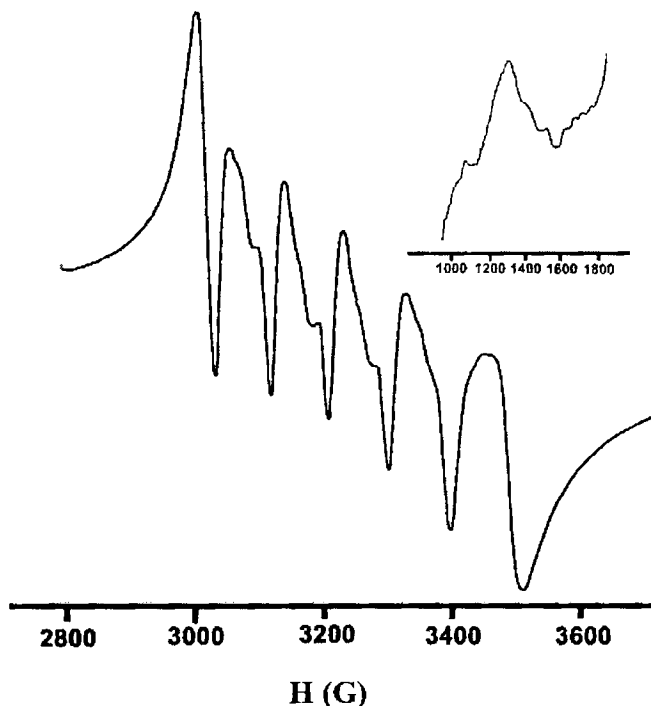
Fig. 4.6. EPR spectrum of compound **14** in DMF at 77 K.

In addition to the hyperfine pattern in the high field signal, a pair of low intensity lines is found in between each of the two main hyperfine lines in the high field signal. These are the forbidden lines corresponding to $\Delta m_I \neq 0$, transitions which arise as a result of the mixing of the nuclear hyperfine levels by the zero-field splitting factor

134

of the Hamiltonian [48]. Thus the general selection rule for the transition, $\Delta m_s = \pm 1$, $\Delta m_I = 0$ is violated. The spacing between the lines in the central hyperfine sextet is estimated to be $A = 100$ G and that for the low field signal is A =115 G.

The polycrystalline state EPR spectrum (Fig. 4.7) of the compound **15** at 77 K shows two g values $g_1 = 2.018$, $g_2 = 4.324$. Both the high-field and low-field signals are devoid of hyperfine splitting pattern.
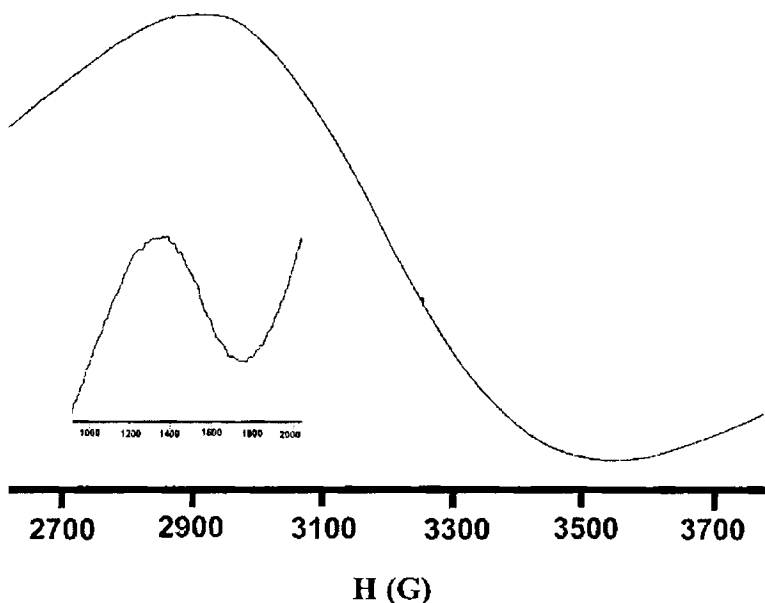
Fig. 4.7. EPR spectrum of compound **15** in polycrystalline state at 77 K.

The spectrum in frozen solution (Fig. 4.8) also displayed two g values, $g_1 = 1.994$, $g_2 = 5.778$. Both the signals show the hyperfine sextet, with the hyperfine coupling constants 106 G and 276 G

respectively for the high-field and low-field transitions respectively.
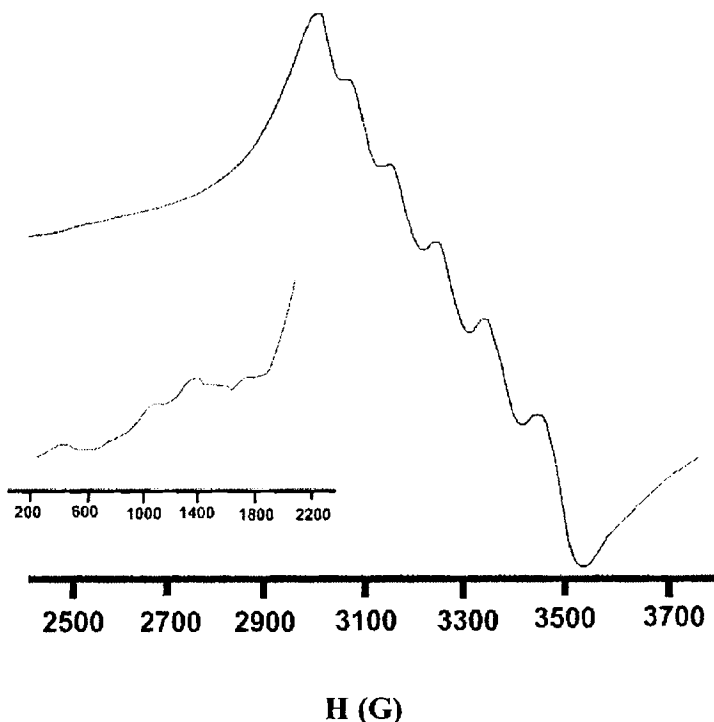
Fig. 4.8. EPR spectrum of compound **15** in DMF at 77 K.

In the X band CW-EPR spectrum of the octahedral Mn(II) complex **16** in polycrystalline state at 77 K (Fig. 4.9), three g values are observed, $g_1 = 1.939$, $g_2 = 2.821$, $g_3 = 5.794$. The three g values imply that the molecule is rhombically distorted. The broadness of the signals is a characteristic feature of Mn(II) complex in the polycrystalline state, which arises due to dipolar interactions and enhanced spin lattice relaxation [46].
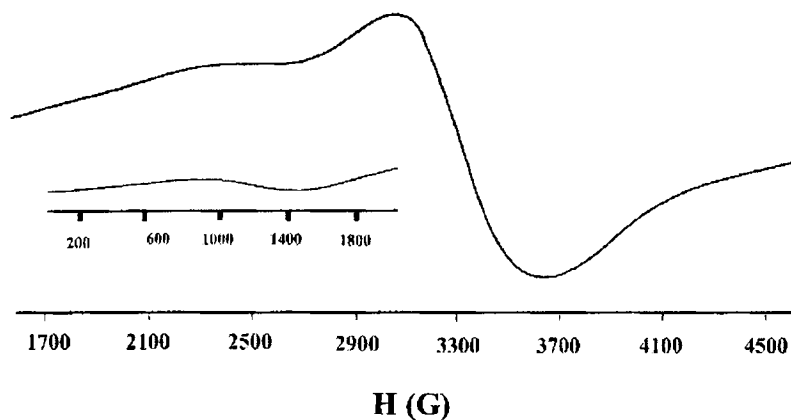
Fig. 4.9. EPR spectrum of compound **16** in polycrystalline state at 77 K.

The EPR spectrum of the complex in DMF solution at 77 K (Fig. 4.10) is isotropic and exhibits a six line manganese hyperfine pattern centered at $g = 1.997$.

H (G)
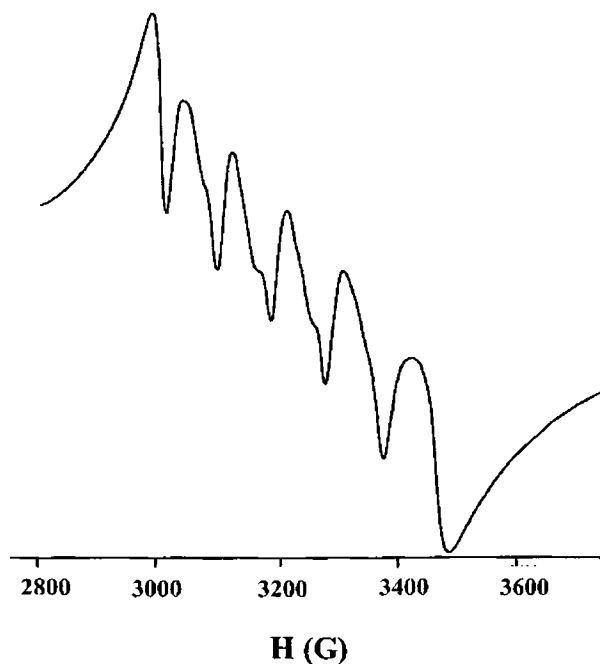
Fig. 4.10. EPR spectrum of compound **16** in DMF at 77 K.

The hyperfine splitting pattern arises due to electron spin-nuclear spin coupling. The hyperfine coupling constant is estimated to be $A = 100$ G. In addition to the hyperfine pattern, a pair of low intensity lines is found in between each of the two main hyperfine lines. These are the forbidden lines corresponding to $\Delta m_I \neq 0$, transitions which arise as a result of the mixing of the nuclear hyperfine levels by the zero-field splitting factor of the Hamiltonian.

The octahedral compound **17a** exhibits EPR features very similar to that of the complex **16**. In the polycrystalline state at 77K (Fig. 4.11), three g values are observed, $g_1 = 1.939$, $g_2 = 2.821$, $g_3 = 5.794$. The three g values indicate a rhombic distortion from the octahedral geometry, which is supported by the crystal structure studies.

| 1000 | 1400 | 1800 | 2200 | 2600 | 3000 | 3400 | 3800 |

H (G)
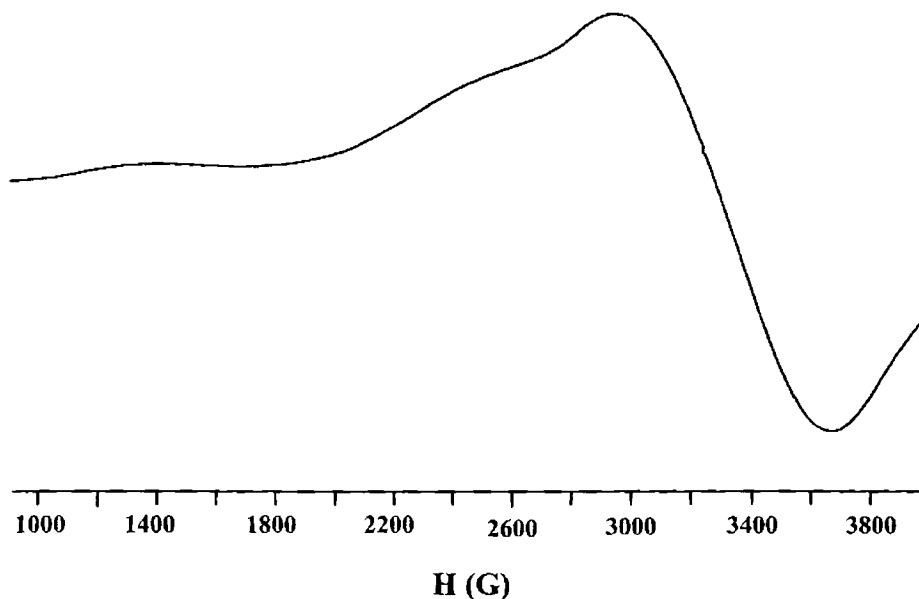
Fig. 4.11. EPR spectrum of compound **17a** in polycrystalline state at 298 K.

The frozen solution spectrum (Fig. 4.12) of the compound in DMF, is also similar in features to the above discussed thiocyanato compound. The spectrum is isotropic and exhibits hyperfine splitting into a pattern of sis lines as a result of the interaction between the electron spin and nuclear spin. The g_{iso} value is found to be 1.999 with a coupling constant of 100 G. Moreover, a pair of low intensity lines is found in between each of the two main hyperfine lines. These are the forbidden lines corresponding to $\Delta m_I \neq 0$, transitions which arise as a result of the mixing of the nuclear hyperfine levels by the zero-field splitting factor of the Hamiltonian.
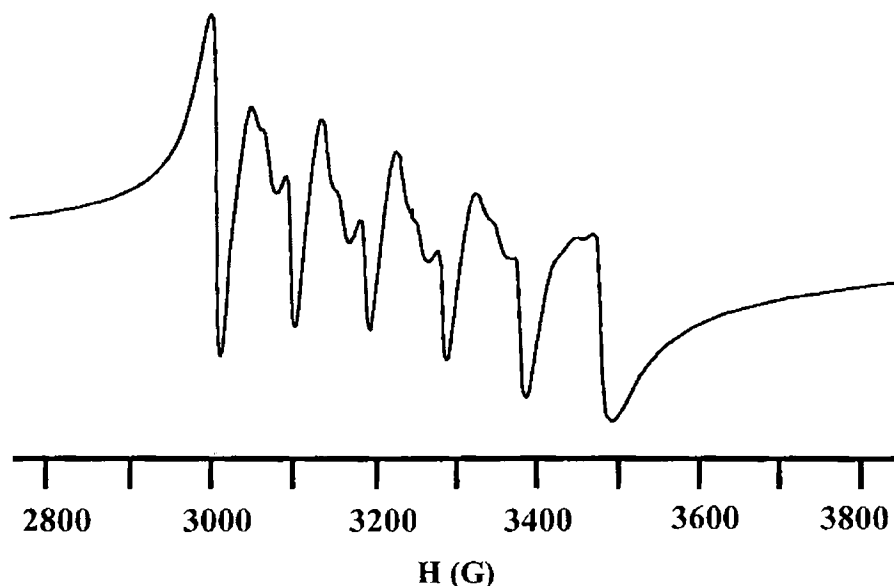
Fig. 4.12. EPR spectrum of compound **17a** in polycrystalline state at 298 K.

For all the complexes, the hyperfine values are lower that that obtained for ionic compounds indicating considerable amount of covalency in the M–L bonds [49,50].

139

4.4.3c *IR spectral studies*

IR spectrum provides a useful diagnostic tool in ascertaining the coordination of different groups and atoms to the metal. This spectroscopic technique becomes particularly useful in the case of complexes of metals with pseudohalogens, for which very strong absorptions are observed in the region above 2000 cm⁻¹.

The IR spectrum of complex **14** (Fig. 4.13) reveals a medium sharp peak at 1589 cm⁻¹, assigned as the v(C=N) stretching mode of the azomethine function of the Schiff base, the position of which is in agreement with the previous reports and is thus indicative of the coordination of azomethine N [23,51]. The band at 1442 cm⁻¹ is attributed to pyridyl ring stretching and the band at 1013 cm⁻¹ is due to pyridyl ring breathing. The in-plane ring deformation of the pyridyl ring and the pyridyl ring out-of-plane bending are observed at 638 and 481 cm⁻¹ as weak bands. The above observations indicate the pyridyl N coordination.

The most relevant and the interesting bands in the IR spectrum of **14** are those associated with the azido groups. A doublet pattern is seen in the spectrum, with two sharp and strong peaks at 2095 and 2058 cm⁻¹, which is assigned as the v_{as} stretching frequency of the azide. A single strong peak at 2033 cm⁻¹ is observed for sodium azide. A shift from that wavenumber (both to higher and lower wave numbers) of the $v_{as}(N_3)$ stretching of the azide indicates that it must be coordinated. The doublet structure is due to the existence of two kinds of azido groups in the complex. The higher wave numbers of the $v_{as}(N_3)$ stretching is probably due to the presence of bridging azides. But in the absence of crystal

140

structure, it is impossible to draw definite conclusions. The $v_s(N_3)$ stretching mode of the azide group is observed at 1329 cm^{-1} as a band of medium intensity. The $v_s(N_3)$ vibration mode in inactive in symmetrical azide groups [52]. The term symmetrical means that there is vary small or negligible difference in the N−N bond lengths in the azide group. The presence of the $v_s(N_3)$ stretching band in the present case rules out the possibility of a highly symmetrical azide groups. The deformation mode of the azido ligand is observed as a weak band at 689 cm^{-1}.
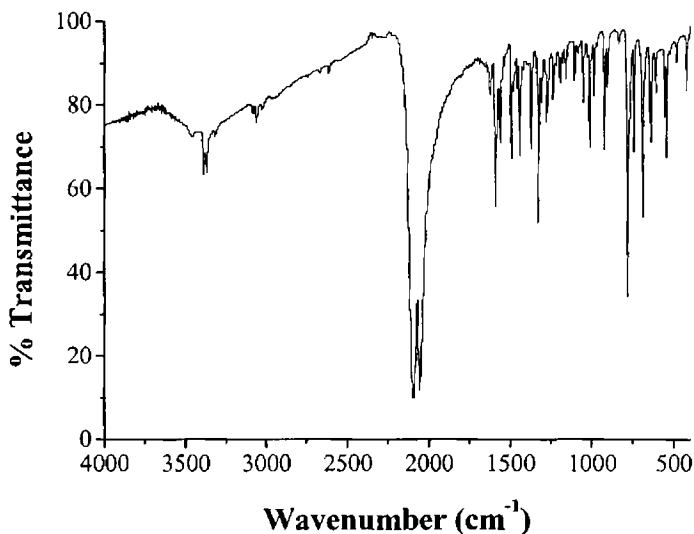
Fig. 4.13. IR spectrum of compound **14**.

A broad band *ca*. 3446 cm^{-1} is due to the presence of lattice water in complex **15** (Fig 4.14). The $v(C=N)$ stretching mode of the Schiff base paa occurs as a medium band at 1593 cm^{-1} and indicates the coordination of azomethine N to the manganese(II). The coordination of the pyridyl nitrogen is confirmed by the presence of pyridyl ring stretch at 1486 cm^{-1},

141

pyridyl ring breathing at 1013 cm^{-1}, pyridyl in-plane ring deformation at 694 cm^{-1} and pyridyl out-of-plane ring deformation at 411 cm^{-1}. The most interesting part of the spectrum is the 2000-2100 cm^{-1} region where the strong absorption bands due to the thiocyanate group is visible. The spectrum of KCNS has a single strong absorption at 2053 cm^{-1} due to the v_{as}(C=N) stretching. A shift from this wavenumber evidently indicates the coordination of the NCS group. The IR spectrum of **15** has a single strong and sharp peak at 2062 cm^{-1} assignable to the v_{as}(C=N) stretching mode of the thiocyanate group. The number and position of the peak suggests the presence of N-bonded bridging thiocyanate group and the thiocyanate groups are equivalent and hence *trans* located in the octahedral complex as suggested by other studies [53]. The v(CS) is found at 775 cm^{-1} and the δ(NCS) bending mode is obtained at 543 cm^{-1} confirming the existence of N-bonded NCS group.
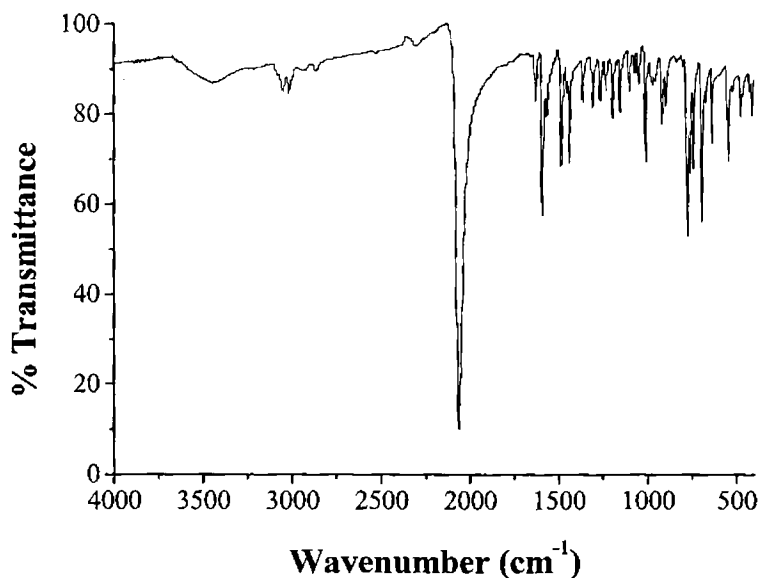
Fig. 4.14. IR spectrum of compound **15**.

In the IR spectrum of compound **16** there are two strong and sharp peaks at 2069 and 2053 cm^{-1}, which are assignable to the v_{as}(C=N) stretching of the thiocyanate groups (Fig. 4.15). This indicates the coordination of the thiocyanate anions and the presence of doublets implies that there are two non-equivalent thiocyanate groups and hence mutual _cis_ coordination. The position of bands (<2100 cm^{-1}) is an evidence for coordination _via_ N atom and also the terminal nature of the thiocyanate groups. All these are confirmed by the crystal structure analysis of complex **16**. v_s(CN) stretching vibration of thiocyanate is _ca._ 1384 cm^{-1} as doublets of medium intensity. Doublets near 789 and 764 cm^{-1} is due to the thiocyanate v_s(CS) stretching vibration. This band is also indicative of N coordination.
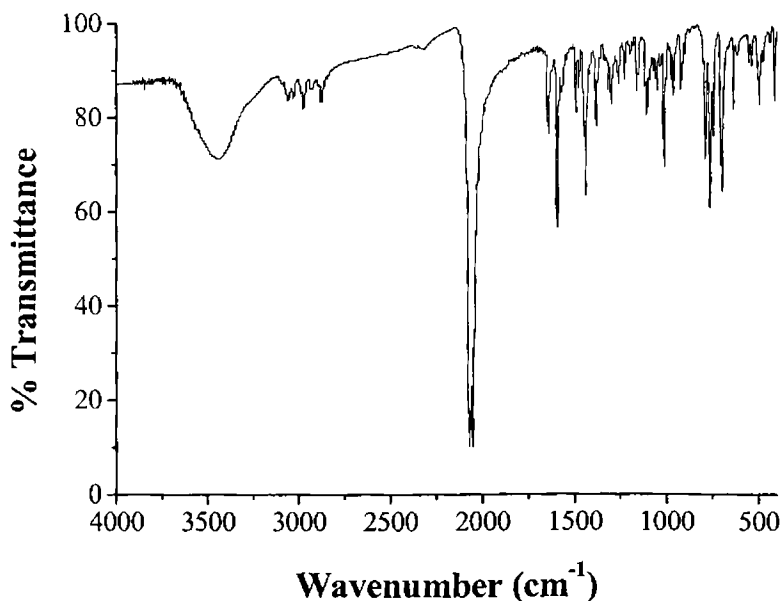
Fig. 4.15. IR Spectrum of compound **16**.

A single sharp peak at 497 cm^{-1} in the IR spectrum of complex **16** is due to the δ(NCS) bending mode. The complex has a sharp peak at 1594 cm^{-1} for the ν(C=N) stretching mode of the Schiff base. The coordination of the pyridyl nitrogen is confirmed by the presence of pyridyl ring stretch at 1440 cm^{-1}, pyridyl ring breathing at 1013 cm^{-1}, pyridyl in-plane ring deformation at 637 cm^{-1} and pyridyl out-of-plane ring deformation at 413 cm^{-1}. The IR data are in conformity with the previous reports dealing with complexes having similar ligand systems [24].

The band at 1579 cm^{-1} in the IR spectrum of compound **17a** is assigned to the stretching vibration of the azomethine group of the Schiff base. The strong bands characteristic of thiocyanato group appears as a doublet at 2063 and 2041 cm^{-1}. The splitting in this band indicates the presence of two thiocyanate groups in the complex. The position of the bands (<2100 cm^{-1}) points out the terminal nature of the thiocyanate and coordination through the N atom. The sharp bands viewed at 1475 cm^{-1} are due to the pyridyl ring vibrations, pyridyl ring breathing at 1015 cm^{-1}, pyridyl in-plane ring deformation at 623 cm^{-1} and pyridyl out-of-plane ring deformation at 409 cm^{-1} confirms the coordination of pyridyl N.

References

[1] J.M. McCord, I. Fridovich, J. Biol. Chem. 244 (1969) 6049.

[2] K. Wieghardt, Angew. Chem. Int. Ed. Engl. 28 (1989) 1153.

[3] V.K. Yachandra, K. Sauer, M.P. Klein, Chem. Rev. 96 (1996) 2927.

[4] W. Rüttinger, G.C. Dismukes, Chem. Rev. 97 (1997) 1.

[5]   C. Tommos, G.T. Babcock, Acc. Chem. Res. 31 (1998) 18.

[6]   V.L. Pecoraro, M.J. Baldwin, A. Gelasco, Chem. Rev. 94 (1994) 807.

[7]   G.C. Dismukes, Chem. Rev. 96 (1996) 2929.

[8]   M.L. Ludwig, A.L. Metzger, K.A. Pattridge, W.C. Stallings, J. Biol. Chem. 219 (1991) 335.

[9]   D.P. Riley, P.J. Lennon, W.L. Neumann, R.H. Weiss, J. Am. Chem. Soc. 119 (1997) 6522.

[10]   R. Sessoli, H.-L. Tsai, A.R. Schake, S. Wang, J.B. Vincent, K. Folding, D. Gatteschi, G. Christou, D.N. Hendrickson, J. Am. Chem. Soc. 115 (1993) 1804.

[11]   E.M. Chudnovsky, Science 274 (1996) 938.

[12]   S.M.J. Aubin, Z. Sun, I.A. Guzei, A.L. Rheingold, G. Christou, D.N. Hendrickson, Chem. Commun. (1997) 2239.

[13]   R. Hage, J.E. Iburg, J. Kerschner, J.H. Koek, E.L.M. Lempers, R.J. Martens, U.S. Racherla, S.W. Russell, T. Swarthoff, M.R.P. van Vliet, J.B. Warnaar, L. van der Wolf, B. Krljen, Science 369 (1994) 637.

[14]   D.E. de Vos, T.J. Ben, Organomet. Chem. 195 (1996) 520.

[15]   C. Zondervan, R. Hage, B.L. Ferigna, Chem. Commun. (1997) 419.

[16]   J.W. Whittaker, M.M. Whittaker, J. Am. Chem. Soc. 113 (1991) 5528.

[17]   Y. Kono, I. Fridovich, J. Bacteriol. 155 (1983) 742.

[18]   Y. Kono, I. Fridovich, J. Biol. Chem. 258 (1983) 6015.

[19]   W.F. Beyer Jr., I. Fridovich, Biochemistry 24 (1985) 6460.

[20]   R.M. Fronko, J.E. Penner-Hahn, C.J. Bender, J. Am. Chem. Soc. 110 (1988) 7554.

[21]   G.S. Waldo, R.M. Fronko, J.E. Penner-Hahn, Biochemistry 30 (1991) 10486.

[22]   G.S. Waldo, S. Yu, J.E. Penner-Hahn, J. Am. Chem. Soc. 114 (1992) 5869.

[23]   E.-Q, Gao, S.-Q. Bai, Y.-F. Yue, Z.-M. Wang, C.-H. Yan, Inorg. Chem. 39 (2003) 3642.

[24]   H.-R. Wen, C.-F. Wang, Y. Song, J.-L. Zuo, X.-Z. You, Inorg. Chem. 44 (2005) 9039.

[25]   G.S. Papaefstathiou, A. Escuer, F.A. Mautner, C. Raptopoulou, A. Terzis, S.P. Perlepes, R. Vicente, Eur. J. Inorg. Chem. (2005) 879.

[26]   G.S. Papaefstathiou, A. Escuer, C.P. Raptopoulou, A. Terzis, S.P. Perlepes, R. Vicente, Eur. J. Inorg. Chem. (2001) 1567.

[27]   F.A. Cotton, G. Wilkinson, C.A. Murillo, M. Bochmann, Advanced Inorganic Chemistry, 6th ed., Wiley, New York (1999) 839.

[28]   Bruker APEX2 Version 1.27, SAINT Version 7.12a and SADABS Version 2004/1, Bruker AXS: Madison, WI, USA, 2005.

[29]   G.M. Sheldrick, SHELXTL Version 5.10, Bruker AXS Inc., Madison, Wisconsin, USA, 1998.

[30]   L.J. Farrugia, J. Appl. Cryst. 30 (1997) 565.

[31]   K. Bradenburg, H. Putz, DIAMOND Version 3.0, Crystal Impact, GbR, Postfach 1251, D-53002 Bonn, Germany, 2004.

[32]   M.A.S. Goher, F.A. Mautner, Polyhedron 12 (1993) 1863.

[33]   M.-G. Zhao, J.-M. Shi, C.-J. Wu, Z. Kristallogr. 218 (2003) 157.

[34]   G. De Munno, G. Viau, M. Julve, F. Lloret, J. Faus, Inorg. Chim. Acta 257 (1997) 121.

[35]   M.G. Barandika, M.L. Hernández-Pino, M.K. Urtiaga, R. Cortés, L. Lezama, M.I. Arriortua, T. Rojo, J. Chem. Soc., Dalton Trans. (2000) 1469.

[36]   D. Cremer, J.A. Pople, J. Am. Chem. Soc. 97 (1975) 1354.

[37]   K. Mitra, S. Biswas, S.K. Chattopadhyay, B. Adhikary, C.R. Lucas, Trans. Met. Chem. 30 (2005) 185.

[38]   P. Bhunia, B. Baruri, U. Ray, C. Sinha, S. Das, J. Cheng, T.-H. Lu, Trans. Met. Chem. 31 (2006) 310.

[39]   A.B.P. Lever, Inorganic Electronic Spectroscopy, 2nd ed., Elsevier Science, Netherlands (1984).

[40]   R. Luck, R. Stosser, O.G. Poluektov, O. Ya. Grinberg, S. Ya. Lebedev, Z. Anorg. Allg. Chem. 607 (1997) 183.

[41]   G. M. Woltermann, J.R. Wasson, Inorg. Chem. 12 (1973) 2366.

[42]   E. Meirovitch, R. Poupko, J. Phys. Chem. 82 (1978) 1920.

[43]   S.K. Misra, J.-S. Sun, Magn. Reson. Rev. 16 (1991) 57.

[44]   Y. Xu, Y. Chen, K. Ishizu, Y. Li, Appl. Magn. Reson. 1 (1990) 283.

[45]   D.J.E. Ingram, Spectroscopy at Radio and Microwave Frequencies, second ed., Butterworth, London (1967).

[46]   B.S. Garg, M.R.P. Kurup, S.K. Jain, Y.K. Bhoon Trans Met. Chem. 13 (1988) 92.

[47]   K.B. Pandeya, R. Singh, P.K. Mathur, R.P. Singh, Trans Met. Chem. 11 (1986) 347.

[48]   W. Linert, F.Renz, R. Boca, J. Coord. Chem. 40 (1996) 293.

[49]   A. Carington, A.D. Mchachlan, Introduction to Magnetic Resonance, Harper & Row, New York (1969) 173.

[50]   B. Bleny, R.S. Rubins, Proc. Phys. Soc. London 77 (1961) 103.

[51]   E.-Q, Gao, Y.-F. Yue, S.-Q. Bai, Z. He, C.-H. Yan, Cryst. Growth Design 5(2005) 1119.

[52]   S.S. Tandon, L.K. Thompson, M.E. Manuel, J.N. Bridson, Inorg. Chem. 22 (1994) 5555.

[53]   K. Nakamato in Infrared and Raman Spectra of Inorganic and Coordination Compounds, 4th ed., John Wiley & Sons, New York, (1986).

✻✻✻✺✺◯◯✺✻✻✻

Syntheses, structural and spectral investigations of nickel(II) complexes of Schiff bases with azide and thiocyanate

5.1 Introduction

The chemistry of nickel has received considerable attention due to its essential role in bioinorganic chemistry and the presence of nickel in several enzymes [1,2]. Nickel enzymes are involved in various biological reactions [3-6]. Morrow and Kolasa reported the cleavage of plasmid DNA by square planar nickel-salen [bis-(salicylidene) ethylenediamine] in the presence of either magnesium mono peroxypthalic acid (MPPA) or iodosulbenzene [7]. The observation of different oxidation states for nickel during the catalytic cycle, has spurred a great interest in the investigation of the electronic and structural factors that contribute to stabilize a particular oxidation state for the nickel center. Several factors have been recognized to be particularly important in the stabilization of the +3 and +1 oxidation states, namely coordination number, geometry, type of donor atom and electronic characteristics of the ligand.

It has been demonstrated that the azido group inhibits enzymatic reactions [8-14]. Thus, the investigation of nickel-azido complexes has become a field of recent interest to understand the role of the metal ions in biological reactions. Moreover, the study of such complexes and

those with other pseudohalogens like thiocyanate is also useful in the context of enhancement of knowledge about magnetic interactions as well as development of magnetic materials. Lin *et al.* synthesized a Ni((II) complex from an imidazole derivative and azido group, which was found to be a feroomagnetically coupled dimer with double end-on azido bridges between the Ni(II) centres [15]. Neutral cubane complexes of Ni(II) were designed from the gem-diol di-2-pyridyl ketone with acetate and dicyanamide [16]. The investigation of the magnetic properties reveal the presence of ferromagnetic exchange mediated through end-to-end thiocyanate bridges in the one dimensional polymer of Ni(II) synthesized from imidazole [17].

5.2 Stereochemistry

Ni(II) species with d^8 configuration are of special interest existing in all coordination numbers from seven through two. Of these some are very common and some rare. The most frequently encountered coordination numbers of Ni(II) are four, five and six. Four coordinate complexes may be tetrahedral or square planar. The five coordinate complexes may exhibit square pyramidal or trigonal bipyramidal geometry. Six coordinate complexes are usually octahedral. The square pyramidal and square planar complexes are obviously related to the tetragonal six coordinate complexes through tetragonal distortion and the removal of one and two ligands respectively from an octahedral array. Distortions from the above mentioned geometries are also possible by means of the variations in the bond lengths and bond angles. The d^8 configuration is especially prone to form four

coordinate diamagnetic square planar derivatives, particularly with stronger field ligands or where steric hindrance impedes higher coordination numbers. The square planar complexes are diamagnetic, while all others are paramagnetic.

5.3 Experimental
5.3.1 Materials

Pyridine-2-carbaldehyde (Sigma Aldrich), 2-benzoylpyridine (Sigma Aldrich), di-2-pyridyl ketone (Sigma Aldrich), 2-hydroxy-4-methoxybenzaldehyde (Sigma Aldrich), aniline (S. D. Fine), _R_-1-phenylethyl amine (Alfa Aeser), 2-aminopyrimidine (Sigma Aldrich), $Ni(ClO_4)_2 \cdot 6H_2O$ (Sigma Aldrich), $Ni(OAc)_2 \cdot 4H_2O$ (CDH), NaN_3 (Reidel-De Haen), KCNS (BDH) and methanol (Merck) were used as received. Ethanol, when used as the solvent was distilled before use.

5.3.2 Syntheses of nickel(II) complexes

$[Ni_2(paa)_2(N_3)_4] \cdot H_2O$ (18): A mixture of pyridine-2-carbaldehyde (0.107 g, 1 mmol) in methanol and aniline (0.093 g, 1 mmol) in methanol were refluxed for 2 hours to obtain a yellow solution of the Schiff base. To this, $Ni(ClO_4)_2 \cdot 6H_2O$ (0.365 g, 1 mmol) dissolved in methanol was added and stirred followed by the slow addition of an aqueous solution of NaN_3 (0.130 g, 2 mmol). The resulting solution was further stirred for 15 minutes. Brown solid separated out after one week, filtered, washed with water, methanol and ether and dried over P_4O_{10} _in vacuo_. Elemental Anal. Found (Calcd.) (%): C, 43.58 (43.16); H, 3.14 (3.33); N, 34.06 (33.55). μ = 2.95 B.M.

[Ni(paa)₂(NCS)₂]·H₂O (19): A mixture of pyridine-2-carbaldehyde (0.107 g, 1 mmol) in methanol and aniline (0.093 g, 1 mmol) in methanol were refluxed for 2 hours. To the yellow solution of the Schiff base thus obtained, Ni(OAc)₂·4H₂O (0.248 g, 1 mmol) dissolved in hot methanol was added. To this solution, a methanolic solution of KCNS (0.194 g, 2 mmol) was added and refluxed for 4 hours. The brown solid separated out was filtered, washed with methanol, water and ether and dried over P₄O₁₀ *in vacuo*. Elemental Anal. Found (Calcd.) (%): C, 55.77 (56.03); H, 3.69 (3.98); N, 15.64 (15.08); S, 11.92 (11.40). μ = 3.28 B.M.

Ni(papea)₂(NCS)₂ (20): Pyridine-2-carbaldehyde (0.107 g, 1 mmol) and *R*-1-phenylethyl amine (0.121 g, 1 mmol) was refluxed in methanol for 2 hours. To this, a methanolic solution of Ni(OAc)₂·4H₂O (0.248 g, 1 mmol) was added followed by an aqueous solution of KCNS (0.194 g, 2 mmol) and refluxed for 4 hours. Greenish blue block shaped single crystals suitable for X-ray diffraction were isolated within a week. The crystals were mechanically separated and dried. Elemental Anal. Found (Calcd.) (%): C, 60.33 (60.52); H, 4.69 (4.74); N, 14.04 (14.11). μ = 3.30 B.M.

[Ni(paap)(NCS)₂]·³/₂CH₃OH·2H₂O (21): A mixture of pyridine-2-carbaldehyde (0.107 g, 1 mmol) in methanol and 2-aminopyrimidine (0.094 g, 1 mmol) in methanol was refluxed for 2 hours. Methanolic solutions of Ni(OAc)₂·4H₂O (0.248 g, 1 mmol) and solid KCNS (0.194 g, 2 mmol) were added to this and refluxed for 4 hours. Greenish brown solid separated out within two days from the reaction

[Ni(paa)$_2$(NCS)$_2$]·H$_2$O (19): A mixture of pyridine-2-carbaldehyde (0.107 g, 1 mmol) in methanol and aniline (0.093 g, 1 mmol) in methanol were refluxed for 2 hours. To the yellow solution of the Schiff base thus obtained, Ni(OAc)$_2$·4H$_2$O (0.248 g, 1 mmol) dissolved in hot methanol was added. To this solution, a methanolic solution of KCNS (0.194 g, 2 mmol) was added and refluxed for 4 hours. The brown solid separated out was filtered, washed with methanol, water and ether and dried over P$_4$O$_{10}$ *in vacuo*. Elemental Anal. Found (Calcd.) (%): C, 55.77 (56.03); H, 3.69 (3.98); N, 15.64 (15.08); S, 11.92 (11.40). μ = 3.28 B.M.

Ni(papea)$_2$(NCS)$_2$ (20): Pyridine-2-carbaldehyde (0.107 g, 1 mmol) and *R*-1-phenylethyl amine (0.121 g, 1 mmol) was refluxed in methanol for 2 hours. To this, a methanolic solution of Ni(OAc)$_2$·4H$_2$O (0.248 g, 1 mmol) was added followed by an aqueous solution of KCNS (0.194 g, 2 mmol) and refluxed for 4 hours. Greenish blue block shaped single crystals suitable for X-ray diffraction were isolated within a week. The crystals were mechanically separated and dried. Elemental Anal. Found (Calcd.) (%): C, 60.33 (60.52); H, 4.69 (4.74); N, 14.04 (14.11). μ = 3.30 B.M.

[Ni(paap)(NCS)$_2$]·^{3}/$_2$CH$_3$OH·2H$_2$O (21): A mixture of pyridine-2-carbaldehyde (0.107 g, 1 mmol) in methanol and 2-aminopyrimidine (0.094 g, 1 mmol) in methanol was refluxed for 2 hours. Methanolic solutions of Ni(OAc)$_2$·4H$_2$O (0.248 g, 1 mmol) and solid KCNS (0.194 g, 2 mmol) were added to this and refluxed for 4 hours. Greenish brown solid separated out within two days from the reaction

medium, filtered, washed and dried over P_4O_{10} *in vacuo*. Elemental Anal. Found (Calcd.) (%): C, 36.14 (36.79); H, 3.60 (4.09); N, 18.80 (18.96). $\mu = 0$ B.M.

[Ni$_2$(dpk·OH)$_2$(N$_3$)$_2$]·3(CH$_3$CH$_2$OH)·3H$_2$O (22): Di-2-pyridyl ketone (0.187 g, 1 mmol) was dissolved in ethanol and aniline (0.093 g, 1 mmol) was added to this. About 4-5 drops of glacial acetic acid was also added and refluxed for 6 hours. To the above solution, Ni(OAc)$_2$·4H$_2$O (0.248 g, 1 mmol) dissolved in hot ethanol was added. An aqueous solution of NaN$_3$ (0.130 g, 2 mmol) was added to the above mixture slowly with stirring. The resulting solution was stirred for 6 hours. The greenish blue product formed was filtered, washed with ethanol, water and ether and dried over P_4O_{10} *in vacuo*. Elemental Anal. Found (Calcd.) (%): C, 41.71 (42.24); H, 5.60 (5.32); N, 17.67 (17.59). $\mu = 0$ B.M.

[Ni(Hhmba)(hmba)(NCS)]·2CH$_3$OH·2H$_2$O (23): 2-Hydroxy-4-methoxybenzaldehyde (0.152 g, 1 mmol) was dissolved in methanol. To this, aniline (0.093 g, 1 mmol) was added. The mixture was refluxed for 2 hours. Ni(OAc)$_2$·4H$_2$O (0.248 g, 1 mmol) dissolved in methanol and an aqueous solution of KCNS (0.094 g, 1 mmol) was added and refluxed for 6 hours. The reaction mixture was filtered and was kept for the evaporation of the solvent. Yellowish green product separated out within a week. Filtered, washed with methanol and water and then with by ether and dried over P_4O_{10} *in vacuo*. Elemental Anal. Found (Calcd.) (%): C, 55.38 (55.54); H, 5.42 (5.56); N, 5.70 (6.27). $\mu = 0$ B.M.

Caution! Although not encountered in our experiments, azide complexes are potentially explosive. Only a small amount of the material should be prepared, and it should be handled with care.

5.4 Results and discussion

The condensation of aldehyde/ketone and amine in 1:1 molar ratio yielded the Schiff base ligands, which were used without further purification for the synthesis of the complexes by reaction in presence of pseudohalides NaN_3/KCNS. All the complexes had the Schiff bases as neutral bidentate *N, N* donors. The nickel(II) complex **22**, which was synthesized from the Schiff base obtained by the condensation of di-2-pyridyl ketone and aniline is not having the Schiff base as the ligand. The Schiff base has undergone hydrolysis in presence of metal to form the gem-diol of di-2-pyridyl ketone. Nucleophilic addition of water to di-2-pyridyl ketone results in the formation of the gem-diol of di-2-pyridyl ketone to undergo metal-mediated nucleophilic addition of small molecules like water or alcohol to the carbonyl group results in the formation of hydrate or hemiacetal [18-22]. It is thus the gem-diol of di-2-pyridyl ketone, which is the ligand in complex **22**. In complex **23**, two Schiff bases are present, of which one coordinates to the metal after deprotonation through the deprotonated O atom and the azomethine N, while in the other there is a free –OH group.

The magnetic susceptibility measurements indicate that the complexes **18**, **19** and **20** are paramagnetic. The complexes **21**, **22** and **23** are diamagnetic, suggesting a four coordinate square planar geometry for them. All the complexes were found to be soluble in

154

DMF, DMSO and acetonitrile, but only partially soluble in other organic solvents such as CHCl₃, ethanol, methanol etc.

5.4.1 Crystallographic data collection and structure analysis

Single crystal X-ray diffraction measurements of complexes **20** were carried out on a Bruker Smart Apex 2 CCD area detector diffractometer at the X-ray Crystallography Unit, School of Physics, Universiti Sains Malaysia, Penang, Malaysia. The unit cell parameters were determined and the data collections were performed using a graphite-monochromated MoKα (λ = 0.71073 Å) radiation at a detector distance of 5 cm at 100(1) K with the Oxford Cyrosystem Cobra low-temperature attachment. The collected data were reduced using SAINT program [23] and the empirical absorption corrections were performed using SADABS program [23]. The structures were solved by direct methods and refinement was carried out by full-matrix least squares on F^2 using the SHELXTL software package [24]. All non-hydrogen atoms were refined anisotropically. Hydrogen atoms were geometrically fixed at calculated positions and allowed to ride on their parent atoms. Molecular graphics employed were ORTEP-III [25] and DIAMOND [26].

5.4.2 Crystal Structure

Ni(papea)₂(NCS)₂ (20): Complex **20** crystallizes in an orthorhombic crystal system with four molecules in the unit cell. It belongs to the chiral space group $P2_12_12_1$. The structural refinement parameters are given in Table 5.1 and the molecular structure of the complex is depicted in Fig 5.1. The important bond lengths and bond angles are given in Table 5.2. The ligand retains its configuration in the complex

as well. In this complex, the carbon atoms C7 and C21 have the R configuration.

Table 5.1. Crystal data and structure refinement

Parameters	Ni(papea)$_2$(NCS)$_2$
Empirical formula	C$_{30}$H$_{28}$NiN$_6$S$_2$
Formula weight	595.41
Temperature	100(1) K
Color	Blue
Nature	Blocks
Wavelength	0.71073 Å
Crystal system	Orthorhombic
Space group	$P2_1P2_1P2_1$ (No:19)
Unit cell dimensions	a = 13.2009(2) Å
	b = 14.6881(2) Å
	c = 14.7152(2) Å
	α = 90.00°
	β = 90.00°
	γ = 90.00°
Volume V (Å^3), Z	2853.22(7), 4
Calculated density (ρ) (Mg m^{-3})	1.386
Absorption coefficient μ (mm^{-1})	0.857
F(000)	1240
Crystal size (mm^3)	1.06x0.34x0.27
θ range for data collection	2.49 - 39.05°
Index ranges	-24≤h≤17, -27≤k≤26, -26≤ l≤26
Reflections collected / unique	73388/19490 [R(int) = 0.0374]
Completeness to 2θ = 42.03	99.1%
Absorption correction	SADABS
Maximum and minimum transmission	0.4633, 0.8009
Refinement method	Full-matrix least-squares on F^2
Data / restraints / parameters	19490/0/352
Goodness-of-fit on F^2	0.994
Final R indices [I>2σ(I)]	R$_1$ = 0.0338, wR$_2$ = 0.0724
R indices (all data)	R$_1$ = 0.0493, wR$_2$ = 0.0724
Largest diff. peak and hole	0.577 and -0.260
Absolute structure parameter	-0.001(4)

Ni(II) has a distorted octahedral NiN$_6$ coordination environment satisfied by two molecules of the neutral bidentate *N, N* Schiff base ligand papea and two thiocyanate anions. The octahedral coordination around Ni(II) is completed by pairs of *trans* pyridyl N (N1 and N3), *cis* azomethine N (N2 and N4) and *cis* thiocyanate N (N5 and N6) atoms.
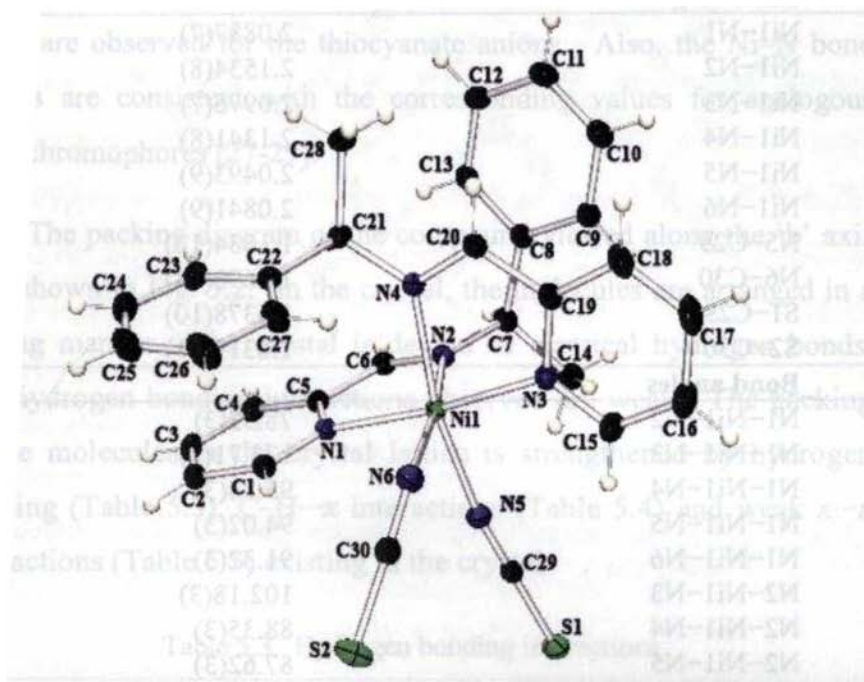
Fig. 5.1. Molecular structure of **Ni(papea)$_2$(NCS)$_2$ (20)**.

The thiocyanate anions act as N-donors as reported for similar structurally characterized complexes [27,28]. The thiocyanate anions are in the terminal mode coordinating through the N atom. The NCS groups are almost linear (N5–C29–S1=179.40(10)° and N6–C30–S2=178.46(9)°). One of the NCS coordinates to the Ni(II) in a linear fashion (C29–N5–Ni1=171.77(8)°), but pronounced bending at the N atom is

observed for the second NCS group (C30–N6–Ni1=133.07(8)°). This behaviour of the thiocyanate is similar to that reported previously for the mixed ligand diethanolamine-Ni[II] complex of thiocyanate [29].

Table 5.2. Selected bond lengths (Å) and bond angles (°) for Ni(papea)$_2$(NCS)$_2$

Bond lengths	
Ni1–N1	2.0887(7)
Ni1–N2	2.1534(8)
Ni1–N3	2.0976(7)
Ni1–N4	2.1341(8)
Ni1–N5	2.0493(9)
Ni1–N6	2.0841(9)
N5–C29	1.1634(13)
N6–C30	1.1690(14)
S1–C29	1.6378(10)
S2–C30	1.6319(11)
Bond angles	
N1–Ni1–N2	78.52(3)
N1–Ni1–N3	173.71(3)
N1–Ni1–N4	95.74(3)
N1–Ni1–N5	94.02(3)
N1–Ni1–N6	91.32(3)
N2–Ni1–N3	102.18(3)
N2–Ni1–N4	88.35(3)
N2–Ni1–N5	87.62(3)
N2–Ni1–N6	169.13(3)
N3–Ni1–N4	78.07(3)
N3–Ni1–N5	92.26(3)
N3–Ni1–N6	88.35(3)
N4–Ni1–N5	168.49(3)
N4–Ni1–N6	96.60(3)
N5–Ni1–N6	89.26(4)
Ni1–N5–C29	171.76(8)
Ni1–N6–C30	133.07(8)
S1–C29–N5	179.40(9)
S2–C30–N6	178.46(9)

The five membered chelate rings give rise to considerable distortion in the octahedral geometry, with bite angles 78.52(3)° and 78.06(3)° for the two Schiff base ligands respectively. This distortion is probably due to the steric requirements of the methyl group on the ligand. As expected, the Ni–N bond lengths are longer for the azomethine nitrogens than the pyridyl nitrogens. The shortest Ni–N bonds are observed for the thiocyanate anions. Also, the Ni–N bond lengths are consistent with the corresponding values for analogous NiN_6 chromophores [27-29].

The packing diagram of the compound viewed along the 'b' axis is as shown in Fig. 5.2. In the crystal, the molecules are arranged in a zig-zag manner. The crystal is devoid of classical hydrogen bonds. The hydrogen bonding interactions observed are weak. The packing of the molecules in the crystal lattice is strengthened by hydrogen bonding (Table 5.3), C–H···π interactions (Table 5.4) and weak π···π interactions (Table 5.5) existing in the crystal.

Table 5.3. Hydrogen bonding interactions

D–H···A	D–H (Å)	H···A (Å)	D···A (Å)	D–H···A (Å)
C(1)–H(1A)···N(6)	0.93	2.61	3.1387(14)	117

D=donor, A=acceptor; Equivalent position code: a =-x, 1/2+y, 3/2-z

Table 5.4. C–H···π interactions

C–H(I)···Cg(J)	H···Cg (Å)	C···Cg (Å)	C–H···Cg (°)
C(21)–H(21A)[1]···Cg(1)[a]	2.78	3.2478(10)	110

Equivalent position code: a = x, y, z
Cg(1) = Ni1, N1, C5, C6, N2
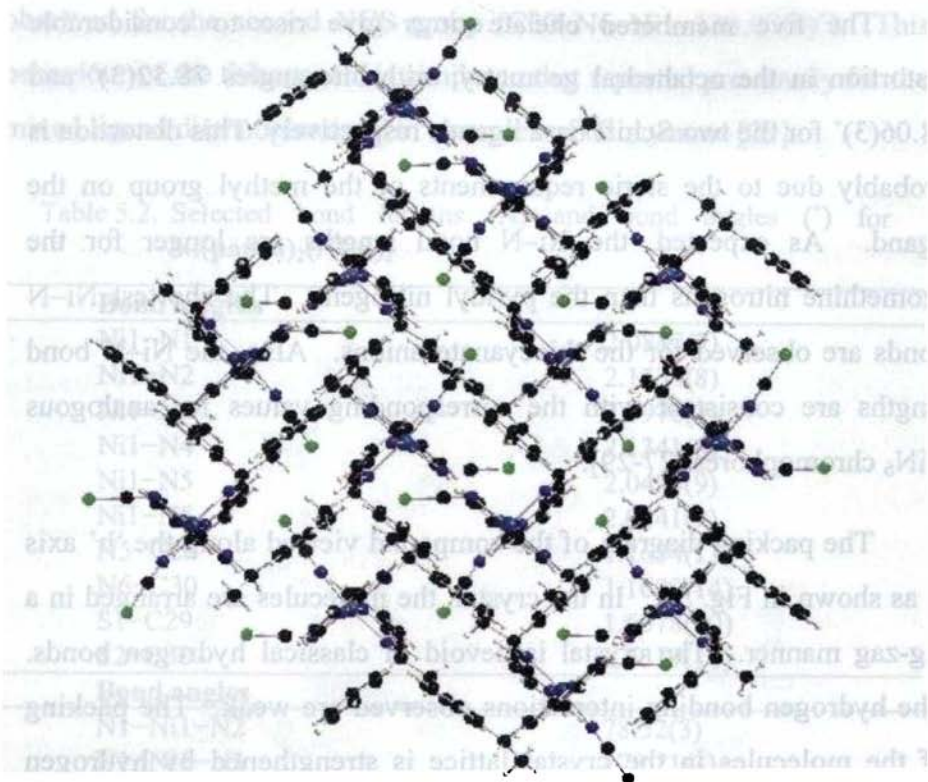
Fig. 5.2. Packing diagram of **Ni(papea)₂(NCS)₂ (20)** viewed along the 'b' axis.

Table 5.5. $\pi\cdots\pi$ interactions

Cg(I)Res(I)···Cg(J)	Cg···Cg (Å)	α (°)	β (°)	γ (°)
Cg(2)[1]···Cg(5)[a]	3.7740(5)	10.63	25.63	30.81
Cg(3)[1]···Cg(5)[b]	3.7224(6)	7.08	26.28	19.40
Cg(3)[1]···Cg(6)[a]	3.9807(6)	11.00	37.64	32.37
Cg(5)[1]···Cg(2)[a]	3.7740(5)	10.63	30.81	25.63
Cg(5)[1]···Cg(3)[c]	3.7224(6)	7.08	19.40	26.28
Cg(6)[1]···Cg(3)[a]	3.9807(6)	11.00	32.37	37.64

Equivalent position code: a = x, y, z; b = 1/2+x,3/2-y,1-z; c = -1/2+x,3/2-y,1-z

Cg(2) = Ni1, N3, C19, C20, N4; Cg(3) = N1, C1, C2, C3, C4, C5; Cg(5) = C8, C9, C10, C11, C12, C13; Cg(6) = C22, C23, C24, C25, C26, C27

160

5.4.3 Spectral characteristics of nickel complexes

5.4.3a *Electronic spectra*

The electronic spectroscopy of Ni(II) ion is of special interest because of the existence of the d^8 in a range of coordination numbers from two to seven. The electronic spectroscopic data available for Ni(II) is probably more that that available for any other metal ion.

For an octahedral nickel (II) complex, three spin allowed transitions are expected *viz.* $v_1 = {}^3T_{2g}(F) \leftarrow {}^3A_{2g}(F)$ (1420–770 nm), $v_2 = {}^3T_{1g}(F) \leftarrow {}^3A_{2g}(F)$ (900–500 nm) and $v_3 = {}^3T_{1g}(P) \leftarrow {}^3A_{2g}(F)$ (520–370 nm) [30]. In addition, two spin forbidden transitions ${}^1E_g(D) \leftarrow {}^3A_{2g}(F)$ and ${}^1T_{1g}(D) \leftarrow {}^3A_{2g}(F)$ are quite prominent. Usually the two spin forbidden transitions remain scrambled due to the fact that the ${}^1E_g$ state lies very close to the ${}^1T_{1g}$ state. The square planar complexes of Ni(II) typically have a single band in the region 650-400 nm. They have no absorption below 1000 nm. The λ_{max} values displayed by the complexes are listed in Table 5.6.

The compound **18** exhibited broad *d-d* bands at 830, 650 and 530 nm, which can be tentatively assigned to the transitions ${}^3T_{2g}(F) \leftarrow {}^3A_{2g}(F)$, ${}^3T_{1g}(F) \leftarrow {}^3A_{2g}(F)$ and ${}^3T_{1g}(P) \leftarrow {}^3A_{2g}(F)$ respectively. This suggests that the Ni(II) ion in complex **18** to be having an octahedral geometry [31-35]. These broad bands might have masked the very low intensity spin forbidden transitions. The broad band observed at 420 nm is attributed to the charge transfer band. The ligand-based transitions were observed at 308 ($\pi \rightarrow \pi^*$) and 343 nm ($n \rightarrow \pi^*$).

161

The electronic spectrum of compound **19** is similar to the above compound and those reported previously. Three weak *d-d* bands were found at 883, 790 and 573 nm, which are the electronic transitions of a six coordinate octahedral stereochemistry. The L → Ni charge transfer band was viewed at 420 nm. The compound reveals $n \rightarrow \pi *$ transition at 346 nm and $\pi \rightarrow \pi *$ transition at 308 nm.

In compound **20**, the three weak bands observed at 880, 662 and 575 nm are due to the $^3T_{2g}(F) \leftarrow \ ^3A_{2g}(F)$, $^3T_{1g}(F) \leftarrow \ ^3A_{2g}(F)$ and $^3T_{1g}(P) \leftarrow \ ^3A_{2g}(F)$ transitions respectively of a distorted octahedral complex. There is a spin forbidden transition $^1E_g(D) \leftarrow \ ^3A_{2g}(F)$ near 785 nm, the presence of which has led to the lowered intensity of v_1 transition [30]. The charge transfer band is observed at 375 nm. The ligand centered transitions are viewed at 345 and 295 nm.

The electronic spectrum of the nickel(II) complex **21** showed a single band *ca.* 620 nm due to the $^3A_{2g}(F) \leftarrow \ ^3B_{1g}(F)$ arising from a square planar geometry [36,37]. The absence of absorption below 1000 nm confirms the square planar stereochemistry of complex **21**. The charge transfer band is seen at 375 nm. The compound reveals $n \rightarrow \pi *$ transition at 346 nm and $\pi \rightarrow \pi *$ transition at 303 nm.

Complex **22** displayed a single band *ca.* 600 nm due to the $^3A_{2g}(F) \leftarrow \ ^3B_{1g}(F)$ of a square planar geometry. The absence of absorption below 1000 nm in this case also confirms the square planar stereochemistry of the complex. The charge transfer band is seen at

425 nm. The compound reveals $n \rightarrow \pi *$ transition at 350 nm and $\pi \rightarrow \pi *$ transition at 292 nm.

The thiocyanato complex **23** has a spectrum indicative of the square planar geometry of the complex. The *d-d* band is observed at 660 nm as a broad band. There are no absorptions below 1000 nm. The charge transfer band is seen at 405 nm. The compound reveals $n \rightarrow \pi *$ transition at 342 nm and $\pi \rightarrow \pi *$ transition at 296 nm.

Table 5.6. Electronic spectral assignments of the nickel(II) compounds in nm

Compounds	Ligand transitions	d-d	Charge transfer
$[Ni_2(paa)_2(N_3)_4] \cdot H_2O$ **(18)**	308, 343	530, 650, 830	420
$[Ni(paa)_2(NCS)_2] \cdot H_2O$ **(19)**	308, 346	573, 790, 883	420
$Ni(papea)_2(NCS)_2$ **(20)**	295, 345	575, 662, 880, 785(sh)	375
$[Ni(paap)(NCS)_2] \cdot ^3/_2 CH_3OH \cdot 2H_2O$ **(21)**	303, 346	620	375
$[Ni_2(dpk \cdot OH)_2(N_3)_2] \cdot 3(CH_3CH_2OH) \cdot 3H_2O$ **(22)**	292, 350	600	425
$[Ni(Hhmba)(hmba)(NCS)] \cdot 2CH_3OH \cdot 2H_2O$ **(23)**	296, 342	660	405

5.4.3b *IR spectra*

IR spectroscopy is a useful tool to confirm the coordination of various atoms and groups to the metal from the position and nature of the bands associated with them.

The IR spectrum of compound **18** (Fig. 5.3) reveals a broad band around 3359 cm^{-1} which corresponds to the lattice water present in the compound. The medium peak at 1590 cm^{-1} is assigned as the v(C=N) stretching mode of the azomethine function of the Schiff base, the position of which is in agreement with the previous reports and is thus indicative of the coordination of azomethine N [38]. The bands at 1561, 1427 and 1021 cm^{-1} are attributed to the vibrations of the pyridyl ring and phenyl ring. The in-plane ring deformation of the pyridyl ring and the pyridyl ring out-of-plane bending are observed at 673 and 489 cm^{-1} as weak bands. The above observations indicate the coordination of pyridyl N to nickel(II).
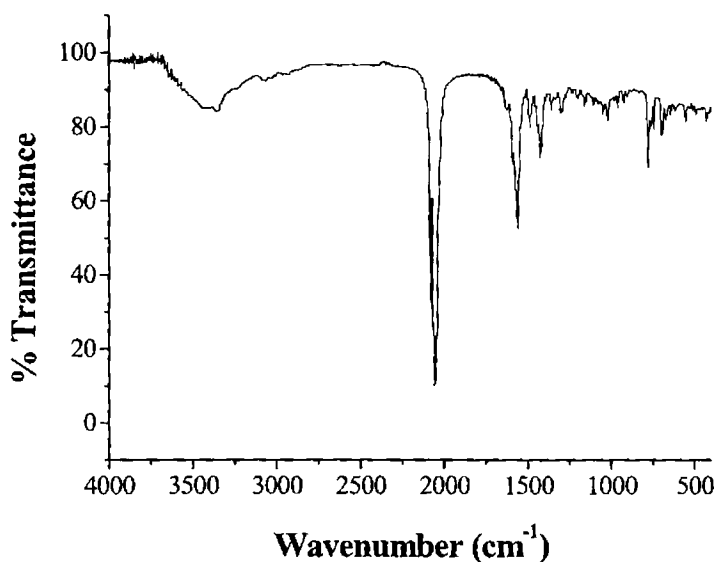
Fig. 5.3. IR spectrum of compound **18**.

The most interesting bands in the IR spectrum of the compound are those associated with the azido groups. There are two strong bands

at 2082 and 2055 cm^{-1} which is associated with the v_{as} asymmetric stretching mode of the azide ligand. The split of this band is indicative of the bridging nature of the azide. The $v_s(N_3)$ stretching mode of the azide group is observed at 1360 cm^{-1} as bands of medium intensity, which rules out the possibility of end-to-end azide bridges since the $v_s(N_3)$ vibration mode in inactive in end-to-end bridges which possess high symmetry [39]. The bending mode of the azido ligand is observed as a weak band at 699 cm^{-1}.

The $v(C=N)$ stretch due to the azomethine group of the Schiff base in compound **19** (Fig. 5.4) occurs as a medium band at 1594 cm^{-1} and indicates that the azomethine N remains coordinated. The coordination of the pyridyl nitrogen is confirmed by the presence of pyridyl ring stretching vibrations at 1633 and 1486 cm^{-1}, pyridyl ring breathing at 1019 cm^{-1}, pyridyl in-plane ring deformation at 642 cm^{-1} and pyridyl out-of-plane ring deformation at 423 cm^{-1}. The most interesting part of the spectrum is the 2000-2100 cm^{-1} region where the strong absorption bands due to the thiocyanate group is visible. There is a single strong and sharp peak at 2086 cm^{-1} assignable to the $v(CN)$ stretching mode of a thiocyanate group. The absence of splitting in this band suggests that the two thiocyanate groups in the complex are trans located and are coordinated to the metal through N atom. The $v(CS)$ is found at 776 cm^{-1} and the $\delta(NCS)$ bending mode is obtained at 556 cm^{-1} confirming the existence of N-bonded NCS group.
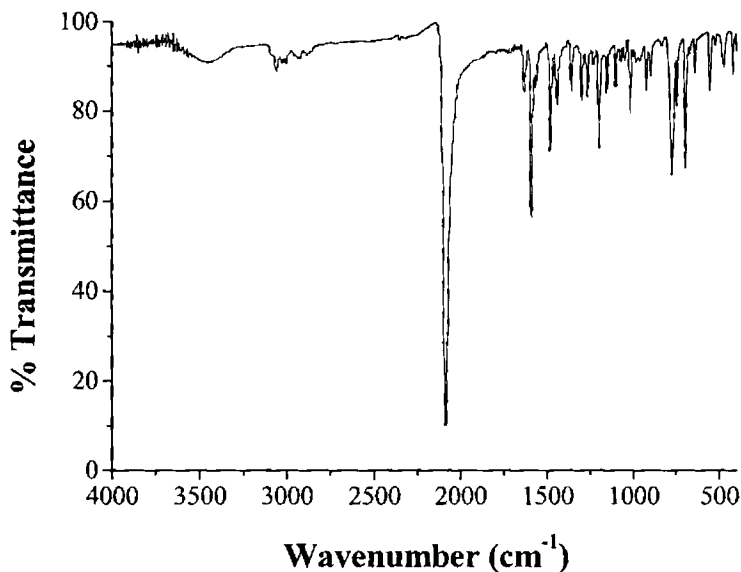
Fig. 5.4. IR spectrum of compound **19**.

In the thiocyanate complex **20** (Fig 5.5), the medium intensity peak at 1597 cm^{-1} is assigned to the absorption of the azomethine function and indicates its coordination. The pyridyl ring stretching and breathing vibrations observed at 1637, 1445 and 1020 cm^{-1} and the pyridyl in-plane ring deformation at 643 cm^{-1} and pyridyl out-of-plane ring deformation at 424 cm^{-1} suggest the coordination of pyridyl N. Two strong peaks observed at 2098 and 2057 cm^{-1} are due to the v(CN) stretching of the thiocyanate group. The position of the peak and the doublet structure points out to the presence of two N-bonded terminal thiocyanate groups in the complex and their cis location in the octahedral complex. The v(CS) of the NCS ligand is seen at 762 cm^{-1} and the bending vibration of the NCS group is at 503 cm^{-1}.

166
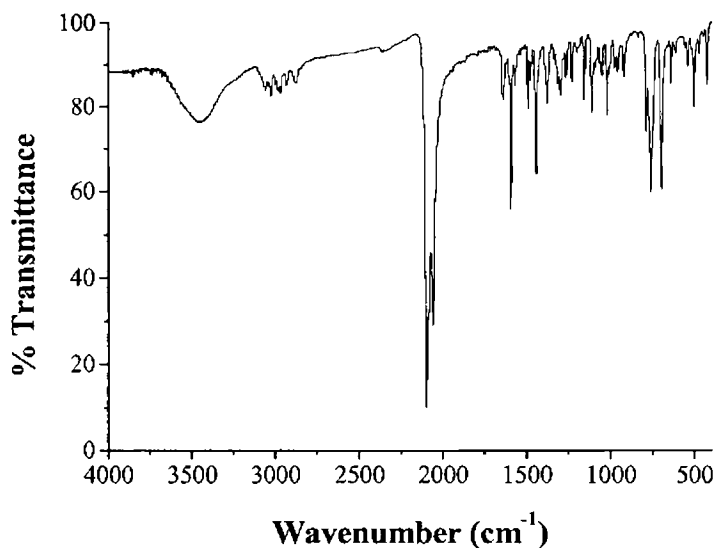
Fig. 5.5. IR spectrum of compound **20**.

Complex **21** (Fig. 5.6) has a medium band at 1568 cm^{-1} assignable to the v(C=N) stretching mode of the azomethine group, indicating the azomethine N coordination. The pyridyl N of the Schiff base is also coordinated as evident from the shifts in the absorption frequencies due to the pyridyl ring. The pyridyl ring stretching is observed as strong bands at 1600 and 1454 cm^{-1}, the breathing mode of the pyridyl ring is at 1068 cm^{-1} and the pyridyl in-plane and out-of-plane ring deformation is at 653 and 422 cm^{-1} respectively. The spectrum is further complicated by the vibrations due to the pyrimidine ring, which also occurs in the same region as that of the pyridine ring. The characteristic asymmetric stretching due to the thiocyanate is observed as a strong peak at 2091 cm^{-1}, which clearly indicates the presence of one type of non-bridging

167

thiocyanate bonded through N atom. This is possible only if the square planar complex **21** has the thiocyanate anions trans with respect to each other. The v(CS) of the NCS ligand is seen at 758 cm^{-1} and the bending vibration of the NCS group is at 474 cm^{-1}. A broad band due to the presence of lattice water in the complex was seen at 3396 cm^{-1}.
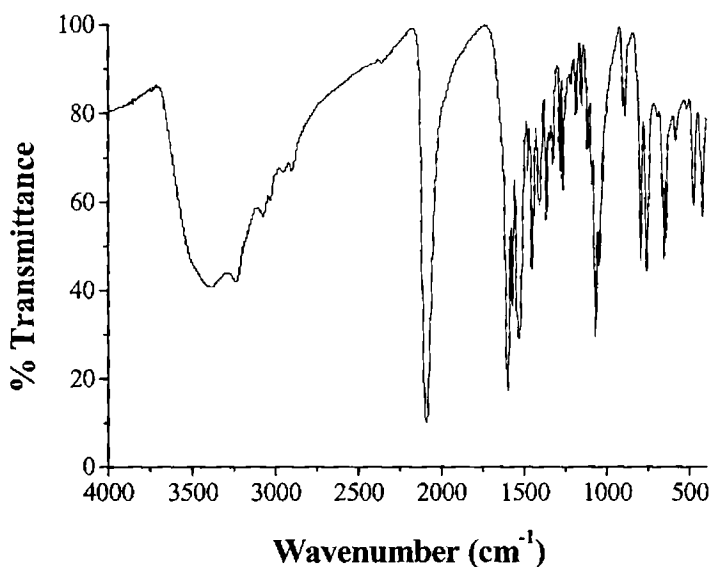
Fig. 5.6. IR Spectrum of compound **21**.

For compound **22** (Fig. 5.7), the broad and medium intensity band at 3377 cm^{-1} is assigned to the v(OH) vibrations. In relation to the absorptions caused by the organic ligand dpk reported elsewhere, it is worth mentioning that the band at 1680 cm^{-1}, assigned to the C=O bond in dpk, is shifted to 1603 cm^{-1} after solvolysis due to the presence of the C–O bond in the complex [18,22,40].

168
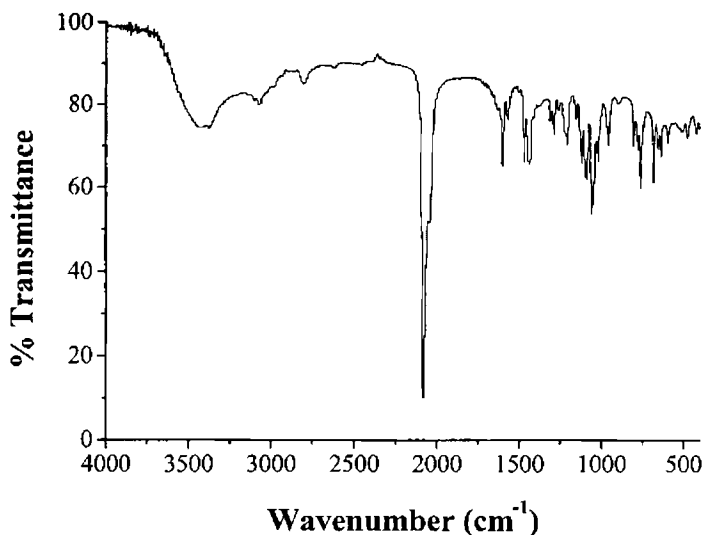
Fig. 5.7. IR spectrum of compound **22**.

Additionally, the IR spectrum of compound **22** revealed the bands corresponding to the skeleton vibrations of the coordinated dpk·OH which appear at slightly shifted frequencies in relation to free dpk. Thus, bands for coordinated dpk·OH (free dpk) are: 1469 (1578) cm^{-1} attributed to the pyridyl ring stretching; 1059 (998) cm^{-1} for the pyridyl ring breathing; 763 (753, 742) cm^{-1} attributed to the pyridyl ring C–H out-of-plane bending and 683 (662) cm^{-1} for the pyridyl ring in-plane vibration. The characteristic $v_{as}(N_3)$ stretching vibrations due to the azide is observed as a strong peak at 2084 cm^{-1}. This suggests the occurrence of bridged azide in the complex. The absence of the symmetric azide absorptions in the 1300 cm^{-1} region implies the bridging azide to be of the end-on type, since the symmetrical $v_s(N_3)$ stretch of end-to-end azide bridge is not IR active.

169

The IR spectrum of compound **23** (Fig. 5.8) can be compared with the spectrum of the ligand Hhmba and the differences in the frequencies of absorption of various functions and groups can be regarded as the evidences for coordination. The spectrum exhibits a broad band *ca.* 3410 cm^{-1} due to the stretching of the –OH group. The ν(C=N) stretching vibration of the azomethine function is observed as a band of medium intensity at 1624 cm^{-1} in the ligand. This band shifts by about 34 cm^{-1} and is seen as a strong intensity band at 1590 cm^{-1} in the spectrum of the complex. This is a very good evidence for the coordination of the azomethine N. Thus, in the complex, two Schiff base ligands are present, out of which one undergoes deprotonation and coordinates to the metal through the oxygen atom and azomethine N while the other remains protonated and has a free –OH and coordinates through the azomethine N alone.
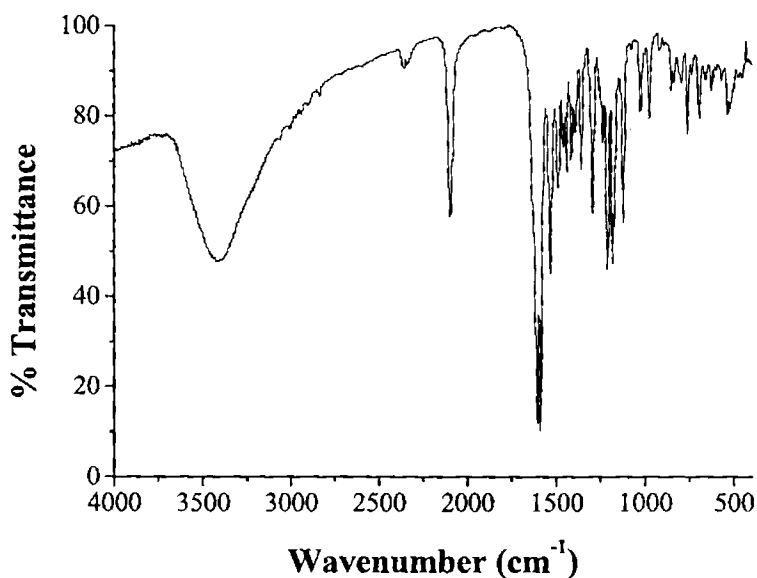
Fig 5.8. IR spectrum of compound **23**.

The fourth coordination of the square planar complex is completed by the N-bonded terminal thiocyanate ligand. This coordination mode of thiocyanate in the complex is supported by the observation of a single peak of medium intensity at 2097 cm^{-1}. The v(CS) of the NCS ligand is seen at 761 cm^{-1} and the bending vibration of the NCS group is at 535 cm^{-1}.

References

[1]   A.F. Kolodziej, Prog. Inorg. Chem. 41 (1994) 493.

[2]   D.X. West, H. Gebremedhin, R.J. Butcher, J.P. Jasinski, A.E. Liberta, Polyhedron 12 (1993) 2489.

[3]   J.R. Lancaster, Jr. (Ed.), The Bioinorganic Chemistry of Nickel, VCH Publishers, New York (1998).

[4]   M.A. Halcrow, G. Cristou, Chem. Rev. 94 (1994) 2421.

[5]   T.I. Doukov, T.M. Iverson, J. Seravalli, S.W. Ragsdab, C.L. Drenman, Science 298 (2002) 567.

[6]   J. Wuerges, J.-W. Lee, Y.-I. Yim. H.-S. Yim, S.-O. Kang, K.D. Carugo, Proc. Natl. Acad. Sci. USA 101 (2004) 8569.

[7]   J.R. Morrow, K.A. Kolasa, Inorg. Chim. Acta 195 (1992) 245.

[8]   E.I. Solomon, U.M. Sundaram, T.E. Machonkin, Chem. Rev. 96 (1996) 2563.

[9]   K.A. Magnus, H. Ton-That, J.E. Carpenter, Chem. Rev. 94 (1994) 727.

[10]   E.I. Solomon, M.J. Baldwin, M.D. Lowery, Chem. Rev. 92 (1992) 521.

[11]   M. Trémoliéres, J.G. Bieth, Phytochemistry 23 (1984) 501.

[12]   A. Rompel, H. Fisher, K. Büldt-Karentzopoulos, D. Miewes, F. Zippel, H.F. Nolting, C. Hermes, B. Krebs, H. Witzel, J. Inorg. Biochem. 59 (1995) 715.

[13]   H.-D. Youn, E.-J. Kim. J.-H. Roe, Y.C. Hah, S.-O. Kang, Biochem. J. 318 (1996) 1452.

[14]   R.K. Watt, P.W. Ludden, J. Bacteriol. 181 (1999) 4554.

[15]   X.-J. Lin, Z. Shen, Y. Song, H.-J. Xu, Y.-Z. Li, X.-Z. You, Inorg. Chim. Acta 358 (2005) 1963.

[16]   G.S. Papaefstathiou, A. Escuer, F.A. Mautner, C. Raptopoulou, A. Terzis, S.P. Perlepes, R. Vicente, Eur. J. Inorg. Chem. (2005) 879.

[17]   B. Żurowska, J. Mroziński, M. Julve, F. Lloret, A. Maslejova, W. Sawska-Dobrowolska, Inorg. Chem. 41 (2002) 1771.

[18]   Z.E. Serna, R. Cortés, M.K. Urtiaga, M.G. Barandika, L. Lezama, M.I. Arriortua, T. Rojo, Eur. J. Inorg. Chem. (2001) 865.

[19]   V. Rattanaphani, W.R. McWhinnie, Inorg. Chim. Acta 9 (1974) 239.

[20]   G.S. Papaefstathiou, A. Escuer, C.P. Raptopoulou, A. Terzis, S.P. Perlepes, R. Vicente, Eur. J. Inorg. Chem. (2001) 1567.

[21]   J.M. Seco, M. Quirós, M.J.G. Garmendia, Polyhedron 19 (2000) 1005.

[22]   Z.E. Serna, M.G. Barandika, R. Cortés, M.K. Urtiaga, G.E. Barberis, T. Rojo, J. Chem. Soc., Dalton Trans. (2000) 29.

[23]   Bruker APEX2 Version 1.27, SAINT Version 7.12a and SADABS Version 2004/1, Bruker AXS: Madison, WI, USA, 2005.

[24]   G.M. Sheldrick, SHELXTL Version 5.10, Bruker AXS Inc., Madison, Wisconsin, USA, 1998.

[25]   L.J. Farrugia, J. Appl. Cryst. 30 (1997) 565.

[26]   K. Bradenburg, H. Putz, DIAMOND Version 3.0, Crystal Impact, GbR, Postfach 1251, D-53002 Bonn, Germany, 2004.

[27]   A. Karadag, A. Buluk, O. Büyükgüngőr, Acta Cryst. C60 (2004) m402.

[28]   V.T. Yilmaz, A. Karadag, C. Thoene, R. Herbst-Irmer, Acta
        Cryst. C56 (2000) 948.

[29]   X.-M. Ouyang, B.-L. Fei, T.-aki Okamura, H.-W. Bu, W.-Y. Sun,
        W.-X. Tang, N. Ueyama, Eur. J. Inorg. Chem. (2003), 618.

[30]   A.B.P. Lever, Inorganic Electronic Spectroscopy, 2nd ed.,
        Elsevier Science Publishers (1984).

[31]   R. Cortés, K. Urtiaga, L. Lezama, J.L. Pizarro, A. Goñi, M.I.
        Arriortua, T. Rojo, Inorg. Chem. 33 (1994) 4009.

[32]   L.J. Wilson, D. Georges, M.A. Hoselton, Inorg. Chem. 14
        (1975) 2698.

[33]   R.D. Hanrock, G.J. McDougall, J. Chem. Soc., Dalton Trans.
        (1997) 67.

[34]   E. Larsen, G.N. Lamar, B.E. Wagner, J.E. Parks, R.H. Holm,
        Inorg. Chem. 11 (1972) 2652.

[35]   K. Wieghardt, W. Schmidt, W. Herrmann, H.-J. Kuppers, Inorg.
        Chem. 22 (1983) 2953.

[36]   D.U. Warad, C.D. Satish, V.H. Kulkarni, C.S. Bajgur, Ind.
        J. Chem. 39A (2000) 415.

[37]   V.G. Gnanasoundari, K. Natarajan, Trans. Met. Chem. 29
        (2004) 511.

[38]   E.-Q, Gao, Y.-F. Yue, S.-Q. Bai, Z. He, C.-H. Yan, Cryst.
        Growth Design 5(2005) 1119.

[39]   J. Nelson, S. M. Nelson, J. Chem. Soc. A (1969) 1597.

[40]   R.R. Osborne, W. R. McWhinnie, J. Chem. Soc. A (1967) 2075.

❀❀❀ℰ✲ℭℛ❀❀❀

Syntheses, structural and spectral investigations of cobalt(II/III) complexes of Schiff bases with azide and thiocyanate

6.1 Introduction

The coordination chemistry of cobalt is of considerable interest since cobalt(II) and cobalt(III) complexes derived from Schiff bases are reported to be biologically active [1-4]. Since cobalt is present in the active sites of several important classes of metalloproteins, their study is of great interest in various aspects of chemistry [5-8]. Vitamin B_{12}, which is involved in the production of red blood cells is a cobalt(III) complex with a substituted corrin macrocycle [9,10]. Cobalt(III) complexes have shown specific hypoxic radiosensitization and thermosensitization as well as anti-tumor activity in vivo [11-16]. The antitumor action of cobalt(III) complexes with tetradentate Schiff bases derived from aliphatic beta-diketones and diamines was observed in the case of ascite form of Erlich carcinoma [17]. Cobalt(III) complexes of Schiff bases are found to be potential antiviral agents [18,19]. Many model complexes of cobalt in both +2 and +3 oxidation states have been prepared and investigated, with particular emphasis on the reactivity of metal ions in the transmethylation reaction and the reversible absorption of molecular oxygen [20-22]. Cobalt complexes are also useful as catalysts in the synthesis and hydrolysis of peptides [23,24]. Azide acts

as an inhibitor for several enzymes like ATPases [25]. Hence the study of metal-azido complexes is very useful for the understanding of biological processes.

The complexes with pseudohalogens like azide and thiocyanate is also interesting for the development of new molecule based magnetic materials because these anions have the capability to link the metal centers through bridges to form compounds with varying topologies and in addition to promote the magnetic exchange interactions between the metal centers. Of these azide is more versatile and efficient magnetic coupler. This spurred the interest in the investigations of coordination compounds containing such anions. Cobalt(II) complex of azide anion with bis(pyrazol-1-yl)methane [26] and cobalt(III) complexes of azide anion with 1,10-phenanthroline [27] and bis(2-pyridyl)amine [28] have been reported. There has been reports on the magnetic studies of dicubane Co(II) complexes with azide bridges synthesized from di-2-pyridyl ketone [29,30]. The compounds were found to be ferromagnetic in nature. One dimensional coordination polymers of Co(II) with double end-to-end thiocyanate bridges synthesized using imidazole as the ligand were found to exhibit long-range magnetic ordering [31].

6.2 Stereochemistry

Co(III) ion has a d^6 configuration and the atomic ground state is ^5D. The six coordinate octahedral geometry is the most commonly observed stereochemistry for the Co(III) ion, but five coordinated complexes have also been reported. Distortions from the regular geometry is frequently observed in the case of Co(III) complexes

176

because of Jahn-Teller effect. Co(II) is a d^7 ion and is known in all coordination numbers from eight through two. However the coordination numbers six and four dominate.

6.3 Experimental

6.3.1 Materials

Pyridine-2-carbaldehyde (Sigma Aldrich), 2-benzoylpyridine (Sigma Aldrich), di-2-pyridyl ketone (Sigma Aldrich), quinoline-2-carbaldehyde (Sigma Aldrich), 2-hydroxy-4-methoxybenzaldehyde (Sigma Aldrich), aniline (S. D. Fine), *R*-1-phenylethyl amine (Alfa Aeser), 2-aminopyrimidine (Sigma Aldrich), $Co(ClO_4)_2 \cdot 6H_2O$ (Sigma Aldrich), $Co(OAc)_2 \cdot 4H_2O$ (Qualigens), NaN_3 (Reidel-De Haen), KCNS (BDH) and methanol (Merck) were used as received. Whenever ethanol was used as the solvent, repeated distillation was carried out before use.

6.3.2 Syntheses of cobalt complexes

$[Co(paa)_2(N_3)_2](ClO_4) \cdot H_2O$ (24): A mixture of pyridine-2-carbaldehyde (0.107 g, 1 mmol) in methanol and aniline (0.093 g, 1 mmol) in ethanol were refluxed for 2 hours. To this $Co(ClO_4)_2 \cdot 6H_2O$ (0.365 g, 1 mmol) dissolved in ethanol and an aqueous solution of NaN_3 (0.130 g, 2 mmol) was added in drops. The resulting brown colored solution was stirred for 15 min. Brown crystalline product formed within one day was filtered, washed with ethanol, water and ether and dried over P_4O_{10} *in vacuo*. Elemental Anal. Found (Calcd.) (%): C, 45.96 (46.13); H, 3.35 (3.55); N, 22.85 (22.42). $\mu = 0$ B.M.

Co(papea)₂(NCS)₂ (25): Pyridine-2-carbaldehyde (0.107 g, 1 mmol) and *R*-1-phenylethyl amine (0.121 g, 1 mmol) were refluxed in methanol for 2 hours. To this, a methanolic solution of Co(OAc)₂·4H₂O (0.249 g, 1 mmol) was added followed by an aqueous solution of KCNS (0.194 g, 2 mmol) and refluxed for 4 hours. Wine red rhombohedral single crystals suitable for X-ray diffraction were isolated within one week. The crystals were mechanically separated and dried over P₄O₁₀ *in vacuo*. Elemental Anal. Found (Calcd.) (%): C, 60.25 (60.49); H, 4.85 (4.74); N, 14.65 (14.11). μ = 4.83 B.M.

[Co₂(paap)₂(N₃)₂(OH)₂]·3H₂O·3CH₃OH (26): A mixture of pyridine-2-carbaldehyde (0.107 g, 1 mmol) in methanol and 2-aminopyrimidine (0.094 g, 1 mmol) in methanol was refluxed for 2 hours. A methanolic solution of Co(ClO₄)₂·6H₂O (0.365 g, 1 mmol) was added to this followed by an aqueous solution of NaN₃ (0.130 g, 2 mmol) in drops. The resulting mixture was stirred for 4 hours and the green product separated out was filtered, washed with methanol, water and ether and dried over P₄O₁₀ *in vacuo*. Elemental Anal. Found (Calcd.) (%): C, 36.14 (36.61); H, 3.95 (4.81); N, 26.25 (25.99). μ = 4.22 B.M.

[Co(paap)₂(NCS)₂]·2H₂O (27): A mixture of pyridine-2-carbaldehyde (0.107 g, 1 mmol) in methanol and 2-aminopyrimidine (0.094 g, 1 mmol) in methanol was refluxed for 2 hours. To this Co(OAc)₂·4H₂O (0.249 g, 1 mmol) was added followed by an aqueous solution of KCNS (0.194 g, 2 mmol) and refluxed for 4 hours. The pink colored crystalline product which separated was filtered, washed with methanol, water and ether and

178

dried over P_4O_{10} *in vacuo.* Elemental Anal. Found (Calcd.) (%): C, 45.48 (45.60); H, 3.60 (3.48); N, 24.36 (24.17). $\mu = 4.80$ B.M.

[Co(bzpa)₂(N₃)₂](ClO₄) (28): 2-Benzoylpyridine (0.183 g, 1 mmol) was dissolved in methanol and to this aniline (0.093 g, 1 mmol) was added the mixture was refluxed for 6 hours. To this, an ethanolic solution of $Co(ClO_4)_2\cdot6H_2O$ (0.365 g, 1 mmol) and NaN_3 (0.130 g, 2 mmol) was added with continuous stirring. The resulting brown solution was left at room temperature for two weeks during which a brown solid separated out. This was filtered, washed with ethanol, water and ether, and P_4O_{10} *in vacuo.* Elemental Anal. Found (Calcd.) (%): C, 57.34 (56.96); H, 3.60 (3.72); N, 18.74 (18.45). $\mu = 0$ B.M.

[Co₂(dpk·OH)₂(N₃)₂]·CH₃CH₂OH·2H₂O (29): Di-2-pyridyl ketone (0.187 g, 1 mmol) was dissolved in ethanol and aniline (0.093 g, 1 mmol) was added to this. About 4-5 drops of glacial acetic acid was also added and refluxed for 6 hours. To the above solution, $Co(ClO_4)_2\cdot6H_2O$ (0.365 g, 1 mmol) dissolved in ethanol was added followed by an aqueous solution of NaN_3 (0.130 g, 2 mmol) slowly with stirring. Stirring was continued for 6 hours. Pink product formed was filtered, washed with ethanol, water and ether and dried over P_4O_{10} *in vacuo.* Elemental Anal. Found (Calcd.) (%): C, 42.31(41.99); H, 3.57 (4.11); N, 21.04 (20.41). $\mu = 3.05$ B.M.

[Co(dpk·OH)₂(NCS)]·4H₂O (30): Di-2-pyridyl ketone (0.187 g, 1 mmol) was dissolved in ethanol and aniline (0.093 g, 1 mmol) was

added to this. About 4-5 drops of glacial acetic acid was also added and refluxed for 6 hours. $Co(OAc)_2 \cdot 4H_2O$ (0.249 g, 1 mmol) was added to the above solution followed by an aqueous solution of KCNS (0.194 g, 2 mmol). The mixture was refluxed for 3 hours. The pink colored solid separated out was filtered, washed with ethanol, water and ether and dried over P_4O_{10} *in vacuo*. Elemental Anal. Found (Calcd.) (%): C, 46.07 (46.70); H, 4.08 (4.43); N, 12.24 (11.84). $\mu = 0$ B.M.

$[Co(qaa)(N_3)_2] \cdot \frac{1}{3}CH_3CH_2OH$ (31): Quinoline-2-carbaldehyde (0.157 g, 1 mmol) was dissolved in ethanol. Aniline (0.093 g, 1 mmol) was added to this. A few drops of glacial acetic acid was also added and refluxed for 4 hours. To this solution, $Co(ClO_4)_2 \cdot 6H_2O$ (0.365 g, 1 mmol) dissolved in ethanol was added. To this an aqueous solution of NaN_3 (0.130 g, 2 mmol) was added slowly in drops. The mixture was stirred for 4 hours and the brown product formed was filtered, washed with ethanol, water and ether. Dried over P_4O_{10} *in vacuo*. Elemental Anal. Found (Calcd.) (%): C, 51.17 (51.25); H, 3.07 (3.61); N, 28.67 (28.69). $\mu = 4.56$ B.M.

$Co(qaa)_2(NCS)_2$ (32): Quinoline-2-carbaldehyde (0.157 g, 1 mmol) was dissolved in methanol. Aniline (0.093 g, 1 mmol) was added to this. A few drops of glacial acetic acid was also added and refluxed for 4 hours. To this, a methanolic solution of $Co(OAc)_2 \cdot 4H_2O$ (0.249 g, 1 mmol) was added followed by the addition of a solution of KCNS (0.194 g, 2 mmol) in water and refluxed for 3 hours. The brown product separated out was filtered, washed with methanol and

ether and dried over P_4O_{10} *in vacuo*. Elemental Anal. Found (Calcd.) (%): C, 63.67 (63.84); H, 3.43 (3.78); N, 13.12 (13.14). $\mu = 4.98$ B.M.

Co(hmba)$_2$(NCS) (33): 2-Hydroxy-4-methoxybenzaldehyde (0.152 g, 1 mmol) was dissolved in methanol. To this, aniline (0.093 g, 1 mmol) was added. $Co(OAc)_2 \cdot 4H_2O$ (0.249 g, 1 mmol) dissolved in water added the above solution followed by an aqueous solution of KCNS (0.194 g, 2 mmol) and the resulting solution was refluxed for 4 hours. The brown product separated out was filtered, washed with methanol followed by ether and dried over P_4O_{10} *in vacuo*. Elemental Anal. Found (Calcd.) (%): C, 61.10 (61.16); H, 4.94 (4.25); N, 7.97 (7.38). $\mu = 0$ B.M.

Caution! Although not encountered in our experiments, azide and perchlorate complexes are potentially explosive. Only a small amount of the material should be prepared, and it should be handled with care.

6.4 Results and discussion

The condensation of aldehyde/ketone and amine in 1:1 molar ratio yielded the Schiff base ligands, which were used without further purification for the synthesis of the complexes by reaction in presence of pseudohalides NaN_3/KCNS.

The complexes **24** and **28** are cationic complexes and can be represented by the formula $ML_2X_2(ClO_4)$, where X= NaN_3. All other complexes are found to be neutral. The complexes **25**, **27** and **32** have the stoichiometry ML_2X_2, while **30** and **31** can be represented as

181

MLX$_2$. The cobalt complexes **26** and **29** have the general formula MLX and that of **33** is ML$_2$X.

The complexes **29** and **30**, which were synthesized from the Schiff base obtained by the condensation of di-2-pyridyl ketone and aniline is not having the Schiff base as the ligand. The Schiff base has undergone hydrolysis in presence of metal to form the gem-diol of di-2-pyridyl ketone. Nucleophilic addition of water to di-2-pyridyl ketone results in the formation of the gem-diol of di-2-pyridyl ketone to undergo metal-mediated nucleophilic addition of small molecules like water or alcohol to the carbonyl group results in the formation of hydrate or hemiacetal [29,30,32-34]. It is thus the gem-diol of di-2-pyridyl ketone, which is the ligand in complexes **29** and **30**. In complex **33**, two Schiff bases are present, both of which coordinates to the metal after deprotonation through the deprotonated O atom and the azomethine N.

All the complexes were found to be soluble in DMF, DMSO and acetonitrile, but only partially soluble in other organic solvents such as CHCl$_3$, ethanol, methanol etc. Room temperature magnetic susceptibility measurements reveal the diamagnetic nature of the complexes **24, 28, 30** and **33**, so cobalt in these complexes is in the +3 oxidation state. All other complexes are found to be paramagnetic and hence are in the +2 oxidation state. Even though several attempts were made to isolate single crystals of all the complexes, we were successful only in the case of two complexes.

6.4.1 Crystallographic data collection and structure analysis

Single crystal X-ray diffraction measurements of complexes **25** were carried out on a Bruker Smart Apex 2 CCD area detector diffractometer and Bruker Smart Apex CCD diffractometer at the X-ray Crystallography Unit, School of Physics, Universiti Sains Malaysia, Penang, Malaysia. The unit cell parameters were determined and the data collections were performed using a graphite-monochromated Mo Kα (λ = 0.71073 Å) radiation at a detector distance of 5 cm at 100(1) K with the Oxford Cyrosystem Cobra low-temperature attachment. The collected data were reduced using SAINT program [35] and the empirical absorption corrections were performed using SADABS program [35]. The structures were solved by direct methods and refinement was carried out by full-matrix least squares on F^2 using the SHELXTL software package [36]. All non-hydrogen atoms were refined anisotropically. Hydrogen atoms were geometrically fixed at calculated positions and allowed to ride on their parent atoms. Molecular graphics employed were ORTEP-III [37] and DIAMOND [38]. S atom on one of the thiocyanate group was found to be disordered with a site occupancy factor of 0.9346(16) and 0.0654(16).

Single crystal X-ray diffraction experiments for the compound **28** were performed on a BRUKER SMART APEX CCD diffractometer equipped with a graphite - monochromated Mo Kα radiation (λ=0.71073 Å) at 293(2) K at the Analytical Sciences Division, Central Salt & Marine Chemicals Research Institute,

Gujarat, India. An omega-phi scan mode was employed for data collection. The collected data were reduced using SAINT [35]. The structure was solved by direct methods with the program SHELXS-97 and refined by full matrix least squares on F^2 using SHELXL-97 [35]. The graphical tools used were ORTEP-III [37] and DIAMOND [38]. All non-hydrogen atoms were refined anisotropically. Hydrogen atoms were geometrically fixed at calculated positions.

6.4.2 Crystal Structures

$Co(papea)_2(NCS)_2$ **(25):** The complex **25** crystallizes into a monoclinic crystal system with the chiral space group $P2_1$. Molecular structure of the complex is displayed in Fig. 6.1. The structural refinement parameters are given in Table 6.1 and significant bond parameters are given in Table 6.2.

In the complex, an inversion in the configuration at C7 and C20 is observed, both the carbon atoms have the S configuration. The coordination sphere around the Co(II) centre is defined by four nitrogens from two molecules of the bidentate Schiff base ligand L and two nitrogen donors from two NCS⁻ anions. The coordination geometry can be best described as a distorted octahedron. The pyridyl nitrogen atoms of the ligands are *trans* to each other, while the azomethine nitrogens and the thiocyanate nitrogens are *cis*. The Co–N distances confirm the divalent nature of the cobalt. The Co–N distances are shortest for the nitrogen atoms of the thiocyanate anions indicating the stronger covalent bonds with the anionic ligands.

184

Table 6.1   Crystal data and structure refinement

Parameters	$Co_2(papea)_2(NCS)_2$
Empirical formula	$C_{30}H_{28}CoN_6S_2$
Formula weight	595.63
Color	Wine red
Temperature (T) K	100.0(1)
Wavelength (Mo Kα) (Å)	0.71073
Crystal system	Monoclinic
Space group	$P2_1$ (No: 4)
Unit cell dimensions	
a (Å)	9.0039(10)
b (Å)	15.1824(3)
c (Å)	11.1332(2)
α (°)	90.00
β (°)	109.2840(10)
γ (°)	90.00
Volume V (Å^3)	1436.53(4)
Z	2
Calculated density (ρ) (Mg m^{-3})	1.377
Absorption coefficient, μ (mm^{-1})	0.773
F(000)	618
Crystal size (mm^3)	1.24x0.74x0.24
θ range for data collection	2.36 - 34.99
Limiting indices	$-14 \le h \le 14$, $-24 \le k \le 18$, $-17 \le l \le 17$
Reflections collected	27190
Unique Reflections (R_{int})	9700 [R(int) = 0.0217]
Completeness to θ	34.99 (99.0 %)
Refinement method	Full-matrix least-squares on F^2
Data / restraints / parameters	9700/3/359
Goodness-of-fit on F^2	1.033
Final R indices [I > 2σ (I)]	$R_1 = 0.0323$, $wR_2 = 0.0814$
R indices (all data)	$R_1 = 0.0347$, $wR_2 = 0.0834$
Largest difference peak and hole (e Å^{-3})	0.869 and -0.709
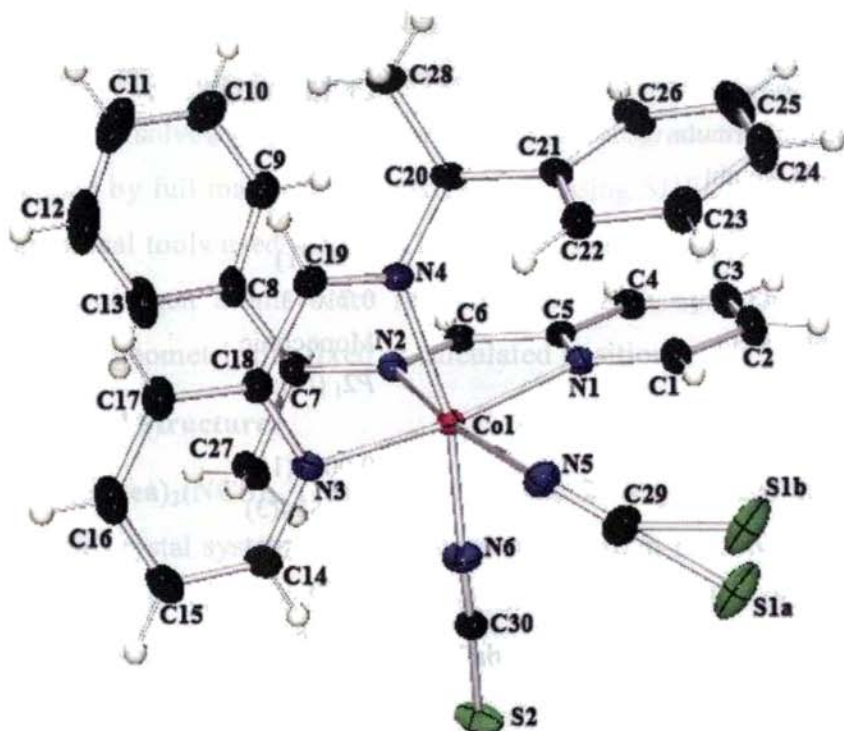
Fig. 6.1. Molecular structure of **Co(papea)₂(NCS)₂ (25)**

The Co(II)–N bond lengths are quite similar to the corresponding distances in similar systems [39,40]. The S atom of one of the thiocyanate groups is disordered with a site occupancy factor of 0.9346(16) for S1A and 0.0654(16) for S1B. The NCS⁻ is almost linear (N5–C29–S1A=178.43(16)° and N6–C30–S2=177.85(16)°). However, the N–C–S bond angle of the disordered S atom at one of the sites is lower (N5–C29–S1B=146.9(4)°). The thiocyanate anion with the disordered S atom is coordinated to the Co(II) centre in a bent manner (C29–N5–Co1=139.46(13)°), while the connection between the second NCS⁻ and the Co(II) is nearly linear (C30–N6–Co1=173.44(15)°).

The two NCS⁻ anions remain as terminal ligands in the complex. The geometry around Co(II) is distorted from the regular octahedral geometry due to the nature of the Schiff base. This is reflected in the small bite angle of 76.25(4)° and 76.25(6)° for the two ligands respectively. Ring puckering analysis reveals the metal chelate ring Cg(1) formed by Co1, N1, C5, C6 and N2 to adopt an envelope conformation on Co1 [$Q(2) = 0.092(1)$ Å, $\Phi = 5.7(10)°$].

Table 6.2. Selected bond parameters of **Co(papea)₂(NCS)₂**

Bond lengths (Å)			
Co1−N1	2.1544(12)	N5−C29	1.165(2)
Co1−N2	2.2353(11)	N6−C30	1.159(2)
Co1−N3	2.1587(12)	S1A−C29	1.6369(18)
Co1−N4	2.1635(14)	S1B−C29	1.642(2)
Co1−N5	2.0894(13)	S2−C30	1.6351(18)
Co1−N6	2.0426(17)		
Bond angles (°)			
N1−Co1−N2	76.25(4)	N6−Co1−N3	93.27(6)
N1−Co1−N3	172.82(6)	N5−Co1−N4	98.82(5)
N1−Co1−N4	96.77(6)	N6−Co1−N4	165.87(5)
N5−Co1−N1	91.73(5)	N6−Co1−N5	90.70(6)
N6−Co1−N1	93.32(6)	C29−N5−Co1	139.46(13)
N3−Co1−N2	101.49(4)	C30−N6−Co1	173.44(15)
N4−Co1−N2	87.74(6)	N5−C29−S1A	178.43(16)
N5−Co1−N2	166.96(5)	N5−C29−S1B	146.9(4)
N6−Co1−N2	85.08(6)	N6−C30−S2	177.85(16)
N3−Co1−N4	76.25(6)	S1A−C29−S1B	33.6(4)

In the crystal lattice of the complex, the molecules pack in a 'head to tail' fashion along the crystallographic 'a' axis. The packing diagram of the compound is given in Fig. 6.2. The crystal structure lacks hydrogen bonds. C−H⋯π interactions (Table 6.3) and π⋯π

stacking interactions (Table 6.4) collectively contribute towards the effective packing of the molecule in the crystal lattice.
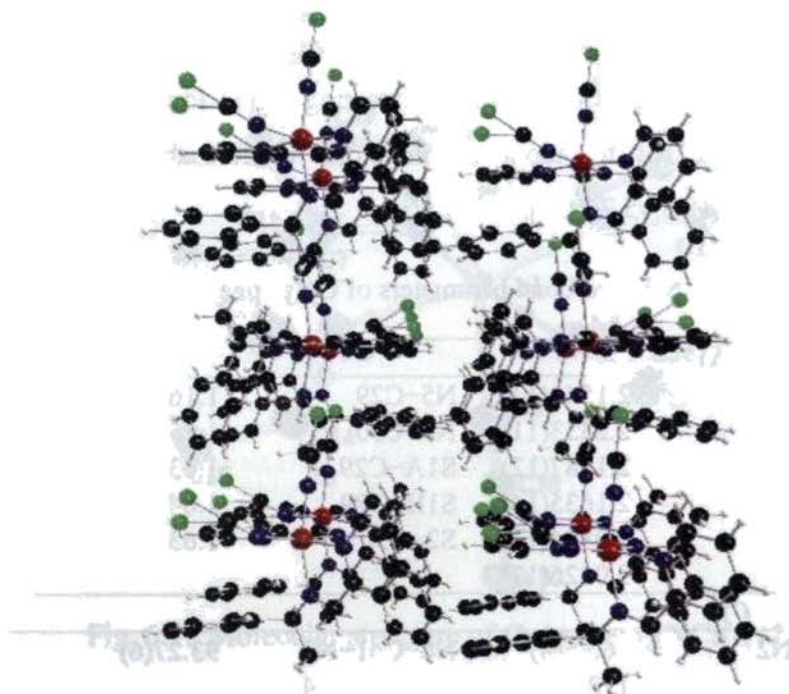
Fig. 6.2. Packing diagram of **Co(papea)₂(NCS)₂ (25)** along the 'a' axis.

Table 6.3. C−H···π interaction parameters

C−H(I)···Cg(J)	H···Cg (Å)	C−H···Cg (°)	C···Cg (Å)
C1−H1A[1]−Cg(6)[a]	3.1365	103.37	3.472(2)
C10−H10A[1]−Cg(3)[b]	3.1796	140.14	3.939(2)
C14−H14A[1]−Cg(6)[c]	3.3040	122.39	3.883(2)
C15−H15A[1]−Cg(6)[c]	3.0245	134.07	3.732(2)
C20−H20A[1]−Cg(1)[a]	2.8278	112.47	3.3278(18)
C23−H23A[1]− Cg(5)[d]	3.1968	133.83	3.8995(19)

Equivalent position code: a = x, y, z; b = -x, -1/2+y, -z; c = 1-x, 1/2+y, -z; d = 1+x, y, 1+z

Cg(1) = Co1, N1, C5, C6, N2; Cg(3) = N1, C1, C2, C3, C4, C5; Cg(5) = C8, C9, C10, C11, C12, C13; Cg(6) = C21, C22, C23, C24, C25, C26

Table 6.4. $\pi\cdots\pi$ interactions

Cg(I)Res(I)···Cg(J)	Cg···Cg (Å)	α°	β°	γ°
Cg(1)[1]···Cg(5)[a]	4.7552(10)	79.01	55.14	63.06
Cg(1)[1]···Cg(6)[a]	4.7996(10)	14.03	47.52	49.74
Cg(2)[1]···Cg(5[a]	4.0298(11)	9.20	24.35	33.01
Cg(3)[1]···Cg(6)[a]	4.2757(11)	17.73	44.21	33.12
Cg(4)[1]···Cg(5)[a]	4.8401(12)	9.73	40.23	49.39
Cg(5)[1]···Cg(2)[a]	4.0298(11)	9.20	33.01	24.35
Cg(5)[1]···Cg(4)[a]	4.8401(12)	9.73	49.39	40.23
Cg(6)[1]···Cg(1)[a]	4.7996(10)	14.03	49.74	47.52
Cg(6)[1]···Cg(3)[a]	4.2758(11)	17.73	33.12	44.21
Cg(6)[1]···Cg(4)[b]	4.9070(11)	88.36	3.58	84.80

Equivalent position code: a = x, y, z; b = 1-x,-1/2+y,-z

Cg(1) = Co1, N1, C5, C6, N2; Cg(2) = Co1, N3, C18, C19, N2; Cg(3) = N1, C1, C2, C3, C4, C5; Cg(4) = N3, C14, C15, C16, C17, C18; Cg(5) = C8, C9, C10, C11, C12, C13; Cg(6) = C21, C22, C23, C24, C25, C26

[Co(bzpa)₂(N₃)₂](ClO₄) (28): Brown needle-shaped single crystals suitable for X-ray diffraction were obtained by the slow evaporation of the complex from a 1:1 mixture of acetone and water. The structure of the cation is given in Fig. 6.3. The structural refinement parameters are given in Table 6.5 and significant bond parameters are given in Table 6.6. The compound crystallizes into the triclinic system with a space group of $P\bar{1}$. There are two crystallographically independent molecules in the asymmetric unit (Fig. 6.4).

Table 6.5. Crystal data and structure refinement

Parameters	Co(bzpa)$_2$(N$_3$)$_2$(ClO$_4$)
Empirical formula	C$_{36}$H$_{28}$ClCoN$_{10}$O$_2$
Formula weight	1518.13
Color	Brown
Temperature (T) K	293(3)
Wavelength (Mo Kα) (Å)	0.71073
Crystal system	Triclinic
Space group	$P\bar{1}$
Unit cell dimensions	
a (Å)	10.9367(9)
b (Å)	18.0817(17)
c (Å)	20.1629(16)
α (˚)	111.342(2)
β (˚)	91.622(2)
γ (˚)	107.5030(10)
Volume V (Å^3)	3499.1(5)
Z	2
Calculated density (ρ) (Mg m^{-3})	1.441
Absorption coefficient, μ(mm^{-1})	0.623
F(000)	1560
Crystal size (mm^3)	0.20x0.16x0.08
θ range for data collection	1.96 - 28.31
Limiting indices	-14≤h≤14, -24≤k≤23, -26≤l≤26
Reflections collected	30575
Unique Reflections (R$_{int}$)	15866 [R(int) = 0.0292]
Completeness to θ	28.31 (91.1 %)
Refinement method	Full-matrix least-squares on F^2
Data / restraints / parameters	15866/0/925
Goodness-of-fit on F^2	1.002
Final R indices [I > 2σ (I)]	R$_1$ = 0.0749, wR$_2$ = 0.2011
R indices (all data)	R$_1$ = 0.1164, wR$_2$ = 0.2289
Largest difference peak and hole (e Å^{-3})	0.907 and -0.522

190
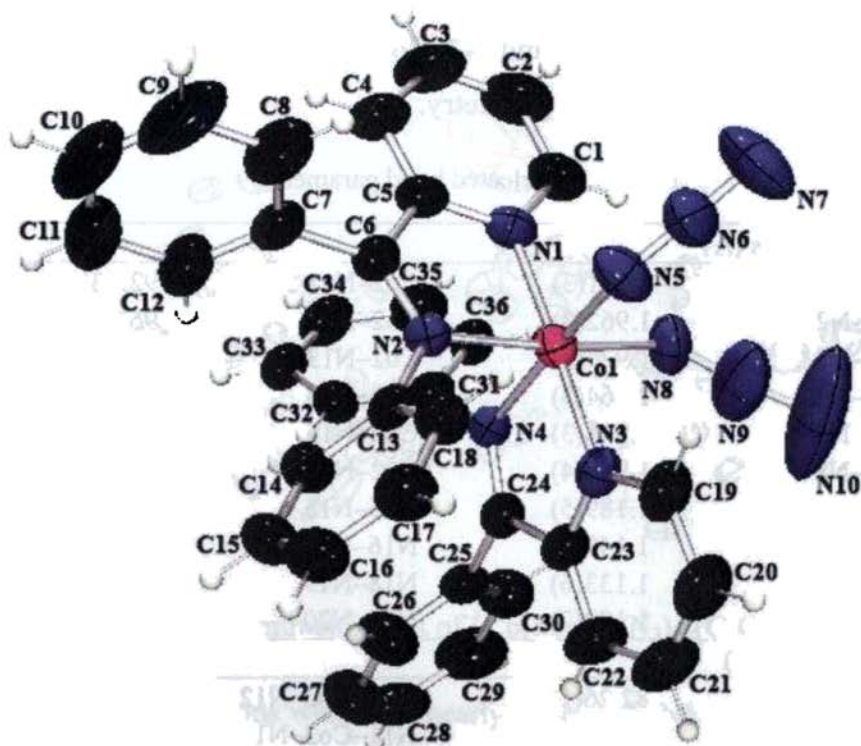
Fig. 6.3. Structure of $[Co(bzpa)_2(N_3)_2]^+$ cation

From Table 6.6, it is clear that the two molecules in the asymmetric unit are almost identical. The bond angles and bond lengths in the two monomers agree with each other. So the discussion can be limited to one of the molecules. The compound consists of cobalt(III) coordinated by four nitrogen atoms from two molecules of the Schiff base and two nitrogen atoms from azide. The N6 coordination of the cobalt(III) is completed by pairs of *trans-* pyridyl N, *cis-* azomethine N and *cis-* azide N to form two five membered chelate rings. The azide anions are terminal. The bond lengths and bond angles reveal significant

distortion in the octahedral geometry. The rather small bite angle [N1–Co1–N2 = 82.26(13)° and N3–Co1–N4 = 82.04(13)°] defines the largest distortion in the geometry.

Table 6.6. Selected bond parameters

Bond lengths (Å)			
Co1–N1	1.921(3)	Co2–N11	1.922(3)
Co1–N2	1.962(3)	Co2–N12	1.966(3)
Co1–N3	1.927(3)	Co2–N13	1.929(3)
Co1–N4	1.964(3)	Co2–N14	1.957(3)
Co1–N5	1.941(3)	Co2–N15	1.944(4)
Co1–N8	1.944(4)	Co2–N18	1.972(4)
N5–N6	1.189(5)	N15–N16	1.187(6)
N6–N7	1.145(6)	N16–N17	1.137(7)
N8–N9	1.133(6)	N18–N19	1.158(6)
N9–N10	1.172(7)	N19–N20	1.151(7)
Bond angles (°)			
N1–Co1–N2	82.26(13)	N11–Co2–N12	82.27(13)
N1–Co1–N3	177.51(13)	N11–Co2–N13	177.24(14)
N1–Co1–N4	95.53(12)	N11–Co2–N14	95.67(13)
N1–Co1–N5	90.19(15)	NL1–Co2–N15	90.81(18)
N1–Co1–N8	90.70(16)	N11–Co2–N18	91.69(16)
N2–Co1–N3	97.17(13)	N12–Co2–N13	96.41(14)
N2–Co1–N4	89.32(12)	N12–Co2–N14	88.59(12)
N2–Co1–N5	87.58(15)	N12–Co2–N15	92.77(17)
N2–Co1–N8	172.62(15)	N12–Co2–N18	173.72(16)
N3–Co1–N4	82.04(13)	N13–Co2–N14	81.86(13)
N3–Co1–N5	92.21(15)	N13–Co2–N15	91.68(18)
N3–Co1–N8	89.78(15)	N13–Co2–N18	89.55(16)
N4–Co1–N5	173.08(15)	N14–Co2–N15	173.51(17)
N4–Co1–N8	89.16(15)	N14–Co2–N18	90.33(15)
N5–Co1–N8	94.68(17)	N15–Co2–N18	89.0(2)
Co1– N5–N6	118.9(3)	Co2–N15–N16	117.8(4)
Co1–N8–N9	119.4(4)	Co2–N18–N19	117.5(3)
N5–N6–N7	175.4(6)	N15–N16–N17	177.3(6)
N8–N9–N10	175.4(9)	N18–N19–N20	177.3(6)
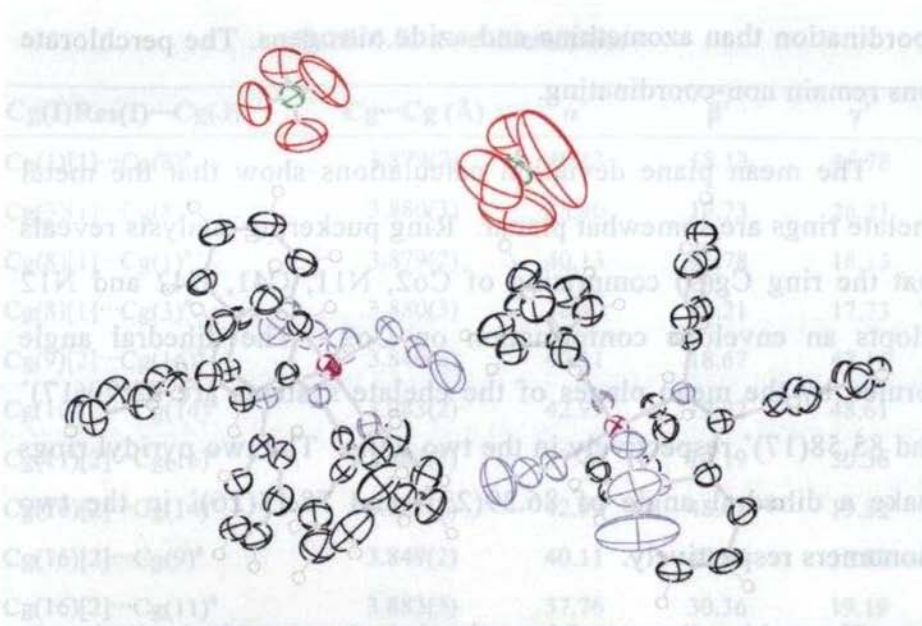
Fig. 6.4. The asymmetric unit of [**Co(bzpa)₂(N₃)₂](ClO₄)** (28).

The azide anions which are nearly linear [N5–N6–N7 = 175.4(6)°
and N8–N9–N10 = 175.4(9)°] are coordinated with a N6–N5–Co1
angle of 118.9(3)° and N9–N8–Co1 angle of 119.4(4)°. The N–N
bond lengths in the azide group are almost equal, with the longer
N–N bonds involving the N atoms coordinated to the metal centre.
However, in N8–N9–N10, the N8–N9 bond [1.133(6) Å] is much
shorter than N9–N10 bond [1.172(7) Å]. This may be attributed to
the stronger C–H···π interaction in N8–N9–N10, which is not
significant in N5–N6–N7. The Co(III)–N bond distances in the
complex are in the range 1.921(3)–1.972(4) Å. This is in agreement
with the previous reports [27,28,41-44]. The Co(III)–N distance is
shorter for the pyridyl nitrogen atoms indicating their stronger

coordination than azomethine and azide nitrogens. The perchlorate ions remain non-coordinating.

The mean plane deviation calculations show that the metal chelate rings are somewhat planar. Ring puckering analysis reveals that the ring Cg(9) comprising of Co2, N11, C41, C42 and N12 adopts an envelope conformation on Co2. The dihedral angle formed by the mean planes of the chelate systems are 88.90(17)° and 85.58(17)° respectively in the two units. The two pyridyl rings make a dihedral angle of 86.39(23)° and 78.15(26)° in the two monomers respectively.

The packing diagram of the molecule in the crystal lattice is given in Fig. 6.5. In the crystal lattice, the molecules are arranged in a 'head to tail' manner. There are no classical hydrogen bonds seen in the crystal structure. The packing of the molecules in the crystal lattice is stabilized by C–H···π interactions (Table 6.7), π···π stacking interactions (Table 6.8) and some weak hydrogen bonding interactions (Table 6.9).

Table. 6.7. C–H···π interaction parameters

C–H(I)···Cg(J)	H···Cg (Å)	C–H···Cg (°)	C···Cg (Å)
N(16)–N(17)[2]···Cg(9)[a]	3.219(7)	53.3(4)	2.697(5)
N(19)–N(20)[2]···Cg(3)[a]	2.954(6)	117.1(6)	3.626(4)
N(19)–N(20)[2]···Cg(10)[a]	3.080(6)	54.4(3)	2.584(4)
N(19)–N(20)[2]···Cg(12)[a]	3.601(7)	74.7(4)	3.479(5)

Equivalent position code: a = x, y, z
Cg(3) = N1, C1, C2, C3, C4, C5; Cg(9) = Co2, N11, C41, C42, N12; Cg(10) = Co2, N13, C59, C60, N14; Cg(12) = N13, C55, C56, C57, C58, C59

194

Table 6.8. $\pi\cdots\pi$ interactions

Cg(I)Res(I)$\cdots$Cg(J)	Cg$\cdots$Cg (Å)	α°	β°	γ°
Cg(1)[1]$\cdots$Cg(8)[a]	3.879(2)	40.13	18.13	46.78
Cg(3)[1]$\cdots$Cg(8)[a]	3.880(3)	38.40	17.73	26.21
Cg(8)[1]$\cdots$Cg(1)[a]	3.879(2)	40.13	46.78	18.13
Cg(8)[1]$\cdots$Cg(3)[a]	3.880(3)	38.40	26.21	17.73
Cg(9)[2]$\cdots$Cg(16)[a]	3.849(2)	40.11	18.67	47.16
Cg(10)[2]$\cdots$Cg(14)[a]	3.983(2)	42.99	19.82	48.61
Cg(11)[2]$\cdots$Cg(16)[a]	3.883(3)	37.76	19.19	30.36
Cg(10)[2]$\cdots$Cg(14)[a]	3.983(2)	42.99	48.61	19.82
Cg(16)[2]$\cdots$Cg(9)[a]	3.849(2)	40.11	47.16	18.67
Cg(16)[2]$\cdots$Cg(11)[a]	3.883(3)	37.76	30.36	19.19

Equivalent position code for $Co(bzpa)_2(N_3)_2(ClO_4)$: a = x, y, z;

Cg(1) = Co1, N1, C5, C6, N2; Cg(3) = N1, C1, C2, C3, C4, C5; Cg(8) = C31, C32, C33, C34, C35, C36; Cg(9) = Co2, N11, C41, C42, N12; Cg(10) = Co2, N13, C59, C60, N14; Cg(11) = N11, C37, C38, C39, C40, C41; Cg(14) = C49, C50, C51, C52, C53, C54; Cg(16) = C67, C68, C69, C70, C71, C72

Table 6.9. H-bonding interactions

D–H$\cdots$A	D–H (Å)	H$\cdots$A (Å)	D$\cdots$A (Å)	D–H$\cdots$A (°)
C1–H1$\cdots$N8	0.93	2.38	2.888(7)	114
C14–H14$\cdots$06[a]	0.93	2.49	3.2742	142
C19–H19$\cdots$N5	0.93	2.43	2.941(7)	114
C35–H35$\cdots$O5[b]	0.93	2.51	3.1711	128
C37–H37$\cdots$N18	0.93	2.43	2.939(8)	114
C50–H50$\cdots$O1[c]	0.93	2.29	3.077(8)	141
C55–H55$\cdots$N15	0.93	2.41	2.912(9)	114
C64–H64$\cdots$O2[d]	0.93	2.51	3.389(10)	158
C68–H68$\cdots$O1[c]	0.93	2.53	3.429(7)	163

D=donor, A=acceptor

Equivalent position code: a = 2-x, 1-y, 1-z; b = 1-x, 1-y, 1-z; c = 2-x, 1-y, 2-z; d = -1+x, 1+y, z

The orientation of the molecules in the crystal lattice is in such a manner that $\pi\cdots\pi$ stacking interactions involving metal-chelate ring, pyridyl and phenyl rings reinforce the packing. The metal chelate ring Cg(1) and pyridyl ring Cg(3) are involved in $\pi\cdots\pi$ interaction with the phenyl ring Cg(8) at average distances of 3.879(2) and 3.880(3) Å. Similar interactions are observed in the second molecule also. In addition, in the second molecule, there is an additional $\pi\cdots\pi$ interaction between metal chelate ring Cg(10) and phenyl ring Cg(14) at average distance of 3.983(2) Å.
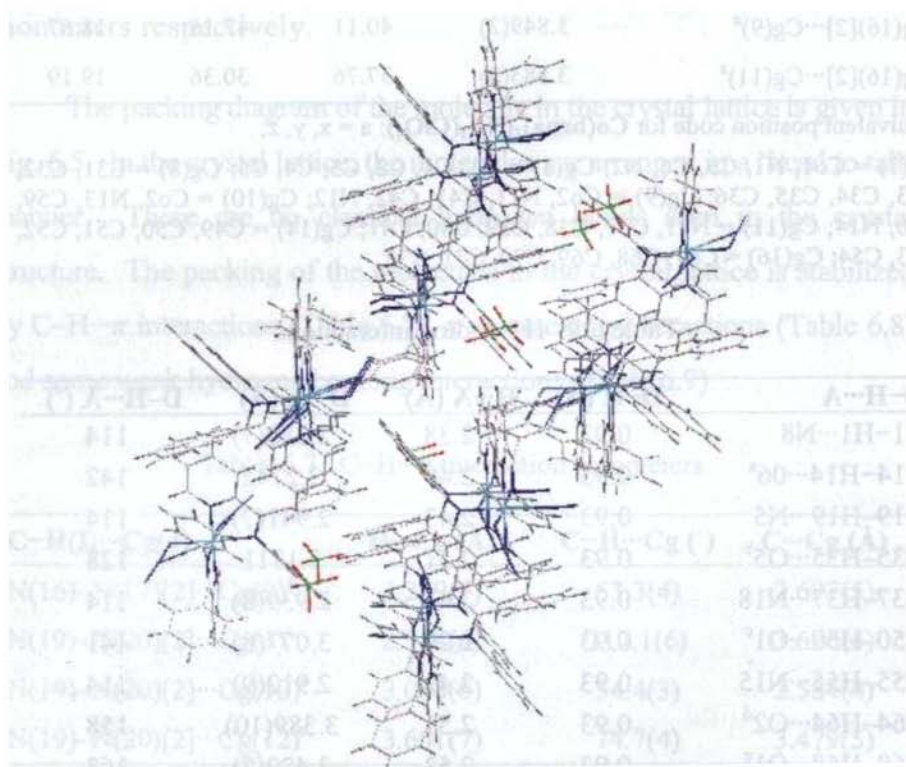

Fig. 6.5. Packing diagram of [Co(bzpa)₂(N₃)₂](ClO₄) (28) viewed along the 'a' axis.

6.4.3 Spectral characteristics of cobalt complexes

6.4.3a *Electronic spectra*

For d^6 Co(III), the atomic ground state is ^5D and the octahedral high spin ground state is $^5T_{2g}$. A single spin-allowed transition to the ^5E_g state is predicted but this will generally be split because the latter suffers Jahn Teller distortion. But only a few high spin six coordinate complexes are known. The six coordinate complexes of cobalt(III) are invariably low spin and have the ground term $^1A_{1g}$. Two transitions viz. $^1T_{1g} \leftarrow {}^1A_{1g}$ and $^1T_{2g} \leftarrow {}^1A_{1g}$ are expected for six coordinate low spin Co(III) complexes [45].

Co(II) is a d^7 species with a ^4F ground term. In six coordinate Co(II), three transitions are expected: $^4T_{2g} \leftarrow {}^4T_{1g}$ (ν_1), $^4A_{2g} \leftarrow {}^4T_{1g}$ (ν_2) and $^4T_{1g}$ (P) $\leftarrow {}^4T_{1g}$ (ν_3). The transition to $^4A_{2g}$ is usually very weak and often appears as a shoulder. For the tetrahedral species also, three transitions are predicted: $^4T_2 \leftarrow {}^4A_2$ (ν_1), $^4T_1 \leftarrow {}^4A_2$ (ν_2) and $^4T_1$ (P) $\leftarrow {}^4A_2$ (ν_3) [45]. All the three transitions can be observed, though ν_1 lies at low energy in the near infrared.

Compound **24** exhibited bands at 800 and 648 nm, which correspond to the *d-d* transitions of Co(III) in a distorted octahedral environment. The CT band is observed at 380 nm. The $\pi \rightarrow \pi^*$ transitions of the ligand are seen as an intense peak at 293 nm. The $n \rightarrow \pi^*$ transitions of the ligand seen at 326 nm are obscured by the broad and intense CT bands.

The thiocyanate complex **25** (Fig. 6.6) displayed a band at 623 nm assignable to the *d-d* transition of an octahedral Co(II). The shoulder observed at 585 nm is probably a spin-forbidden transition. Charge transfer bands are seen at 465 and 407 nm. The lower energy CT band may be assigned to $NCS^- \rightarrow Cu(II)$ LMCT and the higher energy band is due to $N \rightarrow Cu(II)$ LMCT. The $n \rightarrow \pi^*$ and $\pi \rightarrow \pi^*$ transitions due to the ligand are viewed at 340 and 290 nm respectively.

Fig. 6.6. Electronic spectrum of compound **25**.
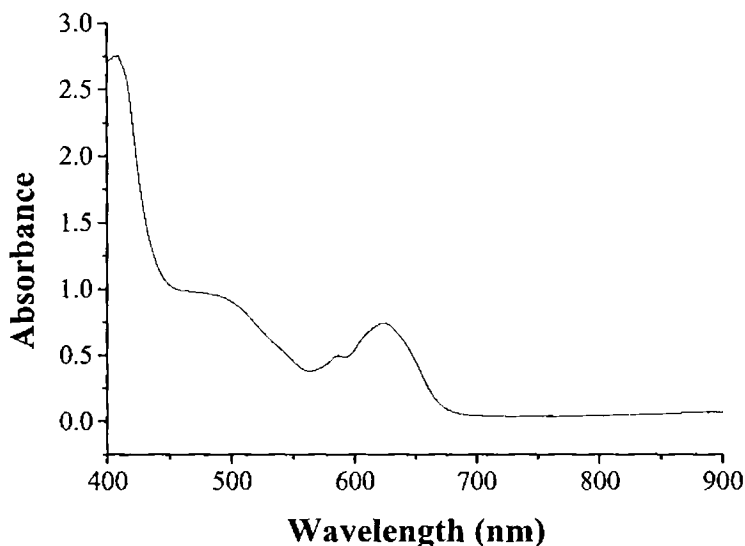
Compound **26** exhibits a broad band at 550 nm assigned to the *d-d* transition and is in accordance with the spectra observed for five coordinate Co(II) complexes. The $\pi \rightarrow \pi^*$ ligand transition is observed at 291 nm and the $n \rightarrow \pi^*$ transition was seen at 312 nm. The $n \rightarrow \pi^*$ peak was very broad that it masked the charge transfer

band. The greater intensity of $n \rightarrow \pi^*$ transition is attributed to the intensity stealing from the charge transfer transitions.

The $n \rightarrow \pi^*$ and $\pi \rightarrow \pi^*$ transitions of the ligand are viewed at 313 and 290 nm respectively in complex **27**. Two charge transfer bands are observed at 471 and 495 nm. Bands observed at 520, 540 and 620 nm correspond to the *d-d* transitions of the octahedral Co(II) complex (Fig. 6.7).

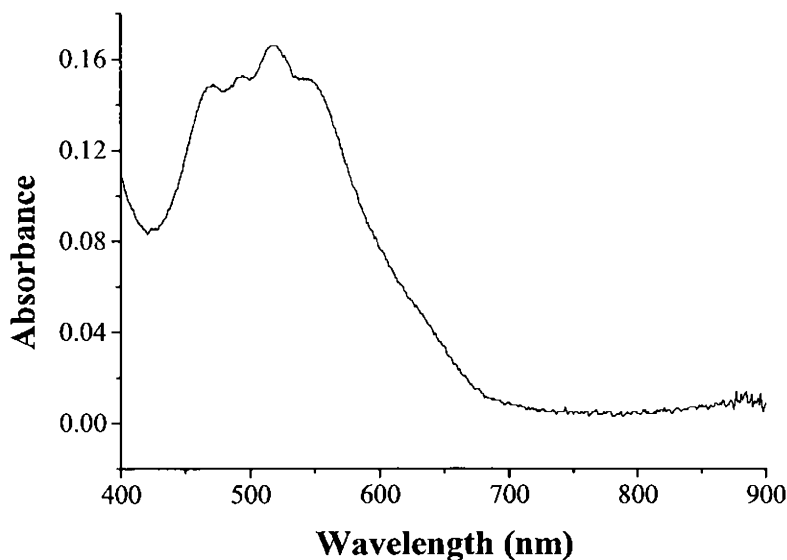Fig. 6.7. Electronic spectrum of complex **27**.

In the Co(III) complex **28**, two *d-d* bands are observed in the regions 820-750 and 660-620 nm. The $n \rightarrow \pi^*$ transition of the ligand was obtained in conjugation with a charge transfer band and was seen at around 347 nm as a very broad band with very high intensity almost equivalent to the intensity of the $\pi \rightarrow \pi^*$

transition of the ligand. The higher intensity of the $n \rightarrow \pi *$ transitions is due to the intensity borrowing from the nearby charge transfer band. The $\pi \rightarrow \pi *$ transition of the ligand is seen at 298 nm.

Co(II) complex **29** exhibits *d-d* bands at 660 and 526 nm suggesting the complex to be tetrahedral. The charge transfer band appears at 482 nm. The ligand centered transitions are seen at 319 and 291 nm. The thiocyanate Co(III) complex **30** has broad bands *ca.* 620 and 524 nm assignable as the *d-d* transition of the Co^{3+} ion. The charge transfer transition in the complex is observed at 483 nm. The $n \rightarrow \pi *$ and $\pi \rightarrow \pi *$ transitions of the ligand are viewed at 312 and 290 nm respectively.

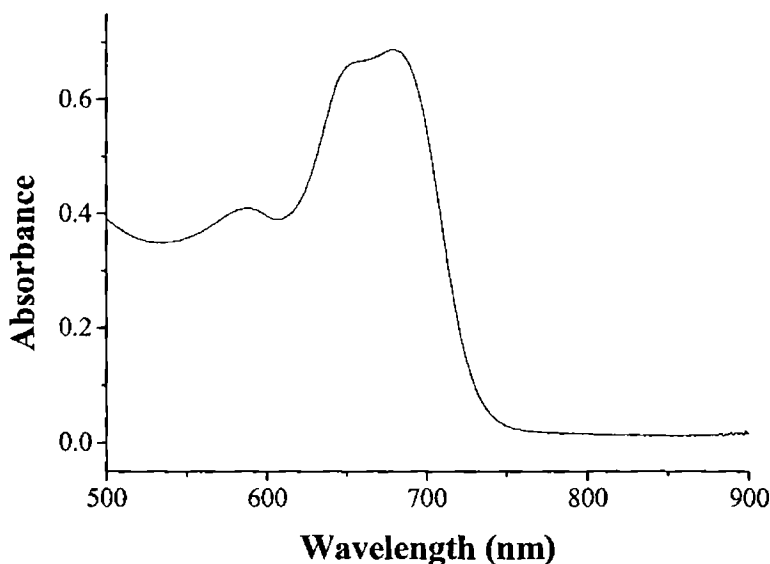The electronic spectrum of compound **31** given in Fig. 6.8.

Fig. 6.8. Electronic spectrum of compound **31**.

In complex **31,** a complicated pattern is displayed with bands at 680, 650 and 589 nm. Considering the intensity of these bands, the one at 680 nm can de assigned as the $^4T_1$ (P)$\leftarrow^4A_2$ of a four coordinate tetrahedral Co(II) species. The other two bands are probably the spin-forbidden transitions, which might have gained intensity by interaction with the visible spin allowed band. The charge transfer transition occurs at 366 nm. The intraligand transitions were obtained at 320 ($n \rightarrow \pi$ *) and 301 nm ($\pi \rightarrow \pi$ *).

The *d-d* transition in complex **32** was obtained as a broad band in the range *ca.* 632 nm, which can be assigned as the $^4T_{1g}$ (P) $\leftarrow^4T_{1g}$ transition of an octahedral Co(II). A shoulder appearing at 560 nm is probably a spin-forbidden transition. The charge transfer band is seen at 420 nm and a higher energy charge transfer band occurs due to N$\rightarrow$Cu(II) transition at 375 nm and the $n \rightarrow \pi$ * and $\pi \rightarrow \pi$ * transitions of the ligand are viewed at 332 and 302 nm respectively.

For complex **33,** *d-d* transition is obtained as a broad band *ca.* 571 nm, which is consistent with the transitions of a five coordinate Co(III) complex. A spin forbidden shoulder was observed at 615 nm. The charge transfer band for the compound is observed in the visible region at 400 nm. The $n \rightarrow \pi$ * and $\pi \rightarrow \pi$ * transitions of the ligand are viewed at 332 and 292 nm respectively in complex. These transitions were observed at 334 and 291 nm respectively in the ligand. The $\pi \rightarrow \pi$ * transitions of the ligand thus show a shift to slightly longer wavelengths in the complex upon complexation. The red shift

in the case of $n \to \pi^*$ transition indicates coordination of the azomethine nitrogen atom of the Schiff base [45].

6.4.3b *IR spectral studies*

IR spectroscopy is a useful tool to confirm the coordination of various atoms and groups to the metal atom from the positions and natures of the bands associated with them. However, it cannot be used alone to determine the stereochemistry and has to be coupled with other spectral techniques like EPR, electronic spectroscopy etc. The interest in the IR spectra of the compounds studied comes mainly from the bands due to the azide and thiocyanate groups. The position of the bands corresponding to the stretching frequency of these groups can be used for characterization of their mode of coordination to the metal ions [46].

The IR spectrum of compound **24** (Fig. 6.9) shows a sharp peak of medium intensity at 1601 cm^{-1}, which is assigned as the $v(C=N)$ stretching mode of the azomethine function of the Schiff base, the position of which is in agreement with the previous reports and is thus indicative of the coordination of azomethine N. The band at 1487 cm^{-1} is attributed to pyridyl ring stretching and the band at 1028 cm^{-1} is due to pyridyl ring breathing. The in-plane ring deformation of the pyridyl ring and the pyridyl ring out-of-plane bending are observed at 658 and 509 cm^{-1} as weak bands. The above observations indicate the pyridyl N coordination. The interest in the IR spectra of azide complexes are focused on the bands corresponding to this versatile ligand. The spectrum of **24** exhibits an intense absorption at 2020 cm^{-1} which is associated with the asymmetric stretching mode of the azide ligand.

The absence of this band indicates the terminal nature of the azide in the complex and suggests the trans location of the two azide groups in the complex. The cis-isomers would have split absorption of the asymmetric stretch of the azide. The $v_s(N_3)$ stretching mode of the azide group is observed as a medium band at 1286 cm^{-1}. The deformation mode of the azido ligand is observed as a weak band at 697 cm^{-1}.

The presence of an unsplit band at 1094 cm^{-1} corresponding to $v_3(ClO_4)$ and at 622 cm^{-1} assignable to $v_4(ClO_4)$ indicate the T_d symmetry of ClO_4^- is maintained in complex **24**. Also, the absence of a band corresponding to v_1 at approximately 920 cm^{-1} is noted. All these suggest that perchlorate is outside the coordination sphere of the complexes and is hence ionic in nature [47-50].
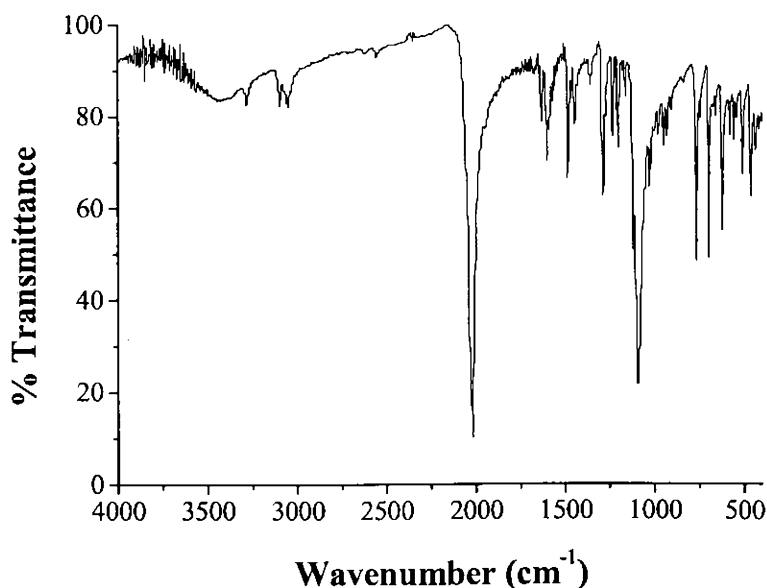
Fig. 6.9. IR spectrum of compound **24**.

The $v(C=N)$ stretch of the azomethine group occurs as a medium band at 1595 cm^{-1} and indicates the azomethine N coordination to the cobalt in complex **25** (Fig. 6.10). The coordination of the pyridyl nitrogen is confirmed by the presence of pyridyl ring stretch at 1444 cm^{-1}, pyridyl ring breathing at 1016 cm^{-1}, pyridyl in-plane ring deformation at 698 cm^{-1} and pyridyl out-of-plane ring deformation at 420 cm^{-1}.
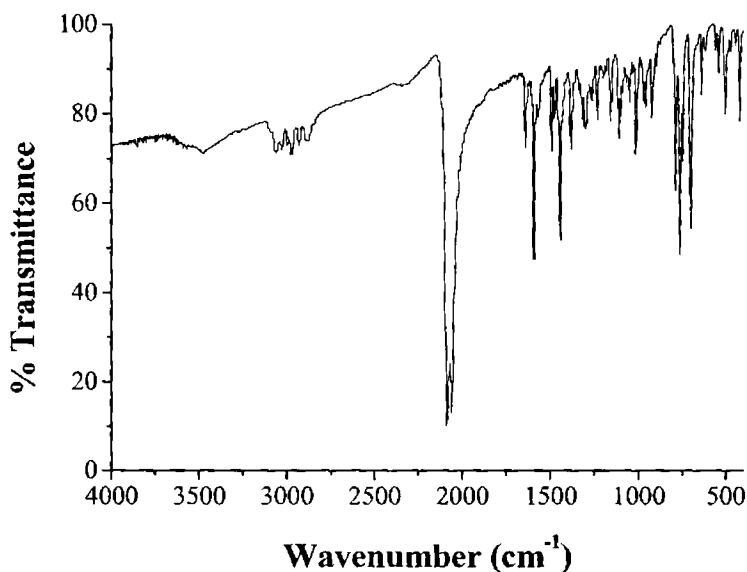
Fig 6.10. IR spectrum of compound **25**.

The IR spectrum of **25** has two strong and sharp peaks at 2088 and 2058 cm^{-1} assignable to the $v(CN)$ stretching mode of a thiocyanate group. The $v(CN)$ of a bridging thiocyanate is usually found to be above 2100 cm^{-1} [46]. In the present case, frequencies of these vibrations are below 2100 cm^{-1} and suggest the presence of

terminal thiocyanate group bonded through the N atom to the metal. Moreover, since this band is a doublet, the NCS groups are non-equivalent. Thus the complex will be a cis isomer, because the trans isomer will have equivalent NCS groups. This is supported by the crystal structure of the complex. The bands corresponding to the stretching frequency v(CS) appear as doublets at 789 and 763 cm^{-1}. The bands belonging to the deformation frequency δ(NCS) were found at 502 and 540 cm^{-1} confirming the existence of N-bonded NCS group. These assignments were made on an observation that the stretching frequency v(CS) in a terminal thiocyanate is lower than in a bridging one [51]. The structure of **25** confirms the hypothesis.

Complex **26** (Fig. 6.11) has a medium band at 1601 cm^{-1} assignable to the v(C=N) stretching mode of the azomethine group, indicating the azomethine N coordination. The pyridyl N of the Schiff base is also coordinated as evident from the shifts in the absorption frequencies due to the pyridyl ring. The pyridyl ring stretching is observed at 1459 cm^{-1}, the breathing mode of the pyridyl ring is at 1052 cm^{-1} and the pyridyl in-plane and out-of-plane ring deformation are at 647 and 420 cm^{-1} respectively.

The characteristic v_{as}(N$_3$) stretch due to the azide ligand in compound **26** is observed as a doublet at 2061 and 2031 cm^{-1}. The splitting of this band is indicative of the bridging performance of the azide in the complex. The presence of the symmetric vibration of the azide at 1282 cm^{-1} suggests the presence of end-on coordination of the

azide since this vibration mode is not usually active in end-to-end azides. The bending mode of the azide is observed at 766 cm^{-1}. Finally, a broad band ca. 3421 cm^{-1} is assigned as the stretching vibration of the –OH group coordinated to the metal.
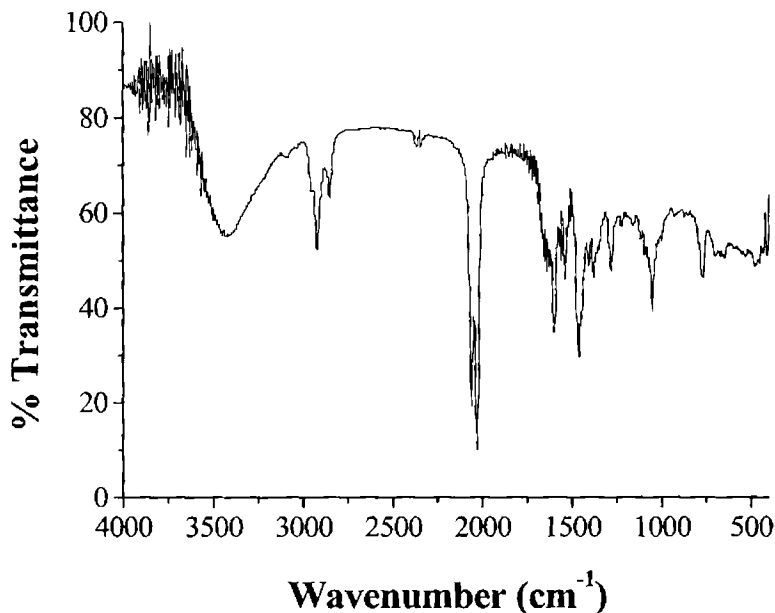
Fig. 6.11. IR spectrum of compound **26**.

Compound **27** (Fig. 6.12) exhibits the v(C=N) of the azomethine function of the Schiff base at 1599 cm^{-1} as a strong band. The band at 1537 cm^{-1} is attributed to pyridyl ring stretching and the band at 1066 cm^{-1} is due to pyridyl ring breathing. The in-plane ring deformation of the pyridyl ring and the pyridyl ring out-of-plane bending are observed at 650 and 579 cm^{-1} as weak bands. The above observations indicate the pyridyl N coordination.
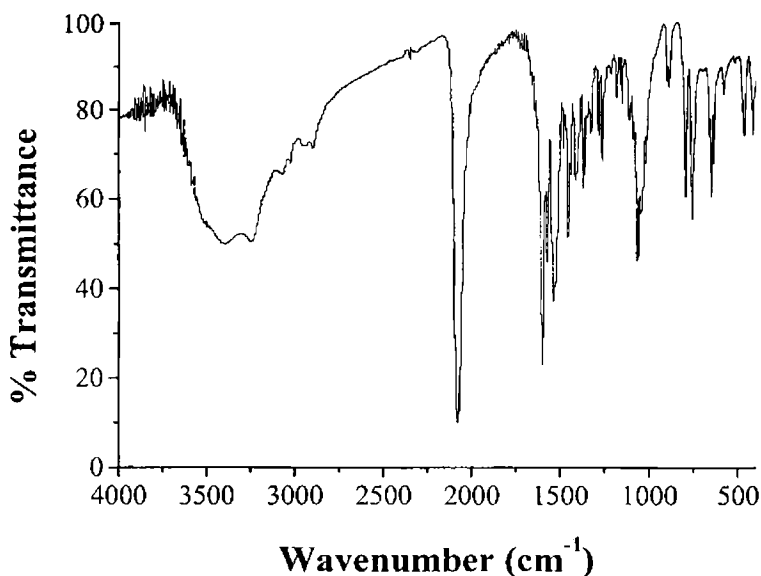
Fig. 6.12. IR spectrum of compound **27**.

The v_{as} stretching due to the thiocyanate groups is observed as a strong band observed at 2079 cm^{-1}. The frequency of absorption below 2100 cm^{-1} indicates the coordination of the NCS group through N atom and the terminal nature of the ligand. The absence of split of the absorption suggests that the complex is a *trans* isomer with the two NCS groups located trans with respect to each other in the octahedral complex and are hence equivalent. The bands corresponding to the stretching frequency v(CS) appear at 757 cm^{-1} and the bands belonging to the deformation frequency δ(NCS) were found at 579 cm^{-1} confirming the existence of N-bonded NCS group.

Complex **28** (Fig. 6.13) exhibits the v(C=N) of the azomethine function of the Schiff base at 1586 cm^{-1} as a medium band. The pyridyl

207

ring vibrations are observed in the usual ranges. The $v_{as}(N_3)$ stretching due to the azide groups is observed as a strong band observed at 2010 cm^{-1} with a small percentage of splitting. This suggests mutual cis coordination of the two azide groups to the metal. The azide symmetric stretch, $v_s(N_3)$, appears at about 1341 cm^{-1} in the compound as a medium band. The band corresponding to the deformation mode (δ) of the azido group can be observed at 685 cm^{-1}.
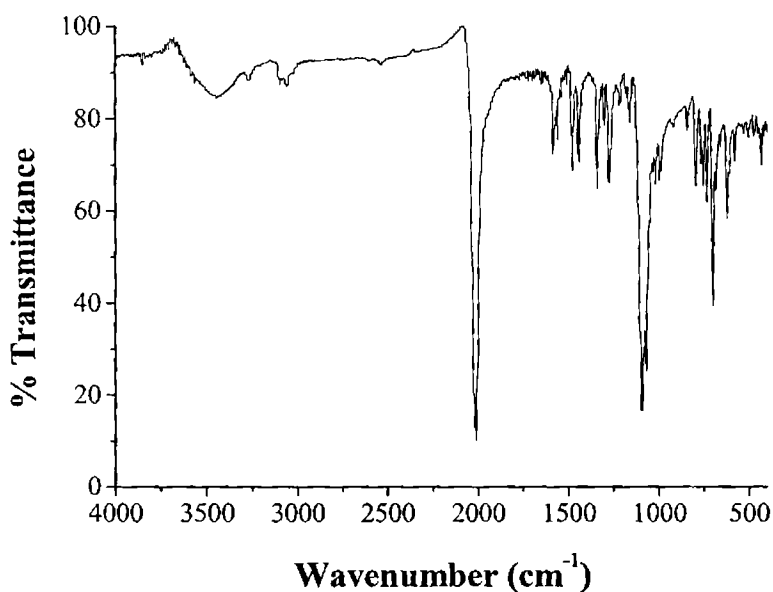
Fig. 6.13. IR spectrum of compound **28**.

According to the elemental analysis, the ligand dpka has undergone hydrolysis to form the gem-diol of dpk, which then forms the metal complex **29**. IR spectral analysis (Fig. 6.14) supports this observation.
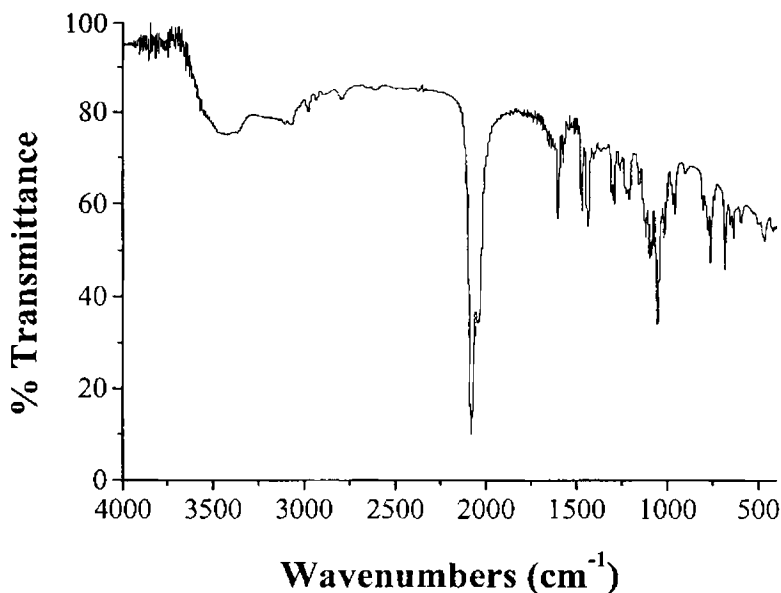
Fig. 6.14. IR spectrum of compound **29**.

The broad and medium intensity band at 3422 cm^{-1} is assigned to the v(OH) vibrations due to the lattice water. In relation to the absorptions caused by the organic ligand dpk reported previously, it is worth mentioning that the band at 1680 cm^{-1}, assigned to the C=O bond in dpk, is shifted to lower frequencies *ca.* 1603 cm^{-1} after solvolysis due to the presence of the C–O bond in the complex [29,30,52]. The bands assigned to the pyridyl ring stretching modes are also remarkably shifted, relative to the free dpk ligand, due to the loss of coplanarity between the pyridyl rings after rehybridisation from sp^2 to sp^3. The pyridyl ring stretching modes in the free dpk at 1578 cm^{-1} is shifted to 1438 cm^{-1}, the ring breathing vibrations in dpk at 998 cm^{-1} suffers a shift to 1056 cm^{-1}, the pyridyl C–H out-of-plane bending in dpk at

753 cm^{-1} shifts to 763 cm^{-1} and the in-plane vibrations of the pyridyl rings shifts to higher frequencies from 662 to 682 cm^{-1} in the complex. The characteristic $v_{as}(N_3)$ stretching vibrations due to the azide ligand is observed as strong doublets at 2080 and 2040 cm^{-1}. The splitting of this vibration indicates the occurrence bridging azide in the complex. The band at 1293 cm^{-1} may be assigned to the $v_s(N_3)$ stretch and is suggestive of the bridging azide to be of the end-on type, since the symmetrical $v_s(N_3)$ stretch of end-to-end azide bridge is not IR active. The band corresponding to the deformation mode (δ) of the azido group can be observed at 636 cm^{-1}.

In complex **30** (Fig. 6.15) the dpk molecule is coordinating in its gem-diol form. The IR pattern is very similar to the complex **29** and the main difference lies in the 2100-2000 cm^{-1} region of the spectrum. Complex **30** exhibits a broad band of medium intensity at 3431 cm^{-1} due to the $v(OH)$ vibrations. The band at 1680 cm^{-1}, assigned to the C=O bond in dpk, is shifted to lower frequencies *ca.* 1601 cm^{-1} in the complex due to the conversion to C–O bond on solvolysis. The vibrations of the pyridyl ring in the free ligand also suffers appreciable shift in frequencies upon complexation. The pyridyl ring stretching modes in the free dpk at 1578 cm^{-1} is shifted to 1434 cm^{-1}, the ring breathing vibrations in dpk at 998 cm^{-1} suffers a shift to 1044 cm^{-1}, the pyridyl C–H out-of-plane bending in dpk at 753 cm^{-1} shifts to 773 cm^{-1} and the in-plane vibrations of the pyridyl rings shifts to higher frequencies from 662 cm^{-1} to 683 cm^{-1} in the complex. In addition a single strong and sharp peak is observed at 2083 cm^{-1}, attributable to

the v(CN) stretching of the N-bonded terminal thiocyanate ligand in the complex. v(CS) is at 752 cm^{-1} and the bending vibration of the NCS group is at 474 cm^{-1}, which again confirms the presence of N-bonded terminal NCS group.
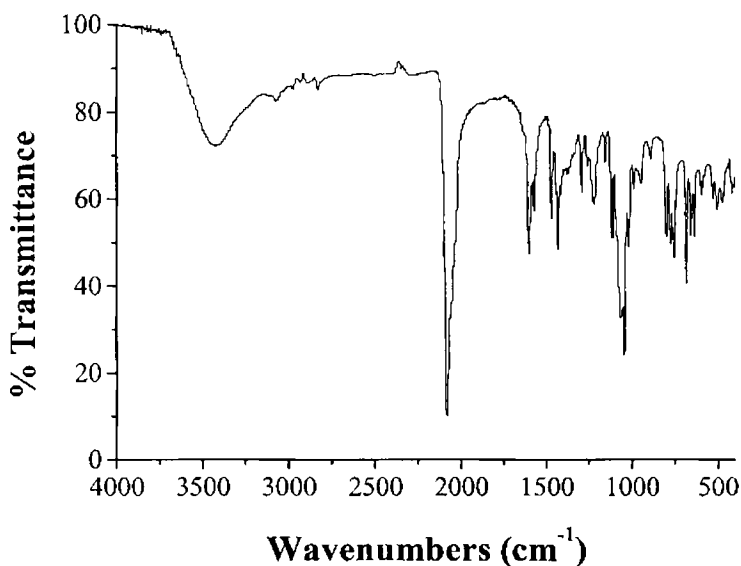
Fig 6.15. IR spectrum of compound **30**.

Complex **31** (Fig. 6.16) has the absorption of the azomethine function of the ligand as a weak band at 1593 cm^{-1}, which supports the coordination of imine N to copper. The pyridyl ring vibrations are shifted appreciably in the complex on comparison with the free pyridyl ring and is thus indicative of coordination through pyridyl N. The v_{as}(N$_3$) stretching vibrations due to the azido ligand exhibits a very strong band at 2065 cm^{-1}. The v_s(N$_3$) stretching mode is observed at 1346 cm^{-1}. The bending mode of the azido ligand is observed at 694 cm^{-1}.
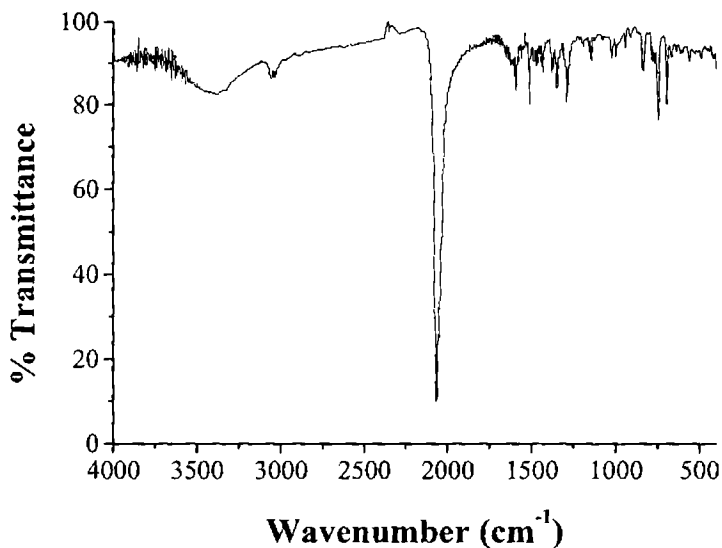
Fig. 6.16. IR spectrum of compound **31**.

In the thiocyanate complex **32** (Fig. 6.17), the medium intensity peak at 1591 cm^{-1} is assigned to the absorption of the azomethine function and indicates its coordination. The pyridyl vibrations are observed in the usual ranges and suggest the coordination of pyridyl N. A very strong peak at 2065 cm^{-1} is due to the v(CN) stretching of the thiocyanate group. The position of the peak indicates the presence of N-bonded terminal thiocyanate group in the complex. The absence of splitting in this absorption is an indication that the complex under study is a *trans* isomer and not a *cis* isomer, because a *cis* isomer will have the split absorption of the asymmetric stretching v(CN). The v(CS) of the NCS ligand at 745 cm^{-1} and the bending vibration of the NCS group is at 490 cm^{-1} also indicates coordination through N atom of the terminal NCS ligand.

212
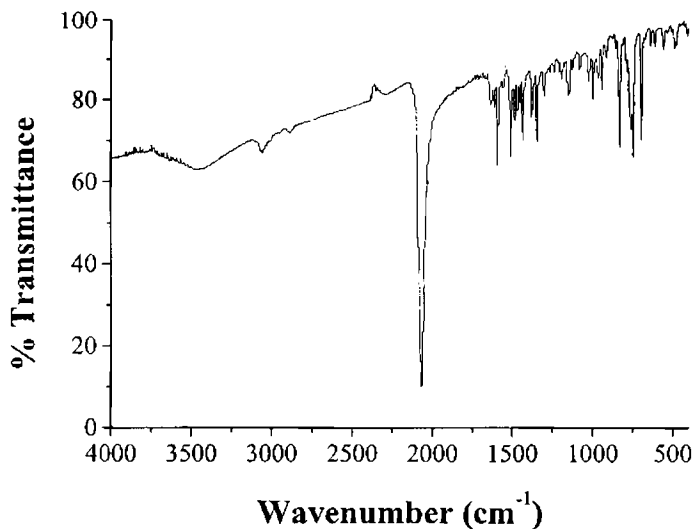
Fig. 6.17. IR spectrum of compound **32**.

The IR spectrum of compound **33** (Fig. 6.18) can be compared with the spectrum of the ligand Hhmba and the differences in the frequencies of absorption of various functions and groups can be regarded as the evidence for coordination. The spectrum of ligand has a broad band at 3445 cm^{-1} due to the stretching mode of the O−H group in the ligand. This band is absent in the complex, which means that the deprotonation of the ligand has taken place the oxygen atom is bonded to the metal. The v(C=N) stretching vibration of the azomethine function is observed as a band of medium intensity at 1624 cm^{-1} in the ligand. This band shifts to lower frequency and is seen as a strong band at 1606 cm^{-1} in the spectrum of the complex. This is a very good evidence for the coordination of the azomethine N. Thus, the deprotonated ligand coordinates to the copper ion through the O atom

213

and the azomethine N. A single strong and sharp peak observed at 2079 cm^{-1} is due to the v(CN) stretching of the thiocyanate ligand, which coordinated through the N atom and exists as a terminal ligand. The v(CS) band is seen at 765 cm^{-1} and the bending vibration of the NCS group is at 466 cm^{-1}.
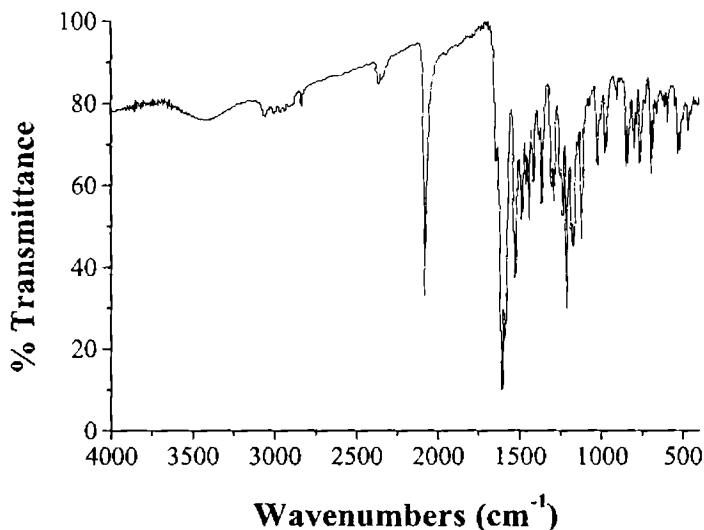
Fig. 6.18. IR spectrum of compound 33.

References

[1]   R.K. Parashar, R.C. Sharma, A. Kumar, G. Mohan, Inorg. Chim. Acta 151 (1988) 201.

[2]   S. Brückner, M. Calligaris, G. Nardin, L. Randaccio, Inorg. Chim. Acta 4 (1968) 386.

[3]   H. Chen, D. Chan, H. Yan, W. Tang, Y. Yang, H. Wang, Polyhedron 12 (1993) 1097.

[4]   A. Böttcher, T. Takeuchi, M.I. Simon, T.J. Meade, H.B. Gray, J. Inorg. Biochem. 59 (1995) 221.

[5]   B. Bosnich, J. Am. Chem. Soc. 90 (1968) 627.

[6]   J.P. Costes, J.M. Dominiguez-Vera, J.P. Laurent, Polyhedron 14 (1995) 2179.

[7]   P.A. Ganeshpure, G.L. Tembe, S.J. Satish, J. Mol. Catal. A113 (1996) L423.

[8]   E.N. Jacobsen, F. Kakiuchi, R.G. Konsler, J.F. Larrow, M. Tokunaga, Tetrahedron Lett. 38 (1997) 773.

[9]   A.R. Battersby, Acc. Chem. Res. 26 (1993) 15.

[10]   S. Balachandran, R.A. Vishwakarma, S.M. Monaghan A. Prelle, P.N. Stanford, F.J. Leeper, J. Chem. Soc., Perkin Trans.1 (1994) 487.

[11]   I.J. Stratford, Int. J. Rad. Oncol. Biol. Phys. 22 (1992) 529.

[12]   B.A. Teicher, M.J. Abrams, K.W. Rosbe, T.S. Herman, Cancer Res. 50 (1990) 6971.

[13]   W.A. Denny, W.R. Wilson, M.P. Hay, Br. J. Cancer Suppl. 27 (1996) S32.

[14]   D.C. Ware, B.D. Palmer, W.R. Wilson, W.A. Denny, J. Med. Chem. 36 (1993) 1839.

[15]   D.C. Ware, H.R. Palmer, P.J. Brothers, C.E.F. Rickard, W.R. Wilson, W.A. Denny, J. Inorg. Biochem. 68, (1997) 215.

[16]   D.C. Ware, H.R. Palmer, F.B. Pruijn, R.F. Anderson, P.J. Brothers, W.A. Denny, W.R. Wilson, Anti-cancer Drug Des. 13 (1998) 81.

[17]   Z. Dori, D. Gershon, US-Patent, Pat. No.5, 258, 403, Date of Patent. Nov 2 (1993).

[18]   E.C. Dunkel, P. Geary, J. Brooks, D. Pavanlangston, 4th Int. Conf. on Antiviral Res. New Orleans (1991) 170.

[19]   H. Devlin, P. Geary, D. Pavanlangston, Z. Dori, E.C. Dunkel, Inv. Ophth-V 34 (1993) 1348.

[20]   J.P. Costes, G. Cros, M.H. Darbieu, J.P. Laurent, Inorg. Chim. Acta 60 (1982) 111.

[21]   A. Böttcher, T. Takeuchi, K.I. Hardcastle, T.J. Meade, H.B. Gray, D.C. Wikel, M. Kapon, Z. Dori, Inorg. Chem. 36 (1997) 2498.

[22]   A. Clearfield, R. Gopal, R.J. Kline, M. Sipski, L.O. Urban, J. Coord. Chem. 7 (1978) 163.

[23]   D.A. Buckingham, L.G. Marzilli, A.M. Sargeson, J. Am. Chem. Soc. 89 (1967) 2772.

[24]   R.J. Brown, D.A. Buckingham, C.R. Clark, P.A. Sutton, Adv. Inorg. Chem. 49 (2000) 307.

[25]   A.F. Knowles, A.K. Nagy, Eur. J. Biochem. 262 (1999) 349.

[26]   L.-F. Tang, H.-Q. Shi, Z.-H. Wang, L. Zhang, J. Chem. Cryst. 39 (2000) 159.

[27]   Q. Zhao, X. Wang, R. Fang, E.R.T. Tiekink, Acta Cryst. E59 (2003) m690.

[28]   M. Du, Y.-M. Guo, X.-B. Leng, X.-H. Bu, Acta Cryst. E57 (2001) m97.

[29]   Z.E. Serna, M.K. Urtiaga, M.G. Barandika, R. Cortés, S. Martin, L. Lezama, M.I. Arriortua, T. Rojo, Inorg. Chem. 40 (2001) 4550.

[30]   Z.E. Serna, R. Cortés, M.K. Urtiaga, M.G. Barandika, L. Lezama, M.I. Arriortua, T. Rojo, Eur. J. Inorg. Chem. (2001) 865.

[31]   B. Żurowska, J. Mroziński, M. Julve, F. Lloret, A. Maslejova, W. Sanda-Dobrowolska, Inorg. Chem. 41 (2002) 1771.

[32]   V. Rattanaphani, W.R. McWhinnie, Inorg. Chim. Acta. 9 (1974) 239.

[33]   G.S. Papaefstathiou, A. Escuer, C.P. Raptopoulou, A. Terzis, S.P. Perlepes, R. Vicente, Eur. J. Inorg. Chem. (2001) 1567.

[34]   J.M. Seco, M. Quirós, M.J.G. Garmendia, Polyhedron 19 (2000) 1005.

[35]   Bruker APEX2 Version 1.27, SAINT Version 7.12a and SADABS Version 2004/1, Bruker AXS: Madison, WI, USA, 2005.

[36]   G.M. Sheldrick, SHELXTL Version 5.10, Bruker AXS Inc., Madison, Wisconsin, USA, 1998.

[37] L.J. Farrugia, J. Appl. Cryst. 30 (1997) 565.

[38] K. Bradenburg, H. Putz, DIAMOND Version 3.0, Crystal Impact, GbR, Postfach 1251, D-53002 Bonn, Germany, 2004.

[39] V.T. Yilmaz, A. Karadag, C. Thoene, R. Herbst-Irmer, Acta Cryst. C56 (2000) 948.

[40] X.-M. Ouyang, B.-L. Fei, T.-aki Okamura, H.-W. Bu, W.-Y. Sun, W.-X. Tang, N. Ueyama, Eur. J. Inorg. Chem. (2003) 618.

[41] J.B. Browne, D.A. Buckingham, A.G. Blackman, C.R. Clark, Acta Cryst. E5 (2002) m125.

[42] Z.-Y. Dong, X.-W. Liu, X.-Q. Wang, R.-J. Wang, G.-Q. Shen, Acta Cryst. E59 (2003) m260.

[43] C.-L. Yuan, Acta Cryst. E61 (2005) m2112.

[44] H.-B. Zhou, D.-Z. Liao, L.-X. Deng, J.-Z. Yu, Y.-P. Gao, X.-F. Yang, Z.-H. Jiang, S.-P. Yan, P. Cheng, Struct. Chem. 17 (2006) 43.

[45] A.B.P. Lever, Inorganic Electronic Spectroscopy, 2nd ed., Elsevier Science, Netherlands (1984).

[46] K. Nakamoto, Infrared and Raman Spectra of Inorganic and Coordination Compounds, 4th ed., John Wiley & Sons, New York (1986).

[47] A.M. Bond, R.L. Martin, Coord. Chem. Rev. 54 (1984) 23.

[48] R. Osterberg, Coord. Chem. Rev. 12 (1974) 309.

[49] S.K. Krishnamurthy, S. Soundararajan, Can. J. Chem. 47 (1969) 995.

[50] S. Prasad, R.K. Agarwal, Trans. Met. Chem. 32 (2007) 143.

[51] M.R. Rosenthal, R.S. Drago, Inorg. Chem. 4 (1965) 840.

[52] R.R. Osborne, W.R. Mc Whinnie, J. Chem. Soc. A (1967) 2075.

❀❀❀❀ℰℭℭ❀❀❀❀

Syntheses, structural and spectral investigations of cadmium(II) complexes of Schiff bases with azide and thiocyanate

7.1 Introduction

Cadmium is an extremely toxic element that is naturally present in the environment and also as a result of human activities. Analysis of biosystems with cadmium ion becomes a problem of particular importance in view of the established toxic influence of this metal, associated with Hg and Pb to the group of the most toxic environmental pollutants [1–4]. Recently, an increase in the concentration of this metal in living organisms has been observed [5]. Its toxicity derives from the fact that it is rapidly localized intracellularly, mainly in the liver, and then bound to metallothionein forming a complex that is slowly transferred to the bloodstream to be deposited in the kidneys. This leads to urinary loss of filterable proteins, calcium and other small molecules, which may produce proteinuria and bone decalcification [3,4,6]. This metal competes with Zn and blocks the active sites of metal-enzymes and as a relatively soft acid it can dislodge Zn(II) in cysteine-coordinated zinc compounds or Ca(II) ions in bone cells [7]. The development of chelating agents is essential for the treatment of cadmium intoxication. *In vivo* cadmium mobilization and an assessment of cadmium chelating drugs have drawn the interest of

many biochemists [8]. For these purposes many kinds of organic compounds (ligands) have been used by many researchers [9,10]. Such an activity is directly attributed to the formation of stable chelates with transition metals that catalyze the corresponding physiological processes [11]. There are several reports of the transition metal complexes including some cadmium complexes containing different types of Schiff base ligands in the literature. Though cadmium has been known as a toxic metal and is often associated with mercury and lead as one of the biologically harmful metal ions, the cadmium(II) ion has recently been found to serve as the catalytic center in a newly discovered carbonic anhydrase [12]. Cadmium complexes of pseudohalogens exhibit interesting NLO, optoelectronic properties and luminescence and are hence useful in the design of new molecule based materials.

Cadmium thiocyanate adducts of organic ligands are an important class of compounds for the design and preparation of functional coordination frameworks [13]. Thiocyanate complexes of cadmium of various dimensionalities have been obtained [14–16]. A major obstacle to a more comprehensive study of such thiocyanate-based polymeric coordination complexes is the lack of a rational synthetic procedure since, given the present knowledge, it is hardly possible to determine which coordination mode will be adopted by the thiocyanate ligand, and whether the sought-after alternating chain structure will finally be formed [17,18]. A number of cadmium(II) thiocyanate complex adducts of monodentate organic ligands, such as methyl-substituted pyridines

[19,20], dibenzylamine [21], dimethyl sulfoxide [22], 4-chloropyridine [23], 1H-1,2,4-triazole [24], imidazole [25,26] and 4-aminopyridine [27] have been reported. All of these adducts exhibit chain structures where each pair of adjacent Cd(II) centers are bridged by thiocyanate ligands and the remaining coordination sites are occupied by monodentate organic ligands. Few thiocyanate bridged cadmium(II) complexes consist of a two-dimensional network [28,29]. Polymeric thiocyanate Cd(II) complexes with bidentate and tridentate ligands have also been reported [26,30,31]. Mononuclear complexes [32] and binuclear complexes [33] of Cd(II)-thiocyanate adducts have also been prepared and characterized. The interest in the study of Cd(II)-thiocyanate complexes of picolinamide lies not only with exploring the coordination abilities of picolinamide, but also in getting some information possibly useful in understanding the role of the thiocyanate ion in biologically important processes recently discovered [34,35].

Though the investigations of the Cd(II)-azido complexes were not as extensively done as the thiocyanate analogues, there are some reports worth mentioning. Polymeric complexes with 1D chain structure have been reported with 3-(2-pyridyl)pyrazole based ligand [32] and other bidentate ligands [36]. Yue _et al._ reported the synthesis and characterization of cadmium(II)-azido polymeric complexes with bidentate diazine Schiff bases having 2D and 3D net topologies [37]. Dimeric complexes of Cd(II) with azide have also been investigated [38-40].

7.2 Stereochemistry

Cd(II) ion with d^{10} electronic configuration permits a wide range of symmetries and coordination numbers. Since the d^{10} configuration affords no crystal field stabilization, the stereochemistry of a particular compound depends on the size and polarizing power of the M(II) cation and the steric requirement of the ligands. Therefore they display a variety of coordination numbers and geometries based on the interplay of electrostatic forces, covalence and the size factor. Cd(II) usually forms four coordinate and six coordinate complexes though Cd(II) six coordinate complexes are found to be more stable than those of Zn(II) because of its larger size.

7.3 Experimental

7.3.1 Materials

Pyridine-2-carbaldehyde (Sigma Aldrich), quinoline-2-carbaldehyde (Sigma Aldrich), 2-hydroxy-4-methoxybenzaldehyde (Sigma Aldrich), aniline (S. D. Fine), *R*-1-phenylethyl amine (Alfa Aeser), 2-aminopyrimidine (Sigma Aldrich), $Cd(OAc)_2 \cdot 2H_2O$ (Qualigens), NaN_3 (Reidel-De Haen), KCNS (BDH) and methanol (Merck) were used as received.

7.3.2 Preparation of cadmium(II) complexes

$Cd_2(paa)_2(N_3)_4$ (34): A mixture of pyridine-2-carbaldehyde (0.107 g, 1 mmol) in methanol and aniline (0.093 g, 1 mmol) in methanol were refluxed for 2 hours to obtain a yellow solution of the Schiff base. To the solution thus obtained, $Cd(OAc)_2 \cdot 2H_2O$ (0.266 g, 1 mmol)

dissolved in methanol and an aqueous solution of NaN_3 (0.130 g, 2 mmol) was added with stirring. The resulting yellow colored solution was stirred for half an hour and the pale yellow product obtained was filtered, washed with methanol followed by ether and dried over P_4O_{10} _in vacuo_. Elemental Anal. Found (Calcd.) (%): C, 38.49 (38.06); H, 2.71 (2.66); N, 30.10 (29.59).

Cd(papea)₂(NCS)₂ (35): Pyridine-2-carbaldehyde (0.107 g, 1 mmol) and _R_-1-phenylethyl amine (0.121 g, 1 mmol) was refluxed in methanol for 2 hours. To this, a methanolic solution of $Cd(OAc)_2 \cdot 2H_2O$ (0.266 g, 1 mmol) was added followed by an aqueous solution of KCNS (0.194 g, 2 mmol) and refluxed for 4 hours. Colorless block shaped single crystals suitable for X-ray diffraction were isolated within one week. Filtered, washed with methanol followed by ether and dried over P_4O_{10} _in vacuo_. Elemental Anal. Found (Calcd.) (%): C, 55.90 (55.51); H, 4.10 (4.35); N, 12.44 (12.95).

[Cd(paap)(NCS)₂]·2CH₃OH·H₂O (36): A mixture of pyridine-2-carbaldehyde (0.107 g, 1 mmol) in methanol and 2-aminopyrimidine (0.094 g, 1 mmol) in methanol was refluxed for 2 hours. $Cd(OAc)_2 \cdot 2H_2O$ (0.266 g, 1 mmol) dissolved in water was added to the above solution followed by an aqueous solution of KCNS (0.194 g, 2 mmol) and refluxed for 4 hours. The yellow product separated out was filtered, washed with methanol followed by ether and dried over P_4O_{10} _in vacuo_. Elemental Anal. Found (Calcd.) (%): C, 33.78 (33.98); H, 3.20 (3.67); N, 17.01 (16.98).

223

Cd(qaa)(N₃)₂ (37): Quinoline-2-carbaldehyde (0.157 g, 1 mmol) was dissolved in methanol. Aniline (0.093 g, 1 mmol) was added to this. A few drops of glacial acetic acid was also added and refluxed for 4 hours. To the deep yellow solution thus obtained, $Cd(OAc)_2 \cdot 2H_2O$ (0.266 g, 1 mmol) dissolved in methanol and an aqueous solution of NaN_3 (0.130 g, 2 mmol) was added slowly in drops. The mixture was stirred for 3 hours. The yellow product obtained was filtered, washed with methanol, water and ether and dried over P_4O_{10} *in vacuo.* Elemental Anal. Found (Calcd.) (%): C, 44.33 (44.82); H, 2.90 (2.82); N, 25.83 (26.14).

Cd₂(qaa)₂(NCS)₄ (38): Quinoline-2-carbaldehyde (0.157 g, 1 mmol) was dissolved in methanol. Aniline (0.093 g, 1 mmol) was added to this. A few drops of glacial acetic acid was also added and refluxed for 4 hours. To the deep yellow solution thus obtained, $Cd(OAc)_2 \cdot 2H_2O$ (0.266 g, 1 mmol) dissolved in methanol and an aqueous solution of KCNS (0.194 g, 2 mmol) was added and the mixture was refluxed for 4 hours. The solution was then left overnight for slow evaporation to obtain a bright yellow solid. The product was filtered, washed with methanol and ether and dried over P_4O_{10} *in vacuo.* Elemental Anal. Found (Calcd.) (%): C, 46.78 (46.91); H, 2.68 (2.62); N, 12.08 (12.16).

[Cd₂(hmba)₂(N₃)₂]·2CH₃OH (39): 2-Hydroxy-4-methoxybenzaldehyde (0.152 g, 1 mmol) was dissolved in methanol. To this, aniline (0.093 g, 1 mmol) was added. The mixture was refluxed for 2 hours. To the above solution, $Cd(OAc)_2 \cdot 2H_2O$ (0.266 g, 1 mmol) dissolved in methanol was added. To this an aqueous solution of NaN_3 (0.130 g, 2 mmol) was then

added slowly. The resulting solution was stirred for 15 minutes and was kept for the evaporation of the solvent. The yellow product obtained within a week was filtered, washed with methanol, water and ether and dried over P_4O_{10} _in vacuo._ Elemental Anal. Found (Calcd.) (%): C, 43.04 (43.65); H, 4.08 (3.91); N, 13.10 (13.57).

[Cd(Hhmba)₂(NCS)₂]·2H₂O (40): 2-Hydroxy-4-methoxybenzaldehyde (0.152 g, 1 mmol) was dissolved in methanol. To this, aniline (0.093 g, 1 mmol) was added. The mixture was refluxed for 2 hours. $Cd(OAc)_2 \cdot 2H_2O$ (0.266 g, 1 mmol) dissolved in methanol and an aqueous solution of KCNS (0.194 g, 2 mmol) was added to the above solution. The resulting mixture was refluxed for 6 hours, filtered and kept for the evaporation of the solvent. Bright yellow product separated out within two weeks was filtered, washed with methanol and ether and dried over P_4O_{10} _in vacuo._ Elemental Anal. Found (Calcd.) (%): C, 49.73 (50.11); H, 4.48 (4.20); N, 8.40 (7.79).

Caution! Cadmium and its compounds are extremely toxic. Although not encountered in our experiments, azide complexes are potentially explosive, especially in the presence of organic ligands. Only a small amount of the material should be prepared, and it should be handled with care.

7.4   Results and discussion

The condensation of aldehyde/ketone and amine in 1:1 molar ratio yielded the Schiff base ligands, which were used without further purification for the synthesis of the complexes by reaction in presence

of pseudohalides NaN_3/KCNS. The complexes **34, 36, 37** and **38** are found to have the stoichiometry $M(L)(X)_2$, where L is the Schiff base and X is the pseudohalogen. However, complexes **35** and **40** had the general formulation $M(L)_2(X)_2$ and complex **39** can be represented as $M(L)(X)$, even though the syntheses of these complexes were done in the molar ratio 1:1:2. The Schiff bases paa, papea, paap and qaa are neutral bidentate N, N donor systems. The Schiff base Hhmba is a monoprotic N, O donor system, which undergoes deprotonation and coordinates through the deprotonated O atom and the azomethine N in complex **39**. However, in complex **40**, it seems that the ligand is not undergoing deprotonation.

The complexes prepared were basically yellow in colour, only the intensities of the color varied in each complex. All the complexes were found to be soluble in CH_3CN, DMF and DMSO, but only partially soluble in other organic solvents such as $CHCl_3$, ethanol, methanol etc. All the complexes are diamagnetic as expected for a completely filled d^{10} system. We could isolate the single crystals of only one Cd(II) complex. All our attempts to get the single crystals of the other complexes went in vain.

7.4.1 Crystallographic data collection and structure analysis

Single crystal X-ray diffraction measurements of complexes **25** were carried out on a Bruker Smart Apex 2 CCD area detector diffractometer and Bruker Smart Apex CCD diffractometer at the X-ray Crystallography Unit, School of Physics, Universiti Sains Malaysia, Penang, Malaysia. The unit cell parameters were determined and the data collections were performed using a graphite-monochromated Mo Kα (λ = 0.71073 Å)

radiation at a detector distance of 5 cm at 100(1) K with the Oxford Cyrosystem Cobra low-temperature attachment. The collected data were reduced using SAINT program [41] and the empirical absorption corrections were performed using SADABS program [41]. The structures were solved by direct methods and refinement was carried out by full-matrix least squares on F^2 using the SHELXTL software package [42]. All non-hydrogen atoms were refined anisotropically. Hydrogen atoms were geometrically fixed at calculated positions and allowed to ride on their parent atoms. Molecular graphics employed were ORTEP-III [43] and DIAMOND [44].

7.4.2 Crystal Structure

Cd(papea)₂(NCS)₂ (35): The complex crystallizes into an orthorhombic crystal system with the chiral space group $P2_12_12_1$. The structural refinement parameters are given in Table 7.1 and the molecular structure of the complex is depicted in Fig. 7.1. The important bond lengths and bond angles are given in Table 7.2. The ligand retains its configuration in the complex as well. In this complex also the carbon atoms C7 and C21 have the R configuration.

Cd(II) centre is six coordinated to four nitrogen atoms from two Schiff base ligands and two N donor thiocyanate anions. The coordination geometry around the Cd(II) centre could be best described as a distorted octahedron with 6N coordination. The Schiff base ligand adopts typical *N, N* bidentate chelating coordination to form a five-membered Cd–N–C–C–N chelating ring. The thiocyanate anions adopt a N-bonded terminal coordination mode. The coordination around

Cd(II) is satisfied by pairs of *trans* pyridyl N (N1 and N3), *cis* azomethine N (N2 and N4) and *cis* thiocyanate N (N5 and N6).

Table 7.1. Crystal data and structure refinement

| Parameters	Cd(papea)$_2$(NCS)$_2$
Empirical formula	C$_{30}$H$_{28}$CdN$_6$S$_2$
Formula weight	649.10
Temperature (T) K	100.0(1) K
Color	Blue
Nature	Blocks
Wavelength (Mo Kα) (Å)	0.71073 Å
Crystal system	Orthorhombic
Space group	$P2_1P2_1P2_1$ (No: 19)
Unit cell dimensions	a = 13.5517(2) Å
	b = 14.0513(2) Å
	c = 15.2805(2) Å
	α = β = γ = 90.00°
Volume V (Å^3), Z	2909.70(7), 4
Calculated density (ρ) (Mg m^{-3})	1.482
Absorption coefficient μ (mm^{-1})	0.924
F(000)	1320
Crystal size (mm^3)	0.52x0.44x0.27
θ range for data collection	2.09 – 42.70°
Index ranges	-24≤h≤25, -26≤k≤26, -29≤ l ≤28
Reflections collected / unique	108229/20479 [R(int) = 0.0411]
Completeness to 2θ = 42.70	99.5%
Absorption correction	SADABS
Maximum and minimum transmission	0.7891, 0.6470
Refinement method	Full-matrix least-squares on F^2
Data / restraints / parameters	20479/0/354
Goodness-of-fit on F^2	1.019
Final R indices [I>2σ(I)]	R$_1$ = 0.0331, wR$_2$ = 0.0568
R indices (all data)	R$_1$ = 0.0422, wR$_2$ = 0.0591
Largest diff. peak and hole	0.769 and -0.389
Absolute structure parameter	-0.013(7)
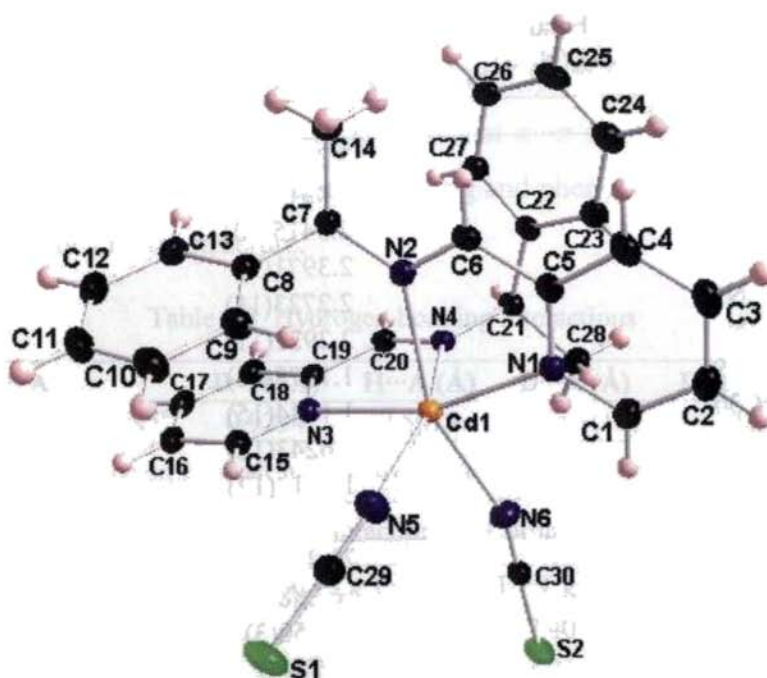
Fig. 7.1. Molecular structure of **Cd(papea)₂(NCS)₂ (35).**

The Cd–N–C bond angles due to the two NCS⁻ anions (C29–N5–Cd1 and C30–N6–Cd1) are significantly bent at 141.32(10) and 160.22(10)° respectively. The thiocyanate groups are linear with the N–C–S bond angles of 178.13(12) and 179.18(12)°. Also, the C–N bond lengths [1.1678(16)° and 1.1644(15)°] and the C–S bond lengths [1.6243(12)° and 1.6313(12)°] in the thiocyanate anions show the normal structure of the thiocyanate [45]. All the Cd–N bond lengths [from 2.2723(11) to 2.4319(8) Å] and the bond angles around Cd(II) [from 70.28(3) 162.88(3)°] are in the normal range expected for similar Cd–NCS complexes with thiocyanate ligand in the terminal coordination mode [32,46-48].

Table 7.2. Selected bond lengths (Å) and bond angles (°) for Cd(papea)$_2$(NCS)$_2$

Bond lengths	
Cd1−N1	2.3551(9)
Cd1−N2	2.4319(8)
Cd1−N3	2.3415(10)
Cd1−N4	2.3971(9)
Cd1−N5	2.2723(11)
Cd1−N6	2.2921(11)
N5−C29	1.1678(16)
N6−C30	1.1644(15)
S1−C29	1.6243(12)
S2−C30	1.6313(12)
Bond angles	
N1−Cd1−N2	70.28(3)
N3−Cd1−N1	162.88(3)
N1−Cd1−N4	104.50(3)
N5−Cd1−N1	97.75(4)
N6−Cd1−N1	89.06(4)
N3−Cd1−N2	92.81(3)
N4−Cd1−N2	87.19(3)
N5−Cd1−N2	101.92(4)
N6−Cd1−N2	157.72(4)
N3−Cd1−N4	70.98(3)
N5−Cd1−N3	88.11(4)
N6−Cd1−N3	107.21(4)
N5−Cd1−N4	157.70(4)
N6−Cd1−N4	90.14(4)
N5−Cd1−N6	88.72(4)
C29−N5−Cd1	141.32(10)
C30−N6−Cd1	160.22(10)
N5−C29−S1	178.13(12)
N6−C30−S2	179.18(12)

The packing diagram of the compound viewed along the 'a' axis is as shown in Fig. 7.2. There are no classical hydrogen bonds in the crystal structure of the complex. The packing of the molecules in the

crystal lattice is reinforced by weak hydrogen bonding interactions (Table 7.3) and C–H⋯π interactions (Table 7.4). The orientation of the molecules in the crystal lattice is such that π⋯π stacking interactions (Table 7.5) between the metal-chelate ring and phenyl and pyridyl rings stabilize the crystal structure.

Table 7.3. Hydrogen bonding interactions

D–H⋯A	D–H (Å)	H⋯A (Å)	D⋯A (Å)	D–H⋯A (Å)
C16–H(16A)⋯N5[a]	0.9294	2.5019	3.2798(17)	141.39

D=donor, A=acceptor; Equivalent position code: a =-x, 1/2+y, 3/2-z

Table 7.4. C-H⋯π interactions of Cd(papea)$_2$(NCS)$_2$

C–H(I)⋯Cg(J)	C⋯Cg (Å)	C–H⋯Cg (°)	C⋯Cg (Å)
C2–H(2A)[1]⋯Cg(5)[a]	3.1004	117.40	3.6239(15)
C7–H(7A)[1]⋯Cg(2)[b]	2.9555	113.20	3.4608(11)
C15–H(15A)[1]⋯Cg(5)[b]	3.0741	92.53	3.2507(12)
C23–H(23A)[1]⋯Cg(3)[b]	3.1364	111.74	3.5869(12)

Equivalent position code: a = 1/2-x,-y,-1/2+z; b = x, y, z
Cg(2) = Cd1, N3, C19, C20, N4; Cg(3) = N1, C1, C2, C3, C4, C5; Cg(5) = C8, C9, C10, C11, C12, C13

Table 7.5. π⋯π interactions of Cd(papea)$_2$(NCS)$_2$

Cg(I)Res(I)⋯Cg(J)	Cg⋯Cg (Å)	α°	β°	γ°
Cg(1)[1]⋯Cg(6)[a]	3.7974(6)	13.34	21.84	29.22
Cg(4)[1]⋯Cg(5)[a]	3.9040(7)	15.27	38.30	24.24
Cg(4)[1]⋯Cg(6)[b]	3.6082(7)	3.56	19.98	16.46
Cg(5)[1]⋯Cg(4)[a]	3.9040(7)	15.27	24.24	38.30
Cg(6)[2]⋯Cg(1)[a]	3.7974(6)	13.34	29.22	21.84
Cg(6)[2]⋯Cg(4)[c]	3.6083(7)	3.56	16.46	19.98

Equivalent position code : a = x, y, z; b= -1/2 +x, 1/2-y,1-z ;c=1/2+x,1/2-y,1-z
Cg(1) = Cd1, N1, C5, C6, N2; Cg(4) = N3, C15, C16, C17, C18, C19; Cg(5) = C8, C9, C10, C11, C12, C13; Cg(6) = C22, C23, C24, C25, C26, C27
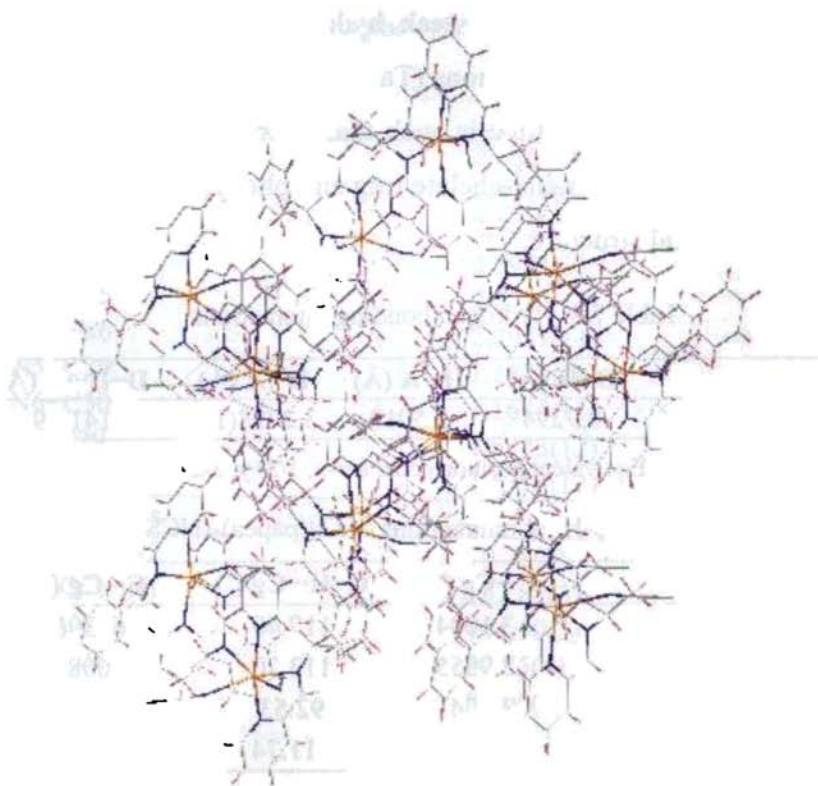
Fig. 7.2. Molecular packing diagram of **Cd(papea)₂(NCS)₂ (35)**.

7.4.3 Spectral characteristics of Cd(II) complexes

7.4.3a *¹H NMR spectra*

For complex **34** (Fig. 7.3), the most downfield signal appears as a singlet at 8.80 ppm and can be assigned to the single proton on the azomethine group [49]. The proton alpha to the pyridyl N suffers a downfield shift and occurs as a doublet at 8.75 ppm due to coupling with the proton on the neighboring C atom. The pyridyl proton present at the para position, by virtue of its position with respect to the pyridyl N is obtained at 8.12 ppm as a quartet through spin-spin coupling with two protons on adjacent carbon atoms. The remianing pyridyl protons

232

resonate at 7.73 and 7.46 ppm as triplet and doublet respectively. In short, all the four pyridyl ring protons resonate as slightly different fields. The protons of the phenyl ring are obtained as multiplet at 7.35 ppm.
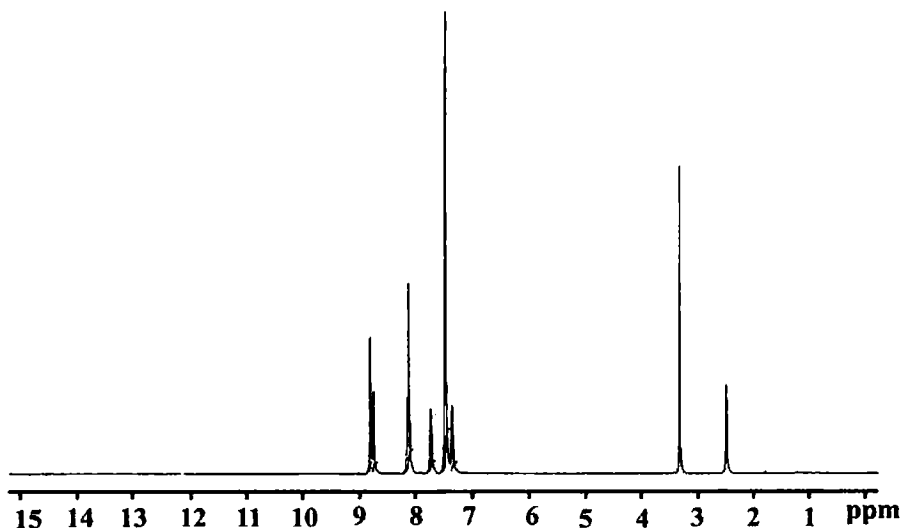

Fig. 7.3. ^{1}H NMR spectrum of compound **34**.

The ^{1}H NMR spectrum of compound **36** (Fig. 7.4) shows a broad signal at 11.10 ppm due to the −OH group of the lattice water. Another broad peak at 10.66 ppm is due to the resonance of the proton of the −OH group of methanol present in the crystal lattice. The broadness of these two signals indicates the existence of hydrogen bonds through water and methanol. The presence of methanol in the lattice sites is also indicated by the singlet appearing at 1.99 ppm assigned as the signal due to the methyl protons of methanol. A broad signal observed at 9.43 ppm corresponds to the proton on the azomethine moiety. The protons of the pyridyl ring resonate at 7.27-8.08 ppm and those of the pyrimidine ring resonate at 8.21-8.79 ppm in the complex.
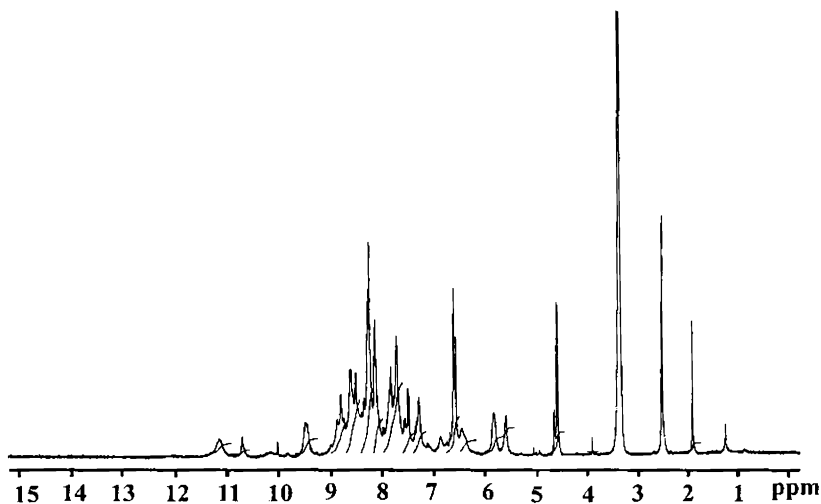
233

Fig. 7.4. ^{1}H NMR spectrum of compound **36**.

In the NMR spectrum of complex **37** (Fig. 7.5), the signal due to the azomethine function occurs as a singlet at 8.79 ppm. The protons of the phenyl ring resonate at 7.33-7.70 ppm and those of the quinoline ring resonate at 8.08-8.53 ppm in the complex as multiplets.
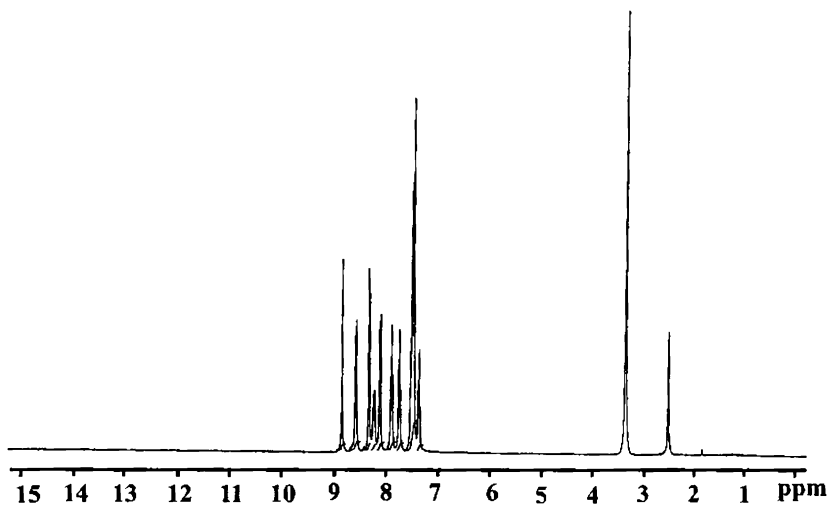

Fig. 7.5. ^{1}H NMR spectrum of compound **37**.

The thiocyanate complex **38** (Fig. 7.6), with the same ligand qaa as that of **37** has a spectrum very similar to the latter. The signal due to the single proton on the azomethine group occurs as a singlet at 8.79 ppm. Multiplets seen at 7.84-8.51 correspond to the protons of the quinoline ring and the multiplets at 7.32-7.69 are due to the protons of the phenyl ring in the complex.
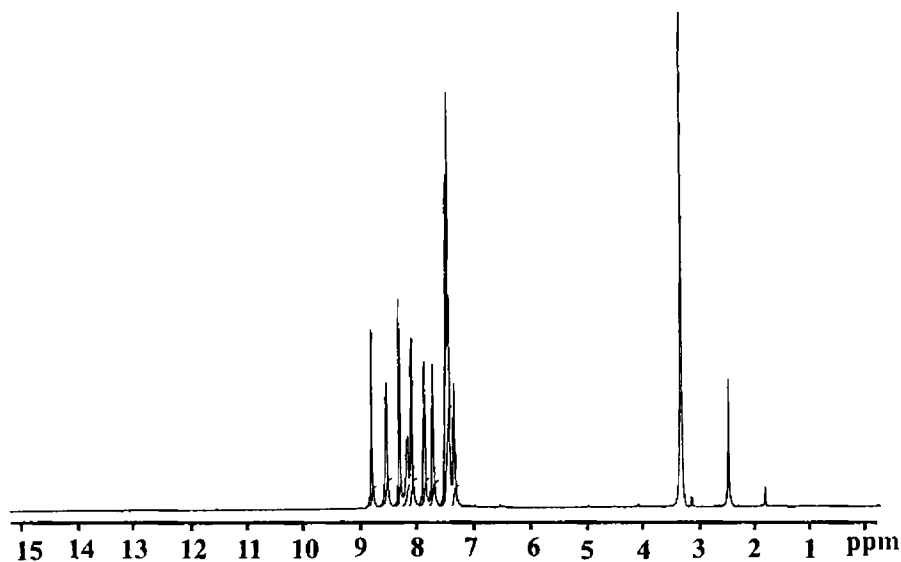
Fig. 7.6. ^{1}H NMR spectrum of compound **38**.

In complex **39** (Fig. 7.7), the singlet appearing at 9.72 ppm corresponding to the single proton of the azomethine moiety, H−C=N in the complex shows an upfield shift of 0.87 ppm in the complex and occurs at 8.85 ppm. The upfield shift may be attributed to the transfer of electrons from the completely filled d orbitals of the metal to the empty antibonding molecular orbitals of N atom of the azomethine group. The protons of the aromatic rings are obtained in the region

235

6.50-7.40 ppm. The methoxy protons appear as a singlet at 3.79 ppm. The presence of methanol is also indicated by the singlet appearing at 1.81 ppm from the protons of the methyl group.
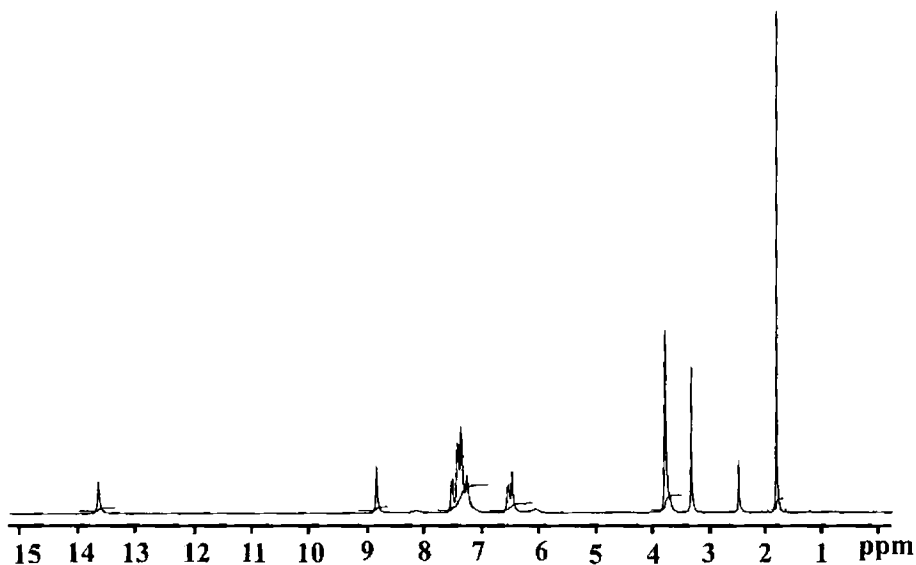
Fig. 7.7. ^{1}H NMR spectrum of compound **39**.

Complex **40** (Fig. 7.8) has a most downfield singlet at 13.36 ppm corresponding to the resonance of the proton of the −OH group of the ligand. This is an evidence for the coordination of the ligand in the neutral form, i.e. without deprotonation. The singlet appearing at 8.85 ppm is due to the resonance of the solitary proton of the azomethine group. This signal has shown an upfield shift due to the metal to N charge transfer from the value of 9.72 ppm in the ligand. The aromatic protons resonate at 6.48-7.52 ppm region and signal corresponding to the protons of the methoxy group appear in the spectrum at 3.79 ppm as a singlet.

236
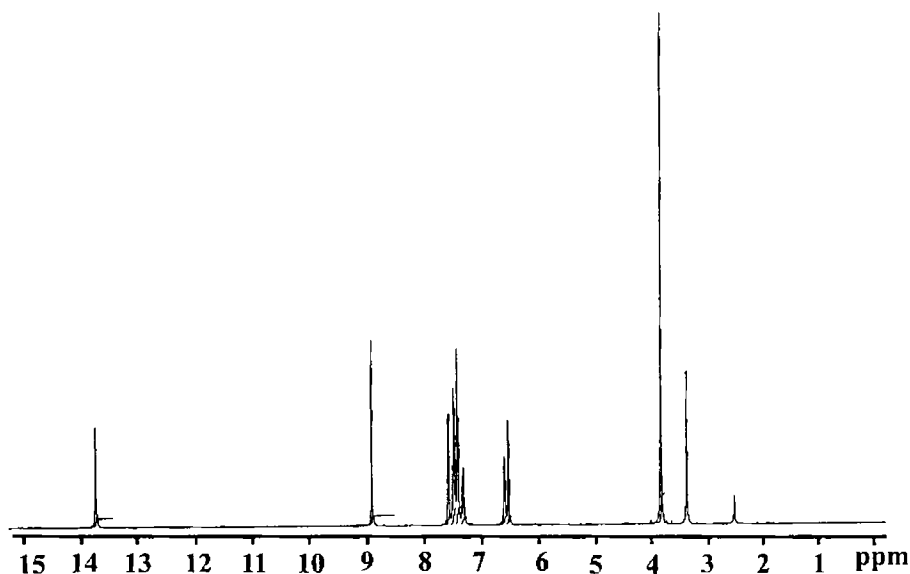
Fig. 7.8. ^{1}H NMR spectrum of compound **40**.

7.4.3b *Electronic spectra*

For cadmium(II) systems no *d-d* transitions are expected since they have a completely filled d^{10} configuration. Table 7.6 lists the various intraligand and charge transfer transitions in the cadmium complexes.

Table 7.6. Electronic spectral data (nm) of Cd(II) complexes

Complex	$\pi \rightarrow \pi^*$	$n \rightarrow \pi^*$	CT
Cd(paa)(N$_3$)$_2$ (**34**)	290	310	410
Cd(papea)$_2$(NCS)$_2$ (**35**)	291	315	390
Cd(paap)(NCS)$_2$·2CH$_3$OH·H$_2$O (**36**)	290	315	400
Cd(qaa)(N$_3$)$_2$ (**37**)	300	320	370
Cd(qaa)(NCS)$_2$ (**38**)	300	325	367, 440, 468
Hhmba	291	334	-
[Cd$_2$(hmba)$_2$(N$_3$)$_2$]·2CH$_3$OH (**39**)	295	335	355, 410
Cd(Hhmba)$_2$(NCS)$_2$·2H$_2$O (**40**)	295	335	356, 410

237

The yellow color of the complexes arises due to charge transfer transitions. Complex **35** is colorless because of the fact that the charge transfer transition in this thiocyanato complex is very weak in intensity that it is almost undetectable. Fig. 7.9 shows the electronic spectrum of compound **34**.
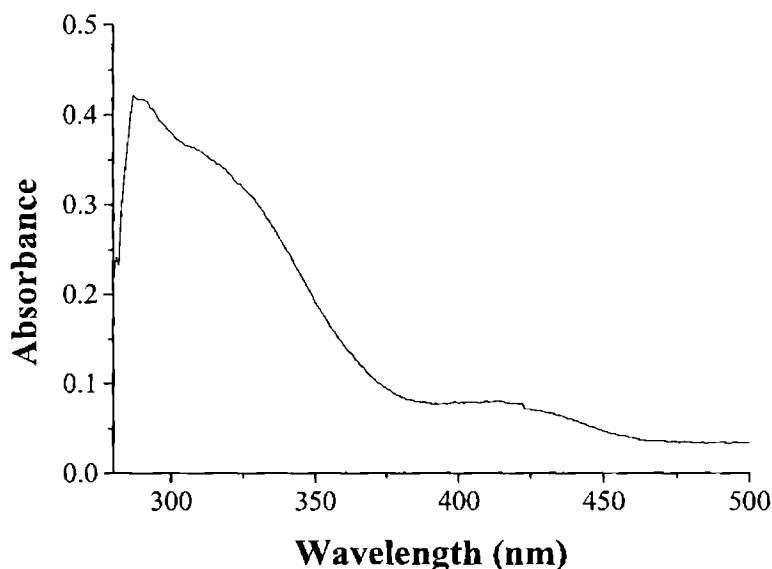
Fig. 7.9. Electronic spectrum of compound **34**.

7.3.2c *IR spectral studies*

Infrared spectroscopy is a very useful tool in determining the coordination of various atoms and groups. It becomes particularly important in the case of complexes containing pseudohalogens like azide and thiocyanate, for which strong absorptions are observed in the $2100-2000$ cm^{-1} region and remain isolated and without any perturbance from the complicated finger print region of the spectrum.

The IR spectrum of compound **34** (Fig. 7.10) has a band of medium intensity at 1591 cm^{-1}, which is assigned as the v(C=N) stretching mode of the azomethine function of the Schiff base. The band at 1437 cm^{-1} is attributed to pyridyl ring stretching and the band at 1013 cm^{-1} is due to pyridyl ring breathing. The in-plane ring deformation of the pyridyl ring and the pyridyl ring out-of-plane bending are observed at 654 and 542 cm^{-1} as weak bands.
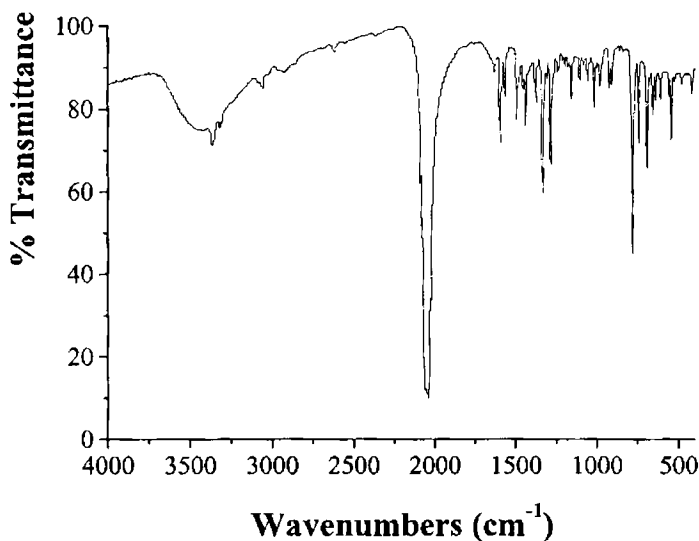
Fig. 7.10. IR spectrum of compound **34**.

The asymmetric stretching of the azide v_{as}(N$_3$) is obtained as a strong doublet at 2059 and 2030 cm^{-1}. This indicates the existence of azide ligand in bridged coordination mode. The v_s(N$_3$) stretching mode of the azide group is observed at 1332 cm^{-1} as a band of medium intensity. The v_s(N$_3$) vibration mode in inactive in end-to-end bridges which possess high symmetry, so the azide bridge may be an end-on

bridge. The deformation mode of the azido ligand is observed as a weak band at 690 cm^{-1}.

The ν(C=N) stretching mode of the Schiff base occurs as a medium band at 1594 cm^{-1} in complex **35** and indicates the coordination of azomethine N to the cadmium(II). The coordination of the pyridyl N is confirmed by the presence of pyridyl ring stretch at 1439 cm^{-1}, pyridyl ring breathing at 1016 cm^{-1}, pyridyl in-plane ring deformation at 639 cm^{-1} and pyridyl out-of-plane ring deformation at 410 cm^{-1}. The asymmetric stretching mode of the thiocyanate group ν_{as}(C=N) is observed as doublets at 2071 and 2050 cm^{-1}. This indicates the coordination of the thiocyanate anions and the presence of doublet implies that there are two non-equivalent thiocyanate groups and hence mutual *cis* coordination of the thiocyanate groups in the octahedral complex. If it were a *trans* isomer only a single peak would have been obtained for the above stretching mode. The position of bands (<2100 cm^{-1}) is an evidence for coordination *via* N atom and also the terminal nature of the thiocyanate groups. All these are confirmed by the crystal structure analysis of complex **35**. Doublets near 788 and 767 cm^{-1} is due to the thiocyanate ν_s(CS) stretching vibration. This band is also indicative of N coordination. A single sharp peak at 497 cm^{-1} is that of δ(NCS) bending mode.

In the thiocyanate complex **36** (Fig. 7.11), the medium intensity peak at 1557 cm^{-1} is assigned to the absorption of the azomethine function and indicates its coordination. The pyridyl ring and pyrimidine ring vibrations are observed in the usual ranges. A strong

broad peak at 2065 cm^{-1} is due to the ν(CN) stretching of the thiocyanate group. The position of the peak and its singlet structure points out to the presence of N-bonded terminal thiocyanate group in the complex. The ν(CS) of the NCS ligand at 753 cm^{-1} and the bending vibration of the NCS group is at 457 cm^{-1} also indicates coordination through N atom of the terminal NCS ligand. The spectrum has a broad band ca. 3300 cm^{-1} due to the ν(O–H) stretching.

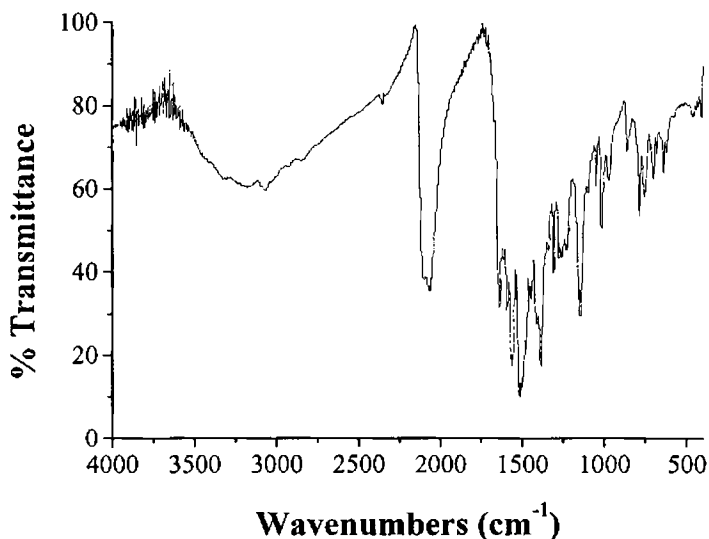Fig. 7.11. IR spectrum of compound **36**.

Complex **37** has the absorption of the azomethine function of the ligand as a medium band at 1592 cm^{-1}, which supports the coordination of imine N. The pyridyl ring vibrations are observed in the usual ranges. The ν_{as}(N$_3$) stretching vibrations due to the coordinated azido ligand occurs as a strong band at 2059 cm^{-1}. The ν_s(N$_3$) peak is

observed at 1333 cm^{-1} and the bending mode of the azido ligand is observed at 689 cm^{-1}.

In the thiocyanate complex **38** (Fig. 7.12), the medium intensity peak at 1589 cm^{-1} is assigned to the absorption of the azomethine function and indicates its coordination. The pyridyl vibrations are observed in the usual ranges. The asymmetric stretching of the thiocyanate ligand v(CN) occurs at 2112 and 2095 cm^{-1}. The position of the peaks and its doublet structure strongly suggest the existence of bridging and terminal thiocyanate group in the complex. The v(CS) of the NCS ligand occurs as a weak doublet at 770 and 745 cm^{-1} and the bending vibration of the NCS group around 460 cm^{-1} occurs as several peaks of low intensity, which also support the presence of bridging thiocyanate ligand in the complex.
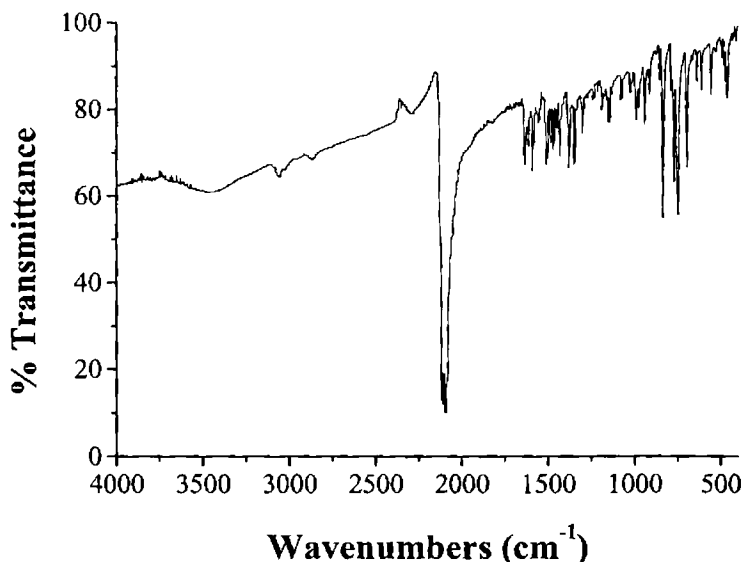

Fig. 7.12. IR spectrum of compound **38**.

The ν(C=N) stretching vibration of the azomethine function is observed as a band of medium intensity at 1624 cm^{-1} in the ligand. This band shifts by about 30 cm^{-1} and is seen as a medium intensity band at 1585 cm^{-1} in the spectrum of the complex **39**. This is a very good evidence for the coordination of the azomethine N. The bands assignable to the ν_{as}(N$_3$) stretching of the azido ligand is visible as a very strong band _ca._ 2066 cm^{-1} and a band of medium intensity at 2032 cm^{-1}. This suggests the presence of different coordination modes of the azide group. The medium band at 1358 cm^{-1} is assigned to the symmetric stretching ν_s(N$_3$) of the azide. The bending vibration of the azide is seen at 690 cm^{-1} as a weak band.

The IR spectrum of complex **40** lacks the band due to the stretching vibrations of the O–H group indicative of the deprotonation of the ligand and coordination through the O atom. The band due to the azomethine group is observed at 1616 cm^{-1} in the complex. The asymmetric ν(CN) stretching of the thiocyanate ligand is observed as a complex pattern of many strong bands at 2124, 2104 and 2088 cm^{-1}, suggesting the existence of different kinds of thiocyanate groups and their different coordination modes. The high frequencies observed indicate the presence of bridging NCS. Many peaks appear in the region 826-753 cm^{-1} due to ν(CS) and the bending vibration of the NCS group occurs as many weak bands near 490 cm^{-1}.

References

[1]   G.D. Munno, S. Mauro, T. Pizzino, D. Viterbo, J. Chem. Soc., Dalton Trans. (1993) 1113.

[2]   Y. Katono,Y. Inoue, R. Chûjô, Polym. J. 9 (1977) 471.

[3]   H.P. Srivastava, D.J. Tiwari, Indian Chem. Soc. 70 (1993) 499.

[4]   M.D. Walker, D.R. Williams, J. Chem. Soc., Dalton Trans. (1974) 1186.

[5]   M.L.S. Simoes Gonçalves, M.M. Correia dos Santos, J. Electroanal. Chem. 187 (1985) 333.

[6]   O. Andersen, Chem. Rev. 99 (1999) 2683.

[7]   W. Kaim, B. Schwederski, Bioinorganic Chemistry: Inorganic Elements in Chemistry of Life, Wiley: New York (1994).

[8]   G.R. Wilkinson, D. Gillard, J.A. McCleverty, Eds. Comprehensive Coordination Chemistry, Pergamon: Oxford 5 (1987).

[9]   R.J. Topping, M.M. Jones, G.R. Gale, A.B. Smith, J. Inorg. Biochem. 36 (1989) 115.

[10]   M.E. Dakanali, T. Kefalas, C.P. Raptopoulou, A. Terzis, T. Mavromoustakos, A. Salifoglou, Inorg. Chem. 42 (2003) 2531.

[11]   I. Geubeur, M. Guekezian, L.H.S.Á. Terra, M.C.B Moraes, C.L. Lago, J.R. Matos, M.E.V. Suárez-Iha, Polyhedron 23 (2004) 2095.

[12]   T.W. Lane, F.M.M. Morel, Proc. Natl. Acad. Sci. USA 97 (2000) 4627.

[13]   H. Zhang, X. Wang, K. Zhang, B.K. Teo, Coord. Chem. Rev. 183 (1999) 157.

[14]   B. Zurowska, J. Mrozinski, M. Julve, F. Lloret, A. Maslejova, W. Sawka-Dobrowolska, Inorg. Chem. 41 (2002) 1771.

[15]   W. Zhang, X. Wu, B. Wu, S. Yu, G. Santoni, D. Rehder, Inorg. Chem. 42 (2003) 1130.

[16]   Z.-L. You, Acta Cryst. C61 (2005) m295.

[17]   J. Fercero, C. Diaz, J. Ribas, E. Ruiz, J. Mahia, M. Maestro, Inorg. Chem. 41 (2002) 6780.

[18]   J.-C. Liu, G.-C. Guo, J.S. Huang, X.-Z. You, Inorg. Chem. 42 (2003) 235.

[19]   M. Taniguchi, A. Ouchi, Bull. Chem. Soc. Jpn. 60 (1987) 1192.

[20] M. Taniguchi, M. Shimoi, A. Ouchi, Bull. Chem. Soc. Jpn. 59 (1986) 2299.

[21] M. Taniguchi, Y. Sugita, A. Ouchi, Bull. Chem. Soc. Jpn. 60(1987) 1321.

[22] A. Chenskaya, A.V. Virovets, S.A. Gromilov, N.V. Podberezskaya, T.G. Cherkasova, Inorg. Chem. Commun. 3 (2000) 482.

[23] M.A.S. Goher, F.A. Mautner, M.A.M. Abu-Youssef, A.K. Hafez, A.M.-A. Badr, C. Gspan, Polyhedron 22 (2003)3137.

[24] J.G. Haasnoot, G.C.M. de Keyzer, G.C. Verschoor, Acta Cryst. C39 (1983) 1207.

[25] H.-J.Chen, G.Yang, X.-M.Chen, Acta Cryst. C55 (1999).2012.

[26] D. Bose, J. Banerjee, Sk. H. Rahaman, G. Mostafa, H.-K. Fun, R.D. Bailey Walsh, M.J. Zaworotko, B.K. Ghosh, Polyhedron 23 (2004) 2045.

[27] S. Banerjee, B. Wu, P.-G. Lassahn, C. Janiak, A. Ghosh, Inorg. Chim. Acta 358 (2005) 535.

[28] N. Mondal, M.K. Saha, S. Mitra, V. Gramlich, J. Chem. Soc., Dalton Trans. (2000) 3218.

[29] G. Yang, H.G. Zhu, B.H. Liang, X.M. Chen, J. Chem. Soc., Dalton Trans. (2001) 580.

[30] M.-C. Suen, J.-C. Wang, J. Coord. Chem. 60 (2007) 257.

[31] M.-C. Suen, J.-C. Wang, J. Coord. Chem. 60 (2007) 2197.

[32] X.-S. Shi, C.-S. Liu, J.-R. Li, Y. Guo, J.-N. Zhou, X.-H. Bu, J. Mol. Struct. 754 (2005) 71.

[33] M. Đaković, Z. Popović, G. Giester, M. Rajić-Linarić, Polyhedron 27 (2008) 210.

[34] M. Rosin, T. Kocher, A. Kramer J. Clin. Peridontol. 28 (2001) 270.

[35] N. Goi, Y. Hirai, H. Harada, A. Ikari, T. Ono, Y. Terashima, N. Kinae, M. Hiramatsu, K. Nakamura, H. Tsuboi, K. Takagi Brain, Behavior and Immunity 20 (2006) e17 (Abstract)

[36]   S.-Q. Bai, E.-Q. Gao, Z. He, C.-J. Fang, C.-H. Yan, Cryst. Eng. Comm. 6 (2004) 606.

[37]   Y.-F. Yue, E.-Q. Gao, S.-Q. Bai, Z. He, C.-H. Yan, Cryst. Eng. Comm. 6 (2004) 549.

[38]   W. Gu, C.-Z. Xie, H.-D. Bian, P. Chen, S.-P. Yan, D.-Z. Liao, Z.-H. Jiang, J. Coord. Chem. 56 (2003) 427.

[39]   Sk. H. Rahaman, R. Ghosh, H.-K. Fun, B.K. Ghosh, Struct. Chem. 17 (2006) 553.

[40]   J.-H. Liu, X.-Y. Wu, Q.-Z. Zhang, X. He, W.-B. Yang, C.-Z. Lu, J. Coord. Chem. 60 (2007) 1373.

[41]   Bruker APEX2 Version 1.27, SAINT Version 7.12a and SADABS Version 2004/1, Bruker AXS: Madison, WI, USA, 2005.

[42]   G.M. Sheldrick, SHELXTL Version 5.10, Bruker AXS Inc., Madison, Wisconsin, USA, 1998.

[43]   L.J. Farrugia, J. Appl. Cryst. 30 (1997) 565.

[44]   K. Bradenburg, H. Putz, DIAMOND Version 3.0, Crystal Impact, GbR, Postfach 1251, D-53002 Bonn, Germany, 2004.

[45]   S.L. Li, Z.Z. Zhang, T.C.W. Mak, Inorg. Chim. Acta 268 (1998) 177.

[46]   A.G. Orpen, L. Brammer, F.H. Aleen, O. Kennard, D.G. Watson, R. Taylor, J. Chem. Soc., Dalton Trans. (1989) S1.

[47]   D.L. Reger, T.D. Wright, M.D. Smith, A.L. Rheingold, S. Kassel, T. Concolino, B. Rhagitan, Polyhedron 21 (2002) 1795.

[48]   S. Sen, P. Talukder, G. Rosair, S. Mitra, Struct. Chem. 16 (2005) 605.

[49]   W. Radecka-Paryzek, E. Jankowska, Inorg. Chim. Acta 134 (1987) 179.

✿✿✿ℰ☯ℂℛ✿✿✿

Summary and Conclusions

Metallo-organic chemistry, incorporating the frontiers of both inorganic and organic chemical aspects, is a topic of utility concern. The first exploration of coordinated metal complexes dates back to the nineteenth century, during the days of Alfred Werner. Thereafter, the inorganic chemistry witnessed a great outflow of coordination compounds, with unique structural characteristics and diverse applications. The diversity in structures exhibited by the coordination complexes of multidentate ligands have led to their usage as sensors, models for enzyme mimetic centers, medicines etc. The ligands chosen are of prime importance in determining the properties of coordination compounds. The presence of more electronegative nitrogen, oxygen and sulfur atoms attached to the ligands increases their denticity thereby enhancing the coordinating possibilities of ligands. Moreover, the presence of these atoms in the coordination sphere leads to their biological activity.

Schiff base ligands are able to coordinate metals through imine nitrogen and another group, usually linked to the aldehyde/ketone. Well-designed Schiff base ligands are considered 'privileged ligands' because they are easily prepared by the condensation between aldehydes and amines. Synthetic catalysts which are enantioselective over a wide range of different reactions were defined as 'privileged' by

247

Jacobsen. Schiff base ligands are able to coordinate many different metals, and to stabilize them in various oxidation states, enabling the use of Schiff base metal complexes for a large variety of useful catalytic transformations. Metal complexes of Schiff bases are useful in the catalysis of many reactions like carbonylation, hydroformylation, reduction, oxidation, epoxidation and hydrolysis etc.

Antimicrobial and antifungal activities of various Schiff bases have also been reported. Many Schiff bases are known to be medicinally important and are used to design medicinal compounds. It has been shown that Schiff base complexes derived from 4-hydroxysalicylaldehyde and amines have strong anticancer activity, e.g. against *Ehrlich Ascites Carcinoma* (EAC).

The pseudohalogens azide and thiocyanate have been demonstrated to be versatile bridging ligands. They are excellent candidates for the design of molecule based magnetic materials. In addition, the azide and thiocyanate anions are observed to inhibit several enzymes like ATPases, cytochrome C oxidase, human carboxy peptidase etc. This makes the study of the metal complexes of these anions very useful for the understanding of biological processes. The use of these anions in conjugation with the Schiff bases for the synthesis of metal complexes can bring about interesting results.

Chapter 1 depicts a brief introduction on Schiff bases, the pseudohalogens azide and thiocyanate and their transition metal complexes. The survey of the previous research works in the field of

248

Schiff bases and their complexes with azide and thiocyanate, their properties and applications is also included. The chapter also contains the objectives of the present study and the details of the different analytical and spectroscopic techniques used for the analysis of the metal complexes.

Chapter 2 deals with syntheses of seven Schiff base ligands. The ligands synthesized are:

1. Pyridine-2-carbaldehyde-aniline (paa)

2. Pyridine-2-carbaldehyde-1-phenylethylamine (papea)

3. Pyridine-2-carbaldehyde-2-aminopyrimidine (paap)

4. 2-Benzoylpyridine-aniline (bzpa)

5. Di-2-pyridyl ketone-aniline (dpka)

6. Quinoline-2-carbaldehyde-aniline(qaa)

7. 2-Hydroxy- 4-methoxybenzaldehyde-aniline (Hhmba)

The ligands paa, papea, bzpa and qaa are neutral bidentate ligands with N, N donor atoms. The ligands paap and dpka are also neutral ligands, but they have additional N donors, which may or may not be coordinated. If all the N atoms of the ligands coordinate to the same metal centre, paap and dpka becomes quadridentate and terdentate respectively. The involvement of the additional N atoms in coordination to the same metal is less probable because of its spatial disposition and the distance from the metal centre. All the above mentioned ligands were obtained as yellow oils and could not be isolated in the solid form even after repeated trials. The ligand Hhmba

could be isolated in the solid form and is a monoprotic bidentate *N, O* ligand, which usually coordinates to the metal through deprotonation. This ligand was characterized by ^{1}H NMR, IR and electronic spectral studies.

Chapter 3 contains the discussion of the thirteen Cu(II) complexes synthesized and characterized by various spectroscopic techniques such as IR, electronic spectral studies and EPR. The magnetic susceptibility measurements reveal some of the complexes to be diamagnetic and many to have low magnetic moments at room temperature. The diamagnetic nature and the low magnetic moments are probably due to an effective antiferromagnetic exchange coupling occurring through the bridging ligands which gives rise to a net spin-pairing effect. In the electronic spectral studies, the broadness of the d-d transitions restricted the assignment of the three d-d transitions. IR spectral studies revealed the coordination of the azomethine N to the Cu(II) centre in the complexes. IR spectroscopy could be used as a very valuable tool to get information regarding the coordination mode of the pseudohalogens. The EPR spectra of all the Cu(II) complexes were recorded both in polycrystalline state at 298 K and in DMF at 77 K. The g values and the various EPR spectral parameters are calculated. The *g* values calculated indicate that in most of the complexes the unpaired electron in Cu(II) resides in the $d_x{}^2{}_{-y}{}^2$ orbital. Some of the complexes were found to be EPR silent in the polycrystalline state, while some others in the powder state displayed very weak Cu^{2+} signals. We could isolate X-ray quality single crystals for one copper

complex and it was found to be a one-dimensional polymer with Cu(II) in an tetragonally elongated octahedral geometry. In the above complex, the ligand papea is found to have undergone metal assisted oxidation and cleavage to give deprotonated pyridine-2-carboxamide, which coordinated to the metal.

Chapter 4 deals with the synthesis and characterization of four Mn(II) complexes. The compounds were characterized by IR, UV-Vis and EPR studies. It was possible to isolate single crystals for two complexes of manganese and in both Mn(II) is in a distorted octahedral geometry. The EPR spectrum of most of the complexes in the polycrystalline state were very broad and it is a characteristic feature of Mn(II) complexes in the polycrystalline state, which arises due to dipolar interactions and enhanced spin lattice relaxation. In the polycrystalline state, two Mn(II) complexes showed two g-tensors, while the remaining two gave three g values. This revealed less zero field splitting (ZFS) effects in former complexes while appreciable ZFS in the latter. The spectra in DMF revealed hyperfine splitting consisting of six lines. In addition to the hyperfine pattern, a pair of low intensity lines is found in between each of the two main hyperfine lines. These are the forbidden lines corresponding to $\Delta m_I \neq 0$, transitions which arise as a result of the mixing of the nuclear hyperfine levels by the zero-field splitting factor.

Chapter 5 describes the synthesis and characterization of six nickel complexes. All the compounds were characterized by various spectral studies. Magnetic susceptibility measurements revealed three of the

nickel complexes to be diamagnetic and hence square planar. We could successfully isolate the single crystals of one nickel complex and the X-ray diffraction studies revealed Ni(II) to be in a distorted octahedral environment in the complex.

Chapter 6 deals with synthesis and characterization of ten cobalt(II/III) compounds. Magnetic susceptibility investigations indicate four complexes to be having cobalt in the +3 oxidation and the remaining to be in the +2 oxidation. Single crystals of two complexes were isolated. The studies reveal one to be having Co(II) and other to be Co(III). The geometry of cobalt in both the compounds is found to be distorted octahedron. The Co(III) complex had two independent molecules in the asymmetric unit.

Chapter 7 describes the synthesis and characterization of seven Cd(II) compounds using various spectral studies like IR and electronic spectra and ^{1}H NMR. The single crystal of one cadmium complex could be isolated. Single crystal X-ray diffraction studies of the compound revealed Cd(II) centres in a distorted octahedral geometry.

Based on the present work, we would like to conclude that the transition metal complexes of Schiff bases and pseudohalides like azide or thiocyanate are promising materials for applications in science and technology. Also, depending up on the metal and the Schiff base used, pseudohalides azide and thiocyanate are found to exhibit different coordination modes in the complexes.

❋❋❋❋ℰℴ ℭℛ❋❋❋❋

SREESHA SASI

Vyshakh
Thacheril Lane
North Fort Gate, Tripunithura
Ernakulam 682 301, Kerala

Ph.No. 9446296572
E-mail: sreeshasasi@yahoo.co.in
sreeshasasi@gmail.com

JOB PROFILE

Working as Lecturer in Chemistry, Government College Malappuram from June 2006.

ACADEMIC PROFILE

Pursuing Ph.D (Inorganic Chemistry)
(2004 – present)
Topic of work: **Structural, Spectral and Magnetic Investigations of some Transition Metal Complexes.**
Supervising Guide: Dr. M.R. Prathapachandra Kurup, Professor, Dept. of Applied Chemistry, Cochin University of Science & Technology, Kochi.

Master of Science
82.1% (2001-2003)
Sacred Heart College, Thevara, Ernakulam
Mahatma Gandhi University, Kottayam

Bachelor of Science (Industrial Chemistry)
91% (1998-2001)
Sacred Heart College, Thevara, Ernakulam
Mahatma Gandhi University, Kottayam

AISSCE (CBSE)
75.6% (1996-1998)
NSS HSS, Tripunithura, Ernakulam

AISSE (CBSE)

89.6% (1996)

NSS HSS, Tripunithura, Ernakulam

ADDITIONAL QUALIFICATIONS

CSIR-UGC (NET) June 2003

CSIR-UGC (NET) December 2002

COMPUTING SKILLS

- Expertise in MS-Office
- ISIS Draw, Chemsketch, Chemdraw
- Familiar with crystallographic softwares
- Expertise in EPR simulation packages

RESEARCH EXPERIENCE

- More than four years research experience in the field of coordination complexes of multidentate ligands such as Schiff bases.

INDUSTRIAL TRAINING

- In-plant training at Hindustan Organic Chemicals from 16th June 2000 to 15th July 2000.

PERSONAL PROFILE

Father's name	Sasi Gopinath
Husband's name	Hareesh N Ramanathan
Date of Birth	12-10-1980
Gender	Female
Marital Status	Married
Nationality	Indian
Languages Known	English, Hindi, Malayalam

POSITIONS OF RESPONSIBILITY

- Member, Organizing committee, National Seminar on Frontiers in Chemistry, FIC-06, Cochin University of Science and Technology
- Coordinator, Career Guidance & Placement Cell, Government College, Malappuram

AWARDS AND HONOURS

- M.V. Varghese Endowment for the best student in Final M.Sc Chemistry (2003-04), Sacred Heart College, Thevara, Ernakulam.
- Endowment for being the topper in science in AISS Examination (CBSE), NSS HSS Thripunithura, 1996

PAPERS/CONFERENCES

- Synthesis and crystal structure of a cobalt(III) complex using a Schiff base and azide, S. Sasi, M.R.P. Kurup, E. Suresh, J. Chem. Cryst, 31 (2007) 37.
- Structure of a one-dimensional coordination polymer of copper(II) with an organic bridging ligand, National Seminar on Frontiers in Chemistry (FIC-06), March 24-25, 2006, Department of Applied Chemistry.
- Thiocyanate complexes of transition metals using a Schiff base, Prof. K.V. Thomas Endowment National Seminar, Sacred Heart College, Thevara, 2007.

❀❀❀ℰᴏᴄ℞❀❀❀